AD 97491

DISCLAIMER NOTICE

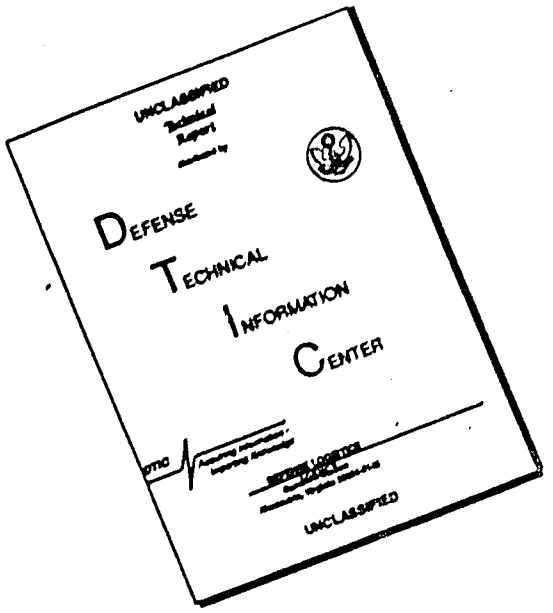

THIS DOCUMENT IS BEST QUALITY AVAILABLE. THE COPY FURNISHED TO DTIC CONTAINED A SIGNIFICANT NUMBER OF PAGES WHICH DO NOT REPRODUCE LEGIBLY.

WADC TECHNICAL REPORT 55-293

DEVELOPMENT AND FABRICATION OF THE F-80C MAGNESIUM ALLOY AIRFRAME

Arthur Kenger
George Leavy

East Coast Aeronautics, Inc.

December, 1955

Structures Branch
Aircraft Laboratory
Contract No. AF 33(038)-5121

WRIGHT AIR DEVELOPMENT CENTER
AIR RESEARCH AND DEVELOPMENT COMMAND
UNITED STATES AIR FORCE
WRIGHT-PATTERSON AIR FORCE BASE, OHIO

FORWARD

This report was prepared by East Coast Aeronautics, Inc., a subsidiary of Barium Steel Corporation, Pelham Manor, New York, under Air Force Contract No. AF 33(038)-5121. It was administered under the direction of Mr. Fred C. Hower, Chief, Development Section, Structures Branch, Aircraft Laboratory, Wright Air Development Center, Air Research and Development Command in conjunction with the Air Materiel Command.

Materials and advice on fabrication and proper use were chiefly supplied by the following:

The Dow Chemical Company for magnesium alloy sheet and extrusions.

American Magnesium Corporation for magnesium alloy sheet and extrusions.

ABSTRACT

The design, fabrication and static test of an all magnesium F-80C airplane is discussed in the following analysis. Temperature limitations for hot forming magnesium alloy and methods employed are presented. Fabrication recommendations for utilizing commercially available high strength magnesium alloys in aircraft primary structures are presented. The present equipment used to fabricate aircraft parts from aluminum alloy can be employed with modifications to incorporate heating devices in order to heat the forming dies and the work. While the necessity for hot working magnesium may, at times, be a drawback in regard to cost of equipment and operation, there are some aspects of the hot working method which, at least partially and often entirely, offset this disadvantage. Hot working of magnesium alloy reduces or eliminates spring-back, thus making greater accuracy possible. In addition, it is generally possible to reduce the number of intermediate draws when hot working magnesium alloy sheet as compared to the number of steps in cold working aluminum alloy sheet. From the machining standpoint, tools for cutting steel will perform satisfactorily on magnesium alloy but better results and a reduction in operating costs may be obtained by modifying the cutting tools to take advantage of the lower cutting resistance of magnesium alloy.

It is concluded from this project that: (a) primary aircraft structural components can be satisfactorily fabricated from the non-strategic magnesium alloys that are commercially available at the present time, (b) the basic design of aircraft can be simplified through the use of thick skin type of construction, (c) primary aircraft structures utilizing thick skin with a minimum of auxiliary stiffeners will compare favorably on a strength-weight basis with conventional reinforced thin-skin type of design.

PUBLICATION REVIEW

This report has been reviewed and is approved.

FOR THE COMMANDER:

TABLE OF CONTENTS

LIST OF ILLUSTRATIONS

LIST OF ILLUSTRATIONS - CONT'D.

LIST OF ILLUSTRATIONS - CONT'D.

LIST OF ILLUSTRATIONS - CONT'D.

LIST OF ILLUSTRATIONS - CONT'D.

INTRODUCTION

Recent developments in the aircraft industry have turned attention to magnesium alloy as a primary material for airframe components. The record shows that strong, light-weight, non-strategic magnesium has established itself as a member of the aircraft family of metals. In a relatively short period, engineers have applied this material into an ever-widening field of aeronautical applications.

The principal factors responsible for the exceptional rapidity of the development of the use of magnesium alloy in the aircraft industry in the past ten years are:

1. The introduction of more suitable alloys, primarily FS1-H24 and ZK60A, which exhibit better strength, ductility and resistance to fatigue as compared to J1-H magnesium alloy previously used in various development programs.

2. Increasing weight savings have been demanded by the aircraft industry.

3. Lower density of magnesium alloys will permit the design of a monocoque type of structure that can carry higher buckling loads for the same weight of structure.

4. The realization of various design simplifications that can be made through the use of a magnesium monocoque type of structure, thus resulting in increased producibility through reduction in overall number of detail parts and fastenings.

5. The cost of design and fabrication can be reduced as a direct result of design simplification.

6. Excellent machining properties.

7. Adaptability of magnesium to many modern processes of fabrication and assembly such as extruding, sand casting, die casting, permanent-mold casting, fusion and resistance welding.

One of the advantages, as well as a weakness of magnesium alloy, is its low modulus of elasticity. Magnesium alloy has a modulus of elasticity of 6-1/2 million as compared to 10 million for aluminum and 29 million for steel. Because of its low modulus, magnesium structures require more cross-sectional area for the same deflection and additional area for the same load due to the lower allowable stresses. Therefore, in many applications the use of magnesium is advantageous in that a thick skin design is possible. This results in greater rigidity and greater resistance to local buckling.

Even though magnesium has a lower strength than aluminum, magnesium can and does compete successfully with denser materials on the basis of strength weight ratio. The reason is that the strength of a part is very often determined more by the geometry of the part than by the basic strength of the

material of which it is made. In aircraft structures, much of the airframe weight is in members for which compressive buckling is a critical condition. The most effective way to boost allowable compressive stresses is to employ thick cross sections. The advantages of magnesium in this regard are obvious. In view of the greater bulk required with magnesium, the problem of local instability may be lessened since under some conditions of loading the strength or stiffness of a structural member increases with the second or third power of the thickness or depth of the member; as a result, heavy-gage monocoque type magnesium sheet structures are practical from both the strength and weight standpoint. This type of construction is often cheaper to manufacture than lighter gage sheet structure of the same weight made of aluminum alloy which requires many rivets and internal stringers to raise the allowable buckling of the skin.

Magnesium alloys have been of immeasurable value in solving the problems which are commonly known as "minimum gage" problems. In stressed skin structural designs where the skins are lightly loaded, a practical minimum gage of skin is used; however, if magnesium skins are used in place of aluminum, considerable weight savings are usually possible.

Several other significant advantages can be realized in utilizing magnesium alloy as primary structural material. Employing heavy-gage monocoque type of construction results in aerodynamic smoothness and increased structural rigidity. These advantages are noteworthy since the demand for even higher speeds has necessitated the development of thinner wings which creates new problems. These problems are partially solved by employing a magnesium monocoque type of structure without paying a penalty in weight.

From the fabrication standpoint, the fabrication of wrought magnesium alloy parts will require new shop tools and technique. This requirement is necessary since many forming operations on magnesium can only be done at elevated temperatures. The strain hardening of the wrought magnesium alloy upon forming permits only a small amount of deformation at room temperature. As the temperature of magnesium alloy is raised above 450°F the magnesium alloy may be more severely worked than most other metals at room temperature. The use of heat on some parts being formed sometimes allows the part to be completely drawn or fabricated in one operation, whereas in other metals several anneals and redraws might be required. Springback is negligible in parts formed at high temperature. In general, magnesium alloys can be formed in more intricate shapes than aluminum alloy parts if the proper tools are used.

In the following analysis, the design, fabrication, and static test of an all magnesium F-80C airplane is discussed. A detail analysis of the assembly procedure employed in constructing the various components of the magnesium airframe is not presented since the method employed is consistent with the experimental nature of this project and is considered as standard practice. The fuselage assembly fixtures, as presented in Figures 6, 8, and 9, are only considered as holding fixtures and are not deemed as production tools.

In Appendix "A", a detail stress analysis of the structural components of the magnesium F-80C airframe is presented.

An analysis of the magnesium wing is not presented since the wing was developed under a separate contract and is completely covered in Air Force Technical Report No. 6194, entitled, "Development of a Thick Skin Magnesium Alloy Wing for F-80 Aircraft," and dated September, 1950.

In the development program of the magnesium airplane, the following parts were not fabricated in magnesium; (a) Ammunition Doors, (b) Nose Landing Gear Doors, (c) Main Landing Gear Doors, (d) Fuselage Fuel Tank Access Door, (e) Upper Engine Access Door, (f) Wing Fillets (up to fuselage station 277.5), (g) Tail Fillets, (h) Internal Air Ducts (portion extending from fuselage station 164 - 224), (i) Louvre and Air Bleed Ducts. For the above mentioned assemblies, it was decided to utilize the standard F-80C aluminum assemblies since the cost of the tools to fabricate these parts in magnesium was not warranted in consideration of the requirements for one airplane and the secondary structural nature of these parts. Based on a design analysis, it was estimated that approximately twenty percent of the structural weight of these assemblies could have been saved if the assemblies were fabricated in magnesium alloy. The magnesium F-80C airplane is shown in Figures 1 and 2.

MATERIALS

The materials used in the fabrication of the F-80C magnesium airplane are as shown in the following table together with the basic allowable stresses used in the detail design of the structure. Attachments were made by 56S aluminum alloy rivets, 75ST aluminum alloy Huck Lockbolts and AN steel bolts and screws except for the following attachments. When aluminum parts were riveted to other aluminum parts, A17ST rivets were used; however, when attaching aluminum to magnesium 56S rivets were used.

The material allowables for the stainless steel used are not presented in the following table since they are generally known.

FIGURE 1 - F-80C MAGNESIUM AIRPLANE

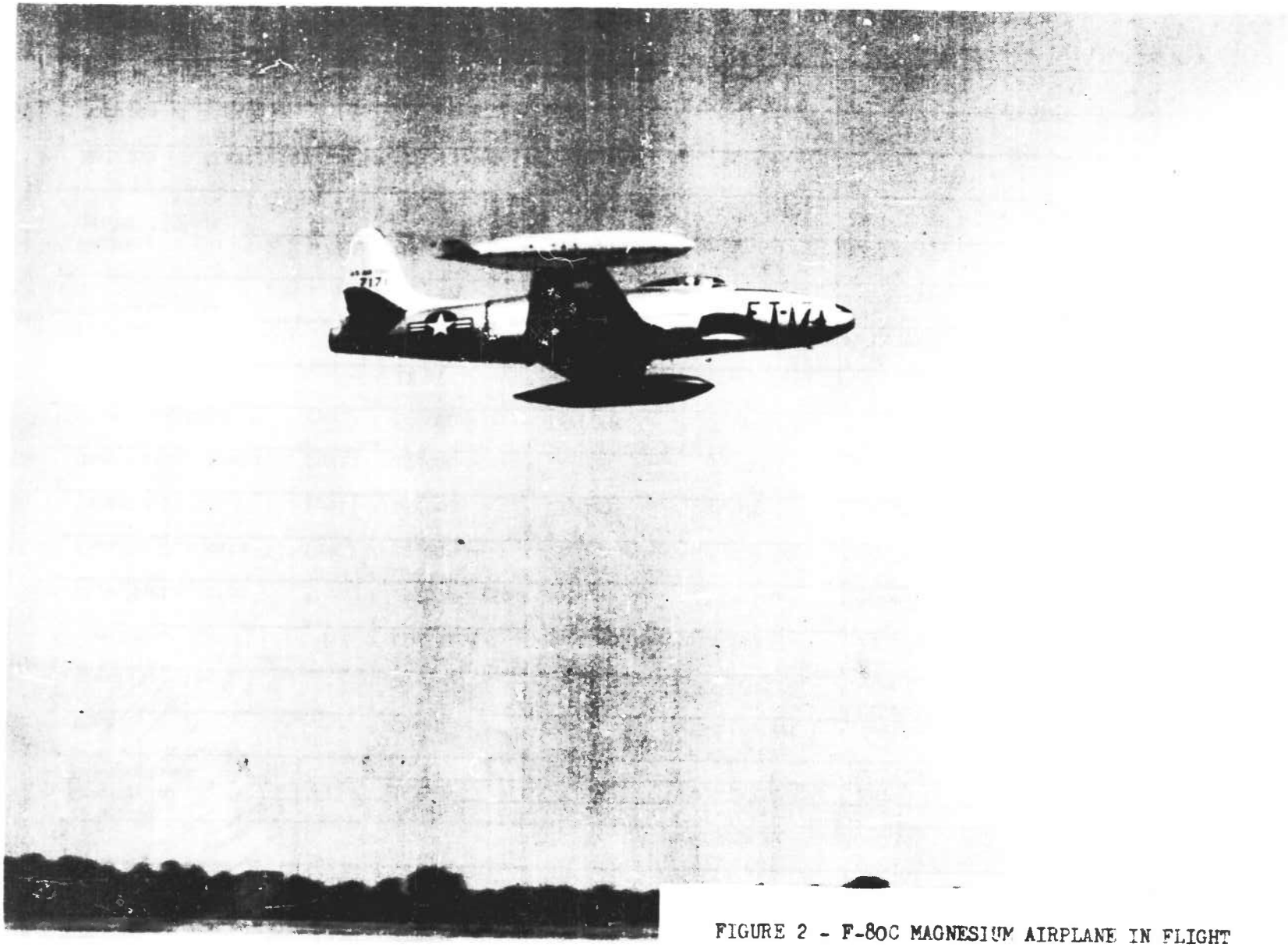

FIGURE 2 - F-80C MAGNESIUM AIRPLANE IN FLIGHT

PHYSICAL PROPERTIES OF MAGNESIUM MATERIALS USED
(DATA FROM ANC-5, TABLES 4.111 (a) & (b) EXCEPT AS NOTED)

Commercial Designation	Dow / Amer.Mag. / ASTM	MAGNESIUM ALLOYS				
		FS1-O / C52S-O / AZ31X	FS1-H24 / C52S-H24 / AZ31X	ZK-60A-T5 / AM-XA76S-T5	H-T4 / AM265-T4 / AZ63-HT	H-T6 / AM265-T6 / AZ63-HTA
Type		Sheet	Sheet	Extrusion	Casting	Casting
Specification		QQ-M-44	QQ-M-44	MIL-M-5354	QQ-M-56 Comp. AZ-63	QQ-M-56 Comp. AZ-63
Condition		Annealed	Hard Rolled	EA (1)	HT (1)	HTA (1)
Size Restriction		.020 - .250	.020 - .128	5-10 ins^2	None	None
Tensile Ultimate	(psi)	32,000	39,000	45,000 (2)	34,000	34,000
Tensile Yield	(psi)	15,000	29,000	36,000 (2)	10,000	16,000
Compressive Yield	(psi)	12,000	24,000	30,000 (3) 25,000 (3)(2)	10,000	16,000
Shear Ultimate	(psi)	17,000	18,000	25,000 (2)	17,000	19,000
% Elongation (e)		12	4	4	7	3
Bearing Ultimate (psi)	E/D = 1.5	50,000	58,000	-	36,000	50,000
	E/D = 2.0	60,000	68,000	76,000 (2)	50,000	65,000
Bearing Yield (psi)	E/D = 1.5	29,000	43,000	-	32,000	36,000
	E/D = 2.0	29,000	43,000	55,000 (2)	36,000	45,000
Modulus of Elasticity		6.50×10^6				
Modulus of Rigidity		2.40×10^6				
Weight/Cubic Inch		0.0645	0.0645	0.0660	0.0664	0.0664

(1) HT = Heat Treated. - EA and HTA = Heat Treated and Aged.
(2) Values shown are minimum mechanical properties per Dow Chemical Co. Bulletin #DM 120.
(3) 30,000 PSI for areas less than 2 Sq. In. - 25,000 PSI for areas from 3 - 5 Sq. In.

DESIGN

The initial step in the design of the experimental F-80C magnesium airframe was to evolve a preliminary layout of the basic internal structure. This preliminary layout in some respects was dictated by contract requirements that the experimental magnesium airframe shall be interchangeable with the prototype aluminum F-80C airframe with respect to the fuselage, wing, aileron, flaps, landing gear and tail assemblies. From an examination of the preliminary layout and the interchangeability criteria it was apparent that no major changes in the internal arrangement of the basic primary structure over that of the prototype could be accomplished; although it was felt that a more efficient magnesium structure could be gained by an original design considering the use of magnesium without being plagued by interchangeability of an existing design in aluminum alloy.

The fuselage structure was designed in three sections similar to that of the prototype fuselage; that is, nose section, mid-section, and aft section. The nose section extends from station 16 to the canted bulkhead station 81.80. This section contains all the armament equipment consisting of six .50 caliber machine guns with ammunition trays for 300 rounds per gun. The mid-section extends from the canted bulkhead station 81.8 to station 277.5 and basically contains the pressurized cockpit, power plant, nose landing gear, self-sealing fuel tank with a capacity of 207 gallons of fuel and two dive recovery flaps located at the bottom of the fuselage forward of station 190.50. The wing is attached to the mid-section at station 190.5 and 228.3. The aft section of the fuselage extends from station 277.5 to station 430. This section incorporates the tail structure and houses the jet engine tail pipe.

The basic structure of the fuselage nose section was unaltered from that of the prototype aluminum structure except for the elimination of the skin stiffeners above the gun deck between station 27 and 47. All skins and bulkheads except the lower skins forward of station 47 which are stainless steel were fabricated from FS1-H24 magnesium alloy sheet. The longerons were fabricated from ZK60A-T5 magnesium extrusions. Stainless steel was also used in the shell ejection region below the gun deck.

The basic structure is shown in Figure 3. A top view and a quarter rear view of the nose section is shown in Figures 4 and 5 respectively. The fittings for the gun mounts are not shown. These fittings were not redesigned and the standard fittings used on the prototype were employed.

In the redesign of the fuselage mid-section, the fuselage frames were placed at the same locations as on a standard Lockheed F-80C airplane; however, practically all of the secondary stringers used on the standard F-80C were eliminated except for the aft lower section of the mid fuselage. The fuselage frames were formed from FS1-H24 magnesium alloy sheet except for special highly loaded frames which were made from AM265-T6 (heat-treated and aged) magnesium alloy castings (Comp. AZ-63). These castings were located at the following stations; 141, 152, 163.875, 190.5, 228.3, 252, and 277.5. At station 141 and 152 only the area of the bulkhead in the region of the pressurized cockpit was made from a magnesium sand

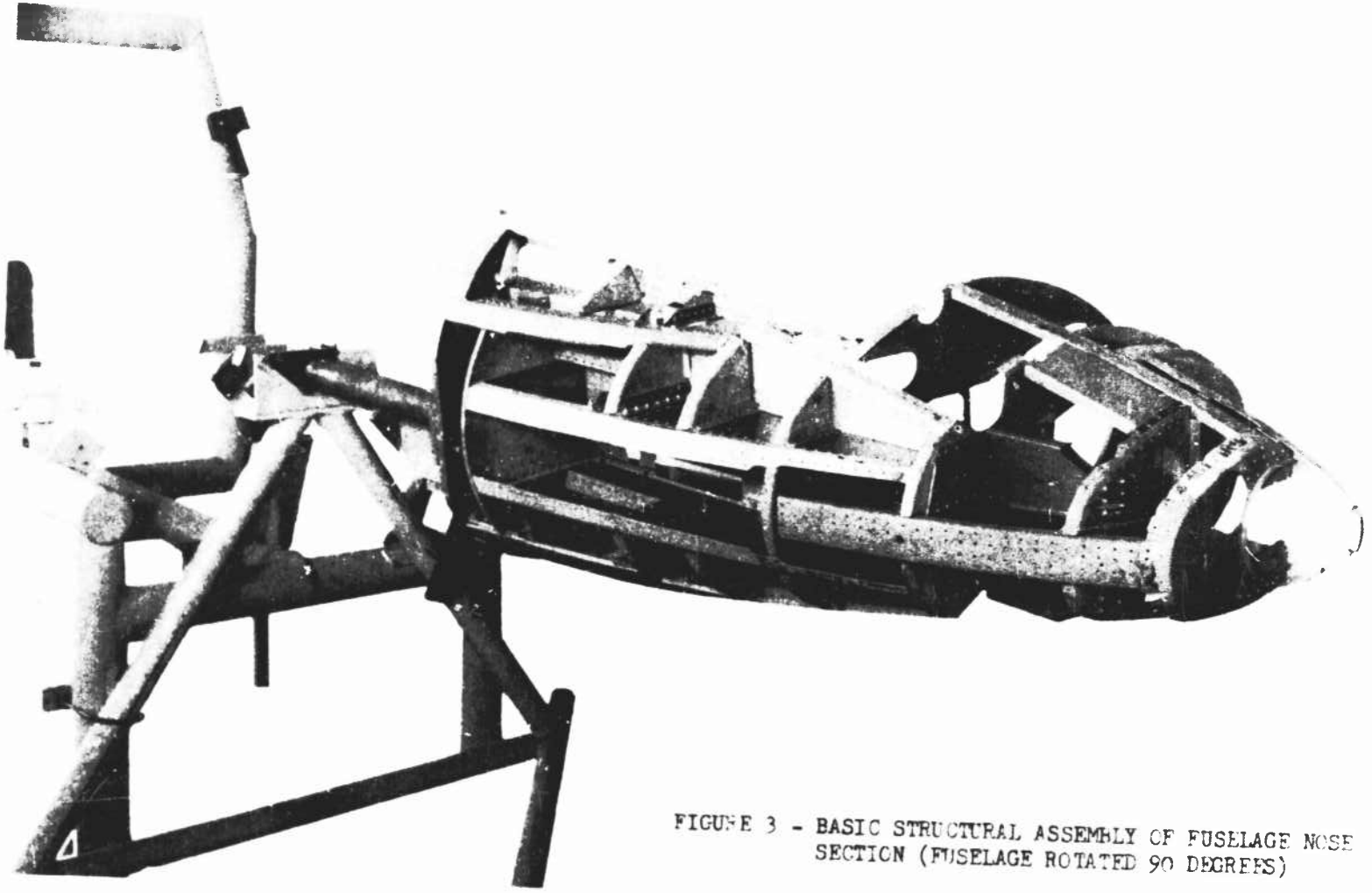

FIGURE 3 - BASIC STRUCTURAL ASSEMBLY OF FUSELAGE NOSE SECTION (FUSELAGE ROTATED 90 DEGREES)

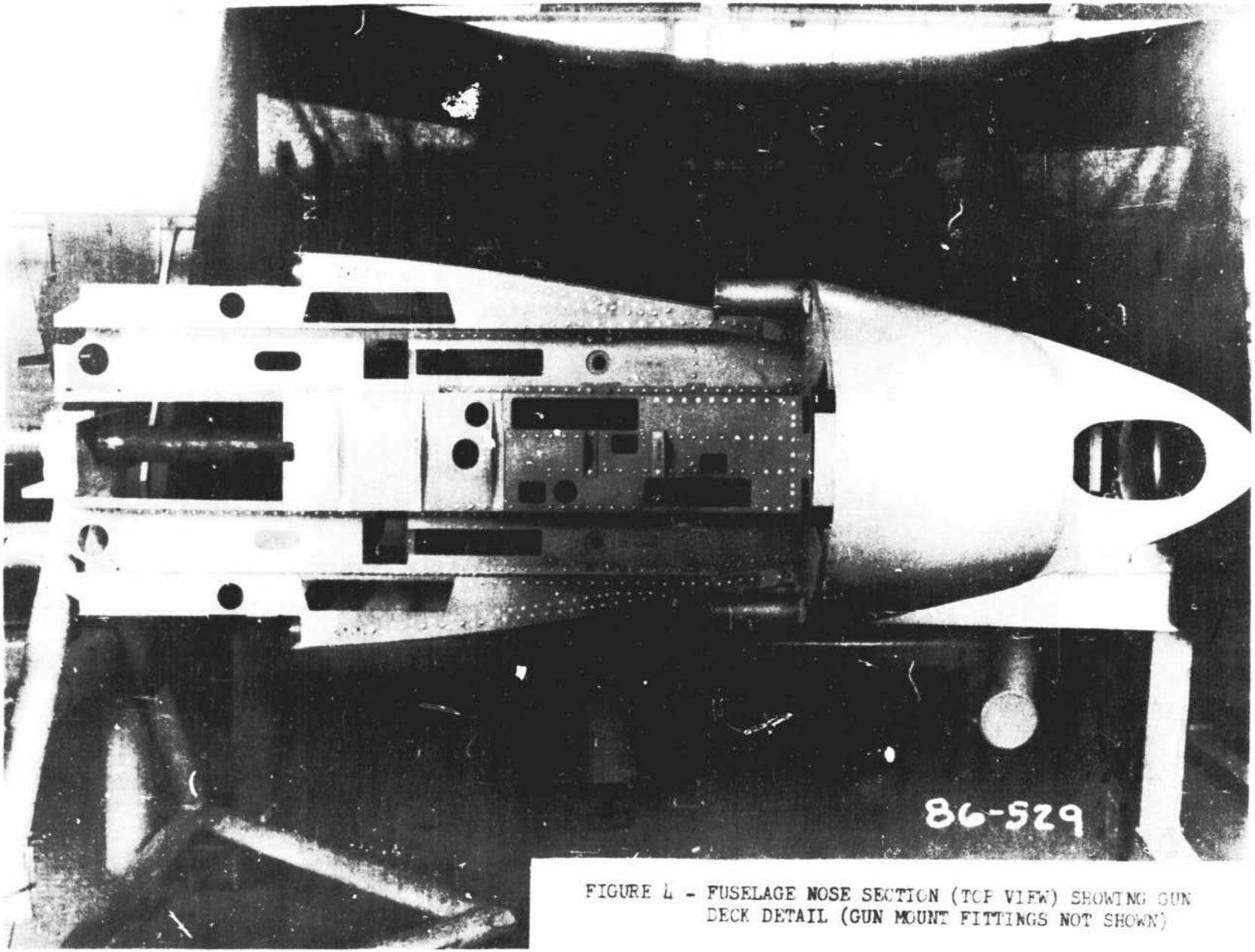

FIGURE 4 - FUSELAGE NOSE SECTION (TOP VIEW) SHOWING GUN DECK DETAIL (GUN MOUNT FITTINGS NOT SHOWN)

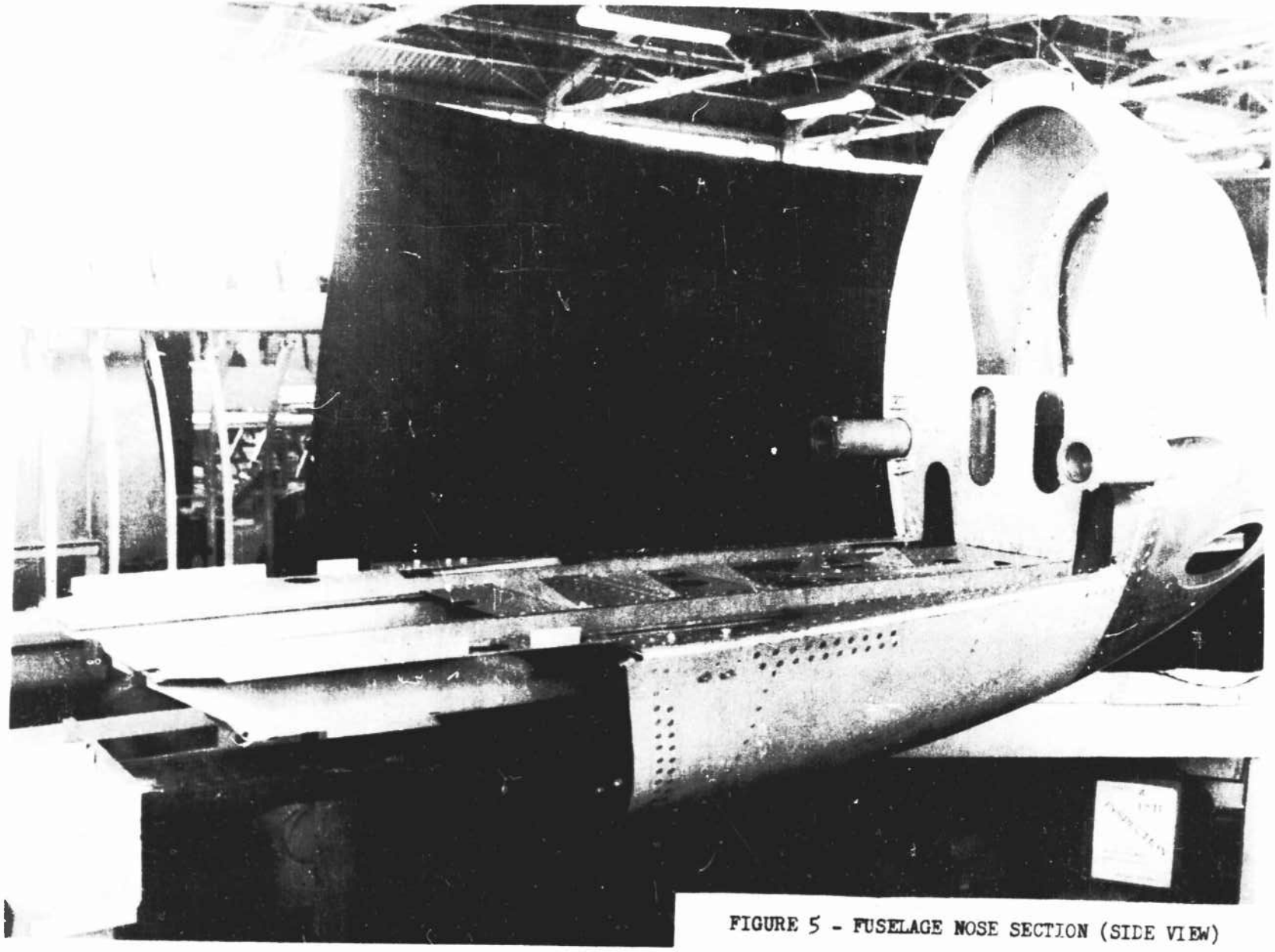

FIGURE 5 - FUSELAGE NOSE SECTION (SIDE VIEW)

casting. In reference to station 163.875, only the air duct region of the bulkhead was designed as a casting. The location of the castings are shown in Figure 6.

The main structural longerons of the fuselage mid-section were fabricated from ZK60A-T5 magnesium alloy extrusions and FS1-H24 magnesium alloy sheet was used as the cover material.

As a result of the static test, additional stiffeners were added as intercostal angles from station 228.3 to 263 at Water Line 97.59 and 106.59. These intercostal stiffeners were clipped to the frames and were made from an equal-leg angle magnesium extrusion of ZK60A-T5 alloy one inch by .125 thick.

The basic structure of the fuselage mid-section is shown in Figures 6, 7, and 8.

The aft fuselage structure was constructed of magnesium alloy except for the fire wall bulkheads and the bulkheads supporting the tail section which were made from stainless steel. The bulkheads were located at the same locations as on the standard Lockheed F-80C airplane with the addition of two bulkheads which were located at stations 288.25 and 388.0; however, all of the secondary stringers used on the Lockheed F-80C were eliminated. The main longerons in the aft fuselage section were made from ZK60A-T5 magnesium alloy extrusions and FS1-H24 magnesium alloy sheet of .064 gage was used as the skin covering as compared to .032 gage aluminum used on the standard F-80C. In the magnesium aft fuselage section, the skin gage for the last 30 inches of the fuselage was reduced to .040. The basic fuselage structure showing the various bulkheads and longerons are shown in Figures 9 and 10.

A comparison of the prototype structure in aluminum alloy and the redesigned fuselage aft section in magnesium alloy is shown in Figures 11 and 12 respectively.

The complete fuselage assembly and empennage for the static test airplane is shown in Figure 13 and the flight test fuselage nose and mid section is shown in Figure 14.

The design of the fin was of conventional design. The front and rear beams were fabricated with ZK60A-T5 extruded magnesium alloy caps and FS1-H24 magnesium alloy webs. The ribs and skins were fabricated from FS1-H24 magnesium alloy sheet. The rudder was fabricated with a FS1-H24 formed sheet channel beam and FS1-H24 ribs and skins.

In the design of the magnesium alloy fin a total of seven ribs were used as compared to eight used on the prototype aluminum conventional F-80C. The skin gage of the magnesium fin was .051 as compared to .032 for the prototype fin.

The magnesium rudder employed eight ribs in its basic structure with a skin gage of .051 although 12 ribs and a skin gage of .032 were employed on the prototype aluminum rudder design.

The basic structure of the fin is shown in Figure 15 and that of the rudder is presented in Figure 16.

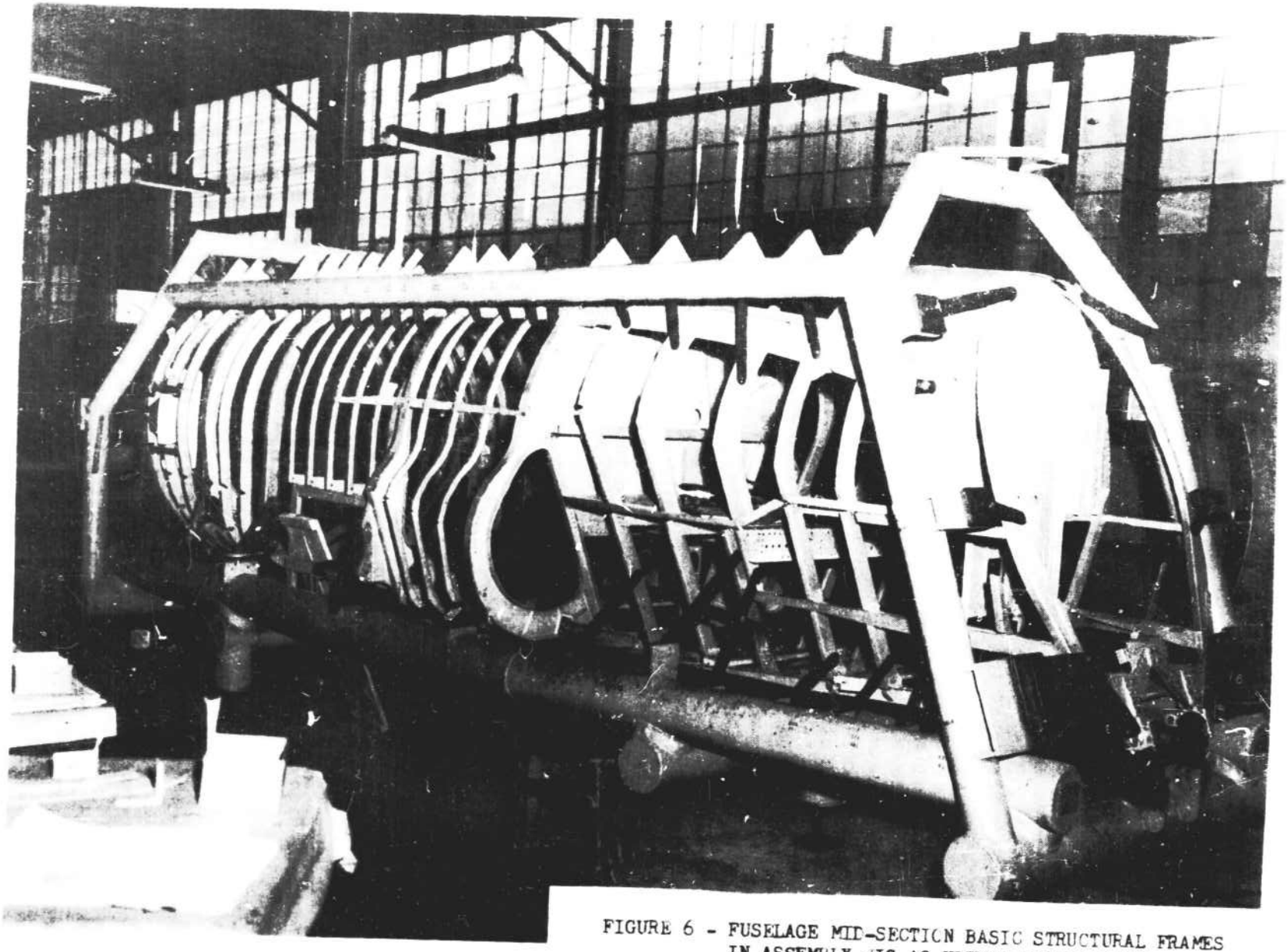

FIGURE 6 - FUSELAGE MID-SECTION BASIC STRUCTURAL FRAMES IN ASSEMBLY JIG AS VIEWED FROM FORWARD END

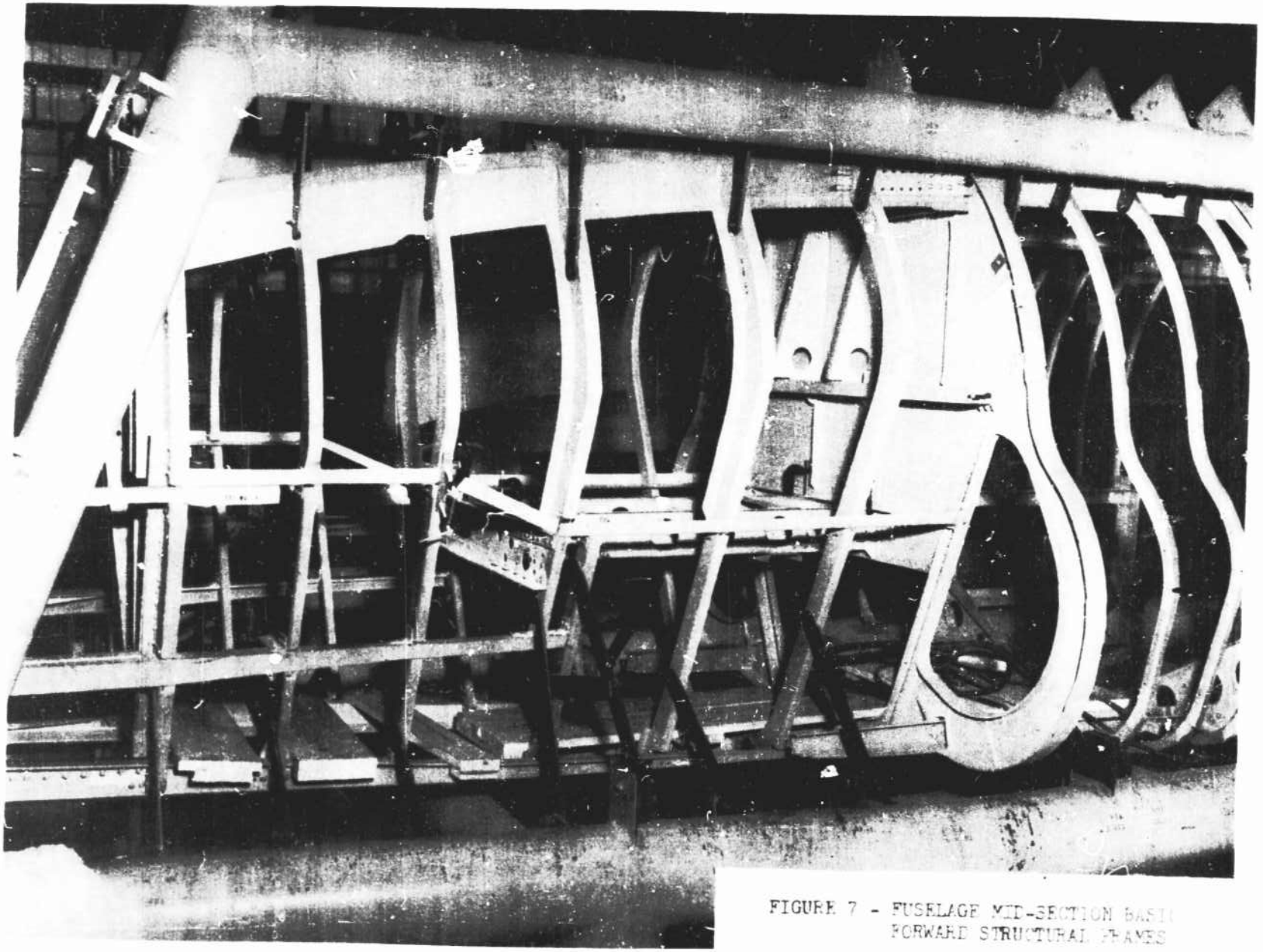

FIGURE 7 - FUSELAGE MID-SECTION BASIC FORWARD STRUCTURAL FRAMES

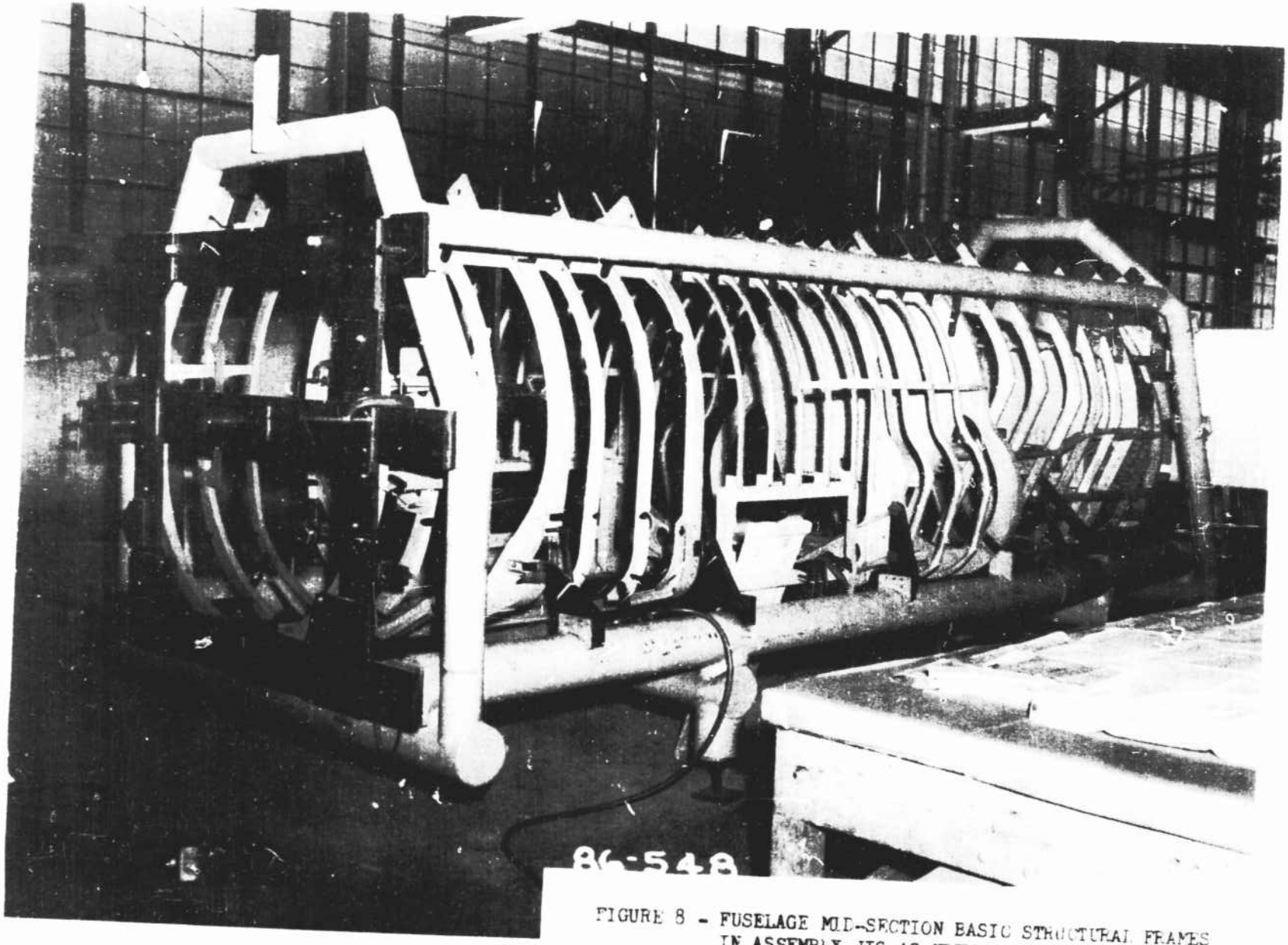

FIGURE 8 - FUSELAGE MID-SECTION BASIC STRUCTURAL FRAMES IN ASSEMBLY JIG AS VIEWED FROM AFT END

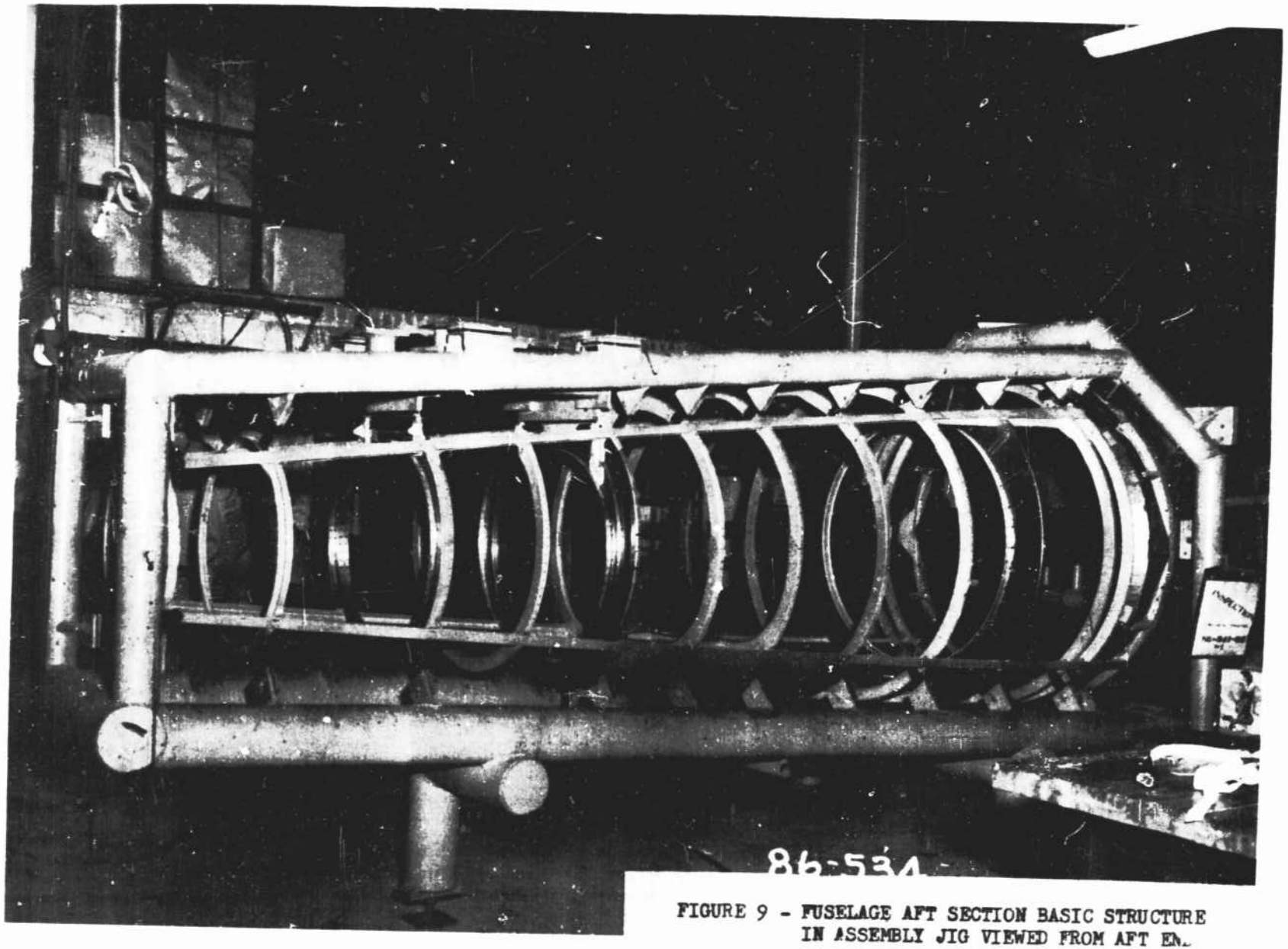

FIGURE 9 - FUSELAGE AFT SECTION BASIC STRUCTURE IN ASSEMBLY JIG VIEWED FROM AFT EN.

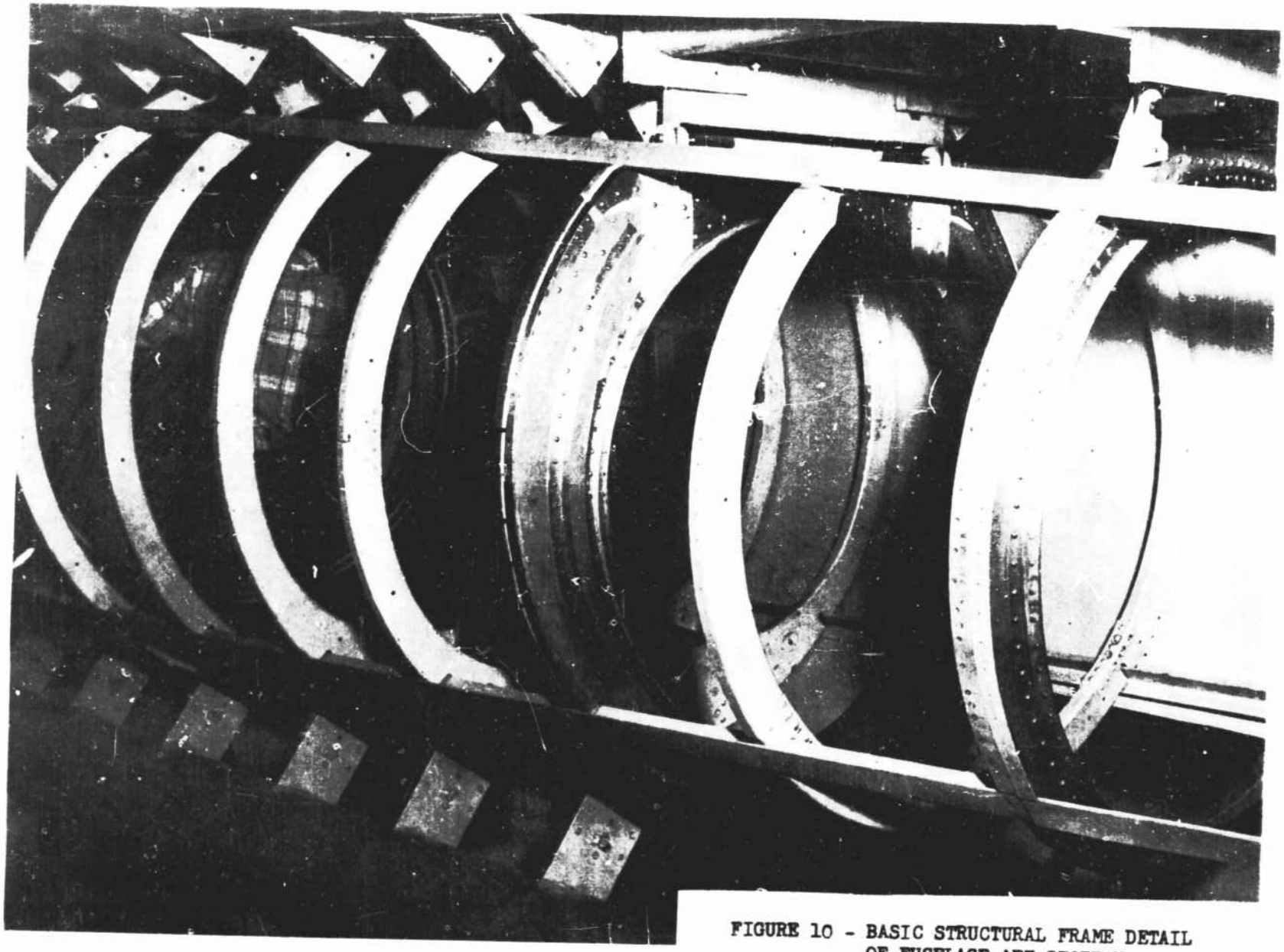

FIGURE 10 - BASIC STRUCTURAL FRAME DETAIL
OF FUSELAGE AFT SECTION

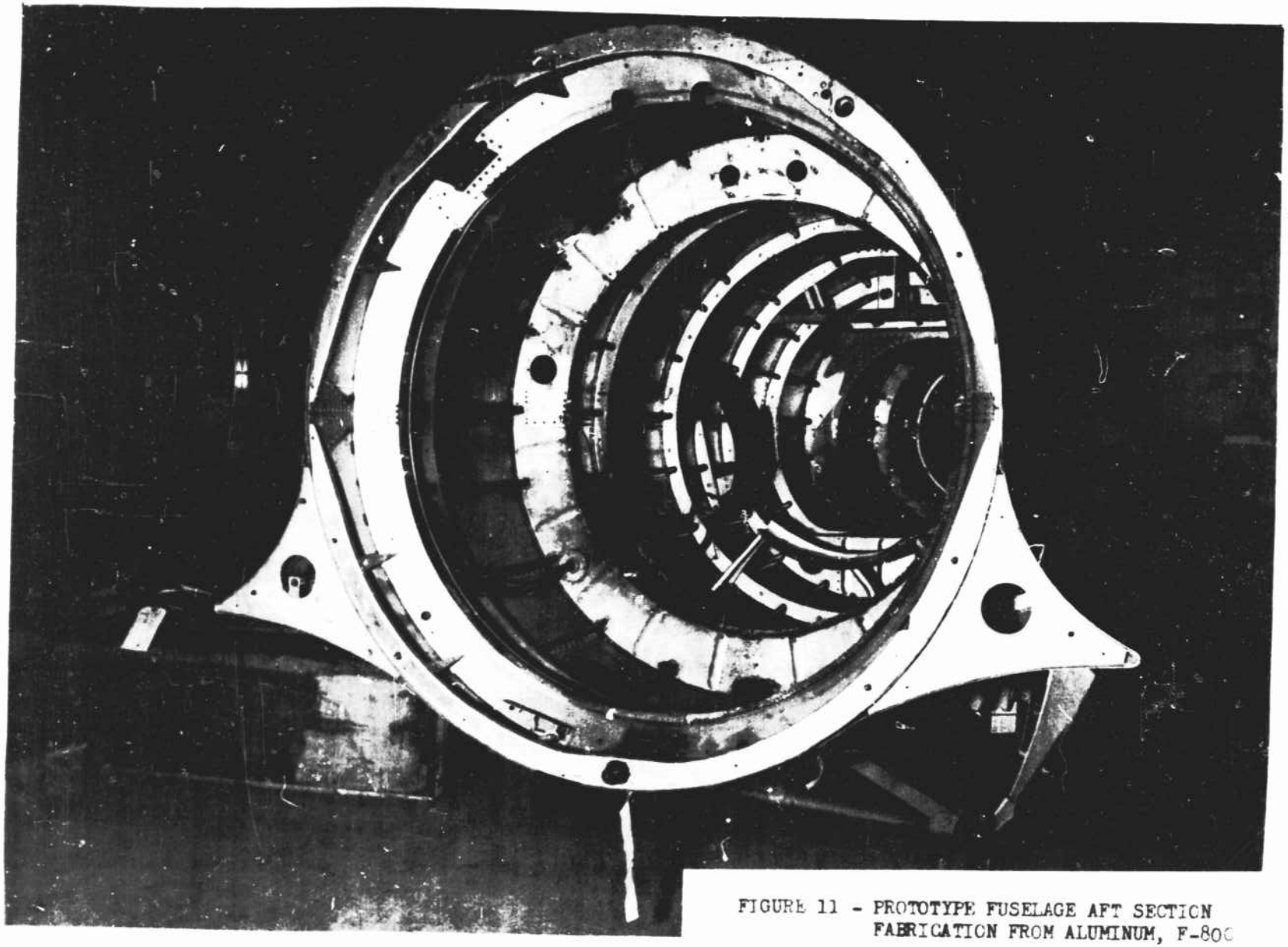

FIGURE 11 - PROTOTYPE FUSELAGE AFT SECTION FABRICATION FROM ALUMINUM, F-80C

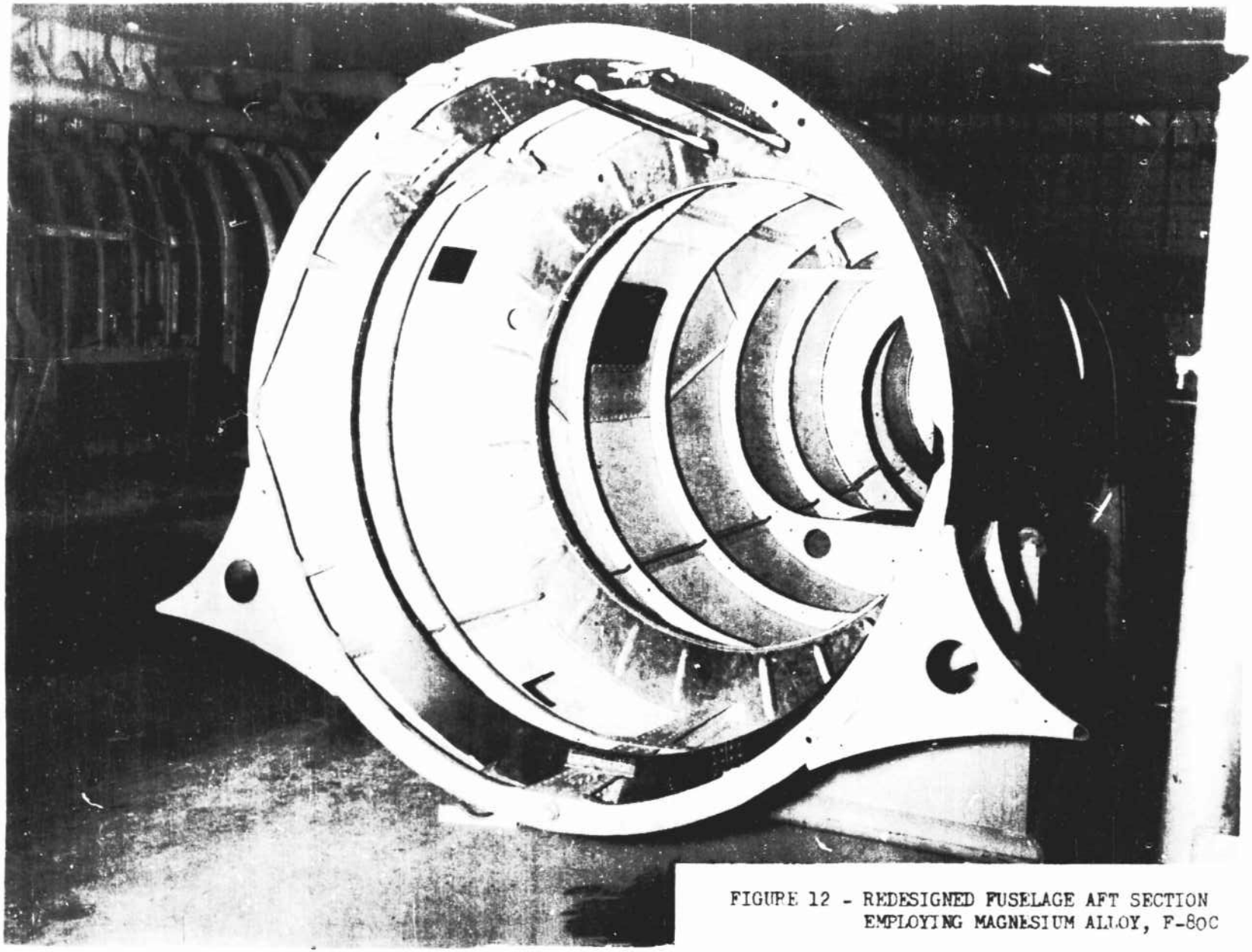

FIGURE 12 - REDESIGNED FUSELAGE AFT SECTION EMPLOYING MAGNESIUM ALLOY, F-80C

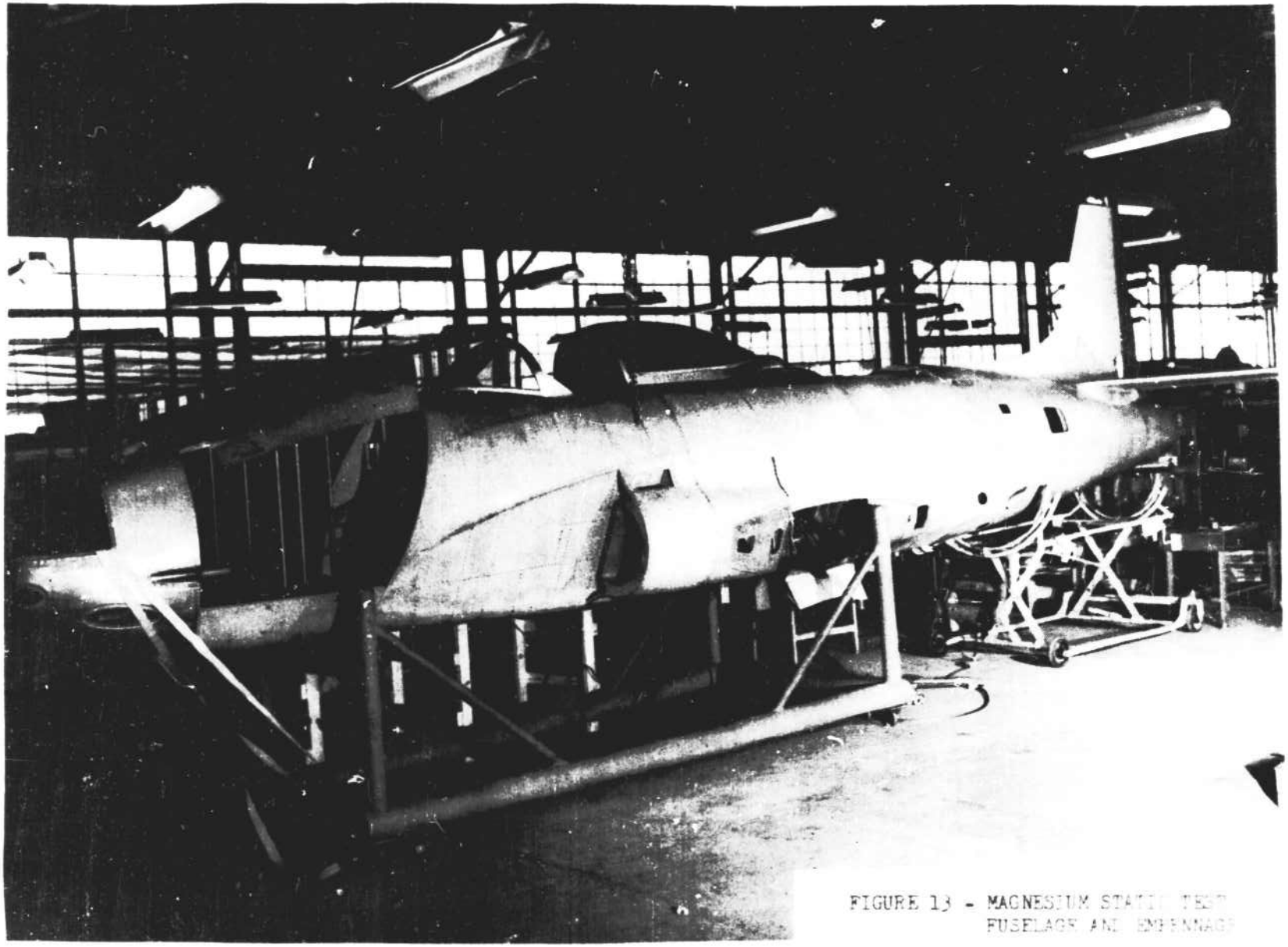

FIGURE 13 - MAGNESIUM STATIC TEST
FUSELAGE AND EMPENNAGE

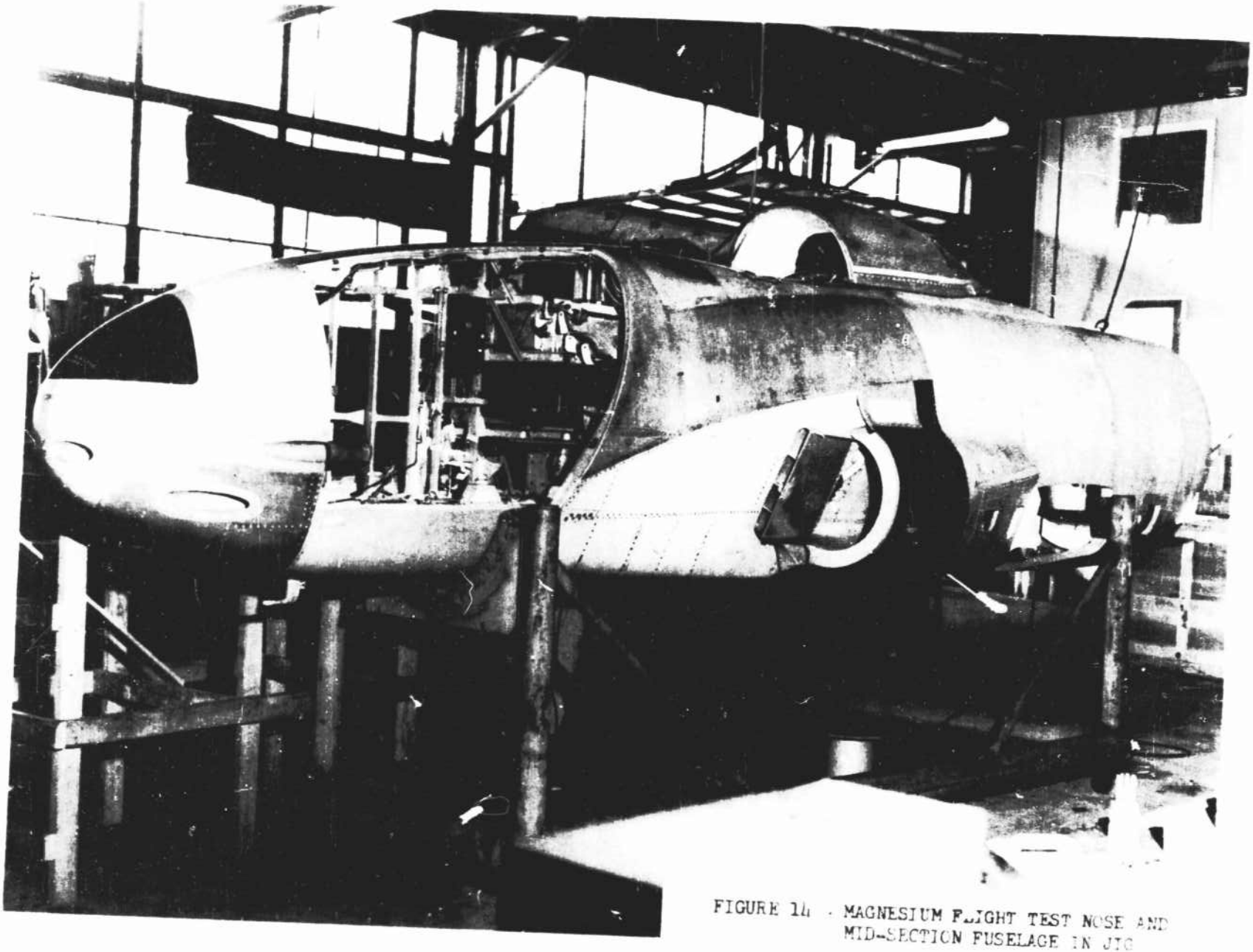

FIGURE 14 - MAGNESIUM FLIGHT TEST NOSE AND MID-SECTION FUSELAGE IN JIG

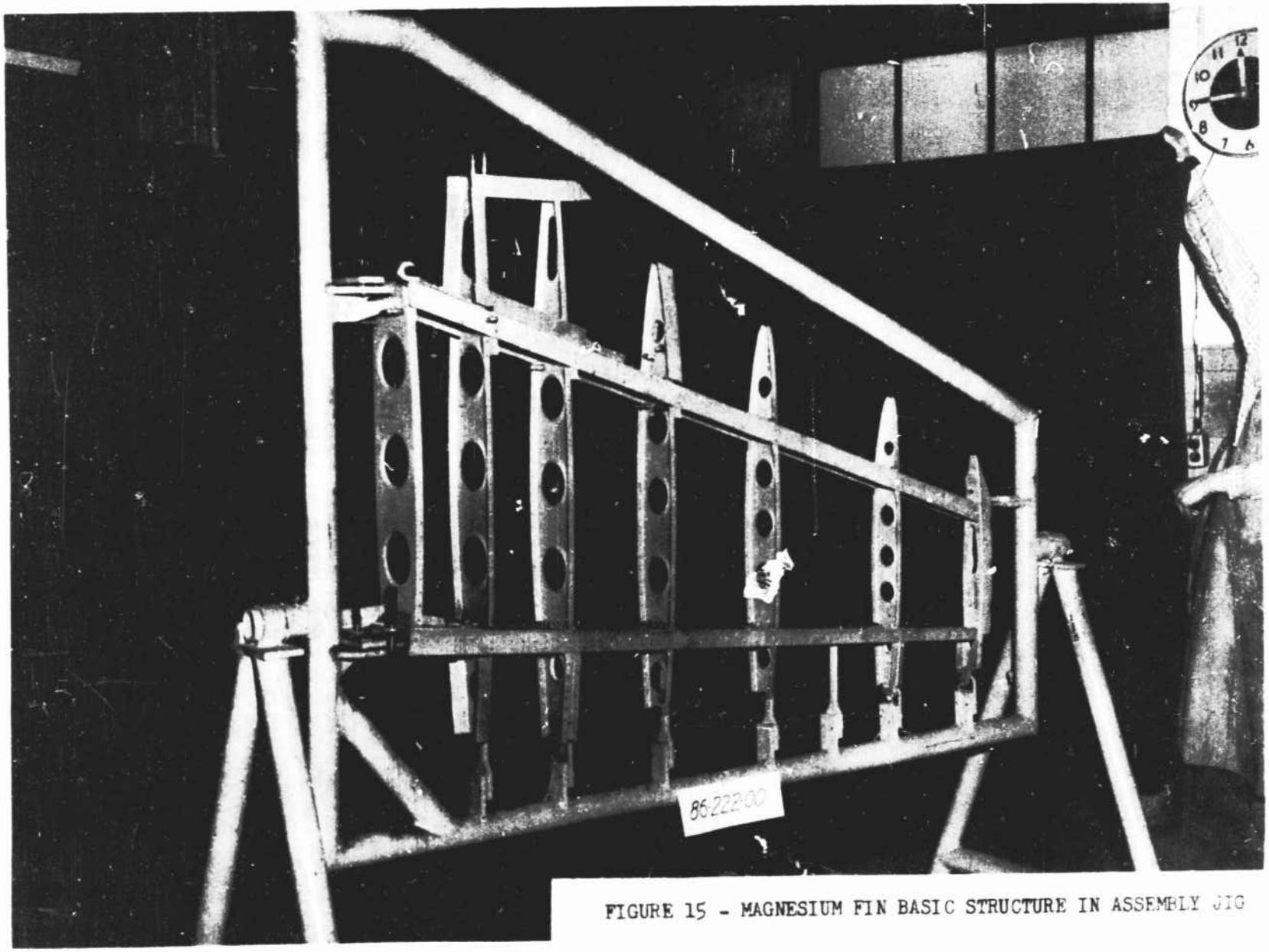

FIGURE 15 - MAGNESIUM FIN BASIC STRUCTURE IN ASSEMBLY JIG

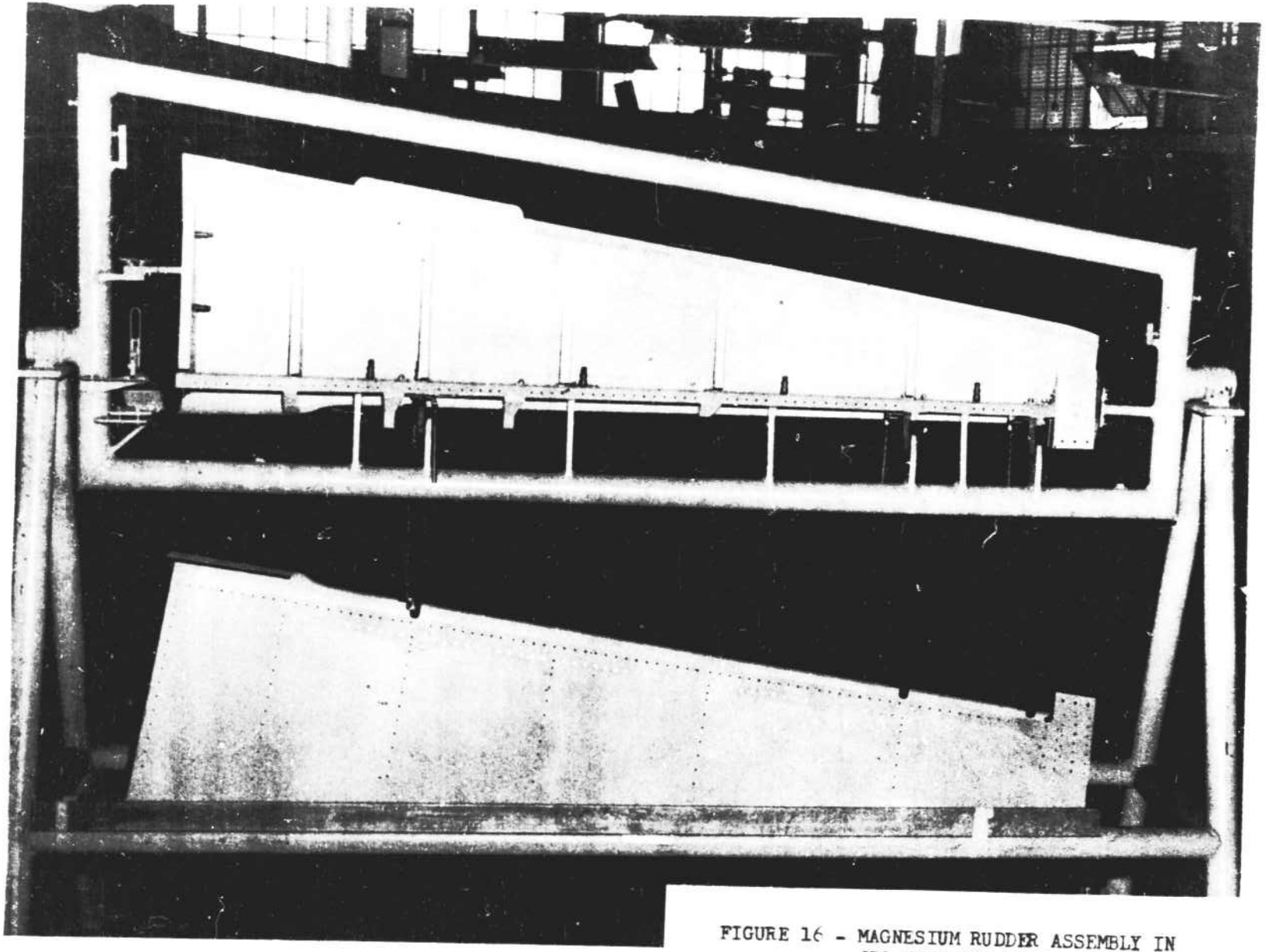

FIGURE 16 - MAGNESIUM RUDDER ASSEMBLY IN JIG WITH ONE SKIN REMOVED

The horizontal stabilizer of the prototype airplane consisted of a two beam construction with longitudinal stringers located approximately five inches apart. These stringers were placed parallel to the rear beam and were dropped as they approached the front beam. Eight chordwise ribs per side, not including the centerline rib completes the basic structural frame. In redesigning the horizontal stabilizer structure from aluminum to magnesium alloy, the prototype structure was changed to a three beam structure utilizing only four ribs per side. In order to obtain maximum beam bending efficiency for minimum weight and to avoid skin splices, the horizontal stabilizer was designed to employ machined tapered magnesium skins that extended from the root section to the tip. These skins were machined from hard rolled magnesium sheet conforming to Federal Specification QQ-M-44, Condition H (Dow FS1-H24). The skins are eighty-two inches (82) long and taper at a rate of .0192 inches per foot and measure .172 inches at the root. The maximum width of the skins was approximately 36 inches.

The problem of forming the leading edge radius was circumvented by employing a machined leading edge insert. This machined leading edge was fabricated from a ZK60A-T5 extruded magnesium bar. At first an attempt was made to cast this leading edge in order to avoid excess machining; however, this casting program was later abandoned due to warpage difficulties encountered.

The three beams of the magnesium horizontal stabilizer were fabricated from ZK60A-T5 magnesium extrusions. The web of the beams was an integral part of the beam caps and was formed by overlapping and riveting the vertical leg of the beam caps. The centerline rib and the ribs located at stabilizer station 10 utilized ZK60A-T5 magnesium extrusion for their rib caps and FS1-H24 magnesium alloy sheet for their webs. All other ribs were formed from FS1-H24 magnesium alloy sheet.

The basic structural configuration of the magnesium horizontal stabilizer is shown in Figure 17.

The elevator was of conventional construction and design and was fabricated with a FS1-H24 magnesium alloy formed sheet channel beam and FS1-H24 ribs and skins.

In order to maintain interchangeability between the magnesium and prototype aluminum empennage, the standard F-80C fin and stabilizer fittings were used.

The flight airplane in the final assembly stages is shown in Figure 18.

DESIGN OF FITTINGS

In order to substantiate the static strength of the most critical fittings used in the design of the magnesium F-80C airplane, all critical fittings were static tested. All fittings chosen for test were originally either forged or cast from aluminum alloy in the prototype airplane. These fittings were redesigned to employ magnesium ZK60A-T5 extrusion alloy or magnesium casting alloy conforming to specification QQ-M-56, Composition AZ63, heat treated and aged.

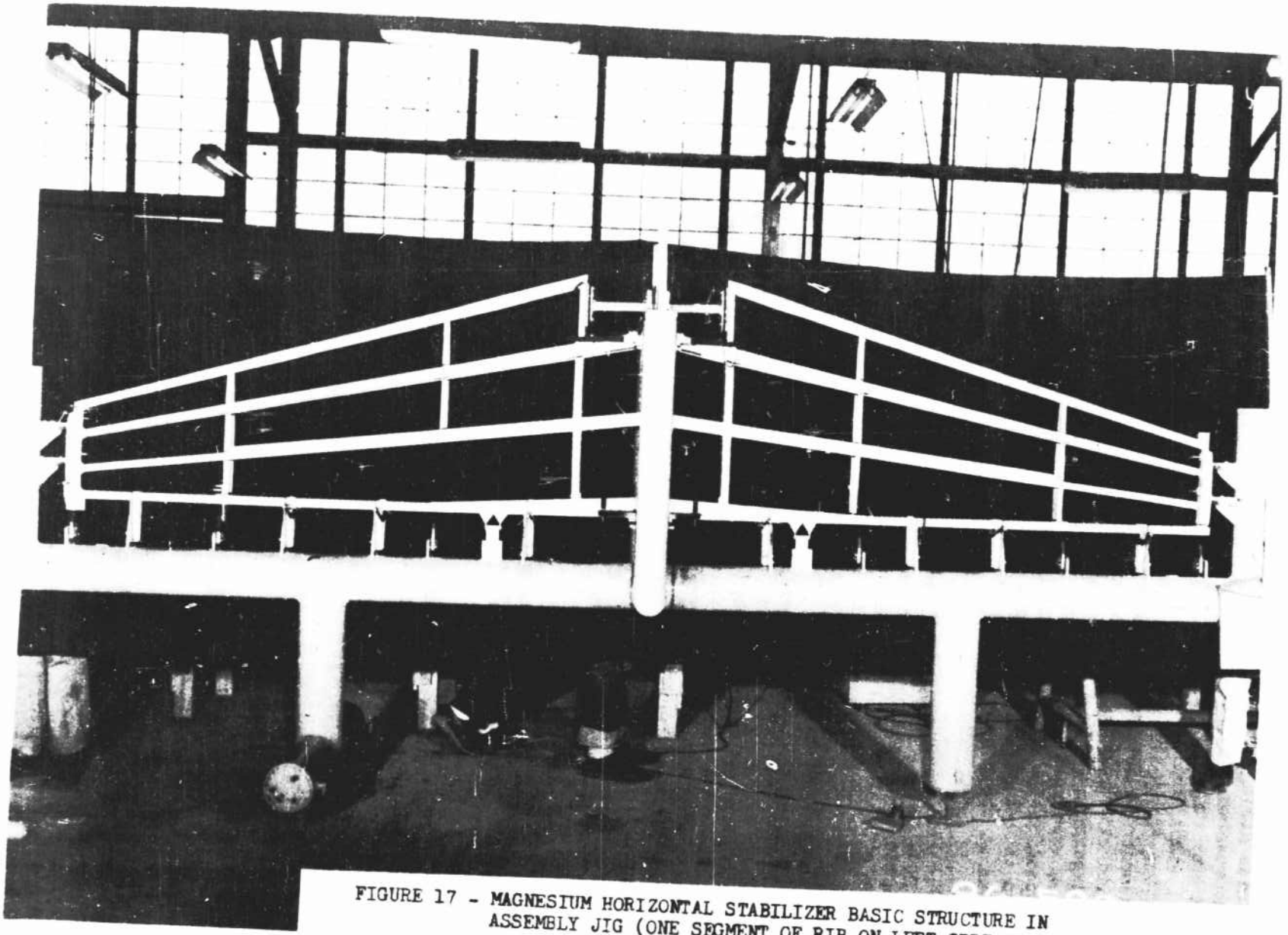

FIGURE 17 - MAGNESIUM HORIZONTAL STABILIZER BASIC STRUCTURE IN ASSEMBLY JIG (ONE SEGMENT OF RIB ON LEFT SIDE OMITTED IN PHOTO)

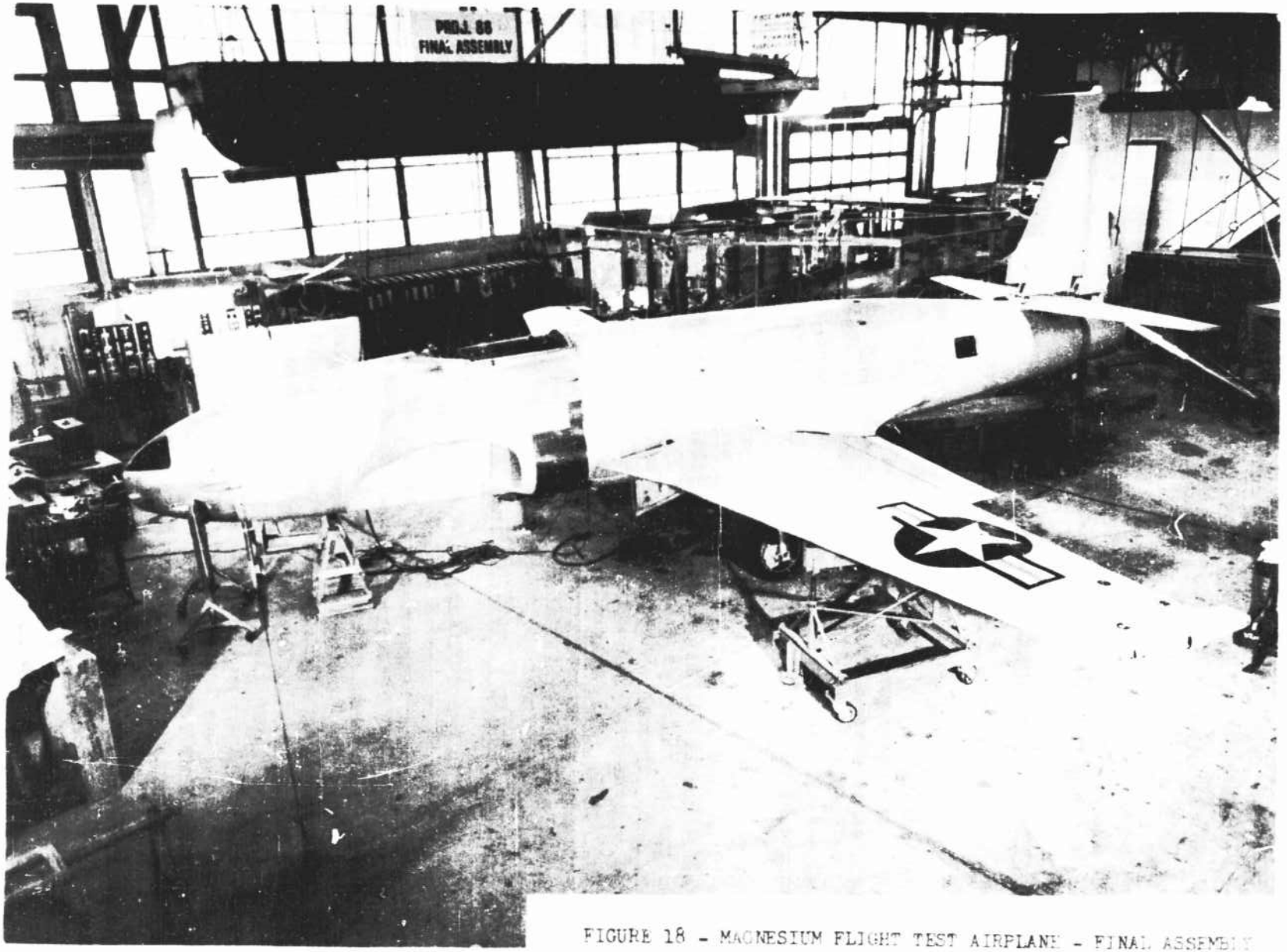

FIGURE 18 - MAGNESIUM FLIGHT TEST AIRPLANE - FINAL ASSEMBLY

The fittings tested are as follows:

FITTING	E.C.A. PART NO.
1 - Bottom Longeron Fitting - Sta. 190.5	86-334-02
2 - Upper Longeron Fitting - Sta. 163.9	86-334-06
3 - Nose Section - Lower Long. Fitting	86-324-02
4 - Upper Long. Aft Fitting - Sta. 277.5	86-344-01
5 - Aileron Push Rod - Attach. Fitting	86-14-09
6 - Elevator Hinge Fitting - Sta. 60.5	86-24-19

Bottom Longeron Fitting - Station 190.5

The bottom longeron fitting is fabricated from a 2.50 x 6.00 inch ZK60A-T5 magnesium alloy extrusion bar. This fitting is critically loaded in compression and is used to transfer the compressive load in the lower centerline longeron to the wing centerline rib casting. Because of the large cross-sectional area of the extrusion the compressive yield strength is only 22,000 psi. In view of the low yield compressive strength a test was conducted to prove the adequacy of the fitting in combination with the longeron material which in itself shows an actual compressive yield strength of 26,000 psi. (Longeron section is machined from an ECA extrusion, number 86-332-15, and is extruded from ZK60A-T5.)

The fitting in combination with the longeron prior to testing is shown in Figure 19 and the test setup is shown in Figure 20. The design ultimate load for the fitting is 70,980 pounds. The fitting was tested to failure in axial compression and failed at a load of 84,500 pounds, or 19 percent above the design ultimate load, through a combination of bending and crushing as shown in Figure 21. The compressive yield strength of the combination based on the static test is 63,200 pounds. In terms of the design ultimate fitting load of 70,980 pounds, the compressive yield load corresponds to a yield point of 89 percent of ultimate load which is substantially above the limit load (67 percent of ultimate).

Upper Longeron Fitting - Station 163.9

The upper longeron fitting at station 163.9 is fabricated from an extruded section of ZK60A-T5 magnesium alloy. This fitting is critical in tension and is used as the upper longeron splice at the aft pressure bulkhead of the pressurized cockpit. The fitting is attached to the inboard face of the upper "Zee Section" longeron. In order to check the fitting and its attachment to the upper longeron, the fitting was attached to a representative piece of "Zee Section" longeron by means of eight AN4 steel bolts. The longeron was formed from FS1-H24 magnesium alloy sheet. The test specimen is shown in Figure 22 and the test set-up is shown in Figure 23.

The fitting was loaded in tension and failed in combined tension and bending through the first row of bolts in the fitting at a load of 19,660 pounds. The failed fitting is shown in Figure 24. The design ultimate fitting load is 21,650 pounds. On the basis of the static test the tensile yield strength of the fitting combination with the representative "Zee Section" longeron is 16,550 pounds which corresponds to a yield point of 76 percent of ultimate design load. From the standpoint of the static test yield load the fitting combination has sufficient

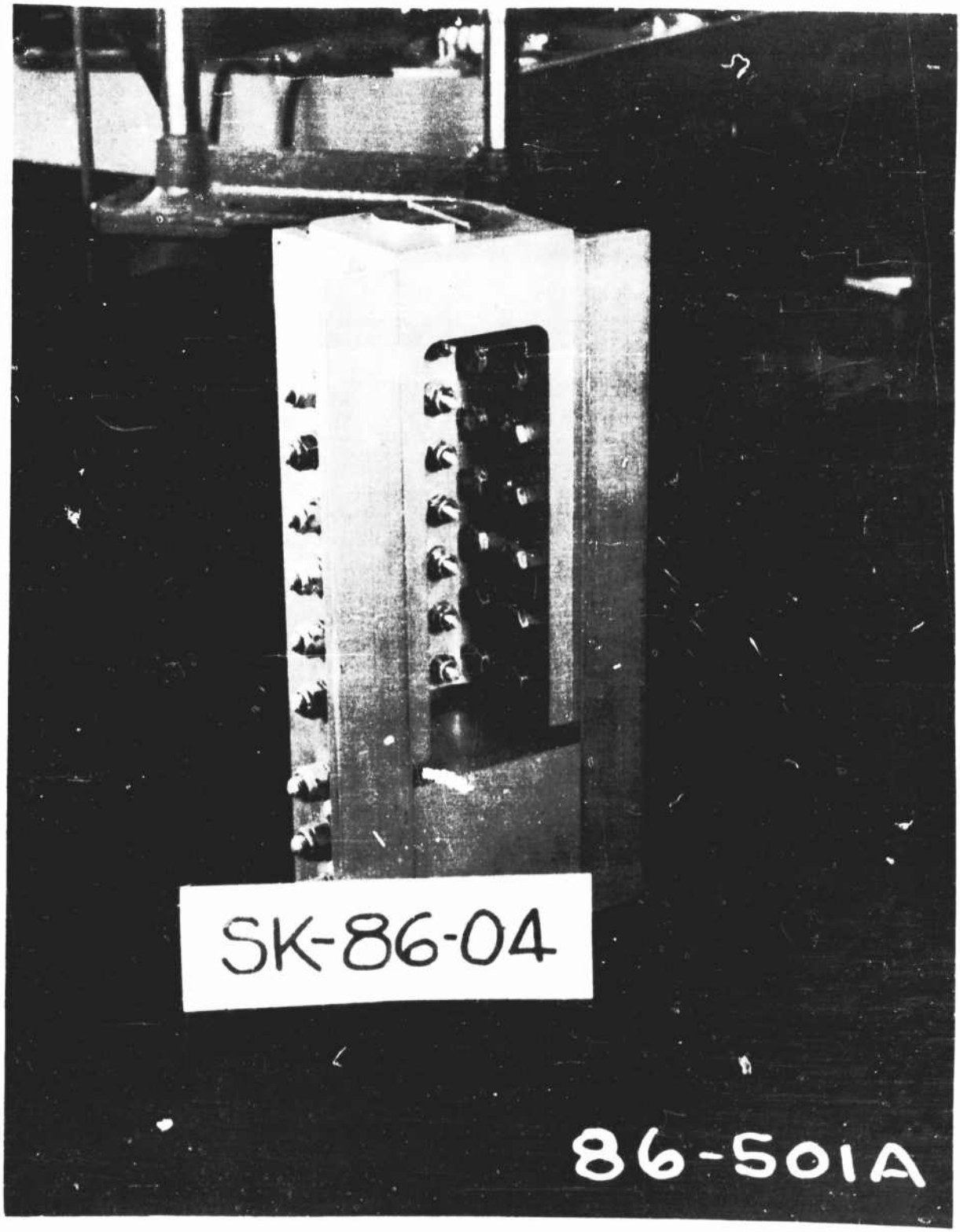

FIGURE 19 - BOTTOM LONGERON FITTING STATION 190.5 PRIOR TO TEST

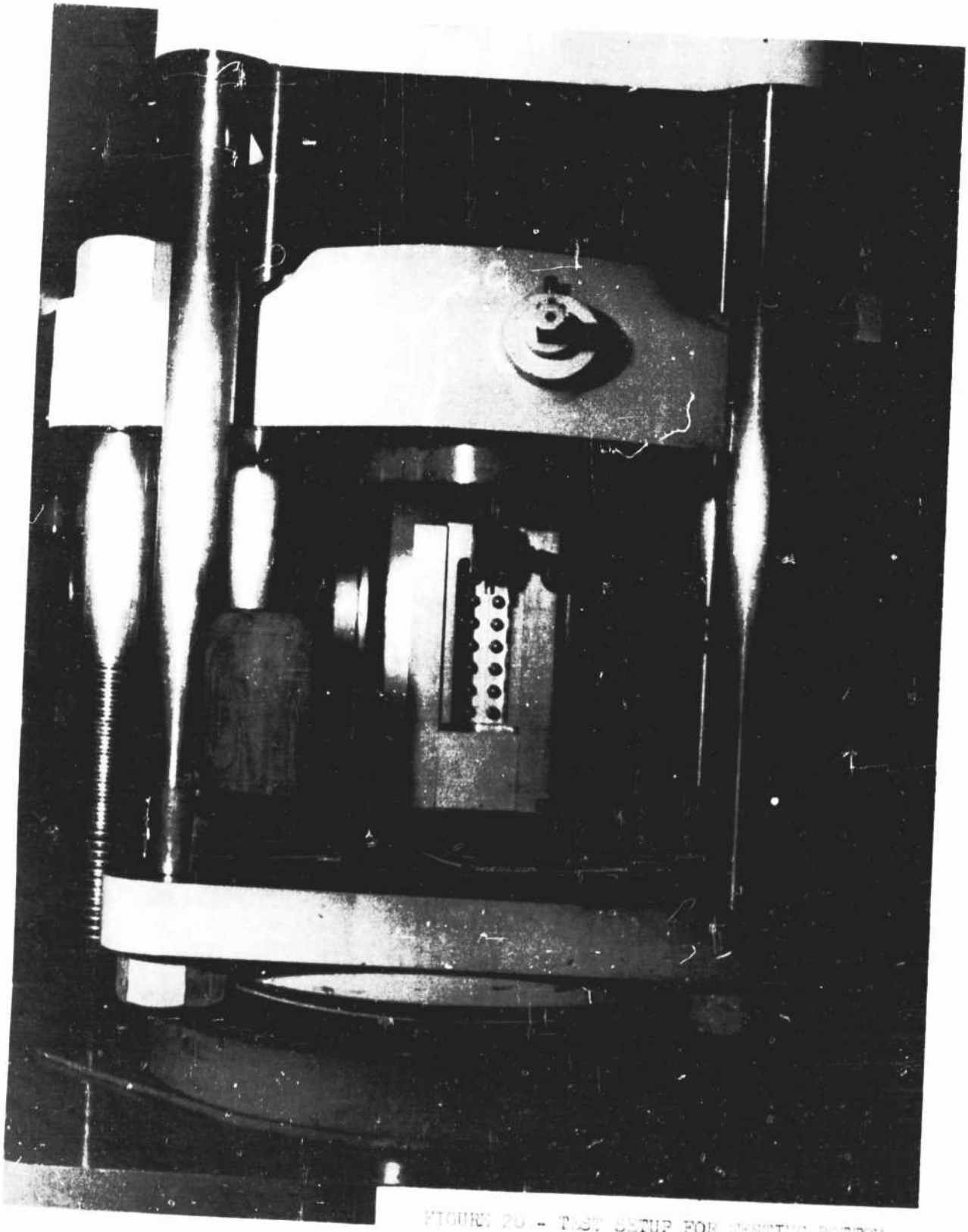

FIGURE 20 - TEST SETUP FOR TESTING BOTTOM LANDING FITTING, STATION 190.5

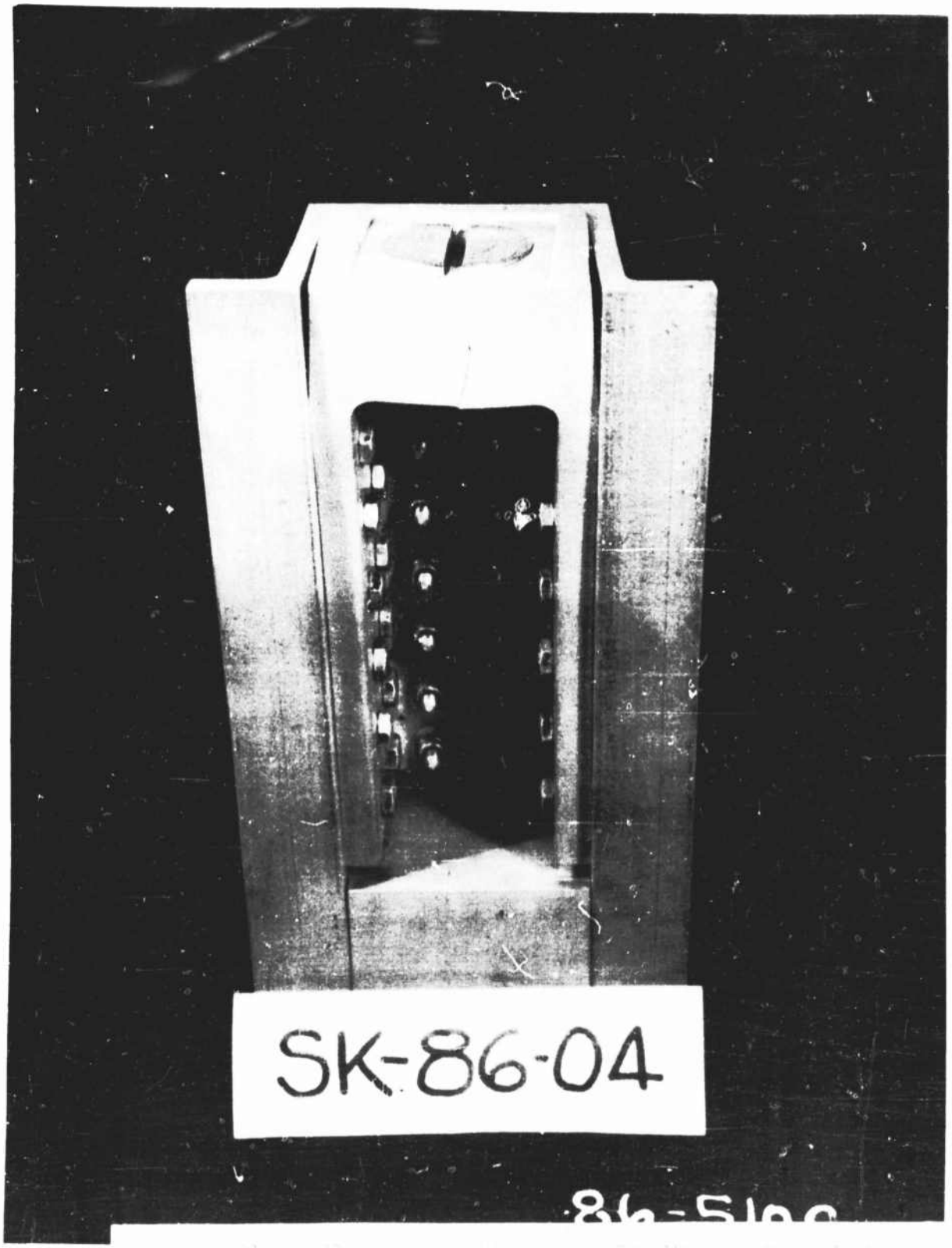
SK-86-04

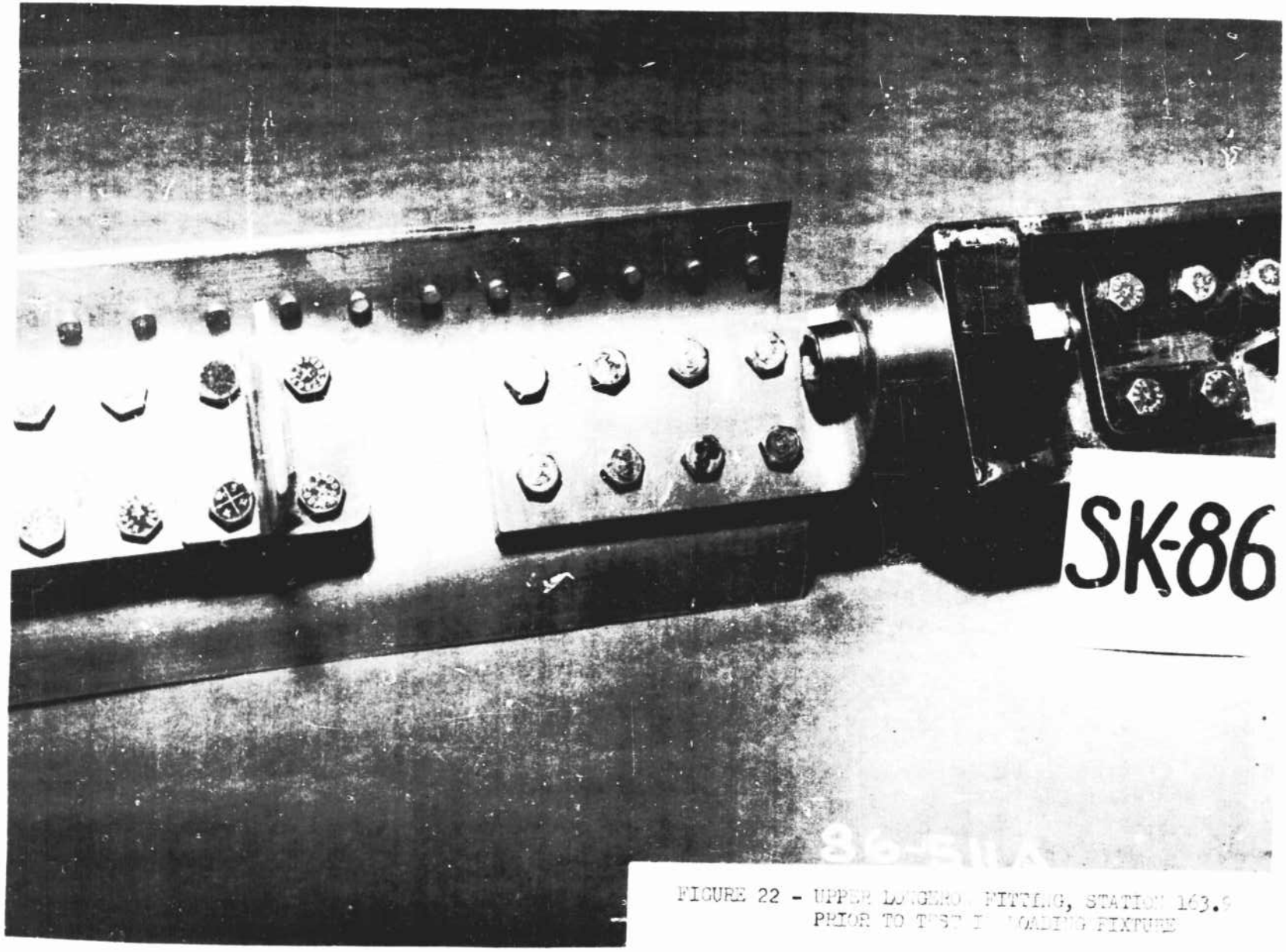

FIGURE 22 - UPPER LONGERON FITTING, STATION 163.5
PRIOR TO TEST IN LOADING FIXTURE

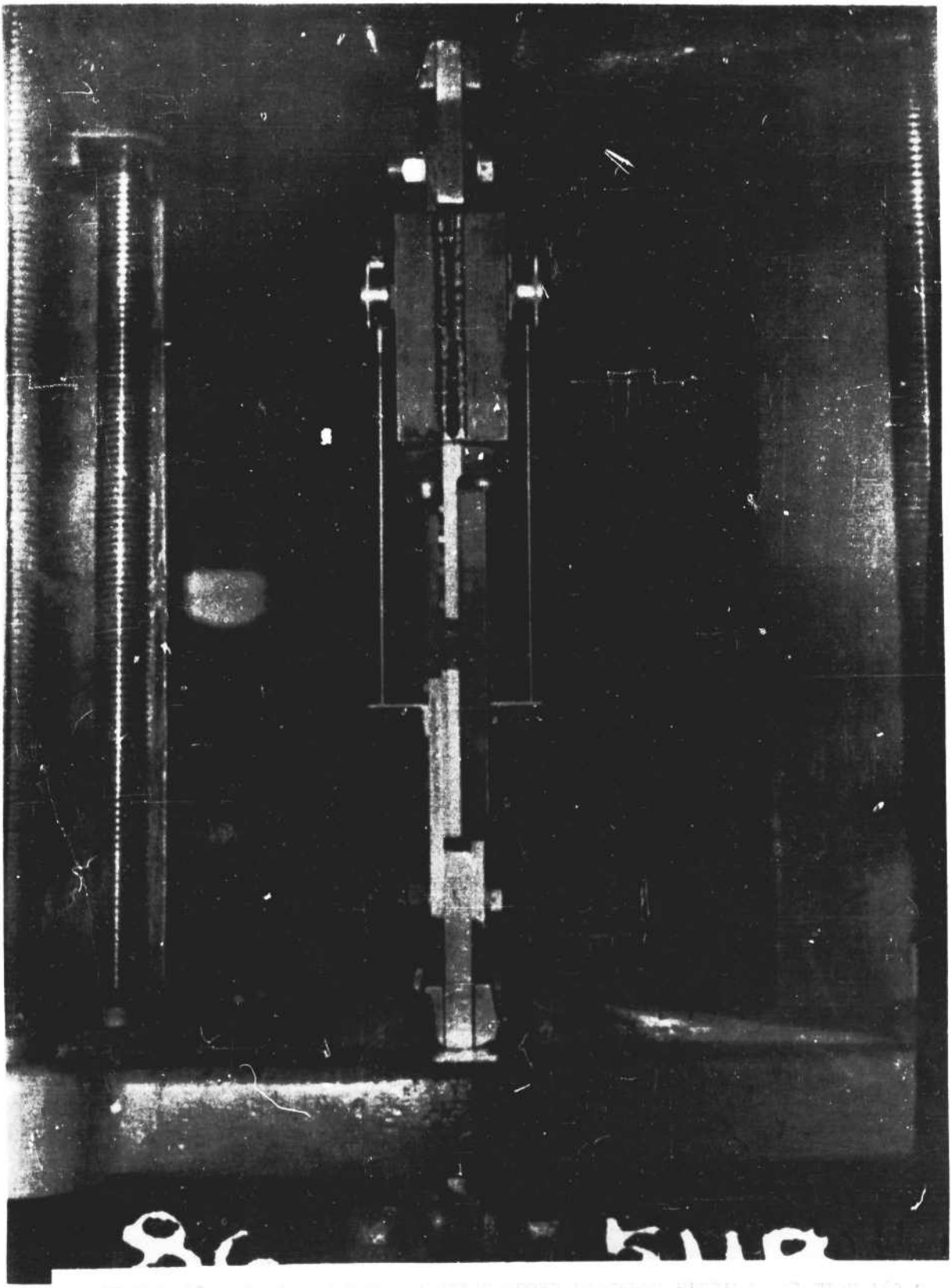

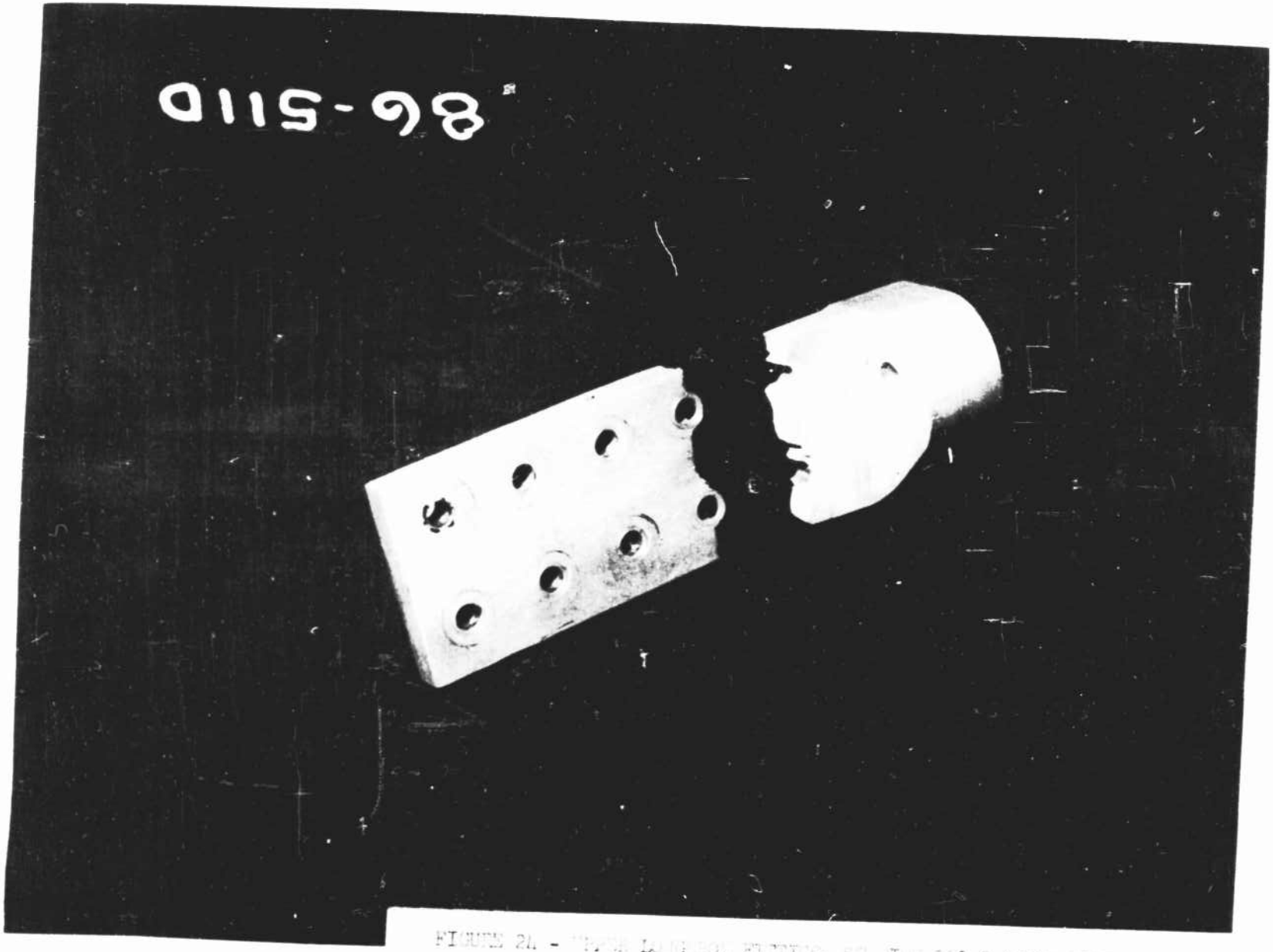

FIGURE 24 - [illegible] FITTING, S/N [illegible] AFTER FIRST [illegible]

strength; however, the ultimate failure load is only 90.8 percent of the required ultimate design load. In view of the location of the failure, the attaching bolt pattern was modified by reducing the number of AN4 bolts from eight to seven. The odd bolt was located at the point of failure. This modification increased the net area through the fitting at its critical section by 16 percent.

The modified fitting combination was tested and failed at a load of 20,650 pounds in combined tension and bending through the last row of bolts through the longeron as shown in Figure 25. The failure load of 20,650 pounds is considered as adequate for the representative structure since the longeron is designed for only 20,600 pounds at the point of failure. Actually, the ultimate design fitting load of 21,650 pounds is quite conservative since it assumes that the full longeron load at station 163.9 is carried entirely through the fitting and none through the external skin splice at this station.

Nose Section - Lower Longeron Fitting

The nose section lower longeron fitting is machined from a 2 x 2.5 inch ZK60A-T5 magnesium alloy extruded bar. Considerable doubt existed as to the adequacy of the strength of this fitting in view of the eccentric nature of the applied bolt load. In addition, the amount of space available for fitting material was severely limited due to the requirements of interchangeability with the prototype structure.

The test specimen in the loading fixture prior to test is shown in Figure 26 and after test in Figure 27.

The specimen failed through the first row of screws as shown in Figure 27 at a load of only 16,500 pounds or 55 percent of ultimate design load of 29,830 pounds.

In view of the low failure load and space limitations caused by the problem of interchangeability it was felt that a further redesign of the fitting in magnesium was not practicable. It was consequently decided to redesign the fitting using 75S-T6 aluminum alloy in place of the ZK60A-T5 material, since only a small increase in sectional area would then be required.

The fitting was not retested since an analysis showed that the calculated strength of the redesigned fitting was adequate based on the increase mechanical properties of 75S-T6 over that of ZK60A-T5 and a further increase in area of the critical section by 13 percent.

The calculated failure load for the redesign fitting is then 111 percent of the ultimate design load of 29,830 pounds.

Upper Longeron Aft Fitting - Station 277.5

The upper longeron aft fitting at station 277.5 is used to transfer the aft fuselage upper longeron loads to the mid-section longeron by means of the fuselage splice bolts at this station. This fitting is critical in tension and is fabricated from ZK60A-T5 magnesium alloy extruded bar.

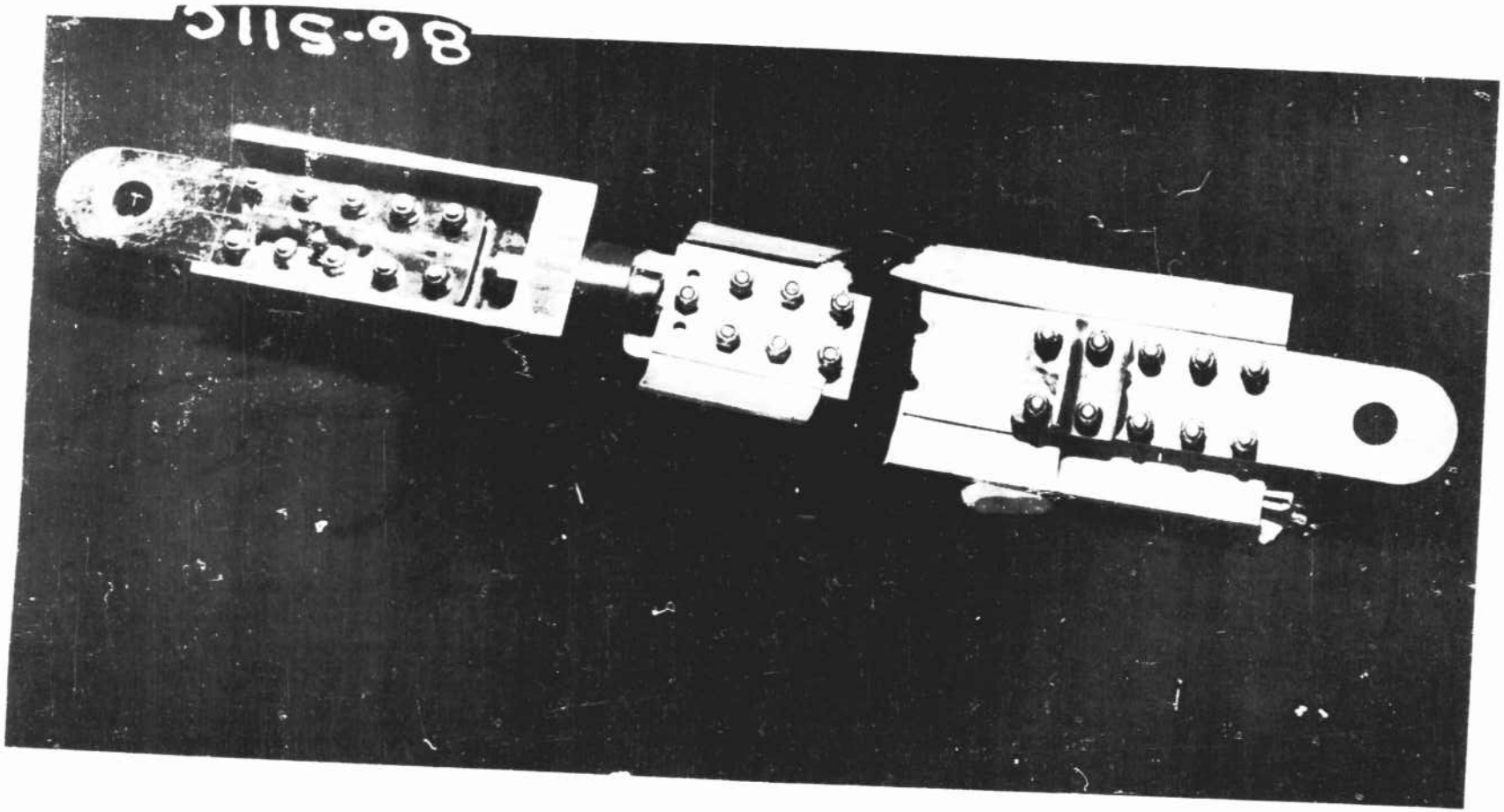

FIGURE 25 - UPPER LONGERON FITTING, STATION 163.4, AFTER FAILURE THROUGH LONGERON

FIGURE 26 - [illegible] LOWER LONGERON FITTING
PRIOR TO TEST IN LOADING FIXTURE

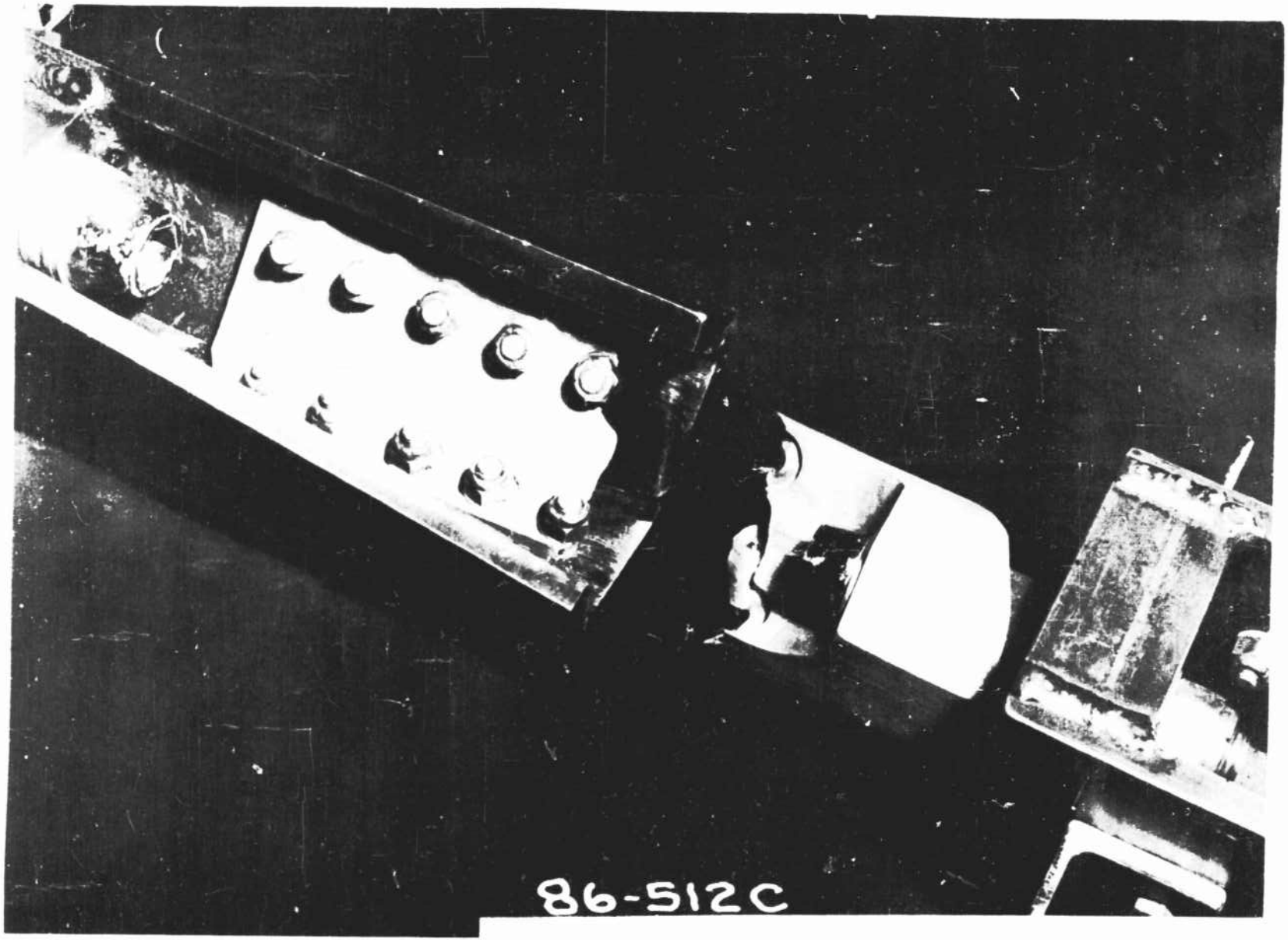

FIG. 27 - MAIN SECTION LOWER LONGERON FITTING AFTER TEST

For test purposes, the fitting was attached to a steel supporting fixture by twenty-four 3/16" diameter steel screws similar to that employed in the airplane. (See Figure 28.)

The specimen failed at a tension load of 35,170 pounds by stripping the threads on the AN365-1016 steel nut used to anchor down the main NAS150 steel bolt. The test specimen after failure is shown in Figure 29. The failure load corresponds to a load of 126 percent of the design ultimate load of 27,880 pounds. Actually, the nut to be used in the airplane will have steel threads with a higher tensile strength than the AN365 nut used in the test. Therefore, it is safe to say that the strength of this fitting will be somewhat higher than the 126 percent of ultimate shown by test.

Aileron Push Rod Attaching Fitting

The aileron push rod attaching fitting as shown in Figure 30 in its supporting steel fixture is machined from ZK60A-T5 magnesium alloy extruded bar. This fitting is critical in tension.

The test fitting was static tested and failed by shear tear-out of the fitting lugs, as shown in Figure 31, at a load of 12,080 pounds. This failure corresponds to a load of 139 percent of the design ultimate load of 8660 pounds.

Elevator Hinge Fittings - Station 60.5

The elevator hinge fitting at station 60.5 is machined from a magnesium alloy casting that conforms to specification QQ-M-56, Composition AZ63-HTA. The fitting in the test fixture after failure is shown in Figure 32. The test specimen failed under load at 4000 pounds by shearing the 1/4" diameter steel hinge pin (125,000 psi H.T.). The casting itself did not fail. The above failure load corresponds to a load of 430 percent of the design ultimate load of 929 pounds.

STATIC TEST PROGRAM

The static test program of the F-80C magnesium airplane was conducted at Headquarters, WADC, Wright-Patterson Air Force Base, Ohio, during the period from 7 October 1953 to 7 January 1954. The structural test article consisted of the complete fuselage structure, horizontal and vertical tail surfaces, one flap. and one aileron constructed of magnesium alloy.

The complete structural test program conducted on the fuselage and empennage consisted of the following loading conditions which were tested for on the following dates:

Condition	Percent Ult. Ld. Supported	Date of Test
1 - Cockpit Pressurization to 9.0 psi	100	7 October '53
2 - Nose Gear and Support Structure		
(a) Static Thrust Condition	100	12 October '53
(b) Condition #1	100	14 October '53
(c) Side Drift Landing	100	14 October '53

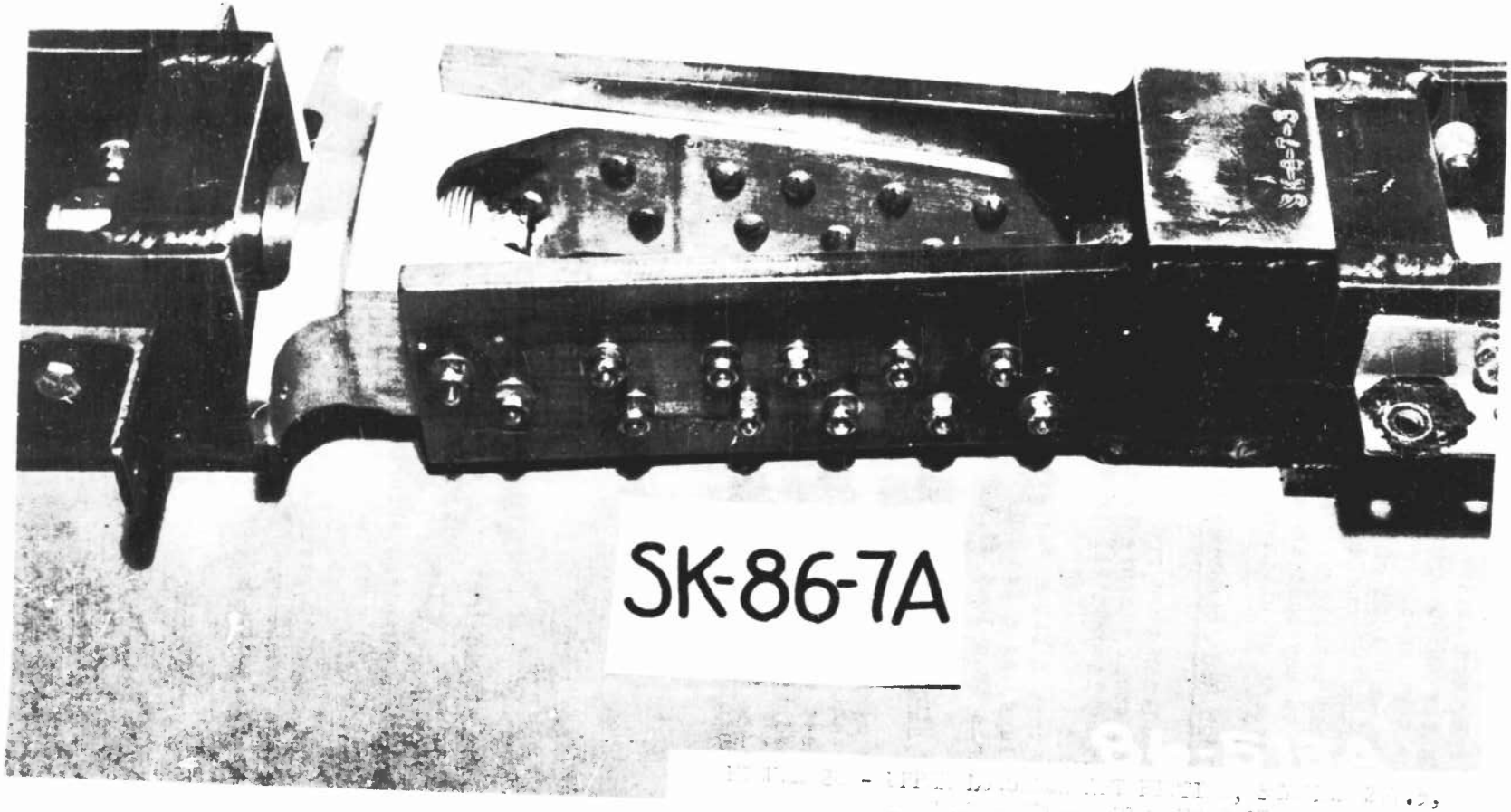
SK-86-7A

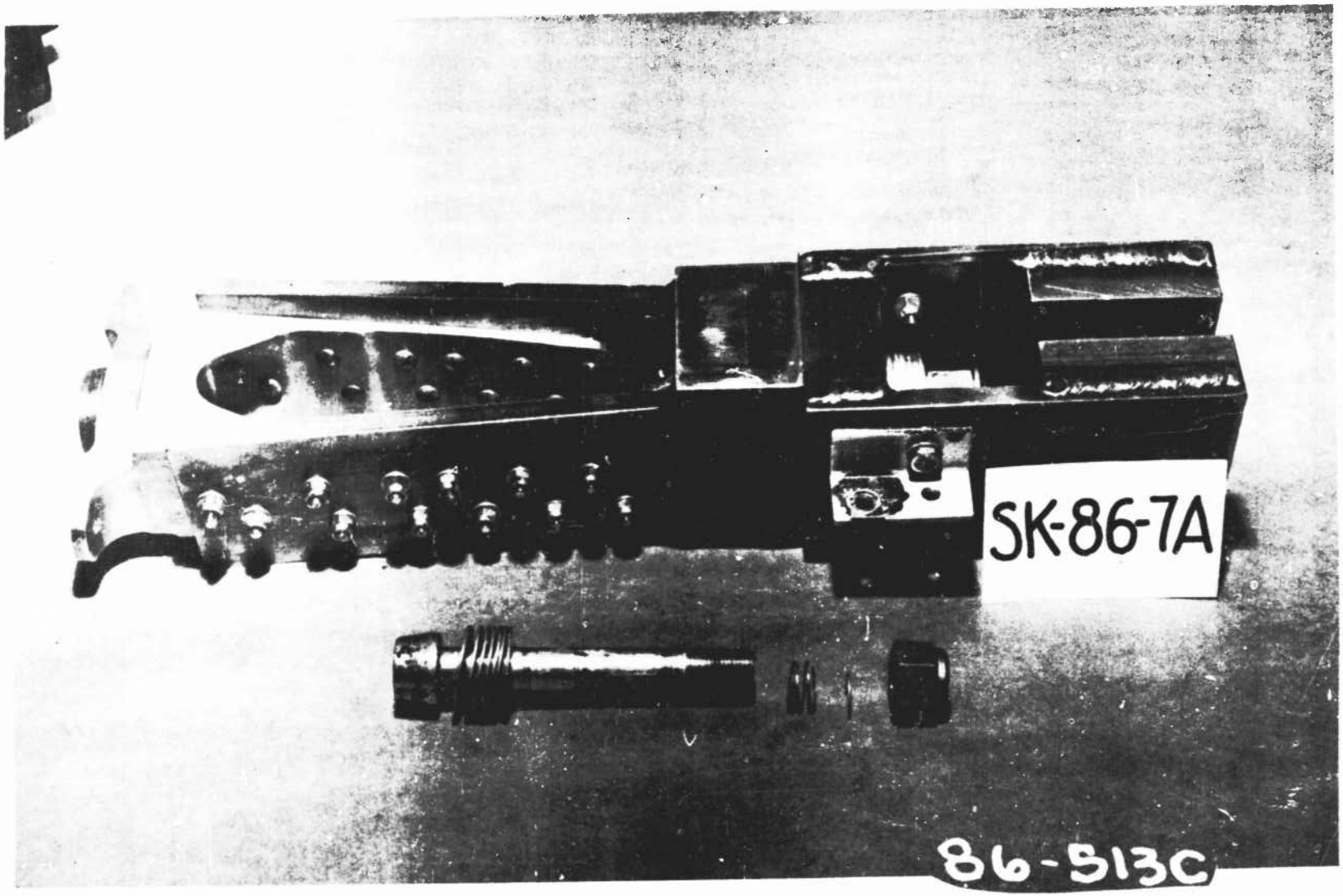

FIGURE 29 - UPPER LONGERON AFT FITTING, STATION 277.5,
AFTER TEST - (NOTE SHEAR FAILURE OF BOLT THREADS)

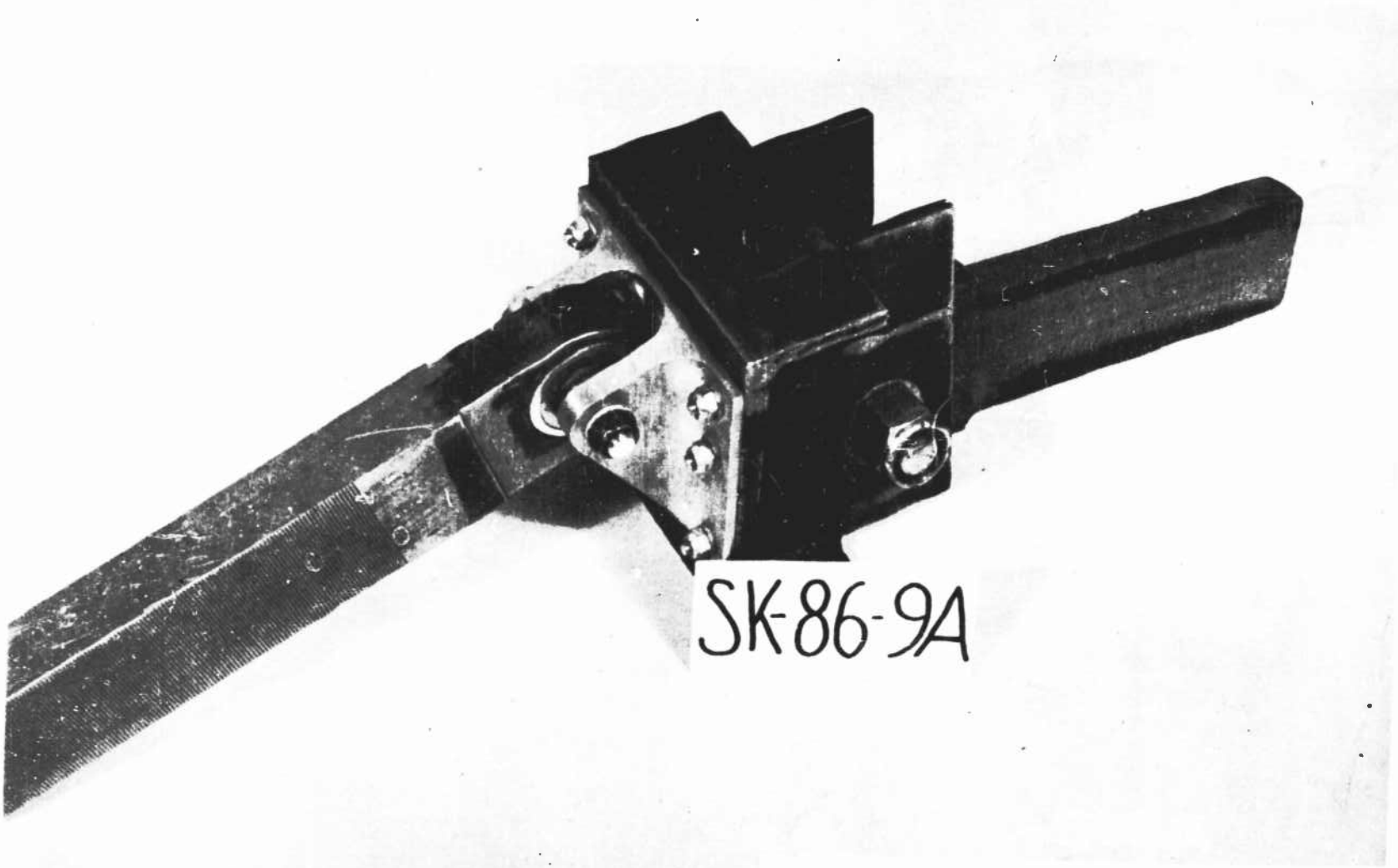

FIGURE 30 - AILERON PUSH ROD ATTACHMENT FITTING PRIOR TO TEST IN LOADING FIXTURE

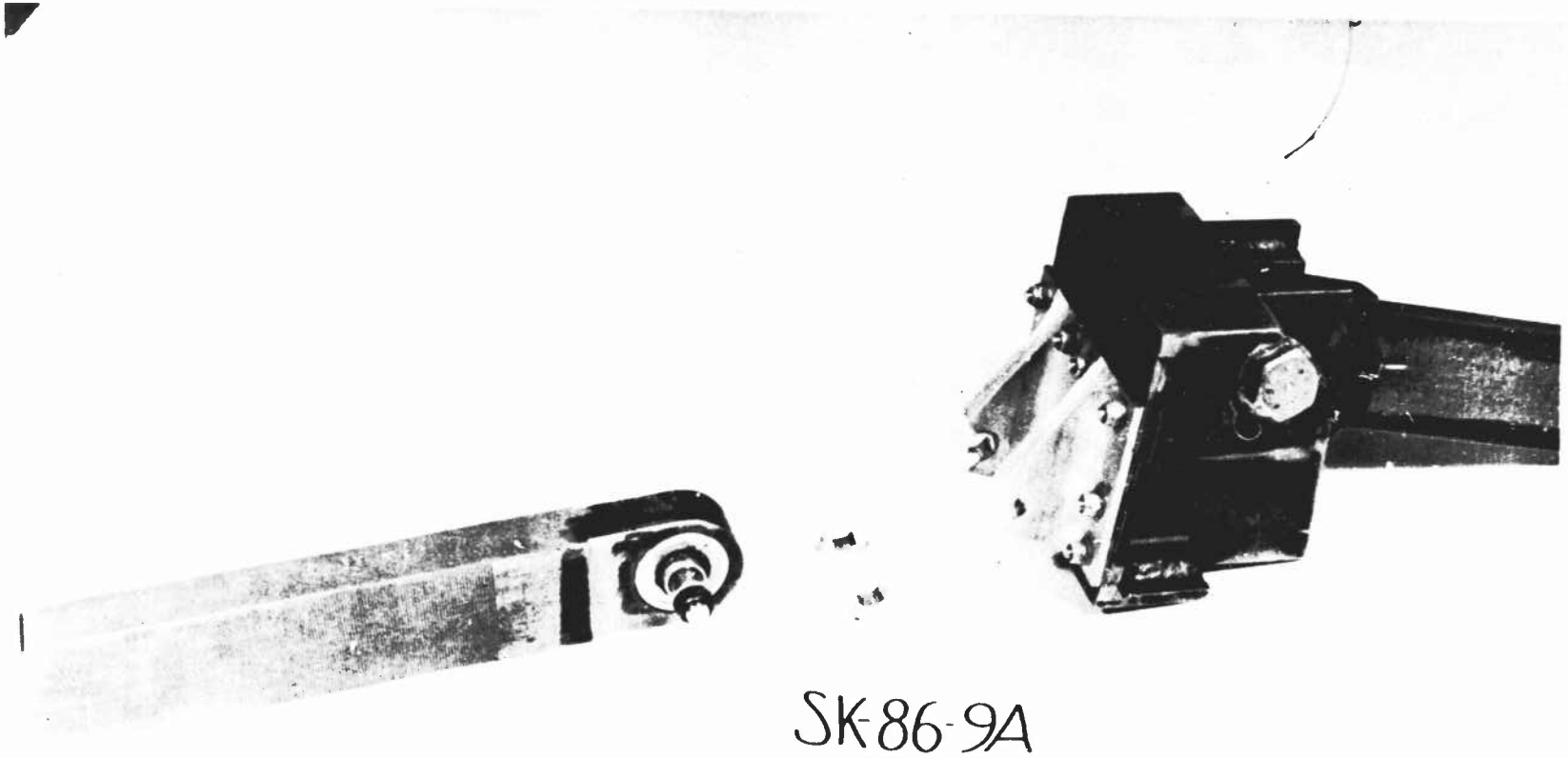

SK-86-9A

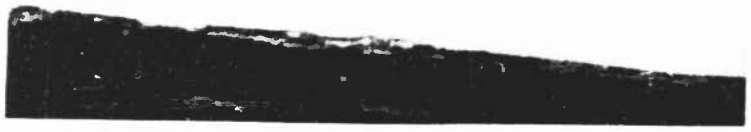

FIGURE 31 - AILERON FIXED ATTACHMENT FITTING AFTER
TEST SHOWING FAILURE OF LUGS

FIGURE 32 - ELEVATOR HINGE FITTING, STATION 0.5,

Condition	Percent Ult. Ld. Supported	Date of Test
3 - Fuselage Condition A-XI	100	16 October '53
4 - Seat Loads		
(a) Seat Dow Load	100	21 October '53
(b) Seat Catapult Load	100	21 October '53
(c) Seat Belt and Shoulder Harness	100	21 October '53
5 - Elevator Control System	100	26 October '53
6 - Condition A-IX	100	27 October '53
7 - Gust Condition	100	28 October '53
8 - Condition A-V	100	29 October '53
9 - Dynamic Symmetrical Condition A	100	29 October '53
10 - Dynamic Symmetrical Condition B	100	29 October '53
11 - Vertical Tail Balance Condition	100	3 November '53
12 - Dive Brake	100	17 November '53
13 - Rolling Pull-Out Condition	100	24 November '53
14 - Combined Dynamic Unsymmetrical Cond. A	100	24 November '53
15 - Combined Dynamic Unsymmetrical Cond. B	100	24 November '53
16 - Combination B	100	25 November '53
17 - Fuselage Condition IV	100	30 November '53
18 - Rolling Pull-Out Condition	100	2 December '53
19 - Aft Fuselage Up Bending Condition	100	2 December '53
20 - Dynamic Symmetrical Condition B	100	2 December '53
21 - Dynamic Symmetrical Condition A	120	2 December '53
22 - Aileron	100	18 December '53
23 - Flap	100	7 January '54

For all tests the empennage was assembled on the complete fuselage which in turn was mounted on a set of F-80 wings. Support for all tests was provided at Wing Station 63 by means of wood and steel formers clamped to the wing structure at that location. A typical setup is shown in Figure 36.

Test loads were applied to the horizontal and vertical tail surfaces by means of hydraulic struts acting through tension patches bonded to the surfaces. Fuselage loads were hydraulically applied through sheet metal straps riveted or bonded to the fuselage structure, engine mount support structure, nose gear supports and machine gun mounts. In each test the loads were carried through the fuselage and reacted at the wing. The correct shear, moment and torsion was maintained through the fuselage where critical. The wing fairing and engine access doors were not installed.

The nose gear and supporting structure was static tested for the following conditions and satisfactorily supported 100 percent ultimate load.

A - Static Thrust Condition

Ultimate Vertical Nose Gear Load = 4130#
Ultimate Aft Nose Gear Load = 6000#
Loads applied at axle centerline with the oleo in static position.
(No relieving loads applied)

B - Condition I

Ultimate Vertical Nose Gear Load = 15,880#
Ultimate Aft Nose Gear Load = 5,240#
Loads applied at axle centerline with the oleo fully extended.
Fuselage Ultimate Inertia Load Factor = 7.136.

C - Side Drift Landing

Ultimate Nose Gear Side Load = 4,350#
Load applied at ground line with the oleo fully extended.
(No relieving loads applied.)

The setup for Condition I is shown in Figure 33.

At the completion of the nose gear test, Fuselage Symmetrical Loading, Condition A-XI, was conducted. This condition corresponds to the Negative High Angle of Attack for a gross weight of 12,200 pounds and an Ultimate Load Factor of 4.50. The test was conducted on the 16th of October 1953 and satisfactorily supported 100 percent ultimate load.

The seat employed in the magnesium F-80C airplane is similar to that of the standard F-80C aluminum airplane. However, in order to check the structural integrity of the supporting structure, the seat installation was tested for the same loads as the prototype airplane. These conditions were as follows:

A - Seat Down Load: 4,000 pounds down on seat bottom.

B - Seat Catapult Load: 6,600 pounds down on seat bottom parallel to rails.

C - Seat Belt and Shoulder Harness: Belt load of 2,880 pounds at 40 degrees to seat bottom plus shoulder harness load of 2.080 pounds.

The seat supporting structure supported the various loads noted and was found to be satisfactory.

The elevator control system was static tested for a control stick force of 450 pounds prior to testing the horizontal tail and fuselage for the critical elevator torque conditions. The control system and supporting structure satisfactorily supported 100 percent ultimate load.

The loading condition of the various tests other than those previously mentioned are as follows:

Horizontal Tail Tests

A - Condition A-IX

Ultimate Stabilizer Load = 16,460# Down
Ultimate Elevator Load = 3,990# Up
Ultimate Trim Tab Load = 170# Down
Ultimate Spring Tab Load = 260# Down

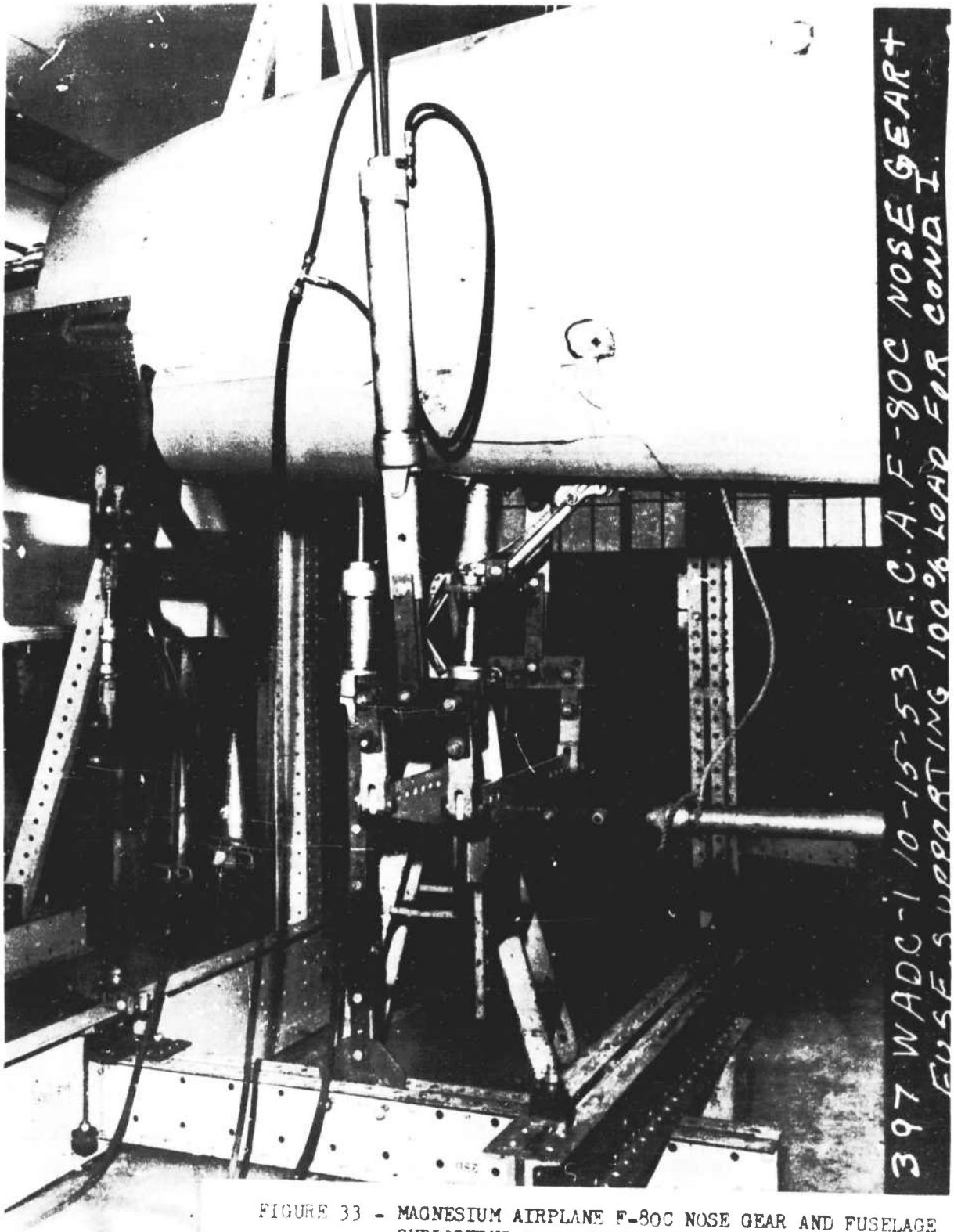

FIGURE 33 - MAGNESIUM AIRPLANE F-80C NOSE GEAR AND FUSELAGE SUPPORTING 100 PERCENT LOAD FOR CONDITION I

B - Condition A-V

Ultimate Stabilizer Load = 13,605# Up
Ultimate Elevator Load = 4,490# Down
Ultimate Trim Tab Load = 170# Up
Ultimate Spring Tab Load = 430# Up

The above loads are total for both sides.
Ultimate Fuselage Inertia Load Factor = 11.0 Down

C - Dynamic Symmetrical Loading Condition A and B

Condition A - Ultimate Horizontal Tail Load = 22,500# Up
- Centroid of Load = 28.5% Total Chord
- Ultimate Fuselage Inertia Load Factor = 28.8 Down

Condition B - Ultimate Horizontal Tail Load = 22,500# Up
- Centroid of Load = 41.4% Total Chord
- Ultimate Fuselage Inertia Load Factor = 28.8 Down

Fuselage Symmetrical Loading Conditions

A - Gust Condition

Ultimate Horizontal Tail Load = 12,795# Down
Centroid of Tail Load = 33.3% Total Chord
Ultimate Load Factor = 0

B - Condition IV

Positive Low Angle of Attack Gross Weight = 9,600#
Ultimate Load Factor = 12

C - Fuselage Up Bending Condition

Ultimate Horizontal Tail Load = 10,700# Up
Centroid of Tail Load = 44.12% Total Chord

The fuselage was relieved at Fuselage Station 277.5.

Vertical Tail Balancing Condition

Ultimate Fin Load = 5,900#
Centroid of Fin Load = 29.5% Total Chord
Ultimate Rudder Load = -975#
Centroid of Rudder Load = 83.3% Total Chord

No fuselage relief applied.

Rolling Pull-Out Condition

Ultimate Fin Load = 6,105#
Centroid of Fin Load = 27% Total Chord
Right Stabilizer Load = 3,500#

Left Stabilizer Load = 2,100# Up
Centroid of Stabilizer Load = 49% Total Chord

Torsion from the unbalanced horizontal tail load adds to torsion from vertical tail.

Fuselage relieving loads at Station 277.5: - Vertical = 13,300#
- Side = 1,914#

Note: During the above test, the additional torsion caused by an increase in vertical tail load to 6,410# was applied to the fuselage by applying vertical couple loads to the horizontal tail.

Combined Dynamic Unsymmetrical Tail Loads

A - Condition A

Ultimate Vertical Tail Load = 4,000#
Centroid of Vertical Tail Load = 28.5% Chord
Ultimate Load Left Stabilizer = 6,710# Up
Ultimate Load Right Stabilizer = 11,250# Up
Centroid of Horizontal Tail Load = 28.5% Chord
Ultimate Fuselage Load Factor = 23 Down

B - Condition B

Ultimate Vertical Tail Load = 4,000#
Centroid of Vertical Tail Load = 28.5% Chord
Ultimate Load Left Stabilizer = 6,710# Up
Ultimate Load Right Stabilizer = 11,250# Up
Centroid of Horizontal Tail Load = 33.3% Chord
Ultimate Fuselage Load Factor = 23 Down

C - Combination B

Ultimate Vertical Tail Load = 4,521#
Centroid of Vertical Tail Load = 28.1% Chord
Ultimate Load Left Stabilizer = 5,813# Down
Ultimate Load Right Stabilizer = 4,354# Down
Ultimate Fuselage Load Factor = 2.625 Down

Aileron Load = 3,228# Ultimate
Load C.P. = .44 $C_{aileron}$
Tab Load = -61# Ultimate

Flap Deflection = 40°
Total Ultimate Flap Load = 2,753#
Load C.P. = .45 C_f aft of

In conducting the combined Dynamic Unsymmetrical Tail Load Condition B, the center of pressure used was 33.3 percent of the horizontal tail chord instead of 41.4 percent as used for the symmetrical condition. This revised center of pressure location was used to obtain a more realistic loading condition.

It should be noted that in the Rolling Pull-Out Condition the vertical tail was tested for an ultimate load of 6,105 pounds even though the Lockheed F-80C airplane was tested for a vertical tail load of 6,410 pounds. When the criterion for the magnesium F-80C airplane was set up, the vertical tail load was set at 6,105 pounds. However, an ammendment to the original criterion was made increasing the load to 6,410 pounds but only after the fin had been fabricated. Since it was not feasible to reinforce the existing fin, a deviation was granted allowing the Contractor to use the 6,105 pounds load. The fuselage was designed for the effects of the 6,410 pounds vertical tail load. Therefore, in conducting the first series of Rolling Pull-Out Condition tests the fin load was limited to 6,105 pounds but the torsion from the larger load was introduced into the fuselage by means of a couple applied to the horizontal tail.

The Rolling Pull-Out Condition was re-run at the completion of the test program for a vertical tail load of 6,410 pounds in order to eliminate the deviation. The correct loading was carried through the aft fuselage up to station 277.5

The first test for the Rolling Pull-Out Condition was conducted on 4 November 1953. This test was discontinued at 70 percent ultimate load due to the formation of sharp buckles in the fuselage side skin between station 263-252 and 238-228 at Water Line 106. Slight skin buckling was also evident below Water Line 100. The skin buckling occurred in the region forward of the engine mounts where the structure is semi monocoque, containing only frames and skin.

The fuselage was reinforced by adding intercostal angles between stations 228.3-238, 238-245.5, 245.5-252, and 252-263 at Water Line 106.59. These angles were clipped to the frames. The intercostal angles were made from an equal-leg magnesium extrusion of ZK60-T5 alloy, one inch by .125 thick.

The second test for the Rolling Pull-Out Condition was conducted on the 19th of November 1953 and was discontinued at 60 percent ultimate load due to the formation of deep skin buckles in the side skin at the same fuselage stations as noted in the previous test but below Water Line 100.

To reinforce the fuselage in the region of the deep buckles, the same reinforcements as used for Water Line 106.59 in the previous test were added at approximately Water Line 97.59. The reinforced fuselage between fuselage stations 228-263 is shown in Figure 34.

The reinforced fuselage was then tested for the Rolling Pull-Out Condition and satisfactorily supported 100 percent ultimate load. At 90 percent ultimate load, the trailing edge skin of the fin at Water Line 140 had a considerable bow. In addition, the fin skin between beams at approximately Water Line 140 had a compression buckle. In reference to the aft fuselage section, skin buckles appeared at 80 percent of ultimate load. These skin buckles were slight and appeared on the upper left side of the fuselage aft of station 277.5. (Note: Fin load applied to the left for this condition.)

The aft section of the fuselage and the empennage in the Rolling Pull-Out Condition at 100 percent ultimate load is shown in Figure 35.

FIGURE 34 - REINFORCEMENT OF FUSELAGE STATION 227.8 - 263; MAGNESIUM AIRPLANE F-80C

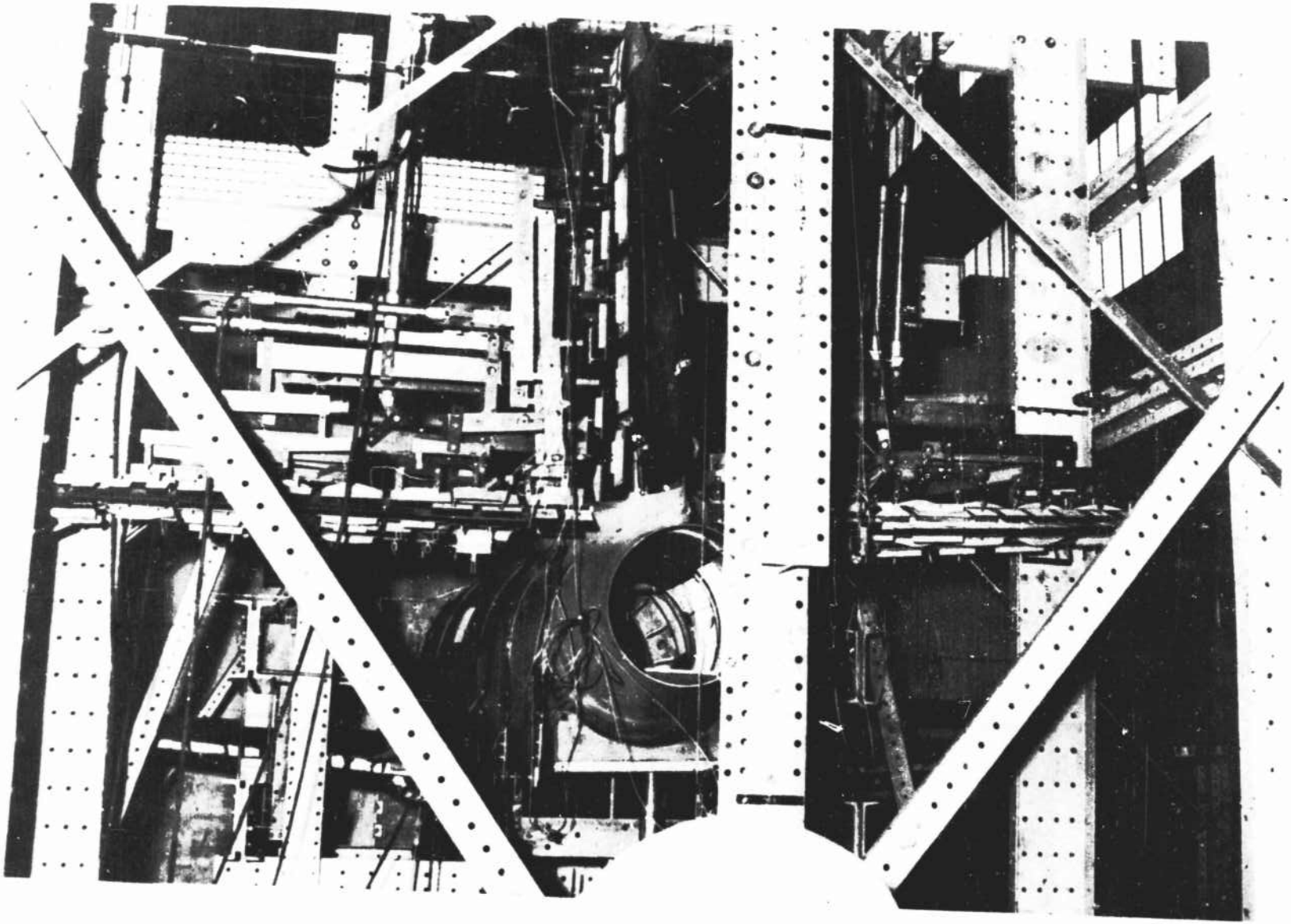

FIGURE 35 - F-80C MAGNESIUM AIRPLANE SUPPORTING 100 PERCENT ULTIMATE LOAD FOR THE ROLLING PULL-OUT CONDITION

The fuselage test for Condition IV was conducted in three steps up to 60 percent ultimate load. Step one, fuselage was loaded to 60 percent with the 12 "G" down load. Step two, test was repeated with the 12 "G" load plus dive brake load and engine thrust up to 60 percent load. Step three, test was repeated with the same load as step two with the addition of cabin pressurization. Step three loads were carried to ultimate. The test setup is shown in Figure 36 for the 80 percent loading condition.

At 70 percent ultimate load for Condition IV, shear buckles became evident in the fuselage side skin between stations 277.5 and 227.8. At 90 percent ultimate load, the fuselage side skin between stations 238 and 263 buckled severely. These buckles are shown in Figure 37. A lower view of that area showing the buckled edge of the skin in the flap motor area cutout is shown in Figure 38.

These buckles between stations 238 and 263 became sharper as more load was applied and between 95 and 100 percent ultimate load the fuselage stringer located 21.75 degrees below Water Line 100 measured from the axis of symmetry of the airplane failed at station 245. (The failed stringer is shown in Figure 39.) The failure appeared to be caused by the instability of the stringer across the top of the flap motor outout between stations 245 and 255. The fuselage momentarily supported 100 percent ultimate load. The failure is shown in Figures 39 and 40.

At ultimate load for Condition IV, the maximum internal pressure applied to the fuselage was 6.45 psi or 95.5 percent of the ultimate pressure of 6.75 psi. However, due to the failure of the fuselage no further pressurization was attempted.

In order to provide additional strength in the flight test F-80C magnesium fuselage it was decided to redesign the failed stringer to achieve at least two times the section modulus of the original section between stations 238 and 263.

The original stringer was a .75 x 1.00 x .063 bulb angle extrusion of ZK60A-T5 magnesium alloy. The section modulus of the bulb angle extrusion was .0277 in^3. The stringer was revised into a channel section of 1.00 inch high having a leg of .75 inches against the skin and an outstanding leg of .50 inches. The thickness of this channel was constant and equal to .125 inches. The section modulus was .0600 in^3 which is 2.16 times that of the original section.

Since the fuselage momentarily supported 100 percent ultimate load no additional tests for Condition IV were necessary.

During the test for Condition IV the dive flap and supporting structure, as previously noted, were tested for an ultimate load of 5,410 pounds per flap at a flap opening of 35 degrees. The dive flap and supporting structure satisfactorily supported 100 percent ultimate load.

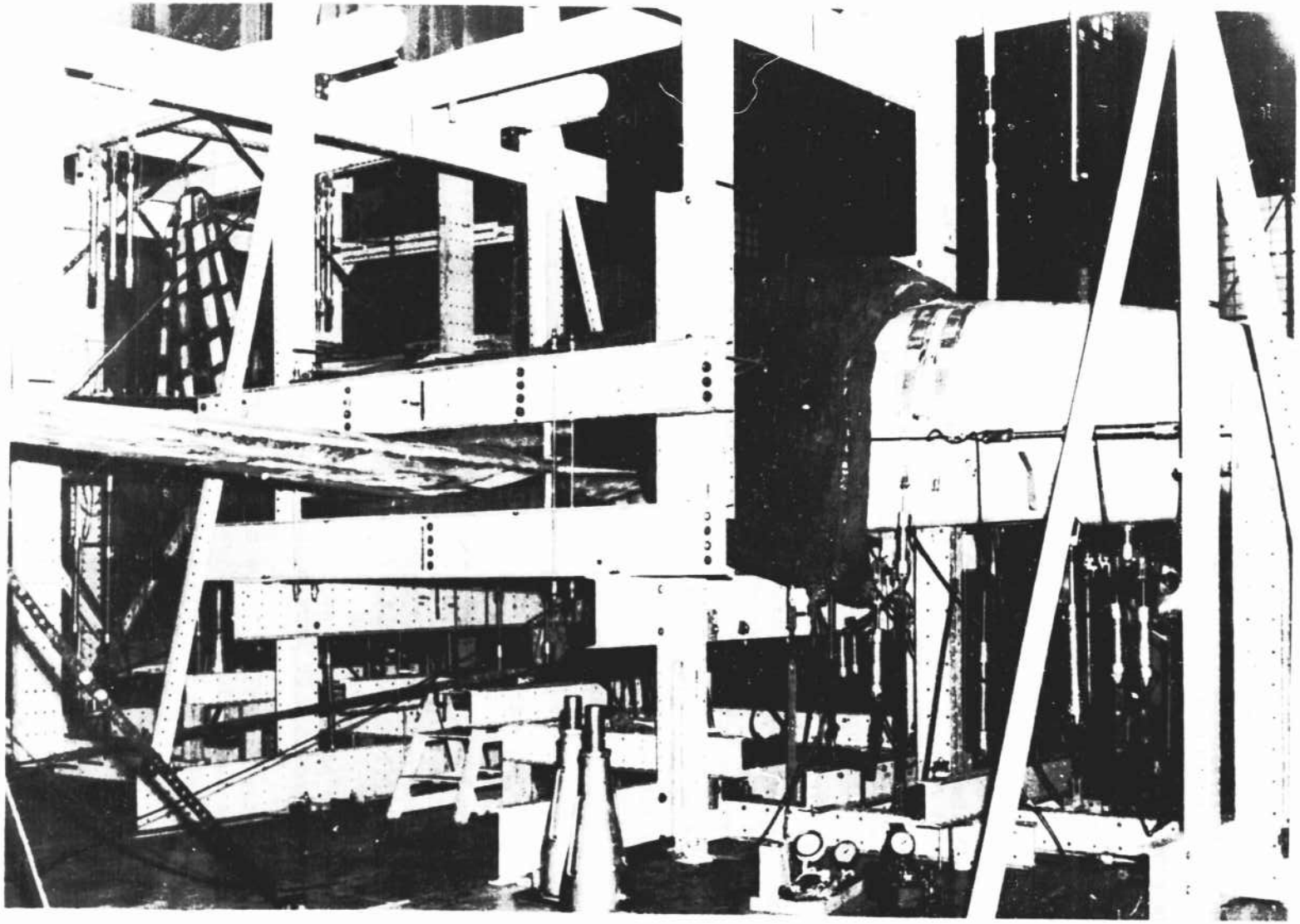

FIGURE 36 - F-80C MAGNESIUM FUSELAGE SUPPORTING 80 PERCENT ULTIMATE LOAD FOR CONDITION IV

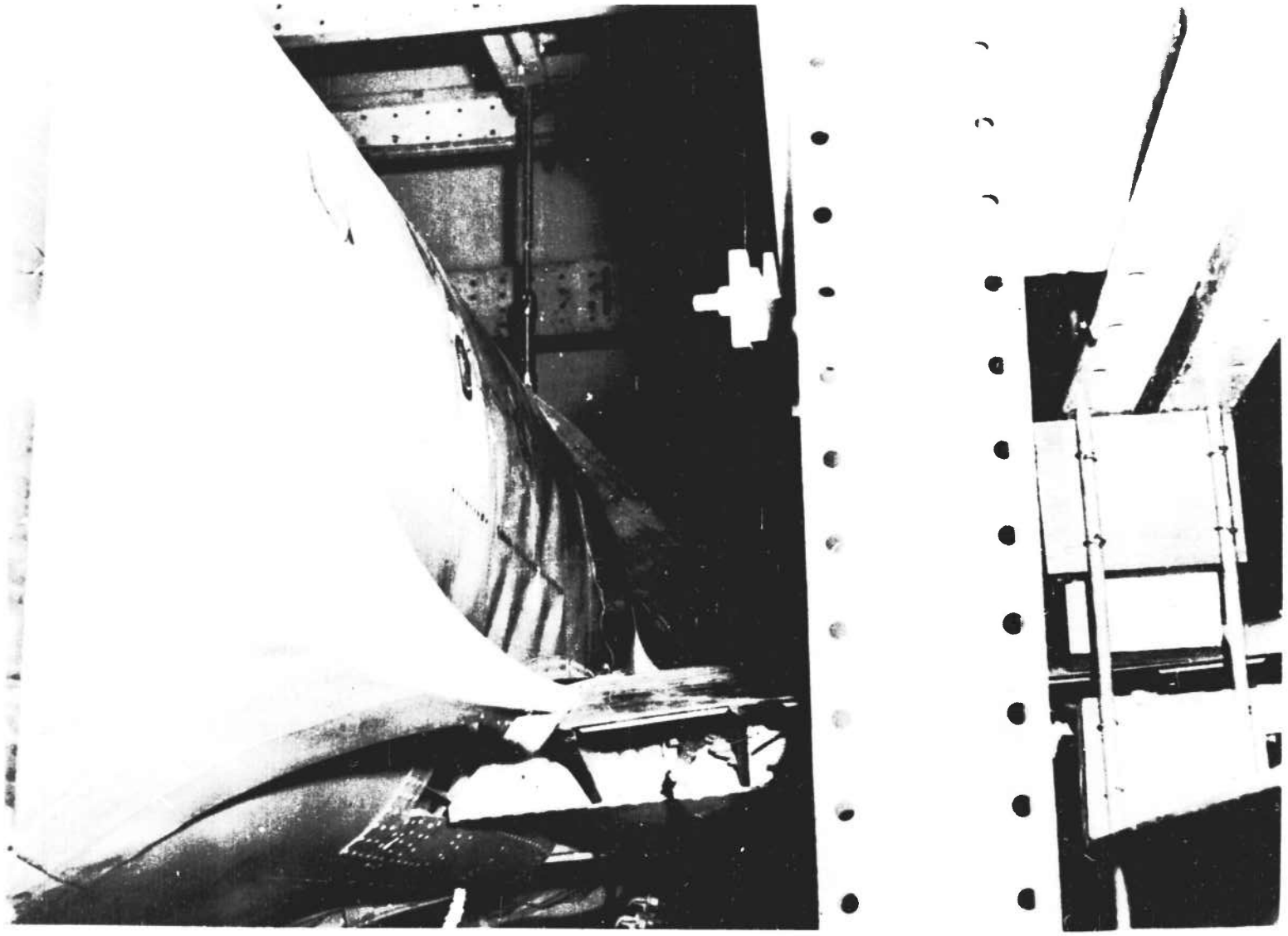

FIGURE 37 - MAGNESIUM FUSELAGE - SIDE SKIN BUCKLES AT 90 PERCENT ULTIMATE LOAD FOR CONDITION IV

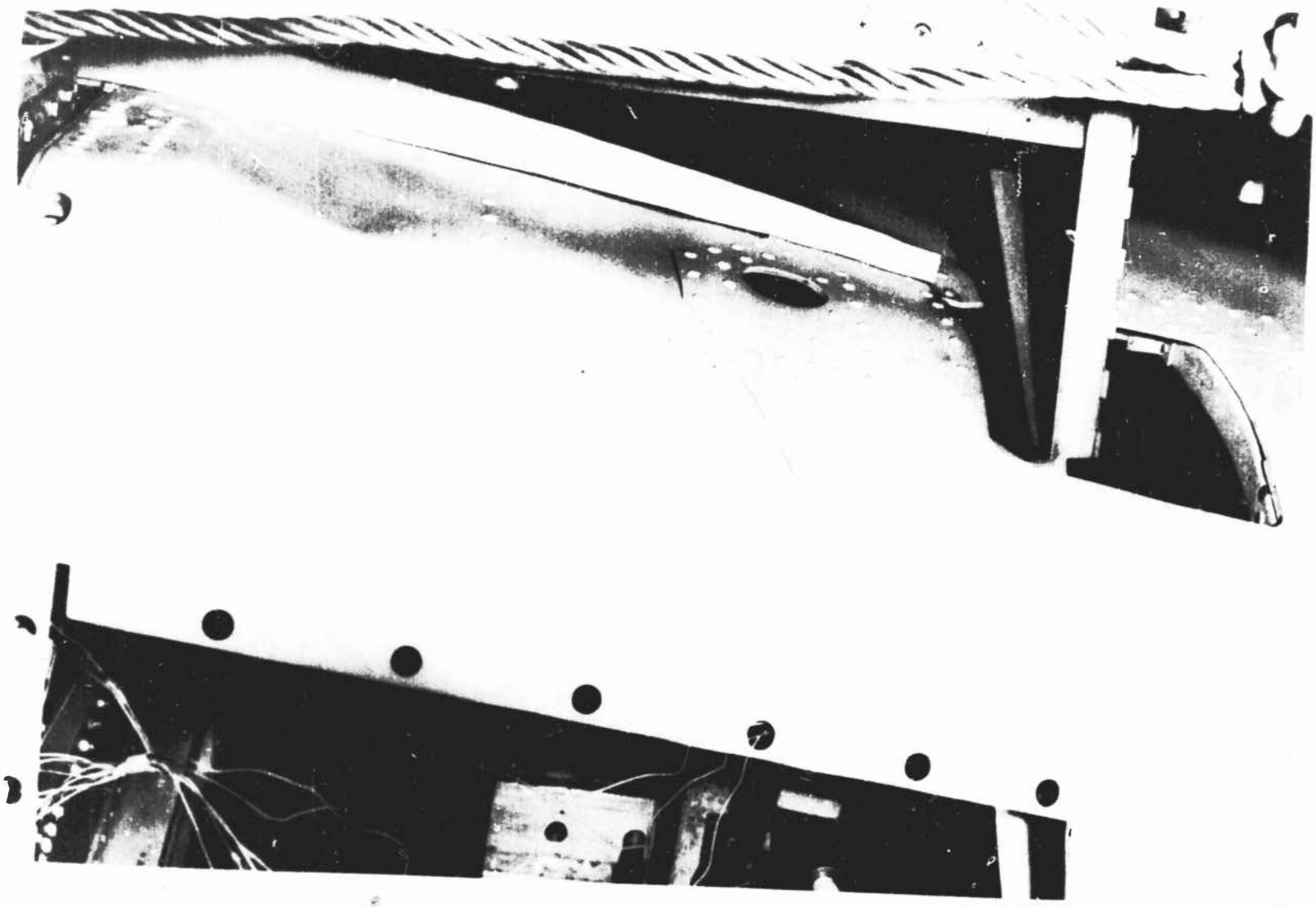

FIGURE 38 - MAGNESIUM F-80C FUSELAGE - LOWER SKIN BUCKLES AT 90 PERCENT ULTIMATE LOAD FOR CONDITION IV (LOWER VIEW)

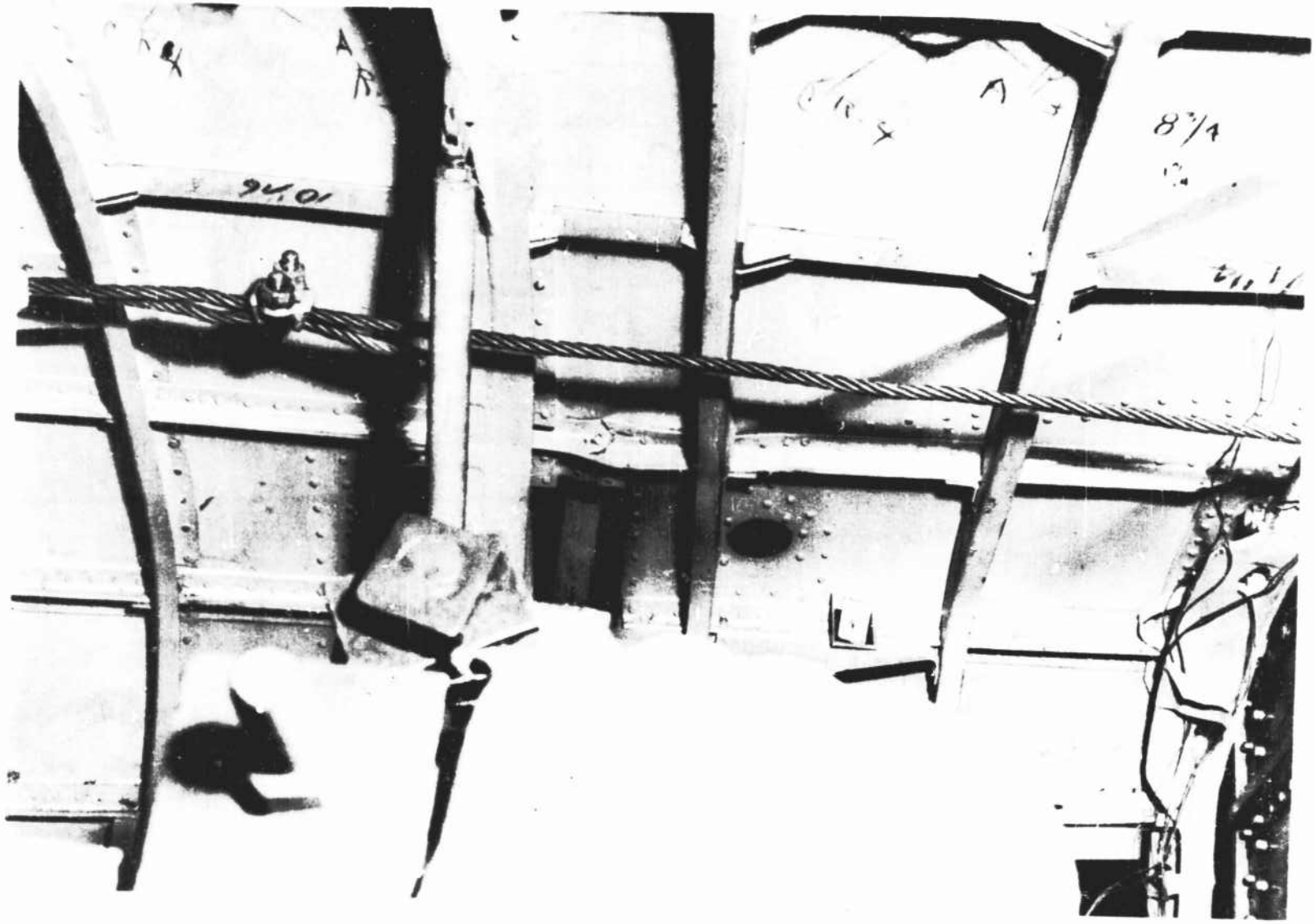

FIGURE 39 - MAGNESIUM F-80C FUSELAGE - STRINGER FAILURE AFTER 100 PERCENT ULTIMATE LOAD FOR CONDITION I?

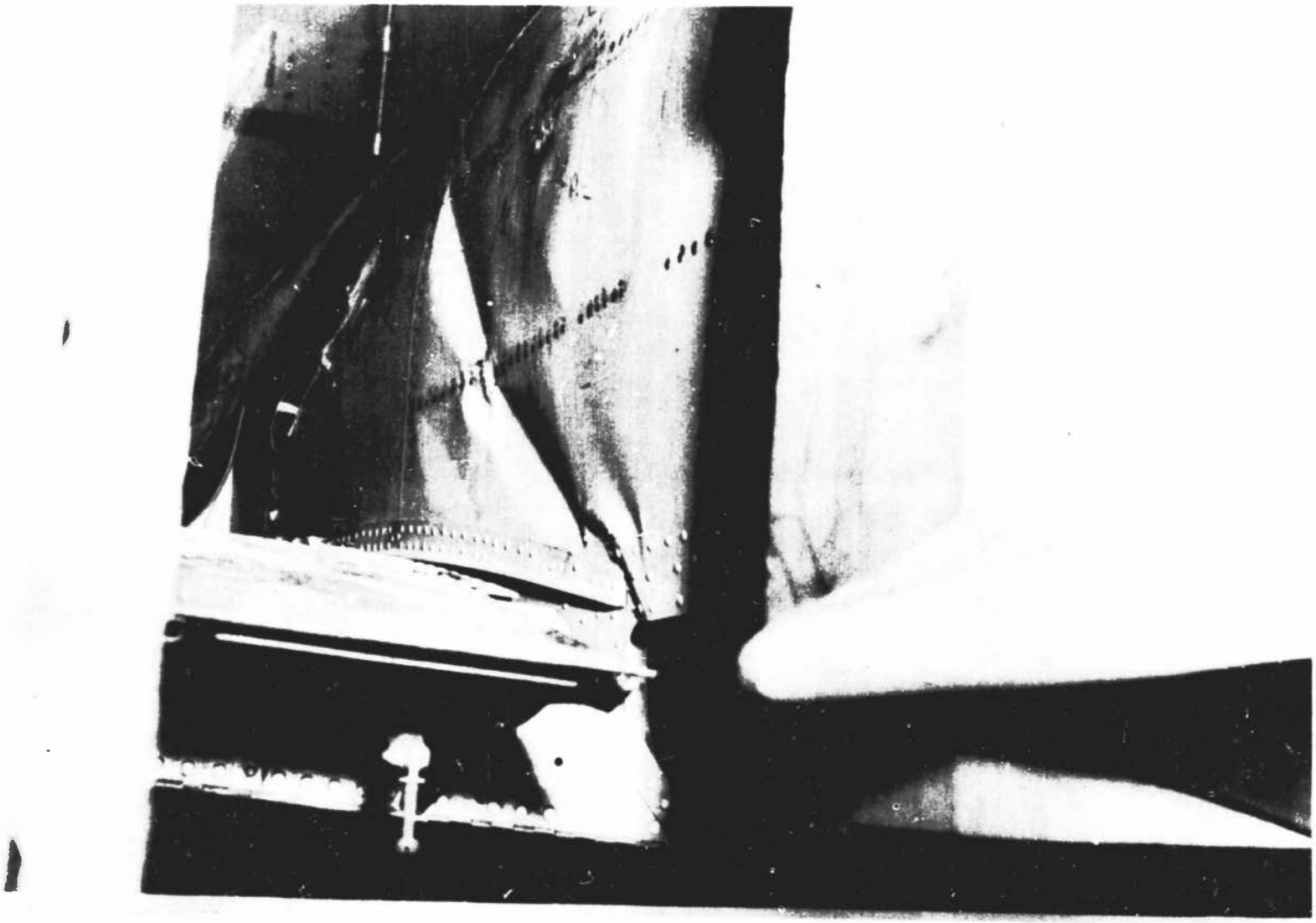

FIGURE 40 - MAGNESIUM F-80C FUSELAGE - SIDE SKIN PERMANENT BUCKLES AFTER 100 PERCENT ULTIMATE LOAD FOR CONDITION IV

With the completion of Condition IV of the static test program, the contractual requirements for the structural integrity were met. However, in order that additional tests could be conducted for comparison purposes with the standard F-80C aluminum parts, the failed fuselage section was arbitrarily reinforced and testing was continued on the empennage and aft fuselage.

The Rolling Pull-Out Condition was re-run for a load of 6,410 pounds on the vertical tail in order to eliminate the load reduction previously mentioned for the magnesium F-80C airplane. The correct loading was carried through the aft fuselage up to station 277.5. Relieving loads were applied to the engine mount to prevent further failure of the fuselage. The empennage and aft fuselage satisfactorily supported 100 percent ultimate load.

During the destruction tests of the standard F-80C aluminum aft fuselage conducted at WADC, the standard aft fuselage supported an ultimate bending moment at station 277.5 of 1,171,000 inch-pounds. In order to check the magnesium aft fuselage for the same condition, this up bending moment was applied to the aft fuselage without failure.

The last series of tests were conducted on the horizontal tail. The horizontal tail of the standard F-80C was tested by Lockheed Aircraft for the Dynamic Symmetrical Up Tail Load of 22,500 pounds for the 25 percent and 50 percent center of pressure locations. The standard tail supported 100 percent ultimate load for the 50 percent center of pressure location and failed between 115 and 120 percent ultimate load for the 25 percent location. These tail loadings were reacted at Bulkhead Stations 376 and 400. The magnesium horizontal tail surfaces were tested for these conditions and satisfactorily supported 100 percent ultimate load for the 50 percent center of pressure location and 120 percent ultimate load for the 25 percent location without failure. The tail was mounted on the aft fuselage for test and the load was partially reacted at Stations 376 and 400.

Typical setups for some of the loading conditions of the static test program are shown in Figures 41, 42, and 43.

EFFECTS OF FORMING TEMPERATURES ON MECHANICAL PROPERTIES OF MAGNESIUM SHEET

Wrought magnesium alloys, in any temper, work harden rapidly when formed at room temperature, hence the cold working possibilities are very limited. In common with most other metals, however, the workability of magnesium alloys is greatly improved at elevated temperatures. It has been generally known that annealing is a function of both time of exposure and temperature of exposure; thus high forming temperatures can be tolerated providing the time at such temperatures is carefully controlled in order to prevent a loss of mechanical properties associated with annealing.

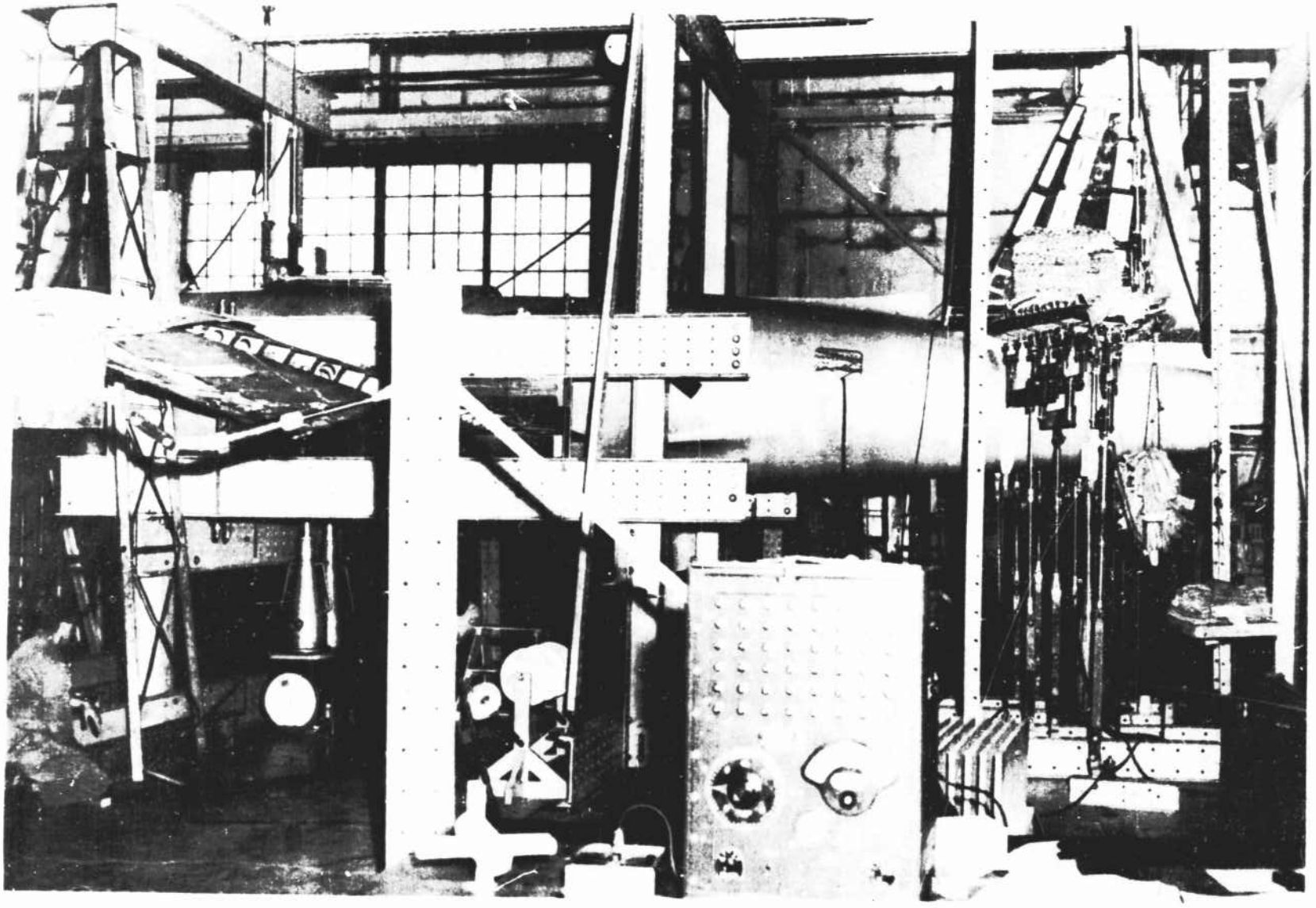

FIGURE 41 - MAGNESIUM F-80C HORIZONTAL TAIL AND FUSELAGE SUPPORTING 100 PERCENT ULTIMATE LOAD FOR CONDITION A-IX

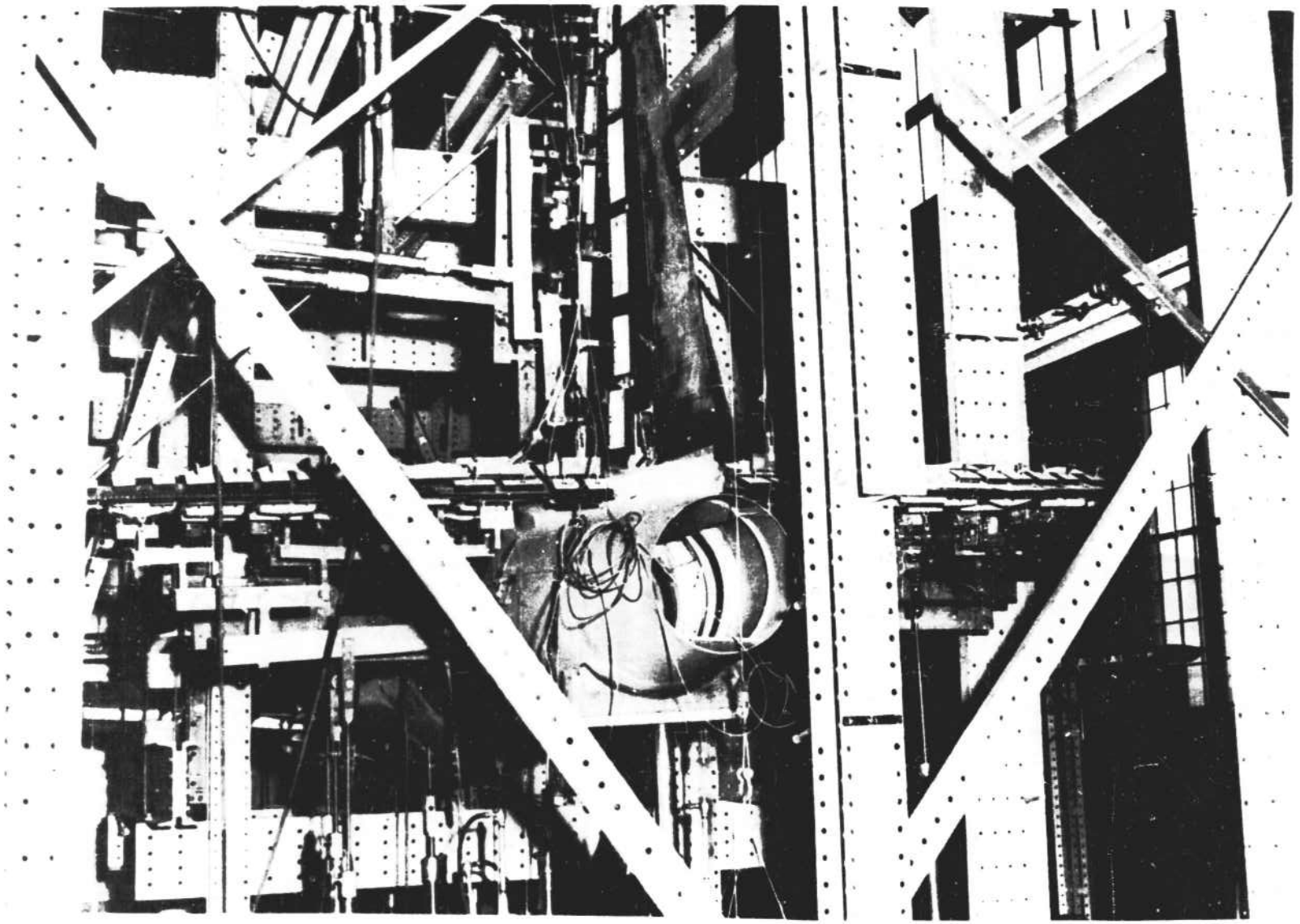

FIGURE 42 - MAGNESIUM F-80C EMPENNAGE AND FUSELAGE SUPPORTING 100 PERCENT ULTIMATE LOAD FOR COMBINATION B

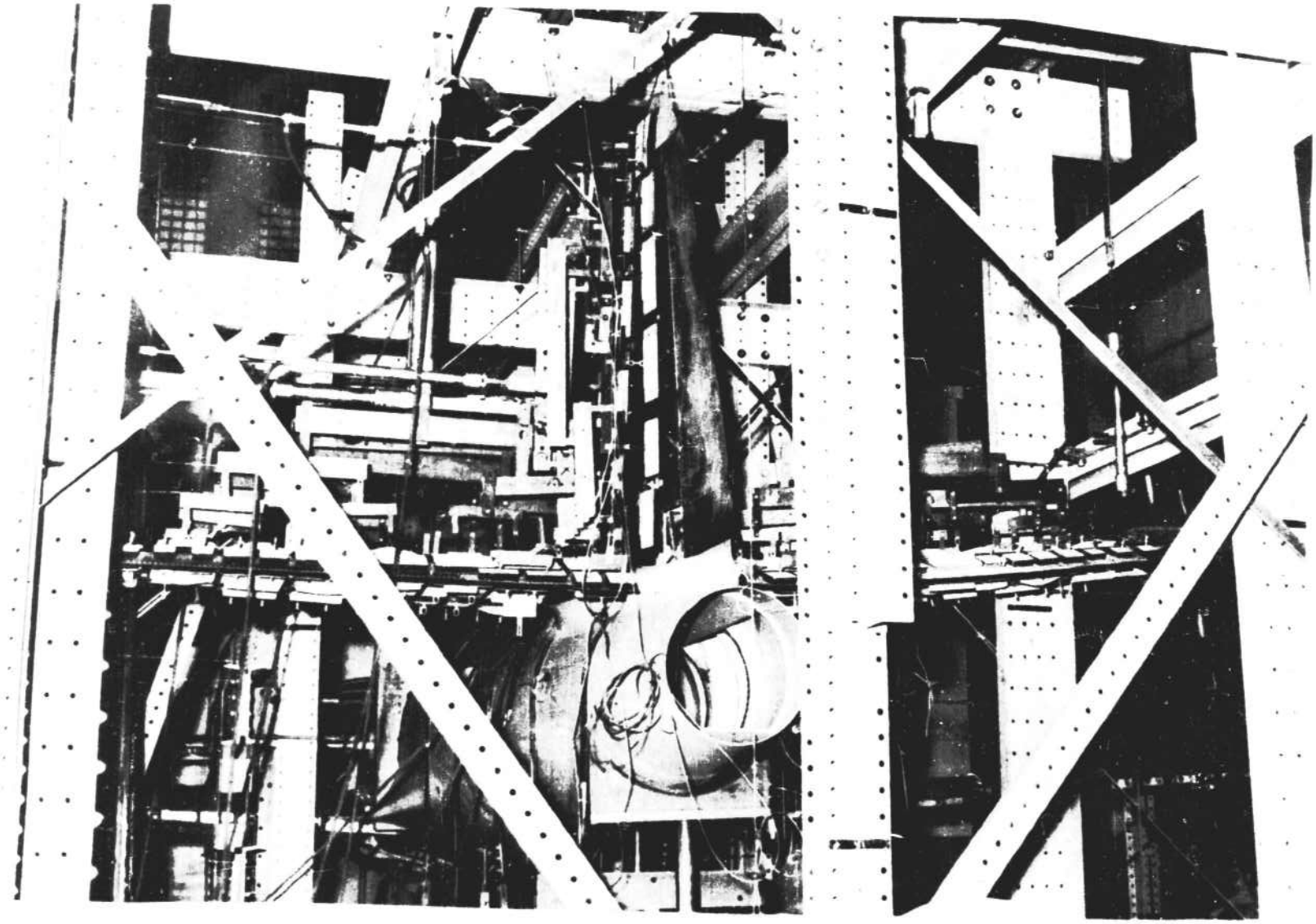

FIGURE 13 - MAGNESIUM F-80C EMPENNAGE & FUSELAGE SUPPORTING 100% ULTIMATE LOAD FOR DYNAMIC UNSYMMETRICAL TAIL LOAD B

The alloy with which the following discussion on forming magnesium at elevated temperatures is concerned, is designated as FS1 by the Dow Chemical Company, AMC52S by the American Magnesium Corporation and QQ-M-44 by the Bureau of Federal Supply. This alloy is a non-heat-treatable alloy furnished in two conditions; "H24" which is cold worked for higher mechanical properties and "O" which is full annealed, sometimes designated as condition "A".

From ANC-5 page 96, Reference 6, the design mechanical properties of this alloy for sheet stock are as follows:

	Annealed	Hard Rolled
Sheet Thickness	0.020 - 0.250	0.020 - 0.128
F_{tu} (psi)	32,000	39,000
F_{ty} (psi)	15,000	29,000
F_{cy} (psi)	12,000	24,000
F_{su} (psi)	17,000	18,000
e, Elongation %	12	4
E in^4	6.5×10^6	6.5×10^6
G in^4	2.4×10^6	2.4×10^6
W, lbs/cu.in.	0.0645	0.0645

It should be noted that the above listed values are minimum guaranteed design properties. However, the typical mechanical properties are somewhat higher as shown in Table 4, Reference 7. For reference purposes, the typical mechanical properties of FS1 are as follows:

	Annealed	Hard Rolled
F_{tu} (psi)	37,000	42,000
F_{ty} (psi)	22,000	32,000
F_{cy} (psi) *	16,000	27,000
e, Elongation %	21	16

* Yield strength is defined as the stress at which the stress-strain curves deviates 0.2% from the modulus line.

An examination of the minimum guaranteed and typical mechanical properties of FS1 magnesium sheet indicates that forming operations can be performed at elevated temperatures without reducing the mechanical properties below the ANC-5 minimum values. As previously stated, in order to guarantee the structural quality of finished parts, it is necessary to confine exposure at temperatures to certain predetermined time-temperature limits. Based on previous tests, the hard rolled magnesium FS1-H24 sheet exhibits, in respect to strength, the property of integrating the effects of time of exposure to temperature. Curves for determining the limiting exposure time for various temperatures are shown in Figures 44, 45, and 46 and were obtained from Reference 8. It should be noted that the curves have been extrapolated above the typical mechanical property levels of the FS1-H24 sheet; however, in using these curves, if the value selected from a given curve should exceed the material's initial property level, the latter figure must, of course, be used.

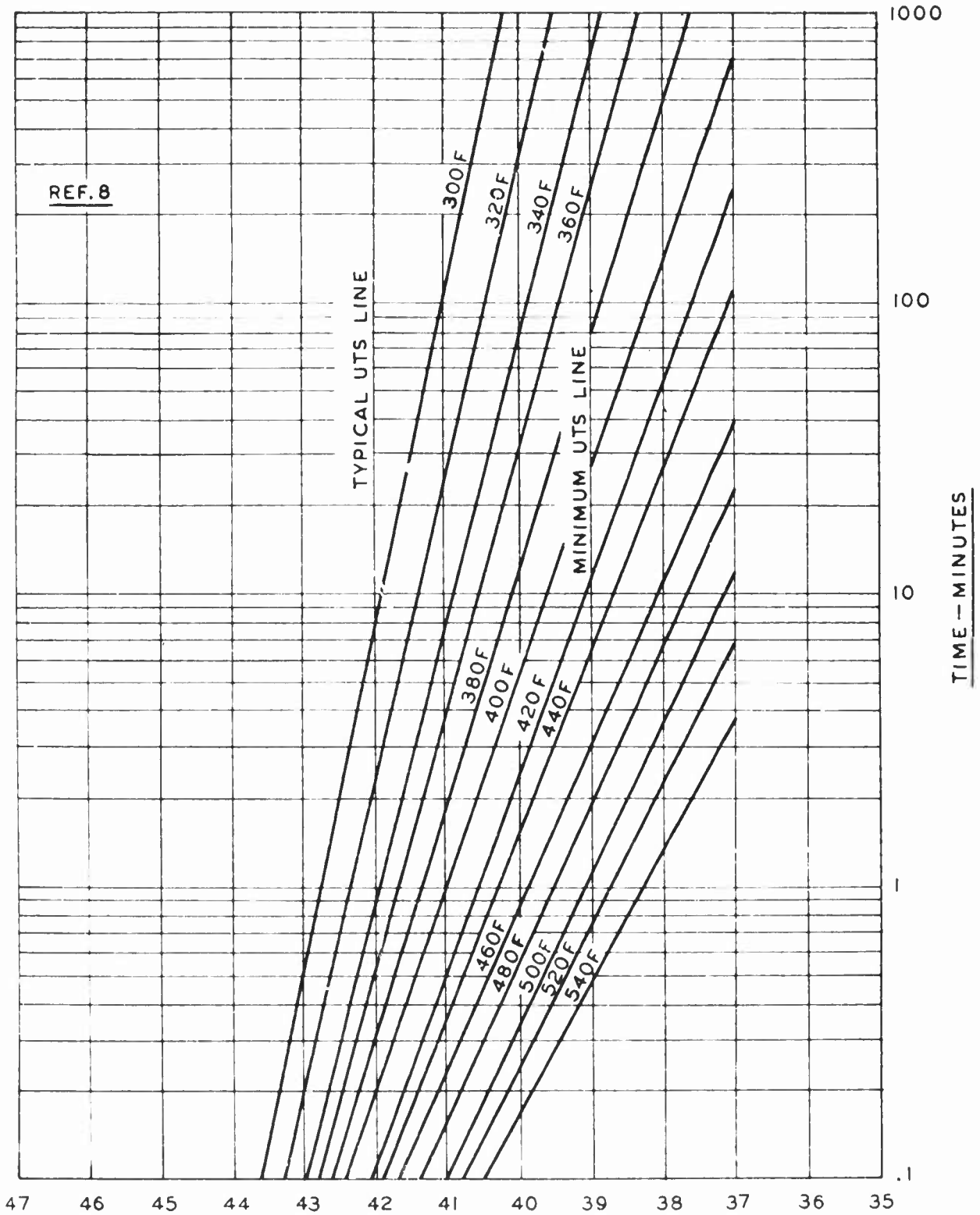

FIG. 44 — ROOM TEMPERATURE PROPERTIES AFTER ELEVATED TEMPERATURE EXPOSURE — MAGNESIUM ALLOY FS1 — H24

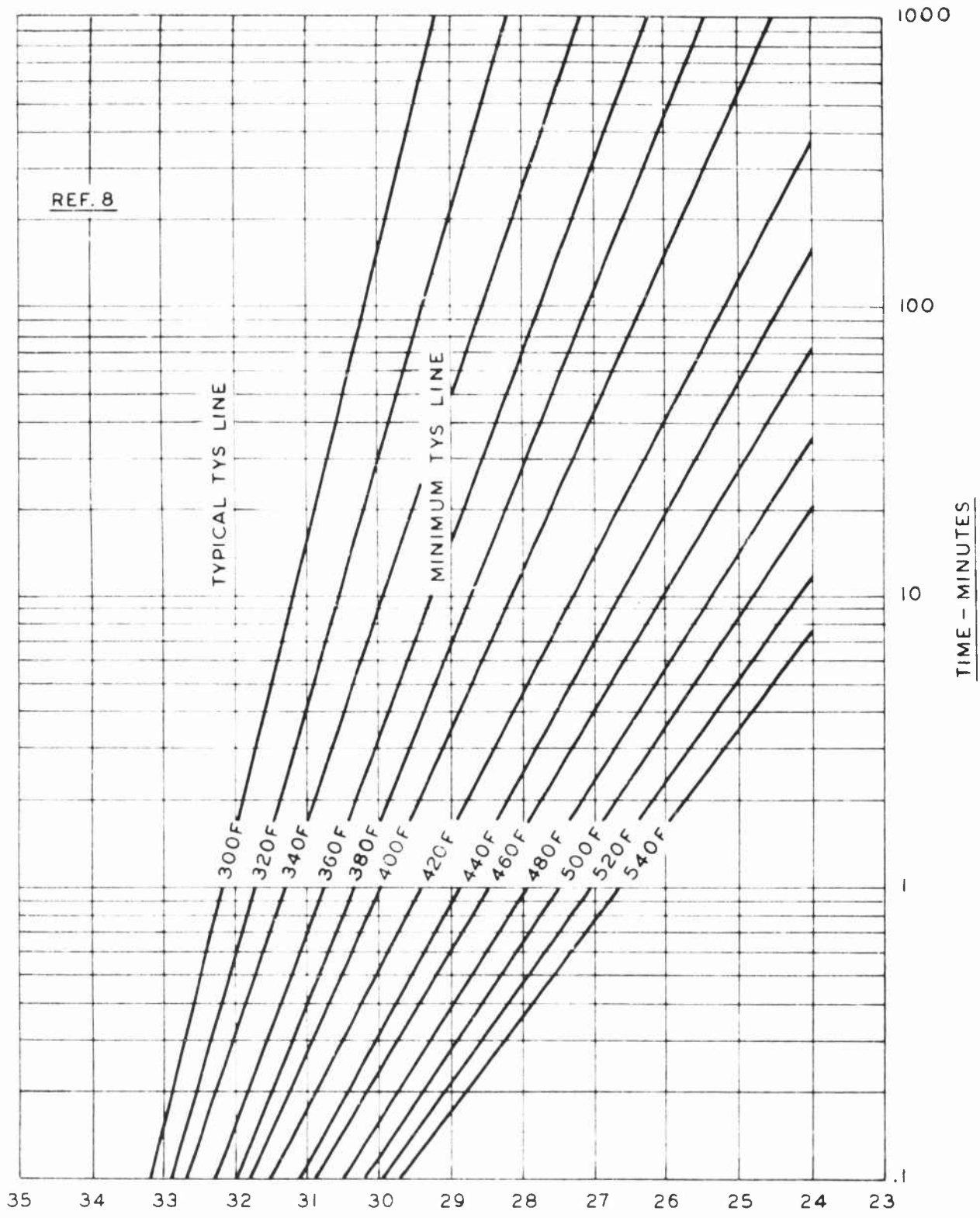

FIG. 45 -- ROOM TEMPERATURE PROPERTIES AFTER ELEVATED TEMPERATURE EXPOSURE - MAGNESIUM ALLOY FSI-H24

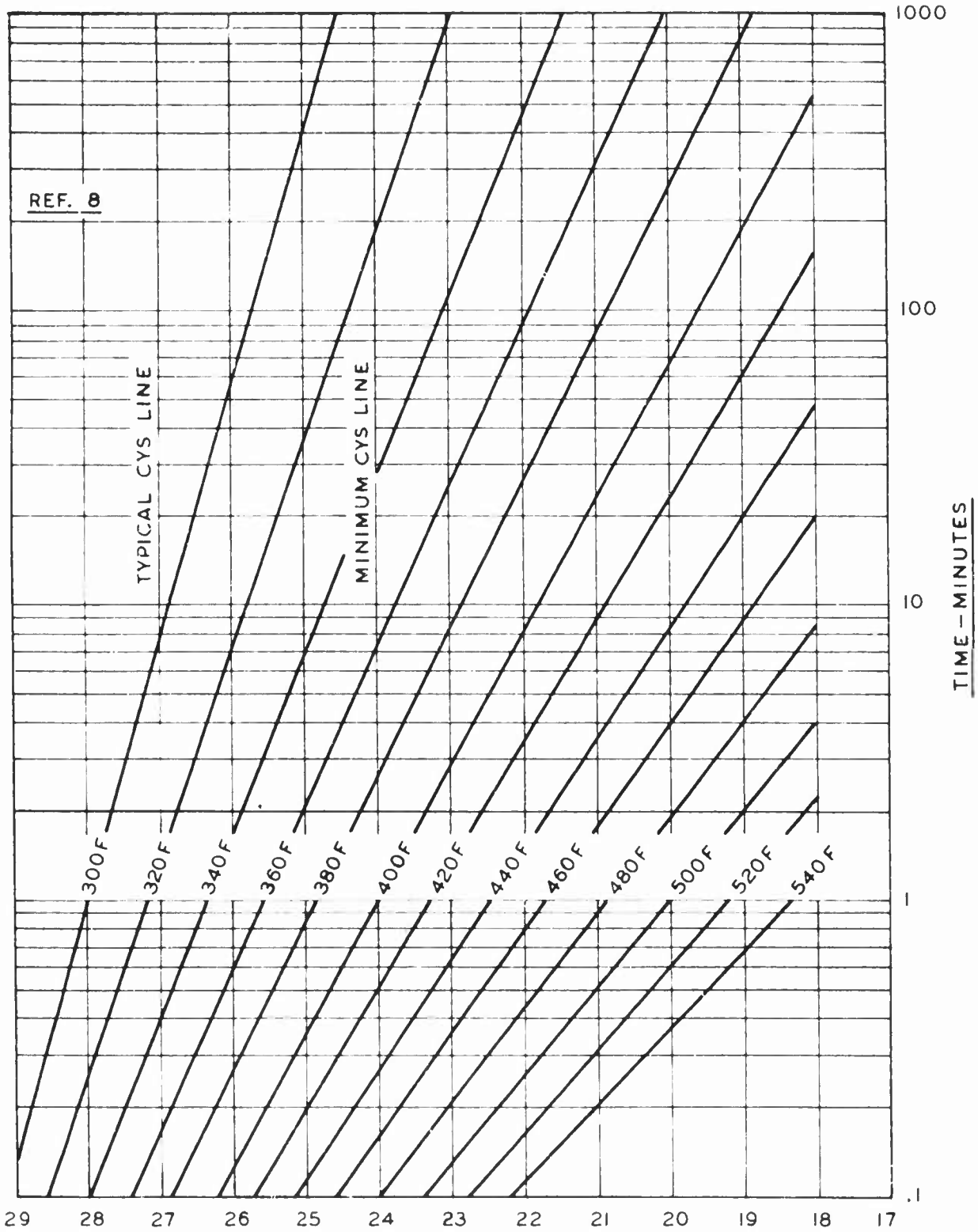

FIG. 46 — ROOM TEMPERATURE PROPERTIES AFTER ELEVATED TEMPERATURE EXPOSURE - MAGNESIUM ALLOY FSI - H24

In using these curves to select a combination of time and temperature for any hot forming operation on FS1-H24 magnesium sheet, a test check should be made for the hot forming operation employed since these curves only predict the effects of time and temperature on the room temperature mechanical strength.

In Figure 47, curves are presented for predicting the maximum permissible combinations of time and temperature to retain the minimum mechanical properties specified in ANC-5. These curves are useful in establishing limits of single exposure for normal forming operations.

Severe forming operations sometimes require repeated exposure to temperature to achieve the desired results. Tests conducted in Reference 2 indicates that the effects of repeated elevated temperatures are cumulative.

In the above reference, tests were conducted to determine the effects of heat cycles on physical properties of magnesium FS1-H24 sheet. The results of these tests are presented in Figure 48 as a ratio of tensile strength after various heating cycles to tensile strength prior to heating versus number of cycles of exposure. In the referenced tests, specimens were subjected to 0, 1, 2, 3, 4, and 5 heat cycles respectively. A heat cycle consisted of heating a specimen to a temperature of 300 - 350 deg. F and maintaining that temperature range for five (5) minutes and then allowing the specimen to cool to room temperature before the heating cycle was repeated.

The results shown in Figure 48 are presented to show the general trend and should not be used for design. However, the curves shown in Figure 44 to 46 may be used to predict the effects of repeated elevated temperature exposures. Using Figure 46 as an example, suppose the magnesium sheet is held at 340 deg. F for five (5) minutes; the resulting design compressive yield stress is then 25,200 psi. Then suppose the part is exposed for 30 minutes at 310 deg. F. Since 80 minutes at 310 deg. F is required to produce the value of 25,200 psi given by five minutes at 340 deg. F, the total equivalent exposure time at 310 deg. F is 110 minutes. Reference to Figure 46, the compressive yield stress is then 25,000 psi.

An examination of Figure 47 indicates that the compressive yield strength dictates the selection of the temperature and time of exposure for hot forming magnesium alloy FS1-H24 sheet and still maintain the minimum design mechanical properties as specified in ANC-5.

For annealed magnesium sheet, the time-temperature relationship is relatively simple since property reduction is not a problem and grain growth becomes the major item of concern in the region over 600 deg. F. To minimize grain growth, a forming temperature of 500 deg. F ±25 deg. is recommended for FS1-0 Dowmetal alloy. Time at temperature can be held for approximately one hour without any appreciable reduction in the mechanical properties of the material.

Dowmetal Mh (or M-H24) may be heated to 375 deg. F ±25 deg. for any length of time without affecting the mechanical properties. A slight reduction in the mechanical properties is obtained if magnesium alloy Mh is heated for any length of time above the recommended temperature. The annealed alloy Ma (or M-0) is similar to that of FS1-0 magnesium alloy insofar as temperature-time relationship except that the maximum temperature limits are 600 deg. F ±25 deg.

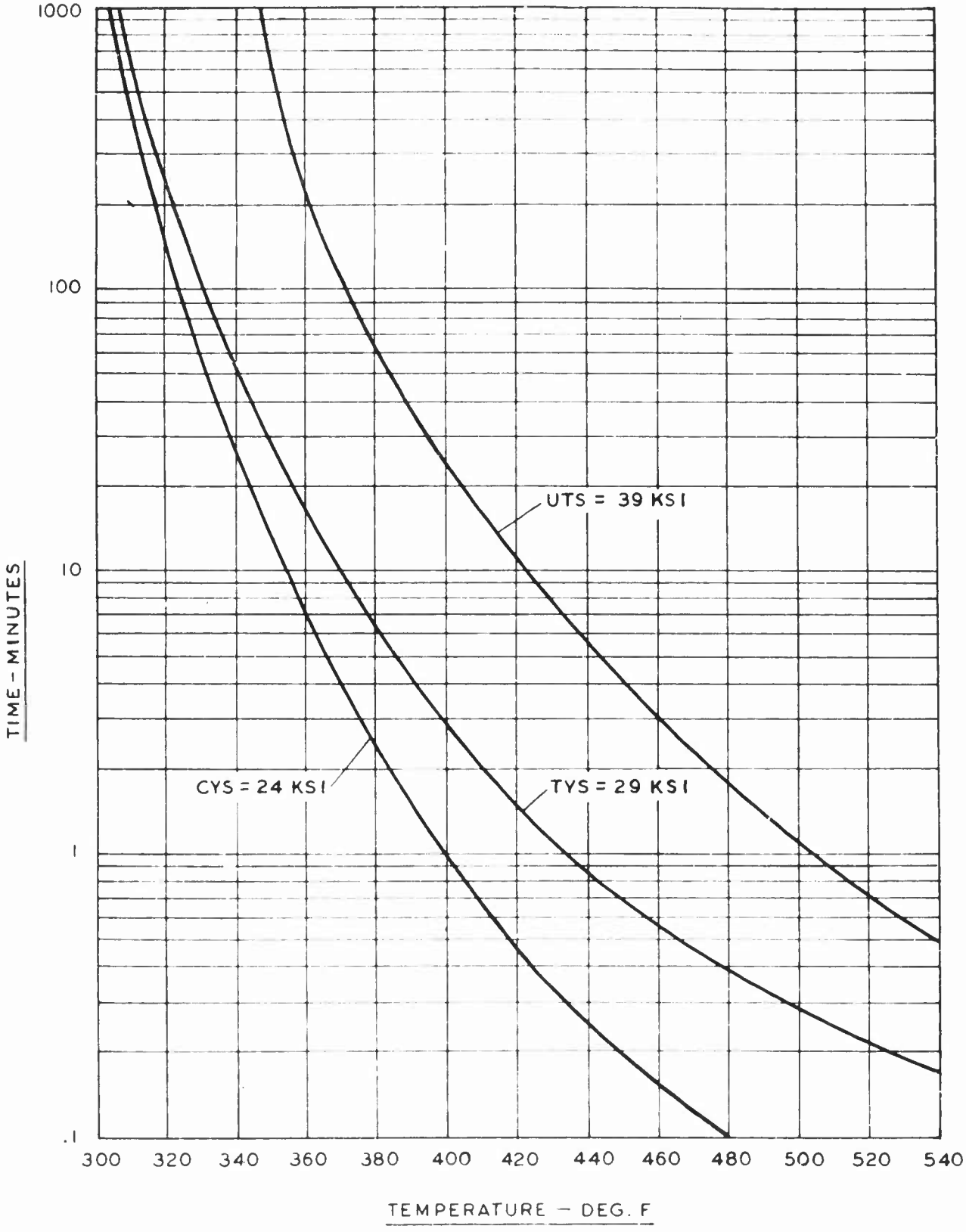

FIG. 47 — PERMISSIBLE COMBINATION OF TIME AND TEMPERATURE FOR FSI-H24 SHEET FOR MAINTAINING ROOM TEMPERATURE PROPERTIES - ANC - 5 MINIMUM VALUES.

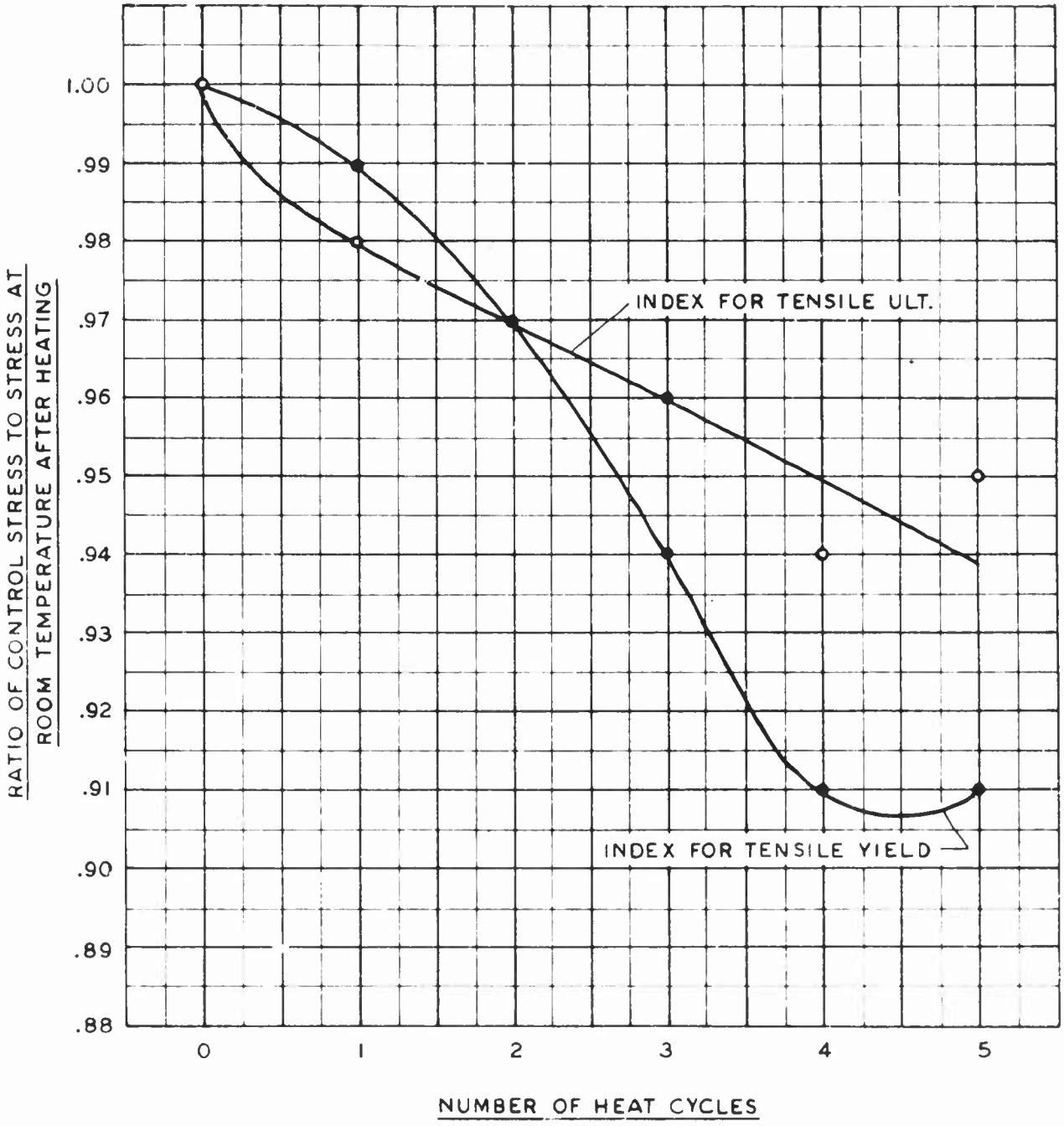

RATIO OF CONTROL VALUE TO ANC-5 VALUE FOR F_{tu} = .89
RATIO OF CONTROL VALUE TO ANC-5 VALUE FOR F_{ty} = .90

FIG. 48 — EFFECTS OF HEAT CYCLES ON PHYSICAL PROPERTIES OF FSI-H24

NOTE: HEAT CYCLE CONSISTS OF HEATING TO 300-350° FOR FIVE MINUTES AND COOLING TO ROOM TEMPERATURE.

EFFECTS OF TEMPERATURE ON THE BEND RADII OF MAGNESIUM ALLOY SHEET

The work hardening properties of wrought magnesium alloy, in any temper, when formed at room temperature presents many pr oblems. Minimum die radii for 90 deg. bends for FS1-O annealed sheet and FS1-H24 hard rolled sheet at room temperature is approximately five times the sheet thickness for the former and approximately eight times the sheet thickness for the latter. Since the workability of magnesium alloy is greatly improved at elevated temperatures, smaller bend radii can be used but controls must be exercised to limit preheating and forming time so that mechanical property specifications are maintained.

The effects of temperature and time on the mechanical properties of FS1-H24 have been previously discussed, however, in order to correlate bend radius and temperature with time of exposure, the curves of Figure 47 have been extended to incorporate allowable die radii vs. temperature. The composite curves are shown in Figure 49.

The allowable die radius vs. temperature for FS1-H24 presented in Figure 49 was obtained from Reference 9 and is based on a resultant 95% acceptable 90 deg. bends. The minimum curve shown is based upon a small production run and is not recommended for large scale production due to the large scrap rate that would result.

Allowable bend radii for FS1-O, Mh, and Ma magnesium alloy are presented in Figures 50 to 52. The effects of temperature and time for the above alloys are not correlated with the mechanical properties since their effects are negligible in the working temperature range as specified for these alloys.

The working temperature range for FS1-O, Mh, and Ma magnesium alloy is that as previously reported and noted below:

Alloy	Forming Temp. (Max.) °F
FS1-O	500°F ±25°
Mh	375°F ±25°
Ma	600°F ±25°

FABRICATION OF MAGNESIUM ALLOY PARTS

The working of magnesium alloys at elevated temperatures involves the development of new shop techniques and methods of heating both equipment and work. While the necessity for hot working magnesium alloy may, at times, be a drawback in regard to cost of equipment and operation, there are some aspects

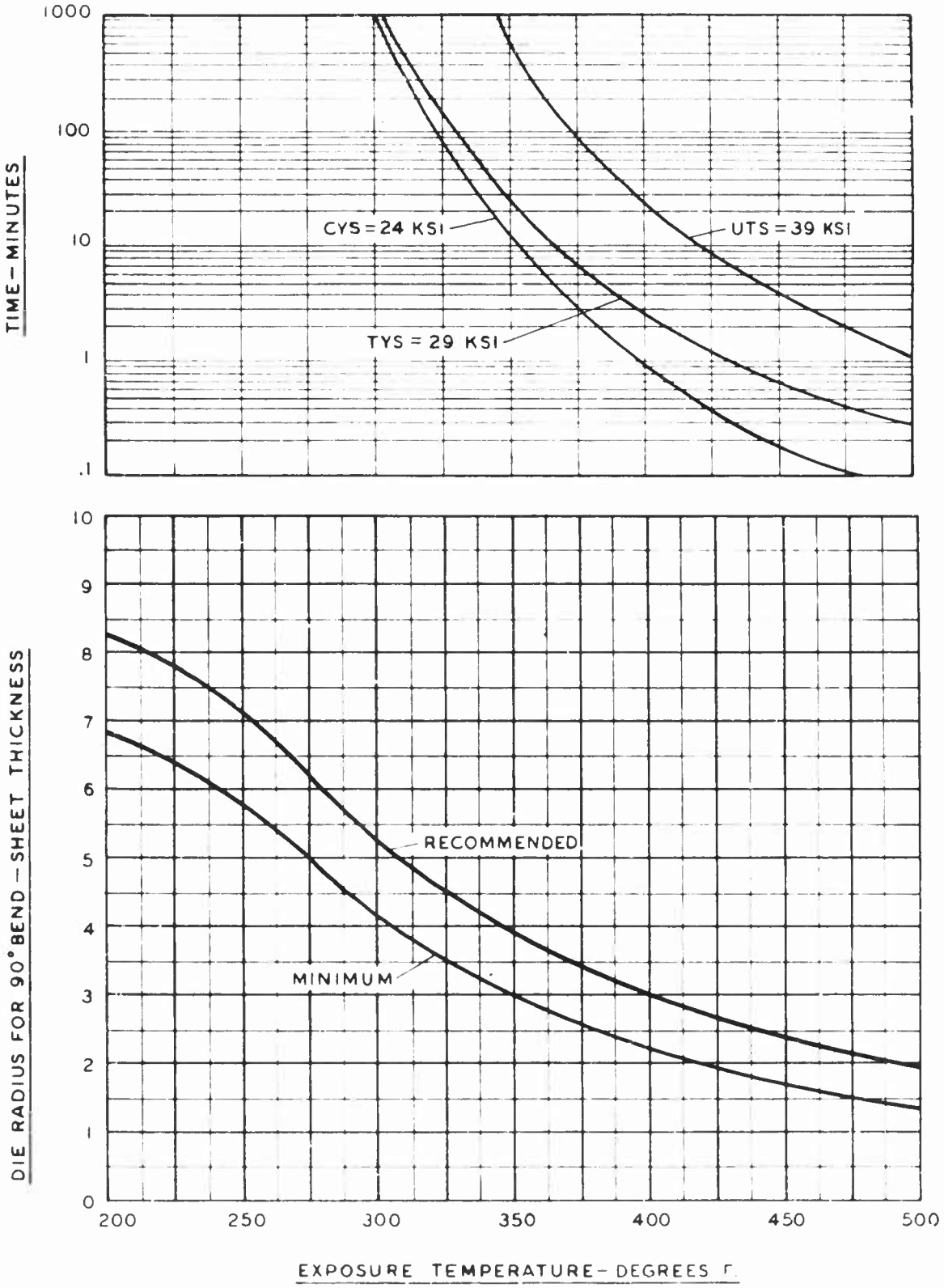

FIG. 49 — EFFECTS OF FORMING TEMPERATURE ON DIE RADII FOR FSI-H24 MAGNESIUM ALLOY SHEET

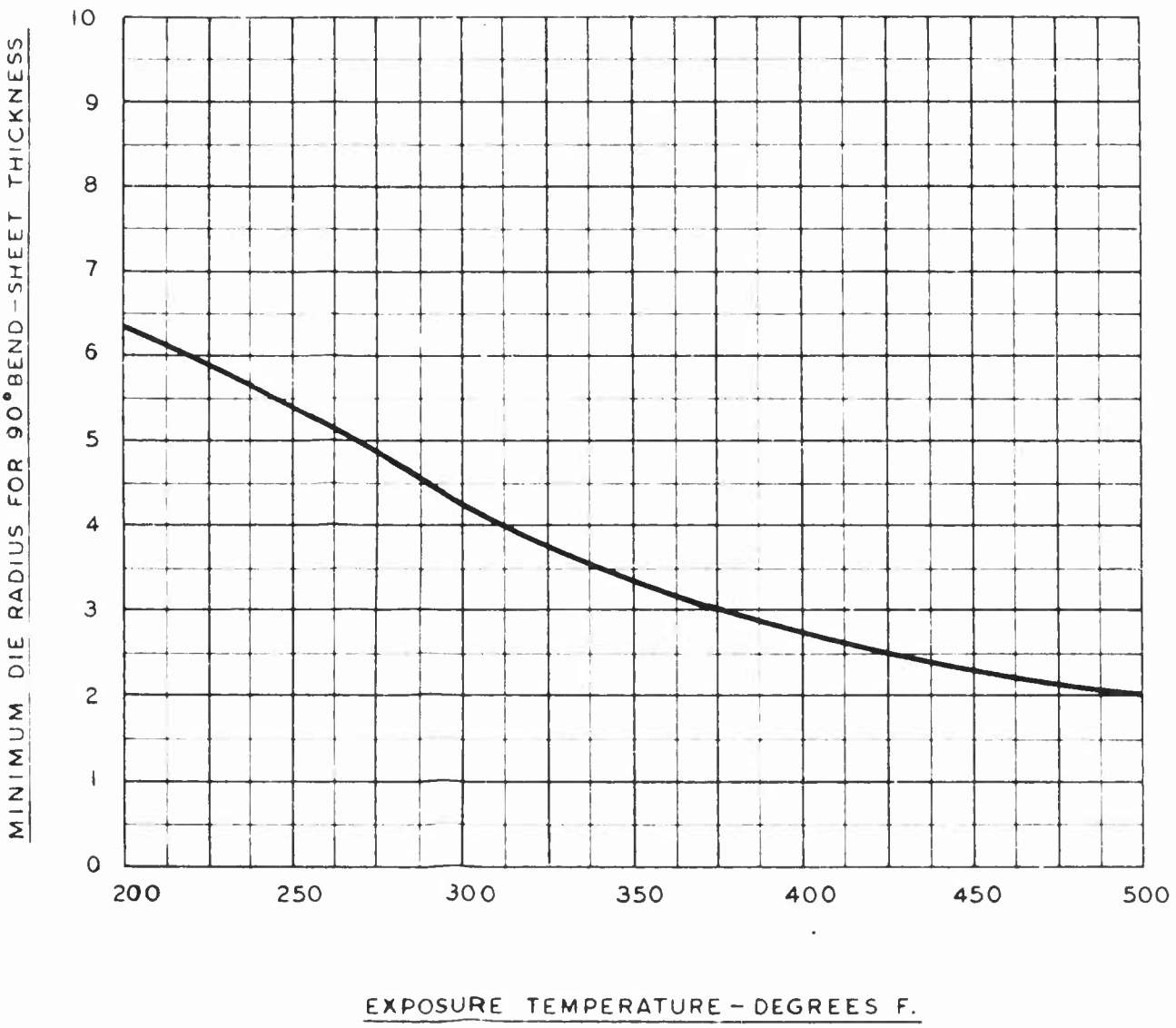

FIG. 50 — EFFECTS OF FORMING TEMPERATURE ON DIE RADII FOR FS-1a MAGNESIUM ALLOY SHEET

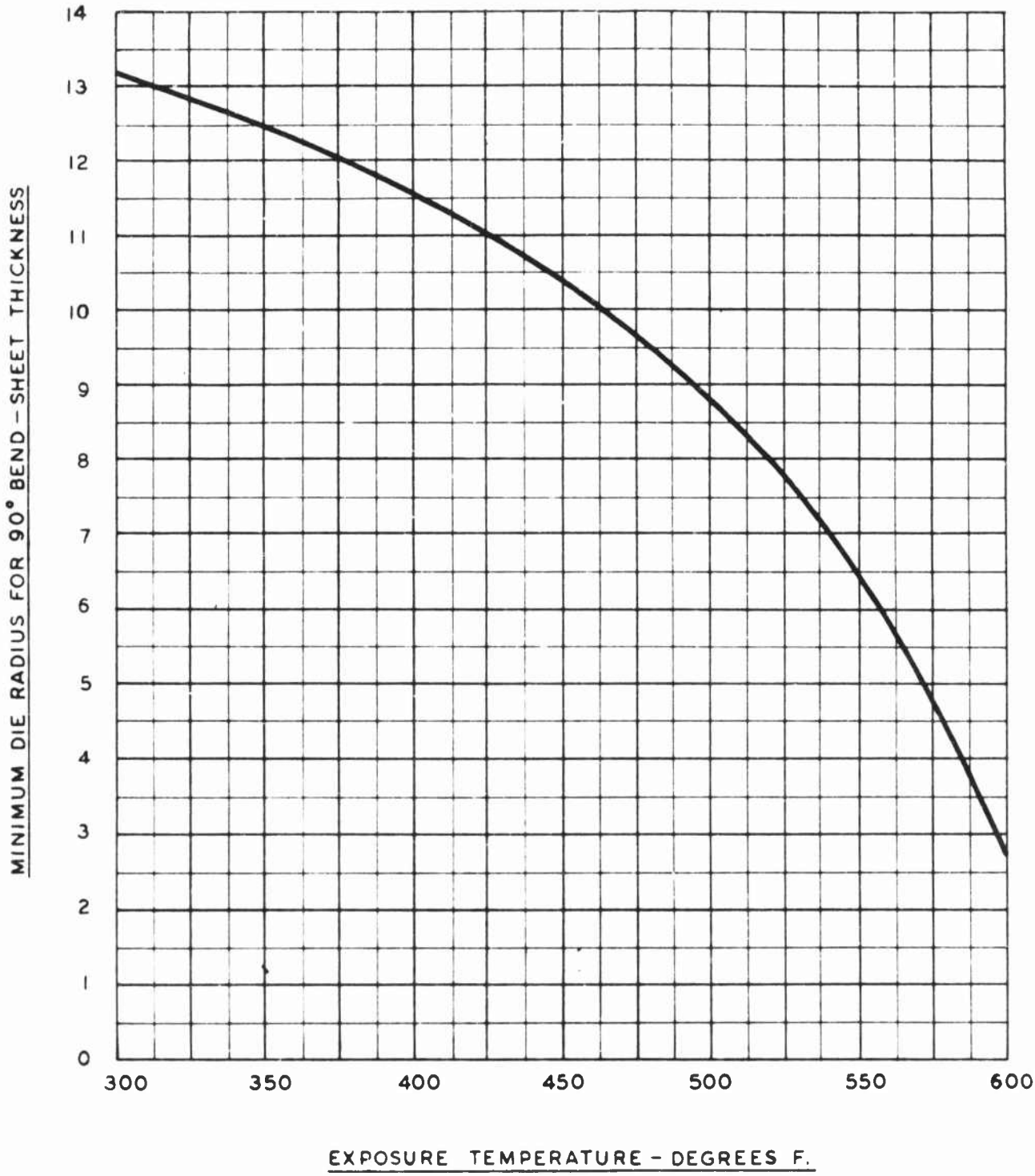

FIG. 51 — EFFECTS OF FORMING TEMPERATURE ON DIE RADII FOR Mh MAGNESIUM ALLOY SHEET

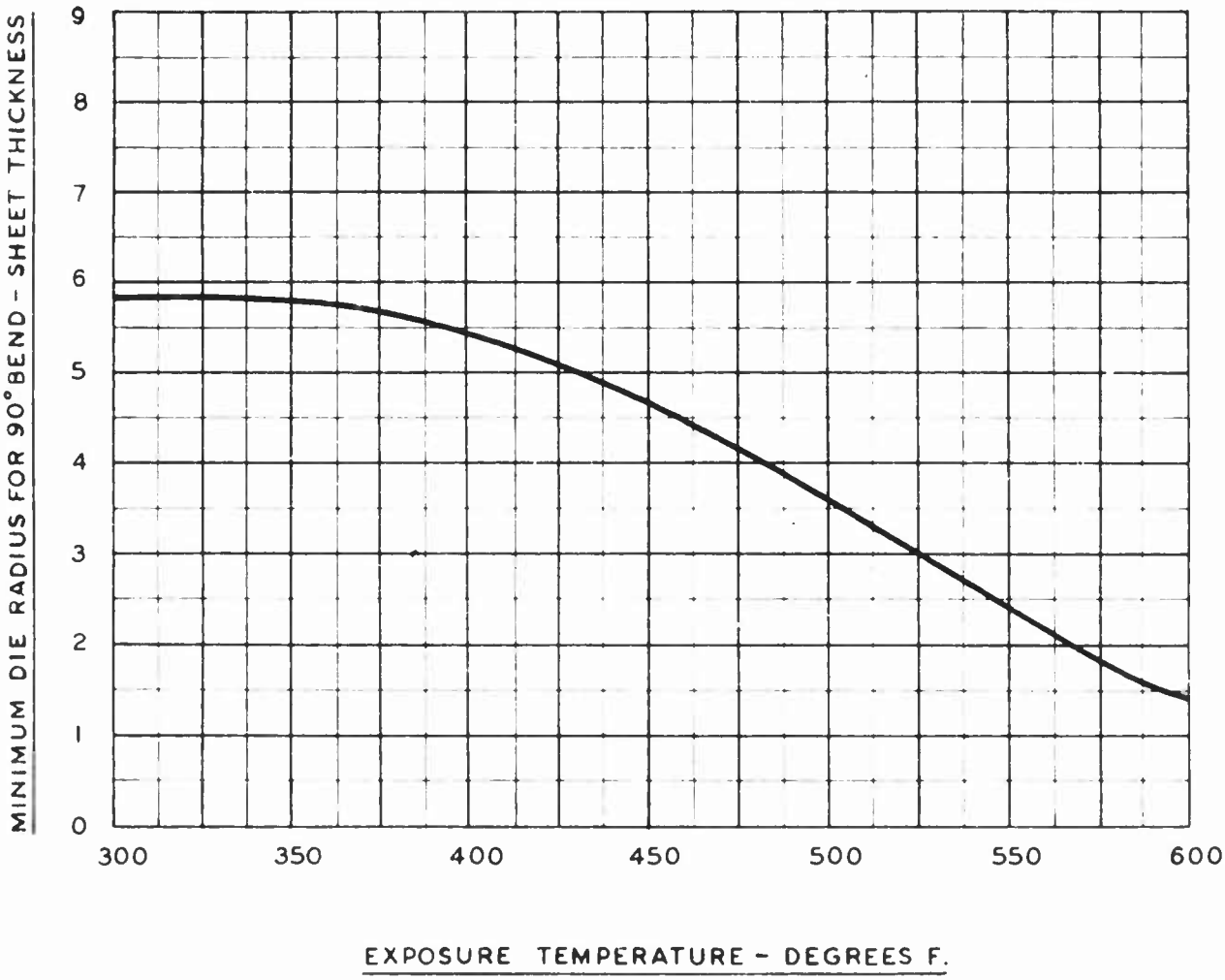

FIG. 52 — EFFECTS OF FORMING TEMPERATURE ON DIE RADII FOR Ma MAGNESIUM ALLOY SHEET

of the hot working method which, at least partially and often entirely, offset this disadvantage. Hot working of magnesium alloy reduces or eliminates springback, thus making greater accuracy possible. In addition, it is generally possible to reduce the number of intermediate draws when hot working magnesium alloy sheet as compared to the number of steps in cold working aluminum alloy sheet.

The methods employed and the equipment used for forming magnesium alloys are the same as those used for other metals, except that the forming of magnesium usually is done at elevated temperatures. Modification to equipment to incorporate heating of the work and tools is all that is necessary.

When magnesium alloys must be hot formed, it is desirable to preheat the sheet or extrusion to the working temperature. Time and temperature for preheating should be determined based on the equipment used to form the part, the amount of forming necessary, and the strength requirements of the part. Gas or electrically heated furnaces and contact type heaters such as hot plates or immersion baths can be used for preheating. The advantages of preheating compared to placing cold sheets in the die, are four-fold. Preheating assures proper forming temperatures, minimizes distortion due to internal stresses, keeps the dies at a uniform temperature, and increases the production rate. However, when parts are relatively small, preheating of the part is not necessary since the part will absorb sufficient heat for forming from the die without reducing the die temperature to any great extent.

It is well to point out that when small quantities of magnesium parts are involved, the easiest and cheapest method of heating small sheets or blanks is to use a gas torch held directly on the work. The torch should be kept constantly in motion to prevent local overheating and the temperature of the part should be checked by means of a contact type pyrometer. While this method requires care to avoid overheating, sufficient experience will enable the operator to handle the torch properly to obtain satisfactory results.

The problem of forming temperature and the time of exposure at temperature and its relation to the mechanical strength of FS1-H24 magnesium alloy sheet is completely covered in the preceeding pages. An examination of the data presented indicates that the maximum forming temperature for FS1-H24 magnesium sheet in consideration of the allowable bend radii is approximately 375 deg. F. This temperature results in a maximum exposure time of only three minutes based on the allowable compressive yield strength as shown in Figure 47. However, a three minute exposure time is too short for practical forming and handling. As a result, a temperature limit of 350 deg. F is recommended for all hot forming operations on FS1-H24 magnesium alloy sheet. This temperature results in a maximum exposure time, reference to Figure 47, of approximately 15 minutes based on the compressive yield strength, and approximately 20 minutes based on the tensile yield strength.

In order to maintain quality control of hot formed magnesium alloy sheet of FS1-H24, the following specification is recommended since most forming operations other than stretch press and drop hammer forming requires a short period of time;

> "Part may be heated to a maximum temperature of 350 deg. F for not over 5 minutes. Four (4) reheates may be permitted."

In the following discussion, several methods used in forming magnesium alloy sheets and extrusions are presented.

Shearing and Blanking

Magnesium alloy sheet can be blanked, punched, and sheared much the same as other metals. On sheets thicker than approximately 0.064 inches, a characteristic rough, flaky fracture is obtained. To minimize this rough fracture and obtain best results, the following procedure is recommended.

For shearing, the clearance between blades should be as small as can be used without scoring the blades. A maximum clearance of three to five percent of the thickness of the sheet is recommended. To reduce the flaky fracture, a shearing or rake angle of 30 to 45 degrees on the upper shear blade should be used. In addition, employing hold-down pressure on the sheet in the shear will improve the edge condition of the sheared sheet.

When a very smooth edge cut is required, the sheared edge may be improved by a double shearing operation known as "shaving". This consists of removing approximately 1/32 to 1/16 of an inch by a second shearing.

Improvement in the condition of sheared edges, particularly on heavy sheet and plate, may be obtained by hot shearing where feasible. Annealed sheet may be heated to 500 deg. F but the maximum temperatures for hard rolled Dowmetal sheet are as follows: FS1-H24 - 250 deg. F; J-1H - 400 deg. F; and MH - 375 deg. F ±25 deg. The temperatures presented for hard rolled magnesium sheet should not be exceeded in order to prevent a loss in the mechanical properties of the material. The effects of heat on the mechanical properties of magnesium alloy sheet has previously been discussed and are not covered in this section.

When hot shearing operations are employed, it is necessary that slight dimensional allowances be made for the thermal expansion of the magnesium alloy sheet.

For blanking and punching operations, small clearances, as required for shearing, are desirable on the tools employed. Dies should be set up with as little clearance as possible to obtain good sheared edges. The clearance between the punch and die should be held to a maximum of three to five percent of the thickness of the material. Clearance angles should be sufficient to permit extraction of punchings and minimize binding of the punch. Shear angles are placed on the female die or the punch depending upon which sheared edge is to have the best surface and should be from two to three degrees.

Blanking and punching operations on magnesium alloy sheet are usually done cold. Hot blanking and punching are possible but not recommended.

If an extremely smooth edge is desired, sheared or blanked parts should be routed or filed.

Hand Forming

When intricate contours are to be developed on small parts and the quantity requirements are small, hand forming may be employed. However, this method

is not recommended on large parts requiring a great deal of forming since it is difficult to maintain time of exposure at temperature within the specified limits and still complete the necessary forming.

In hand forming, aluminum alloy form blocks and backing plates are used. The block and backing plate are brought up to working temperature on a hot plate. The preheated blank to be formed is clamped between the heated form block and backing plate. Form blocks and backing plates are usually heated to 375 - 400 deg. F to compensate for loss of temperature from transferring dies from hot plate to set up area. The heated assembly is then placed in a vise and deformation is carried out by hammering with a leather maul. The assembly is maintained at the working temperature by applying torch heat to the die block as required. A contact pyrometer should be used to check the working temperature and to avoid overheating of the work.

In hand forming operations, the maximum exposure time of 20 minutes is sometimes exceeded but, it is felt that the exposure time can be extended to twice that amount since the time at 350 deg. is very small due to heat loss. In addition, the mean temperature during the hand forming operation is estimated to be 330 deg. F. Reference to Figure 47 indicates that an exposure time of 70 minutes can be employed at a temperature of 330 deg. F based on the compressive yield stress at room temperature. Therefore, extending the exposure time to 40 minutes is considered conservative.

Typical hand formed parts are shown in Figure 53. The tools employed for two of the parts shown are presented in Figure 54 and the hot plate used for preheating the form block and backing plate is shown in Figure 55.

It is to be noted that the lightening holes are preformed in a press by employing standard dies. These dies are preheated to 375 deg. F and the work obtains its heat by contact. The time of exposure to temperature for forming the lightening holes is approximately 60 seconds and is, therefore, not considered.

Bending

Machine bending is frequently used for the manufacture of stringers, clips, stiffeners, and other parts which can be readily formed by bending sheet or strip. A press-type brake is used almost exclusively because of the ease with which it can be equipped with strip electric heaters on either side of the dies. Bends of the smallest possible radii are obtainable if a very slow press speed is used to finish the bend. When possible, both the dies and the work should be heated. If the dies alone are heated, the work will absorb heat by contact. If the work alone is heated, the bending operation must be rapid, before the dies dissipate the heat at the bend. Heat dissipation to the die can be retarded by heating the die with a torch. A contact pyrometer should be used to avoid overheating of die.

Bend radii of 90 deg. bends for various working temperatures are presented in Figures 49 to 52. In forming hard rolled FS1-H24 magnesium sheet the maximum allowable working temperature is 350 deg. F as previously noted. Reference to Figure 49, the minimum allowable bend radii is then 3t where "t" is the thickness of the material. However, for large production runs a 4t bend radius is recommended in order to reduce the scrap rate due to cracked parts.

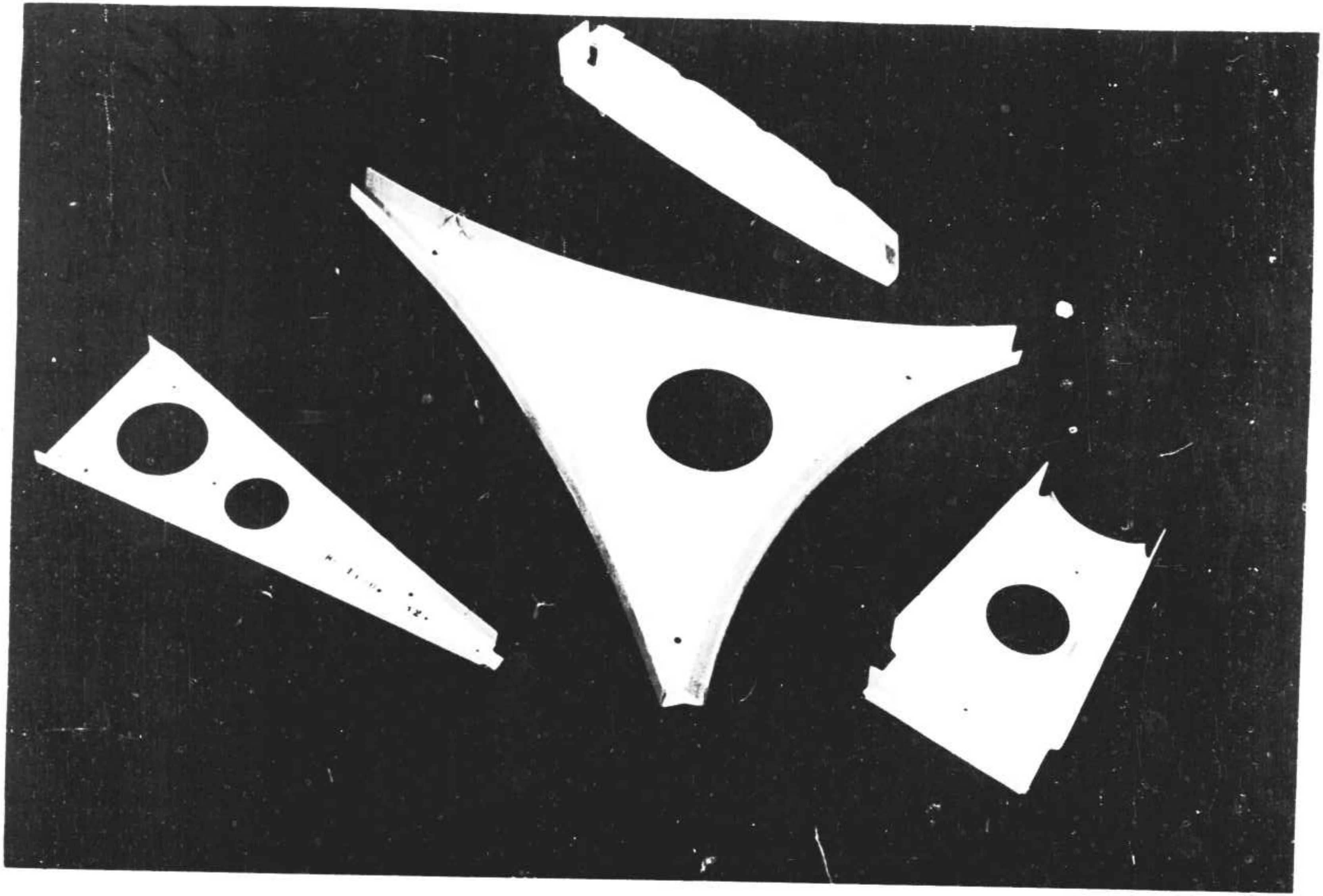

FIGURE 53 - TYPICAL HAND FORMED PARTS OF MAGNESIUM ES1-[illegible] [illegible]

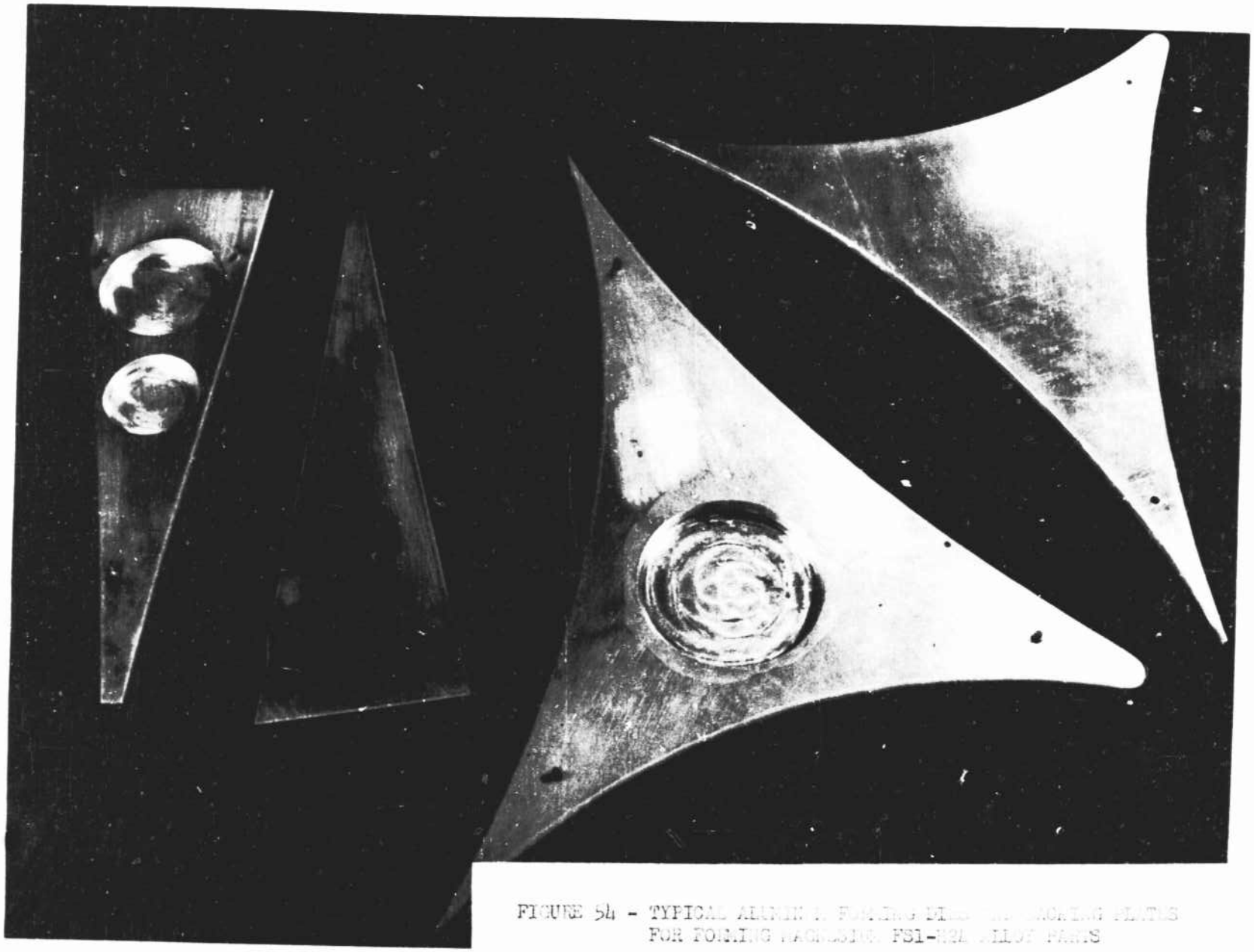

FIGURE 54 - TYPICAL ALUMINUM FORMING DIES AND MATCHING PLATES FOR FORMING MACHINING FS1-HSA SKIN PANELS

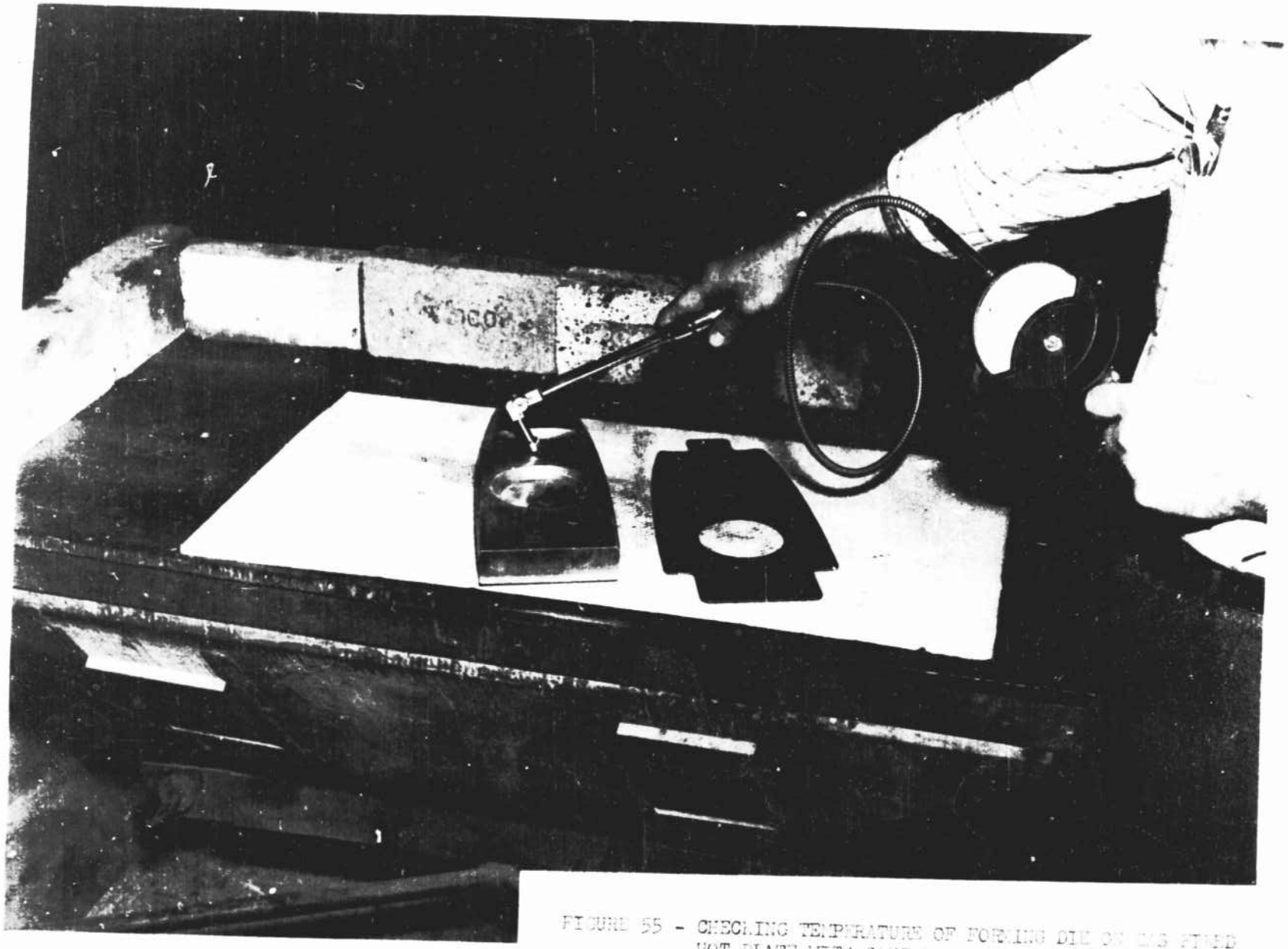

FIGURE 55 - CHECKING TEMPERATURE OF FORMING DIE ON [illegible] HOT PLATE WITH CONTACT PYROMETER

In preparing the blank material for bending, it is necessary to deburr and polish the ends of the blank in the region of the bend in order to prevent cracking of the material. Whenever possible, bends should be made parallel to the grain direction because of the greater elongation of magnesium sheet in the transverse direction.

Typical brake bend formed parts of FS1-H24 magnesium sheet are shown in Figures 56 and 57. Flanged lightening holes are preformed prior to brake bending.

When the radius of bend is large enough to permit cold forming, ordinary bending rolls are satisfactory for forming single-curvature magnesium alloy sheet and extrusion.

Extrusion Bending

Bars and extrusions can be bent in production on standard equipment, such as angle rolls, stretch formers, tangent benders or in press dies. Parts are preheated depending on the severity of the bend, shape, size, and alloy of the material. Torch heating and hand forming are often used where small number of parts are to be formed.

The maximum formability of ZK-60-A magnesium alloy extrusions is obtained at about 500 deg. F. In the aged condition (ZK-60A-T5), the metal is formed at 350 deg. F or less to prevent loss of room temperature properties. If the time at these temperatures is limited to 1/2 hour, there will be no significant decrease in room temperature tension or compression properties.

Allowable bend radii depend on the shape and cross section of the extrusion. On simple sections, bend radii of 2t have been obtained at 500 deg. F, increasing to 8t at 300 deg. F, and 10t to 12t at room temperature for ZK-60A magnesium alloy extrusion. For ZK-60A-T5 magnesium alloy extrusion in the heat-treated and aged condition, allowable bend radii of 8t at a working temperature of 350 deg. F can be obtained on a simple section.

Shallow Drawing and Pressing

In shallow drawing, the parts are more pressed than drawn, since there is very little metal flow. Wing ribs, door-reinforcing panels, and fairings are typical examples of parts fabricated by this method. The Guerin process of using a rubber pad as the female die is most frequently used. In the Guerin process, a rubber pad 6 to 10 inches thick of about 60 Durometer is contained in a metal box and acts as the female die. In adapting this process to magnesium forming, it is necessary to use heated dies. This is accomplished by placing the dies on a heated platen or for more complicated dies, by inserting heating elements into the die itself. When parts are relatively small and flat, they will absorb sufficient heat for forming from the dies; however, work blanks for larger and more intricate parts should be preheated.

To prevent the rubber from sticking to the formed part, cornstarch or flaked mica is spread on the backing plate and along the exposed parts of the blank prior to pressing. Ordinary rubber is satisfactory for temperatures up to 350 deg. F. Synthetic rubbers or specially compounded natural rubbers are required for higher working temperatures up to 450 deg. F.

In preparing the blank material for bending, it is necessary to deburr and polish the ends of the blank in the region of the bend in order to prevent cracking of the material. Whenever possible, bends should be made parallel to the grain direction because of the greater elongation of magnesium sheet in the transverse direction.

Typical brake bend formed parts of FS1-H24 magnesium sheet are shown in Figures 56 and 57. Flanged lightening holes are preformed prior to brake bending.

When the radius of bend is large enough to permit cold forming, ordinary bending rolls are satisfactory for forming single-curvature magnesium alloy sheet and extrusion.

Extrusion Bending

Bars and extrusions can be bent in production on standard equipment, such as angle rolls, stretch formers, tangent benders or in press dies. Parts are preheated depending on the severity of the bend, shape, size, and alloy of the material. Torch heating and hand forming are often used where small number of parts are to be formed.

The maximum formability of ZK-60-A magnesium alloy extrusions is obtained at about 500 deg. F. In the aged condition (ZK-60A-T5), the metal is formed at 350 deg. F or less to prevent loss of room temperature properties. If the time at these temperatures is limited to 1/2 hour, there will be no significant decrease in room temperature tension or compression properties.

Allowable bend radii depend on the shape and cross section of the extrusion. On simple sections, bend radii of 2t have been obtained at 500 deg. F, increasing to 8t at 300 deg. F, and 10t to 12t at room temperature for ZK-60A magnesium alloy extrusion. For ZK-60A-T5 magnesium alloy extrusion in the heat-treated and aged condition, allowable bend radii of 8t at a working temperature of 350 deg. F can be obtained on a simple section.

Shallow Drawing and Pressing

In shallow drawing, the parts are more pressed than drawn, since there is very little metal flow. Wing ribs, door-reinforcing panels, and fairings are typical examples of parts fabricated by this method. The Guerin process of using a rubber pad as the female die is most frequently used. In the Guerin process, a rubber pad 6 to 10 inches thick of about 60 Durometer is contained in a metal box and acts as the female die. In adapting this process to magnesium forming, it is necessary to use heated dies. This is accomplished by placing the dies on a heated platen or for more complicated dies, by inserting heating elements into the die itself. When parts are relatively small and flat, they will absorb sufficient heat for forming from the dies; however, work blanks for larger and more intricate parts should be preheated.

To prevent the rubber from sticking to the formed part, cornstarch or flaked mica is spread on the backing plate and along the exposed parts of the blank prior to pressing. Ordinary rubber is satisfactory for temperatures up to 350 deg. F. Synthetic rubbers or specially compounded natural rubbers are required for higher working temperatures up to 450 deg. F.

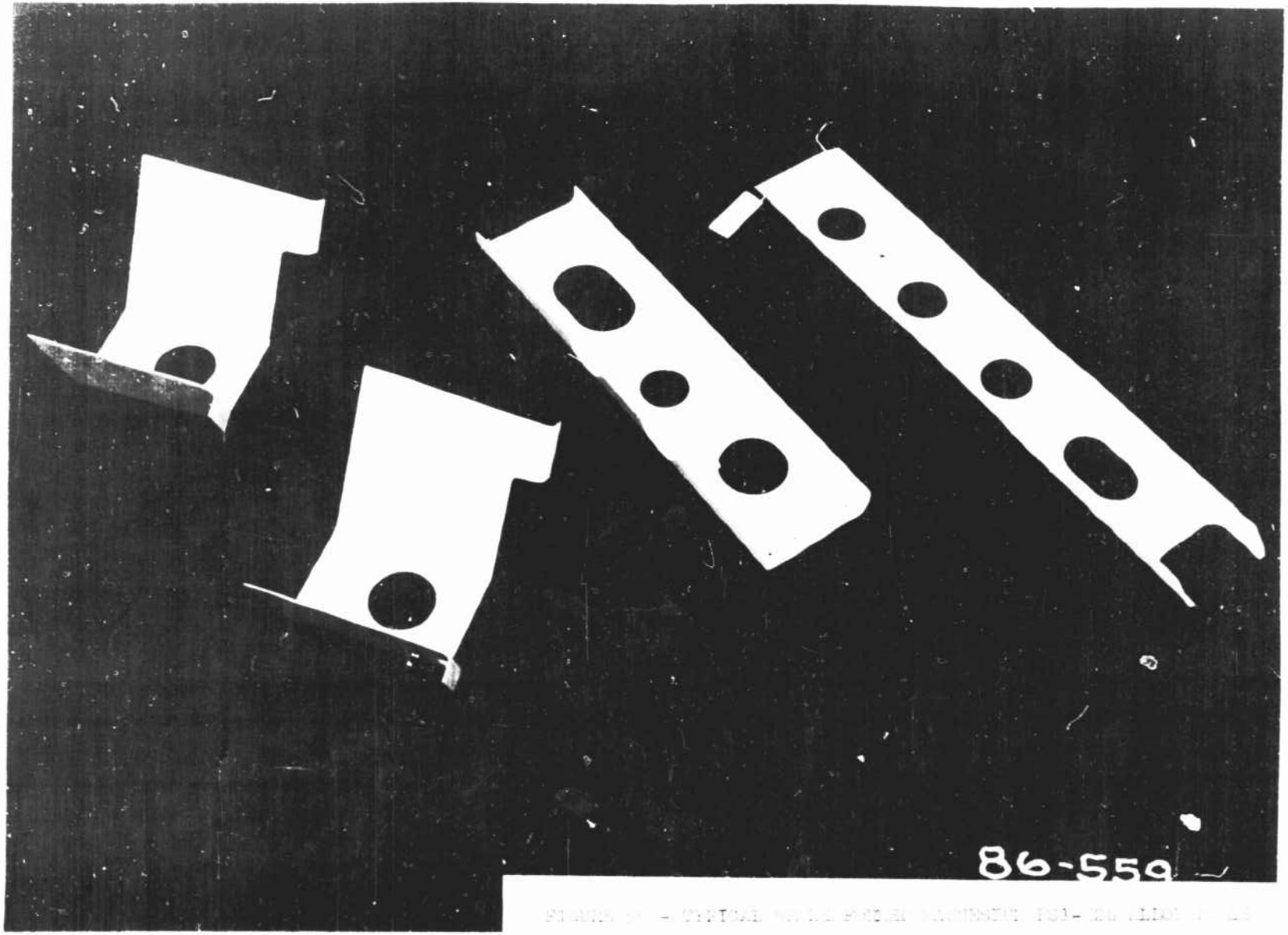
86-559

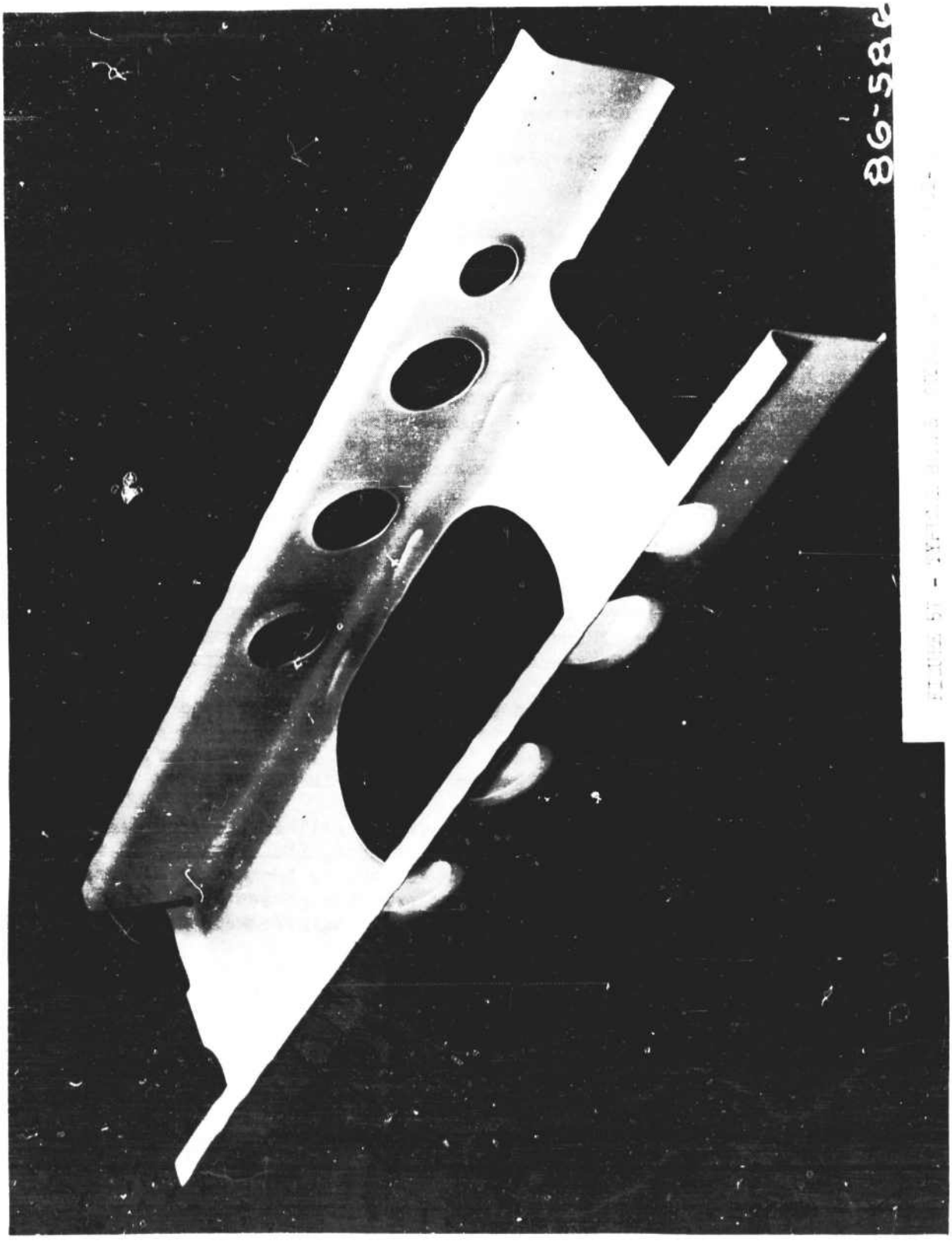
86-58

In using the Guerin process for forming ribs and bulkheads, a metal backing plate should be used in conjunction with the die. This backing plate, when placed over the blank to be formed, would stabilize the web thus reducing the tendency for the web to wrinkle. The use of the backing plate results in less rework of formed parts.

If a few parts are required and the forming die is relatively small, preheating of the die and backing plate can best be done on a hot plate. The hot plate should be placed close to the press and a thin asbestos sheet should be placed between the die and the press platen in order to avoid loss of heat to the press platen.

Some typical formed parts are shown in Figures 58 to 61. Typical aluminum dies and backing plates are shown in Figure 62.

Drop Hammer Forming

Magnesium alloy sheet is most formable by methods involving slowest rates of loading which is definitely not the characteristic of the drop hammer. This means that maximum temperatures must be used to take advantage of the higher elongation and the rapid impact action of the hammer must be slowed to a minimum. The forming machines that can be used include the free fall, rope controlled hammers, and the pneumatic Chambersburg Cecostamps.

Die heating is accomplished in two ways, either by an electrically heated platen installed on the bed of the hammer or by torch heating the die. In order to prevent creep or the danger of flattening, the Kirksite die which is normally used, is limited to a temperature of 300 deg. F. This temperature is considered the maximum allowable temperature for Kirksite. The temperature of the lead punch is maintained at 200 deg. F and is heated by conduction from the die. It is felt that the maximum permissible temperature for the lead punch is 200 deg. F.

For heating of flat sheet or formed parts, circulating air type ovens are recommended. However, a Propane burning torch may be used for small production runs providing a contact pyrometer is used to check the temperature of the work so as to avoid overheating. A typical set up is shown in Figure 68.

In order to reduce the tendency for magnesium to gall at elevated temperatures, a drawing lubricant is necessary. Colloidal graphite suspended in a suitable carrier can be used providing the formed part is thoroughly cleaned after forming. However, it is well to point out that graphite presents a difficult cleaning problem. A satisfactory substitute such as vegin reduces the problem of cleaning to some extent.

In order to take advantage of the higher mechanical properties of hard rolled magnesium alloy sheet FS1-H24, an attempt was made to form .064 gage FS1-H24 magnesium alloy sheet by means of the drop hammer. Based on minimum mechanical properties of the material, the time-temperature relationship was limited to 350 deg. F $\pm$25 deg. This limitation on the temperature range was felt to be the maximum allowable temperature consistent with the strength requirements.

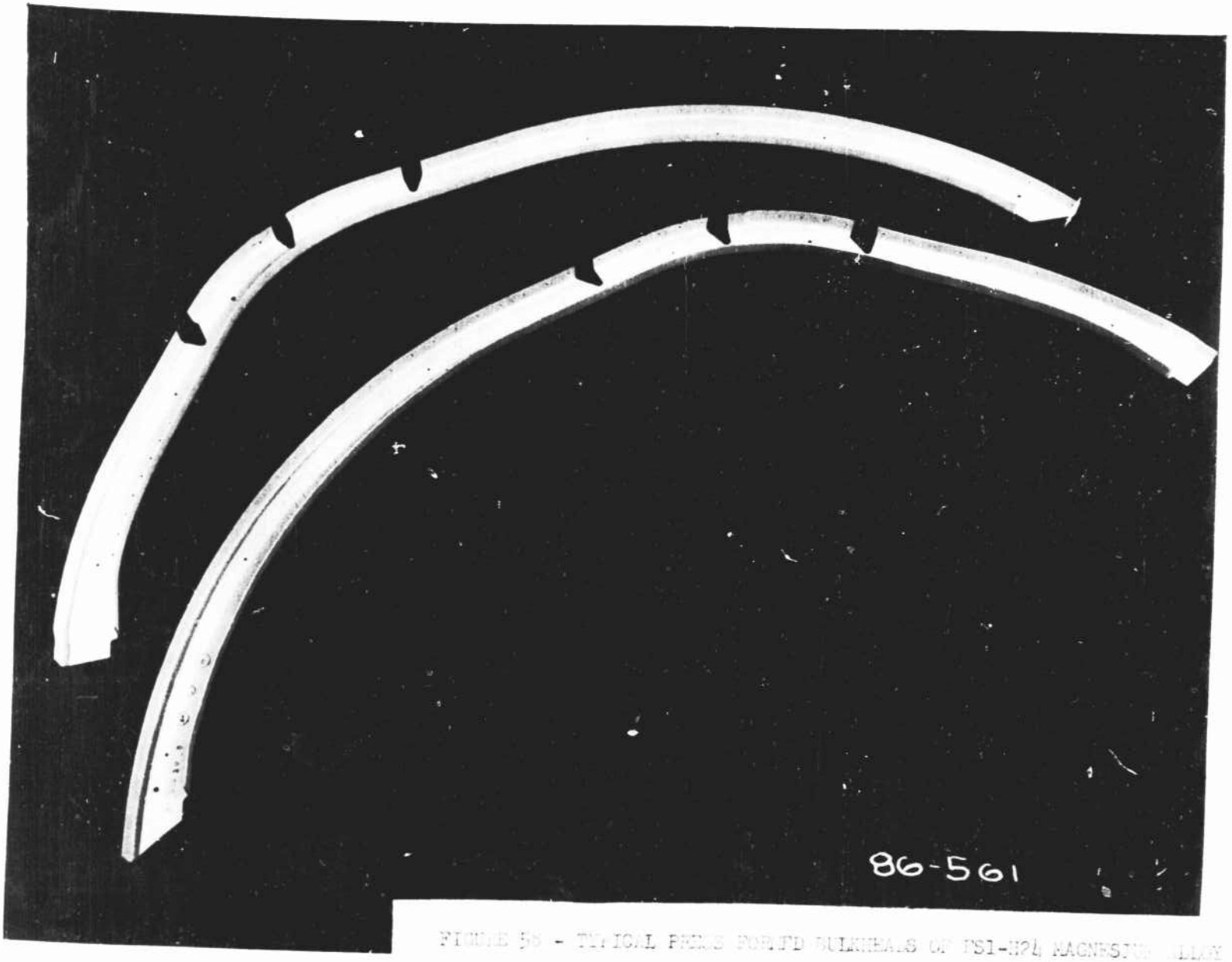

FIGURE 56 - TYPICAL FIELD WELDED BULKHEADS OF TSI-H24 MAGNESIUM ALLOY

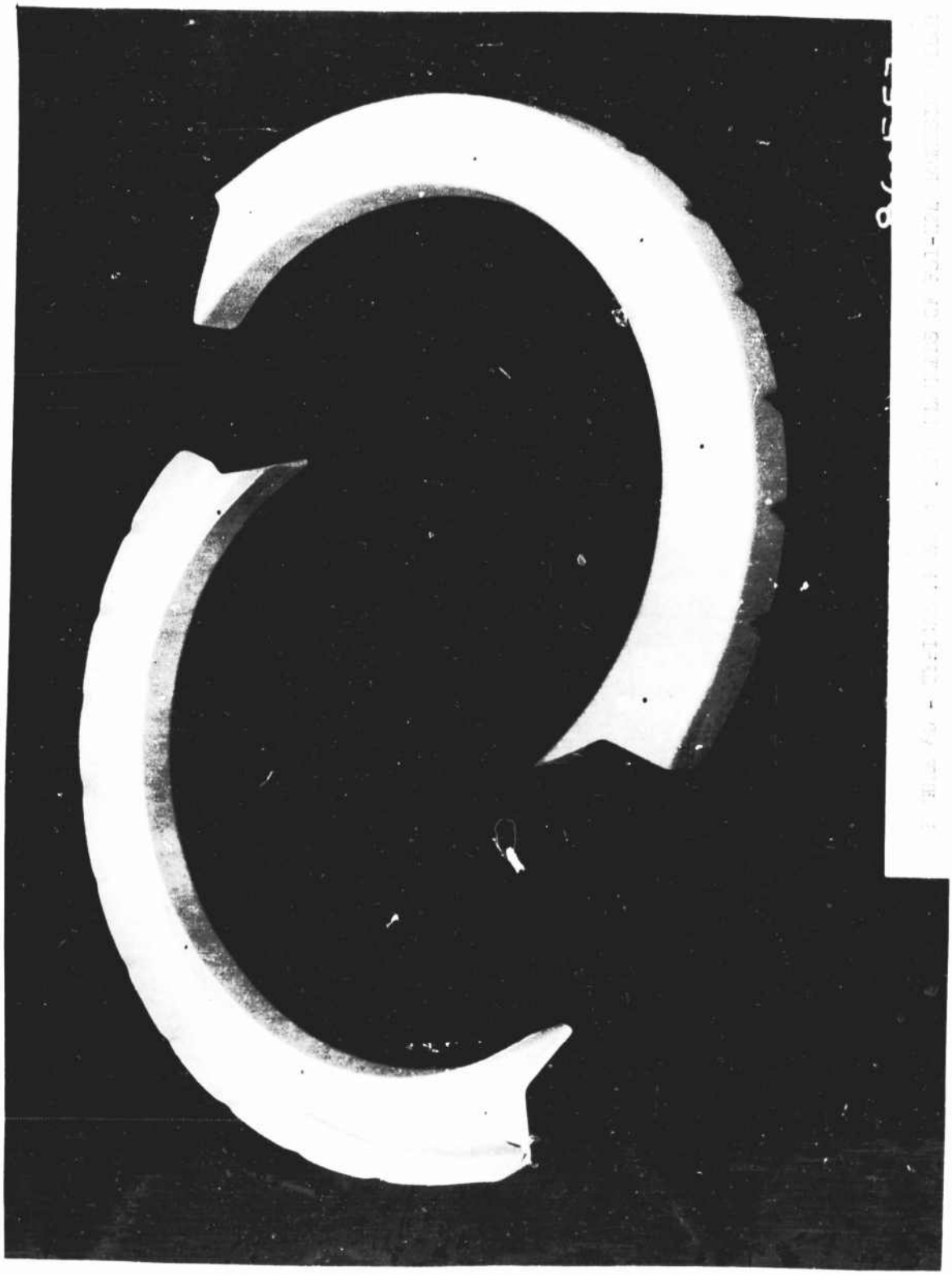

86-587

Numerous tests were conducted without any success. A typical failure specimen is shown in Figure 63. It is well to point out that the formability of the material would increase with a further increase in temperature but, the time of exposure at temperature is not considered practical as can be seen from an examination of Figure 47.

Based on the tests conducted on FS1-H24 magnesium alloy sheet, the use of the drop hammer in hot forming FS1-H24 magnesium alloy sheet is not recommended unless forming is limited to simple shapes having maximum compression of approximately five percent or pure stretch of about ten percent.

Additional tests were conducted to form FS1-O magnesium sheet in the annealed condition. It has been found that this material is more suitable for drop hammer forming.

For annealed magnesium sheet the time-temperature relationship is relatively simple since property reduction is not a problem and grain growth becomes the major item of concern in the region over 600 deg. F. As a result 500 deg. F was chosen for the maximum allowable temperature and the time of exposure was chosen as one hour.

Typical hammer formed parts from annealed magnesium sheet are shown in Figures 69 and 70.

The Kirksite dies used for the drop hammer work were fabricated from a male template build-up. This build-up is used as the mold pattern after the voids in the build-up are filled with plaster of paris and also used as a check fixture to check the contour of the formed parts.

Typical build-ups are shown in Figures 71 and 72.

Based on results obtained, magnesium alloy sheet in the annealed condition is as formable in the upper temperature limit as 3S-O aluminum sheet. Fewer compression wrinkles occur from the use of magnesium sheet than from the use of 24S-O in the same die. However, when severe drawing is necessary, drop hammer forming is not recommended. Drop hammer forming of magnesium alloy should be limited to shallow draws and stampings which should be done at approximately 500 deg. F.

The formability of hard rolled sheet in the drop hammer at 375 deg. F is only slightly better than that of 75S-T6 aluminum alloy at room temperature.

MACHINING OF MAGNESIUM

One of the outstanding advantages of magnesium alloy is its excellent machining characteristics. Magnesium alloy can be machined at extremely high speeds; usually at the maximum obtainable on modern machine tools. Heavier depths of cut and higher rates of feed than are used on other metals are possible with magnesium. In spite of this, the life of cutting tools is excellent, especially when using carbide tipped tools. The surface finish when

#1-375

FIGURE 61 - KIRSITE DROP HAMMER PIE

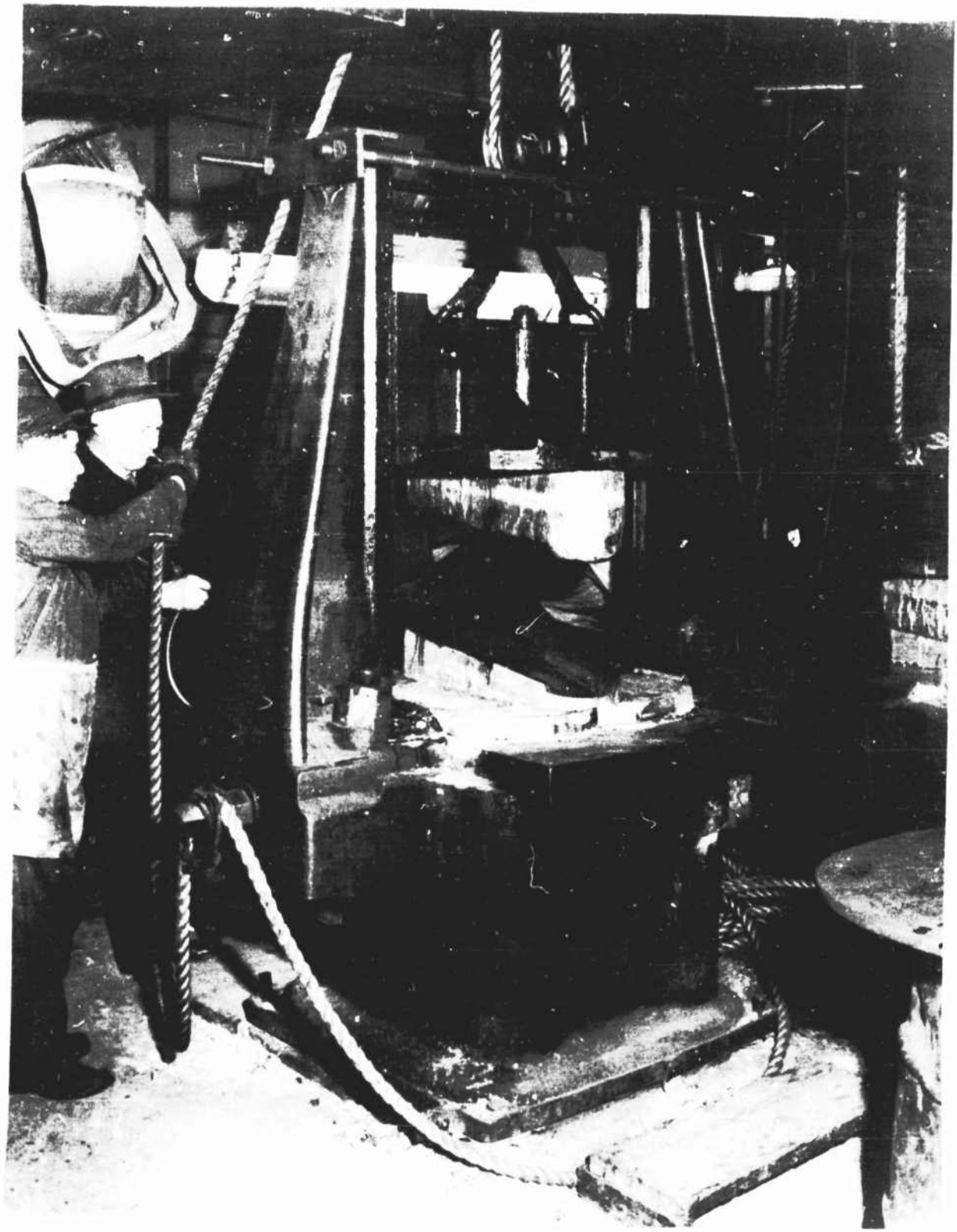

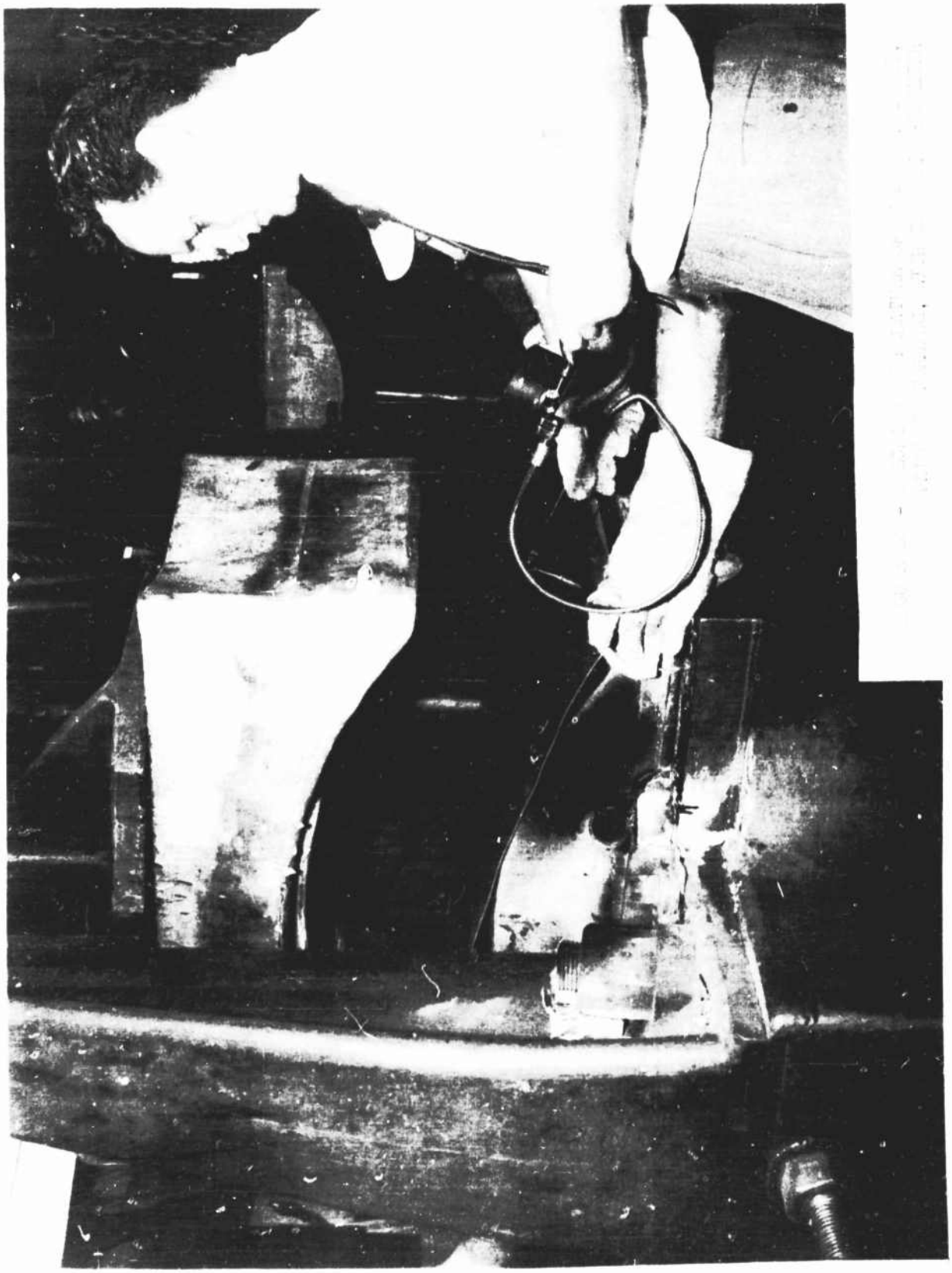


86-520

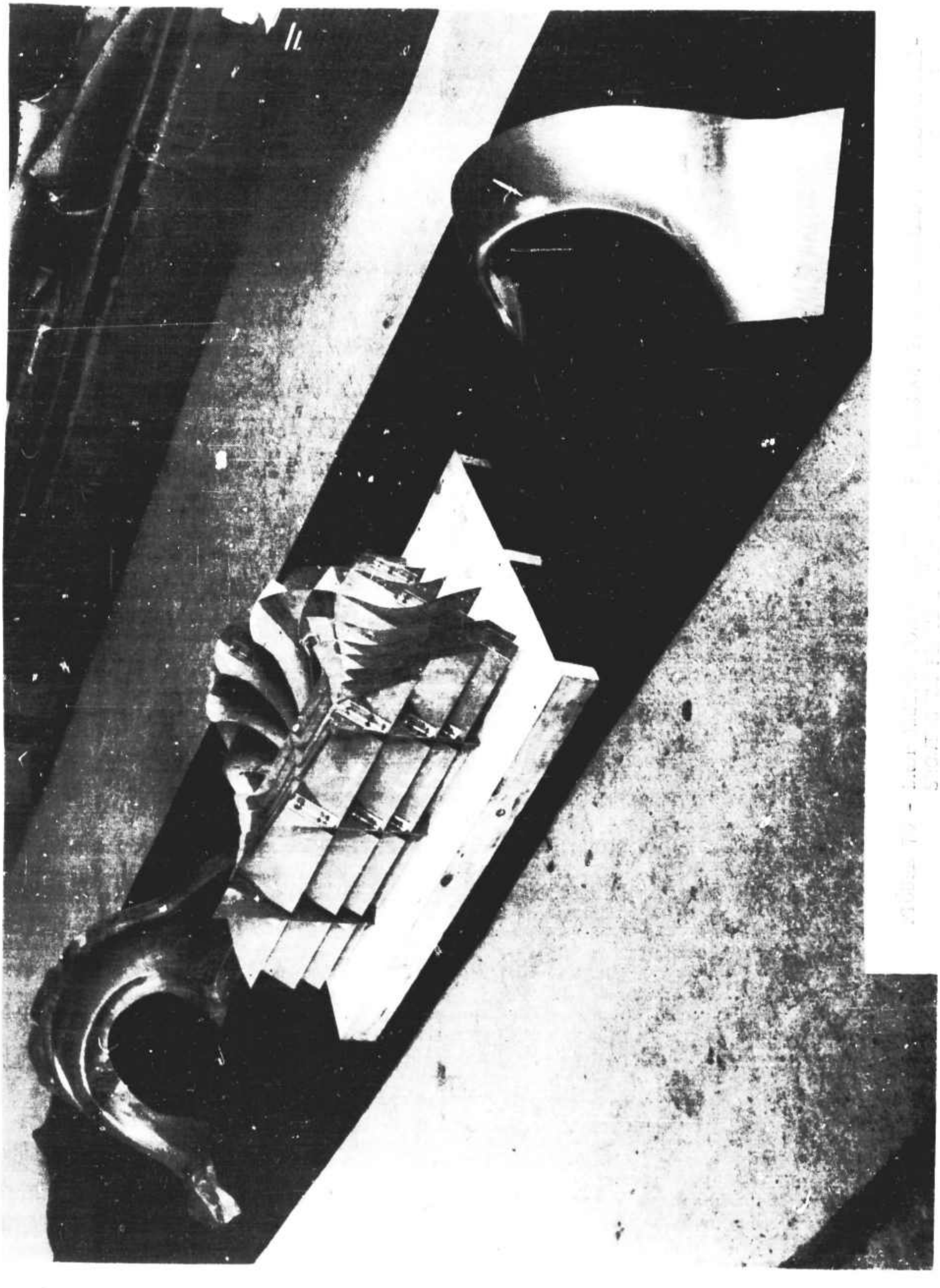

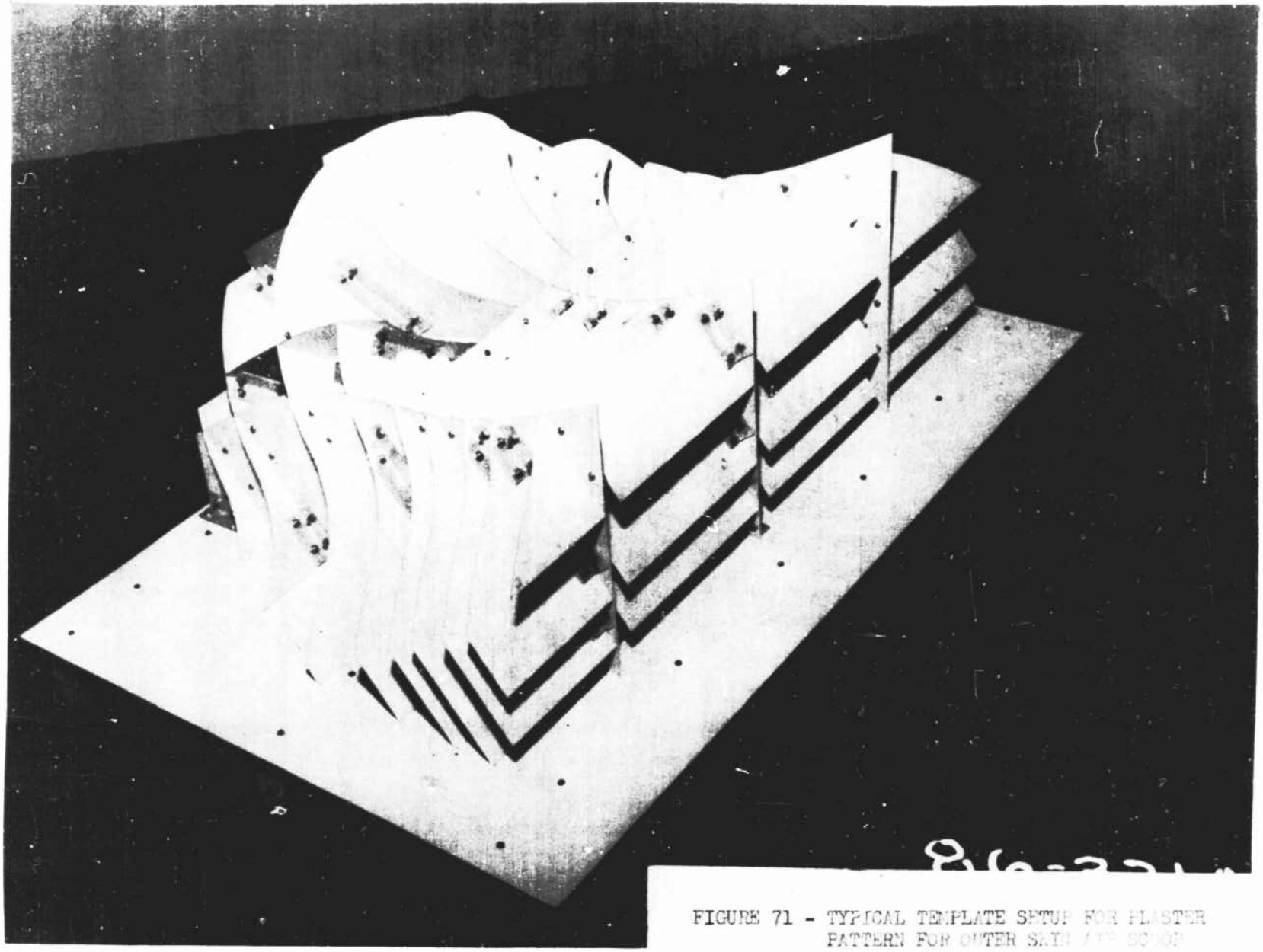

FIGURE 71 - TYPICAL TEMPLATE SETUP FOR PLASTER PATTERN FOR OUTER SKIN AFT DOOR

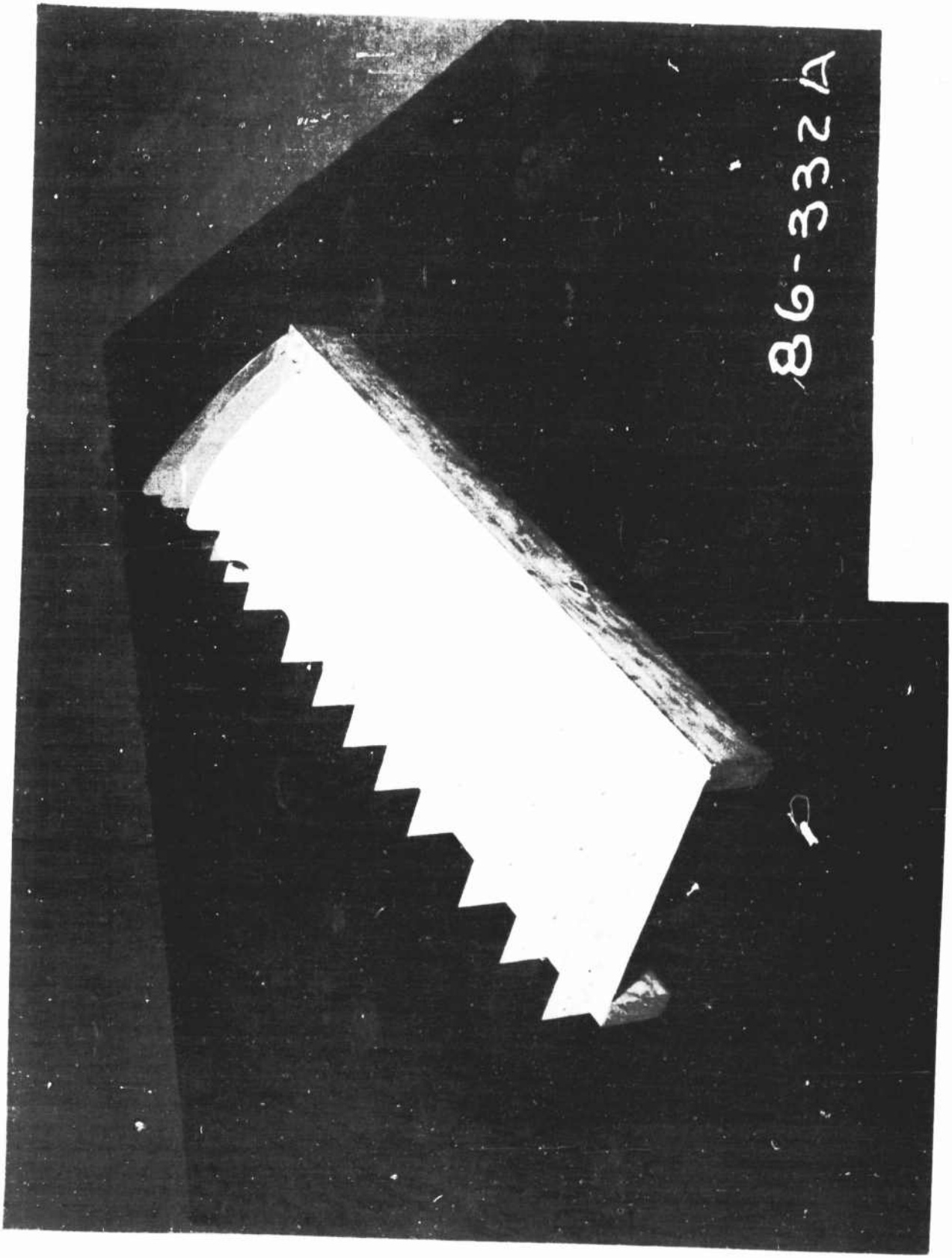
86-332A

machining magnesium is excellent because there is no tendency for the metal to tear or drag. The free cutting action of magnesium produces well broken chips which do not obstruct the cutting tools or the machine. Extremely accurate parts with dimensional tolerances of only a few ten thousandths of an inch can be made by standard machining operations. The power required to remove a given amount of metal is much lower for magnesium than for any other commonly used metal.

Tools for cutting steel will often perform satisfactorily on magnesium; however, better results may be obtained by modifying the cutting tools to take advantage of the lower cutting resistance and lower specific heat.

When machining magnesium, tools can generally be ground with sharper cutting angles, since required cutting pressures are lower than with other metals and the edge consequently requires less backing. It is essential that the cutting edges be kept sharp and that the tool faces be polished in order to insure free cutting action and also to reduce the tendency for magnesium particles to adhere to the tool tip. The tool clearances should be large, 10 to 15 degrees, and tools should be designed to allow for ample chip room. Large feeds may be used as this will reduce the amount of frictional heat developed.

Turning and Boring

Lathe set-ups, with due consideration of the more careful chucking of magnesium and slight differences in tool design, are similar to that used for steel. The turning tool design may be considered as a compromise between the conflicting requirements of high cutting capacity and long tool life. It should be noted that an increase in rake will reduce the cutting power required; however, it would also reduce the tool life.

Typical turning tool angles for cutting magnesium are shown in Table I. Included in this table are the values for other metals. The terminology employed is that of the American Standards Association as shown in Figure 73.

Table I - Typical Turning Tool Angles

	Soft Steel *	Magnesium	Aluminum **
Back Rake	8°	10 - 20°	30 - 50°
Side Rake	22°	5 - 10°	10 - 20°
Side Relief	6°	8 - 15°	8 - 10°
End Relief	6°	8 - 15°	8 - 10°
End Cutting Edge Angle			
Roughing Tool		15°	
Finishing Tool	6°	5°	
Side Cutting Edge Angle			
Roughing Tool		15 - 25°	
Finishing Tool	45°	10°	

* Reference 4, page 905.

** Reference 4, page 1315.

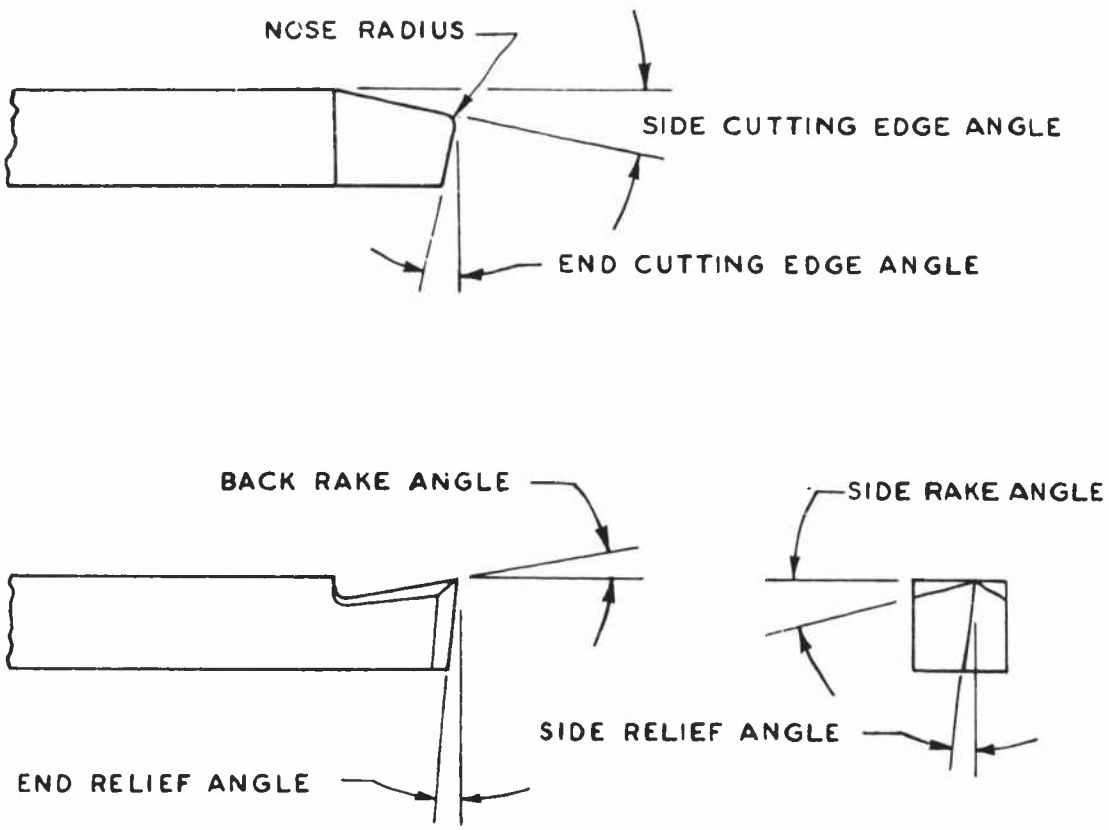

FIG. 73 — TERMINOLOGY OF SINGLE POINT TOOLS ACCORDING TO THE AMERICAN STANDARDS ASSOCIATION

When carbide tipped tools are used, the rake angles noted in Table I should be slightly smaller to provide more support for the cutting edge. In reference to the side and end cutting edge angles, they may be varied widely to suit the particular job, but side cutting edge angles above approximately 40 deg. may cause chatter. Nose radii should be kept small to avoid rubbing of the work on the end of the tool thus avoiding overheating of the work and reducing the fire hazard.

For the speeds, feeds, and depths of cut for turning and boring magnesium, the general rule is to turn and bore magnesium as fast as the machine tool, fixture, and work will allow.

Table II presents general recommendations for determining depths of cut, feed, and speeds for turning and boring magnesium. The data was obtained from Table 3 of Reference 5.

Table II - Recommended Speeds, Feeds, and Depth of Cut For Turning and Boring Magnesium

Operation	Speed fpm	Feed ipr	Max. Depth of Cut Inches
Roughing	300 - 600	0.030 - 0.100	0.500
	600 - 1000	0.020 - 0.080	0.400
	1000 - 1500	0.010 - 0.060	0.300
	1500 - 2000	0.010 - 0.040	0.200
	2000 - 5000	0.010 - 0.030	0.150
Finishing	300 - 600	0.005 - 0.025	0.100
	600 - 1000	0.005 - 0.020	0.080
	1000 - 1500	0.003 - 0.015	0.050
	1500 - 2000	0.003 - 0.015	0.050
	2000 - 5000	0.003 - 0.015	0.050

Shaping and Planing

Practically the same tool design and machining recommendations as outlined for turning and boring can be applied to the shaping and planing of magnesium. Deviations from the recommended tool shapes can be made in accordance with the particular job as long as sharp cutting edges and sufficient relief angles are used.

In shaping and planing, the maximum cutting speeds are much lower than the recommended cutting speeds for turning and boring. Economies in operation are usually affected through use of heavy feeds and depths of cut which are made possible by the lower power required to machine magnesium. Cutting fluids are usually unnecessary inasmuch as the cutting speeds used do not create a fire hazard.

Milling

Milling operations provide an opportunity to take full advantage of the excellent machining characteristics of magnesium. Heavy feeds and extremely

high milling speeds can be used to remove metal rapidly with excellent surface finish.

The tooth design of the milling cutter for magnesium is similar to that for aluminum alloys, but differs from that customarily used for steel by having higher rakes, greater reliefs and increased chip space. For a given cutter diameter, the recommended number of teeth for cutting magnesium is about two-thirds of that used for aluminum, and one-half to one-third of that used for steel. This reduction is made possible by the low cutting resistance of magnesium. Furthermore, fewer teeth are desirable in order to reduce the amount of heat generated in cutting and to provide ample chip space.

High-speed steel can be used satisfactorily on all types of milling cutters but cemented carbides are superior for inserted tooth face mills and fly cutters which operate at high speeds. Single and multiple tooth fly cutters perform exceptionally well on magnesium alloys.

Approximate tool angles for various types of milling cutters are shown in Figure 74. Negative face rake angles are sometimes used on face mills to throw the chips out of the cutter. Helical slab mills should have helix angle of approximately 45 degrees.

If a limited production is required, it has been found that standard milling cutters used for aluminum can be used for machining magnesium alloy providing that the teeth are ground to provide for larger peripheral clearance of approximately 10 deg. followed by a secondary clearance of approximately 20 deg. When using standard cutters reground as noted, the cutting speeds must be reduced due to the increase in frictional heat generated by the larger number of cutting teeth and the reduced chip clearance.

Approximate cutting speeds to be used in milling operations for magnesium alloy are presented in Table III and were obtained from Table 4, Reference 5. Since a wide variety of feeds and depths of cut are possible, only general recommendations are presented.

Table III - Recommended Speeds, Feeds, and Depths of Cut For Milling Magnesium

Operation	Speed fpm	Feed		Depth of Cut Inches
		In/Min.	In/Tooth	
Roughing	Up to 900	10 to 50	0.005 to 0.025	Up to 0.500
	900 to 1,500	10 to 60	0.005 to 0.020	Up to 0.375
	1,500 to 3,000	15 to 75	0.005 to 0.010	Up to 0.200
Finishing	Up to 900	10 to 50	0.005 to 0.015	Up to 0.075
	1,000 to 3,000	10 to 70	0.004 to 0.008	0.005 to 0.050
	3,000 to 5,000	10 to 90	0.003 to 0.006	0.003 to 0.030
	5,000 to 9,000	10 to 120	0.002 to 0.005	0.003 to 0.030

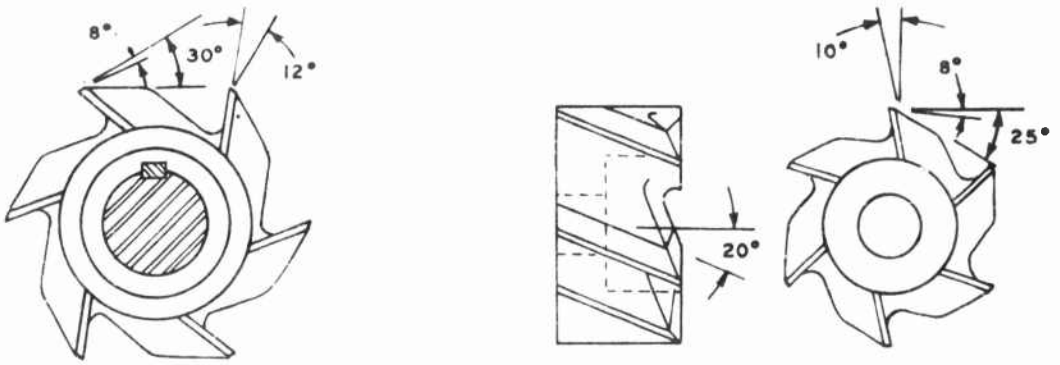

COARSE TOOTH MILLING CUTTER

SHELL END MILL

FIG. 74 — TYPICAL MILLING CUTTERS RECOMMENDED FOR USE ON MAGNESIUM

Drilling

Best results in drilling magnesium alloy are obtained if the drills are correctly designed for the type of drilling being performed. Three types of drills will effectively service all drilling operations. These types of drills include drills for sheet metal, shallow holes (depth less than five times the drill diameter), and deep holes.

Standard high speed twist drills with a helix angle of approximately 35 - 40 deg. and standard point angles of 118 deg. are satisfactory for drilling magnesium alloy providing that the flutes are highly polished to facilitate the flow of chips out of the hole. It is also extremely important, no matter what type of drill is used, that the cutting edges be kept sharp. Dull drills give poor surface finish, undersized holes and burrs, and tend to heat up the work.

For maximum production and quality of drilled holes, slight modifications of standard drills are recommended for drilling sheet and deep holes. The modified drill for drilling magnesium sheet should have a point angle of approximately 60 deg. in order to prevent "walking" of the drill, the reduce thrust, and to prevent abrupt change of thrust when breaking through. A helix angle of approximately 10 deg.will prevent the work from climbing the drill on the break-through.

Drilling deep holes in magnesium produces an appreciable quantity of chips which must be guided out of the hole through a considerable length of drill flute. High-helix drills (40 - 45 deg.) will do this satisfactorily. Flutes should be opened and polished to provide larger chip spaces and smooth surfaces to aid in chip removal. Drills with low helix angles and with unopened flutes may cause chips to jam, resulting in high torques and poor surface finish. The latter type of drill will have to be withdrawn frequently to clear the flutes, whereas a high-helix drill can penetrate to 25 times the drill diameter in a single pass.

In reference to the chisel edge angle of the drill for deep-hole drilling in magnesium alloy, angles of 135 - 150 deg. are recommended and are considered essential in order to provide a good surface finish and to minimize the tendency of spiralling in the hole. Angles smaller or larger than those recommended cause difficulties due to improper relief at the cutting edge and the lack of proper centering of the drill. The standard drill point angle of 116 - 118 deg. has been found to be the most satisfactory; however, to reduce spiralling and to insure straight smooth holes, a spur or pilot point of 60 deg. ground at the center of the drill is recommended.

The fact that a drill made to the design recommendations for deep hole drilling in magnesium alloy can be used to drill holes up to 25 times the drill diameter without withdrawing the drill to clear the flutes is of particular importance in the use of multiple spindle or automatic drilling machines.

Recommended speeds and feeds for drilling magnesium are presented in Table IV. Wide deviations from the recommended feeds can be used when drilling shallow holes but the recommendations for deep hole drilling should be closely followed for best results.

Table IV - Recommended Speeds and Feeds for Drilling Magnesium

Drill Dia. Inches	Speed fpm	Sheet	Feed - ipr	
			Shallow Holes*	Deep Holes**
1/4	300	0.005 to 0.030	0.004 to 0.030	0.004 to 0.008
1/2	to	0.010 to 0.030	0.015 to 0.040	0.012 to 0.020
1	2,000	0.010 to 0.030	0.020 to 0.050	0.015 to 0.030

Table IV was obtained from Reference 5.

* Depth less than 5 times drill diameter.
** Depth greater than 5 times drill diameter.

Reaming

For most reaming of magnesium alloy, carbon tool steel reamers are quite satisfactory. High-speed steel tools (or carbide-tipped, in some cases) are more feasible for long production runs.

Reamers for magnesium alloys should have fewer flutes than normal for best results. Reamers under approximately one inch in diameter should have four flutes, while those over one inch in diameter should have six flutes. The flutes may be straight (0 deg. helix angle) or have a negative helix angle of approximately 10 degrees.

For best results, reamer blades should have a positive rake of about 5 to 9 deg., a marginal width of 0.010 to 0.025 inches, ground to a relief of about 4 to 7 deg. and blending into a 15 to 20 deg. clearance angle.

The reaming allowance on drilled holes should be sufficient to permit the reamer to take a positive cut, thereby avoiding compression of the metal through burnishing and resultant poor finish and undersized holes. An allowance of approximately 1/32 of an inch on a diameter should be sufficient for reaming holes in magnesium alloys.

Cutting Fluids

The use of cutting fluids when machining magnesium is primarily to cool the work and reduce the possibility of distrotion of the work and ignition of fine chips. The improvement in surface finish and increased tool life which cutting fluids accomplish on other metals are minor considerations in the machining of magnesium. Such fluids are referred to as "coolants" when used on magnesium.

While less heat is generated in cutting magnesium than is the case with other metals, the high cutting speeds, the high thermal expansion, and the low heat capacity of magnesium make it necessary in some machining operations that the heat developed in cutting be dissipated. Machining heat may be reduced by correct tooling and machining techniques, but is often of such intensity that application of cutting fluids is necessary. The machining of irregular shapes or thin sections which might be easily distorted and multi-tool set-ups which create much local heating, are examples of cases where cooling should be employed.

When high cutting speeds and low feeds are used in machining magnesium alloy, a fire hazard sometimes exists, particularly when fine chips are being produced. Although sharp tools greatly reduce this hazard and cutting feeds must be in the range of 0.001 inch and less to start fires, uncertainties in operations make it necessary to take precautions against this hazard. A stream of cutting fluid, of four to five gallons per minute per tool, is sufficient to practically eliminate the fire hazard. If a particular job or machine tool prohibits the use of a cutting fluid, cutting speeds should be reduced to below 500 feet per minute and the recommendations regarding sharp tools and feeds should be rigorously followed. In all machining operations where a low cutting speed is used, magnesium may be safely machined without a cutting fluid, but safe practice dictates that where high cutting speeds are used cutting fluids should also be used.

A wide variety of mineral oil cutting fluids will function satisfactorily on magnesium.

Properties of cutting fluids recommended for machining magnesium are as follows:

Specific Gravity	0.79 to 0.86
Viscosity (Saybolt) @ 100°F	Up to 55 sec.
Flash Point - Min. Value (Closed Cup)	160°F
Saponification No. (Max.)	16
Free Acid (Max.)	0.2%

The chemical nature of magnesium makes it necessary that the free acid content of cutting fluids be below 0.2% and that the use of vegetable or animal oils, which may oxidize and increase the acid content, be restricted.

Water soluble oils, oil water emulsions or water solutions of any kind, although they are good coolants, should not be used on magnesium. Water will greatly intensify any chip fires which might accidently be started.

Fire Hazard Due to Machining

Magnesium alloys must be heated to their melting points before they will ignite. Roughing cuts and medium finishing cuts produce chips of such a size that they are not readily ignited during machining. Fine cuts, however, produce chips which sometimes will ignite if produced at high cutting speeds. Stopping the feed and letting the tool dwell before disengagement, and letting the tool or tool holder rub on the work will produce extremely fine chips; consequently, these practices should be avoided.

Factors tending to increase the fire hazard are: high cutting speeds, extremely fine feeds, dull or chipped tools, improperly designed tools, and poor machining techniques. With sharp cutting tools, it is necessary to use a feed of less than 0.001 inches and cutting speeds in excess of 1,000 feet per minute to create a serious fire hazard. Even under the most adverse conditions, that is with dull tools and fine feeds, the fire hazard is very slight at speeds below approximately 700 feet per minute.

Sand cast surfaces, oxide inclusions, and ferrous inserts which will cause sparks when hit by the cutting tool, increase the possibility of fire.

The use of a sufficient quantity of cutting fluids will practically eliminate any possibility of fire when machining magnesium at any cutting speeds.

Distortion of Machined Parts

Distortion of magnesium parts occurs infrequently during machining and usually can be attributed to heating of the part or to improper chucking.

The problem of distortion caused by heating of the part during machining can be reduced by using sharp, properly designed tools and relatively large feeds and depths of cut to prevent excessive heating. An adequate quantity of cutting fluid also will remove the heat developed in cutting and eliminate thermal expansion.

The fact that magnesium will spring more easily than most metals makes it essential that parts be chucked in such a manner that the clamping pressure is applied to heavy sections and that the pressure is not great enough to cause distortion. Special attention should be paid to light parts which might easily be distorted by chucking or heavy cuts. Once acquainted with this characteristic of magnesium alloys, the machinist can easily avoid difficulties due to chucking.

Distortion of magnesium parts is seldom due to stresses induced during casting, forging, or extruding; but may be due to stresses caused by straightening of parts. These stresses can be relieved prior to machining by heating at 325 - 450 deg. F for 1 to 2 hours depending on the alloy and temper, and slowly cooling. If distortion of parts occurs after rough machining, the size of cuts should be decreased and the cutting tools inspected to insure that they are properly ground and in good condition. These steps usually eliminate any difficulties but it may be necessary to stress relieve or store parts for two or three days prior to finish machining. This procedure usually is necessary only on complex parts having extremely close tolerances.

MACHINE-TAPERED MAGNESIUM SKINS

To obtain maximum beam bending efficiency for minimum weight and to avoid skin splices, the horizontal stabilizer of the magnesium F80-C airplane was designed to employ machine-tapered magnesium skins that extended from the root section to the tip. These machine-tapered skins were 82 inches long and tapered from .172 inches thick at the root to .040 inches at the tip. The maximum width of the skin was approximately 36 inches.

To machine the tapered skins for the horizontal stabilizer an Onsrud Model A-32 GA arm router was used. In order to utilize the arm router to perform a milling operation, it was necessary to lock the router head to prevent any movement in the vertical direction. In addition, all bearing play in the arms was removed so that the cutter would generate a plane when moved about the pivot points of the arms. The machine was then leveled and bolted to the floor.

The cutting tool used was a double tool fly cutter of high speed tool steel. Tool bits on the fly cutter were set at approximately .40 inches off center and balanced to prevent any vibration that might occur at the high router rpm of 20,000.

The work was held on a surface-ground vacuum bed. Sealing of the edges of the work on the vacuum bed was achieved by applying zinc chromate paste.

A problem of deflection was anticipated, therefore, the vacuum bed was so designed that the deflection of the magnesium sheet being machined was controlled by vented hollow cylindrical supports arranged within the vacuum chamber. The cylindrical supports were spaced in number to provide increasing frequency of support at the end where the greatest thickness of stock was to be removed which in turn would cause the largest amount of deflection of the work. The design criteria for the spacing of the supports were based on a requirement that the work should not deflect beyond .001 of an inch at a vacuum pressure of 29 inches of Hg.

In order to provide for leveling of the vacuum bed and also a means for tilting the bed for the required taper, six adjusting screws were provided. Four adjusting screws were located at each corner and two were located at the mid-points of the long side of the vacuum bed. To adjust the vacuum bed for the proper taper the bed was first leveled so that the plane generated by the router cutting head was parallel to that of the vacuum bed. Once this was accomplished, the vacuum bed was tilted by means of the adjusting screws to a slope of .0192 inches per foot.

To gage the depth of cut, check pads of known thickness were located at various points at the edge of the vacuum bed.

A check run of the above setup was made to determine the overall tolerance that can be maintained. It was found, as was expected, that the depth of cut can be changed .010 of an inch by varying the pressure on the cutting head especially when the arms of the router were fully extended. In view of this, it was decided to machine the tapered skins to approximately .015 of an inch over the nominal specified and perform the final cleanup by sanding.

The vacuum bed designed for the above operation is shown in Figure 75 and the complete setup is shown in Figures 76 and 77.

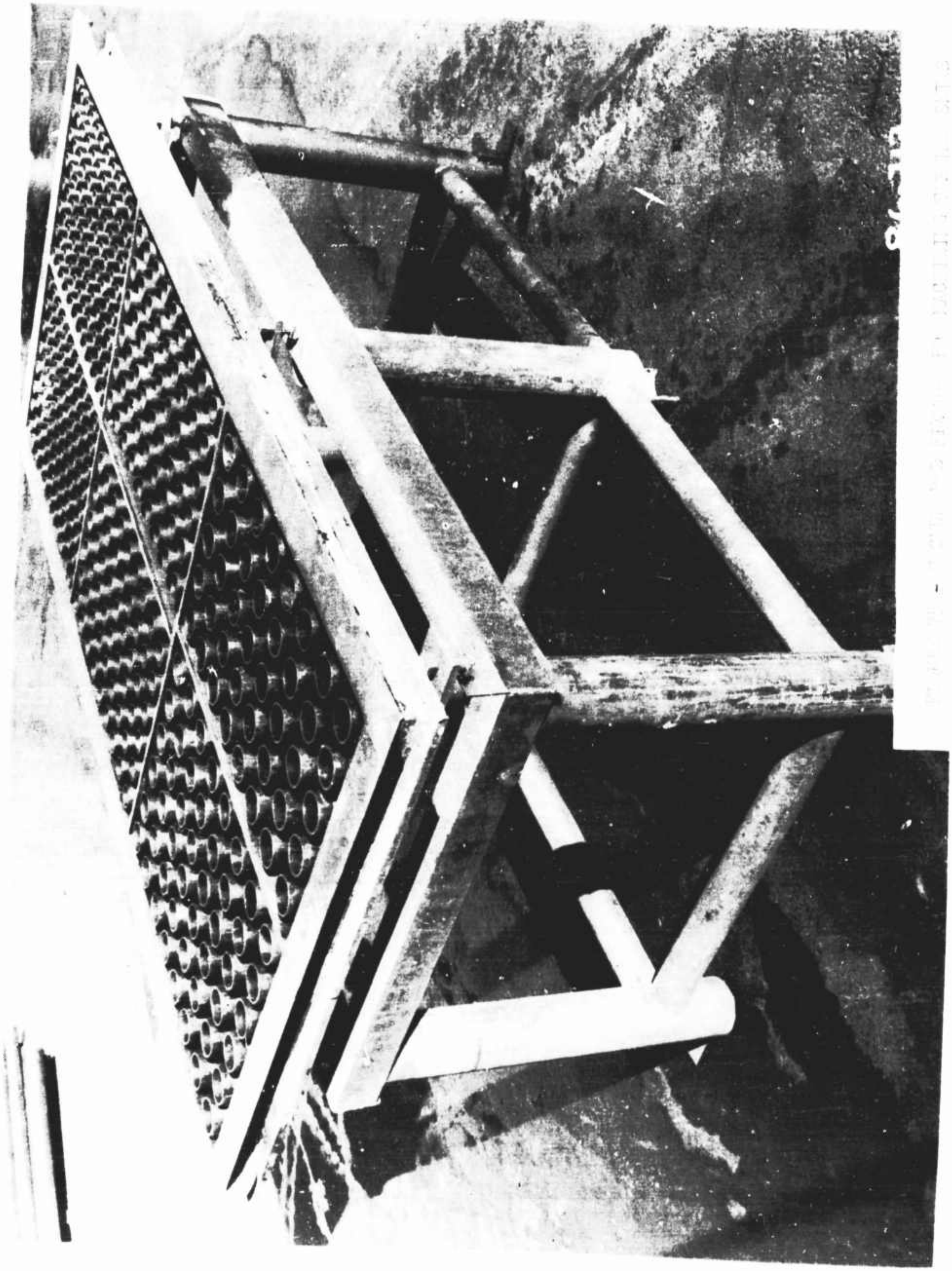

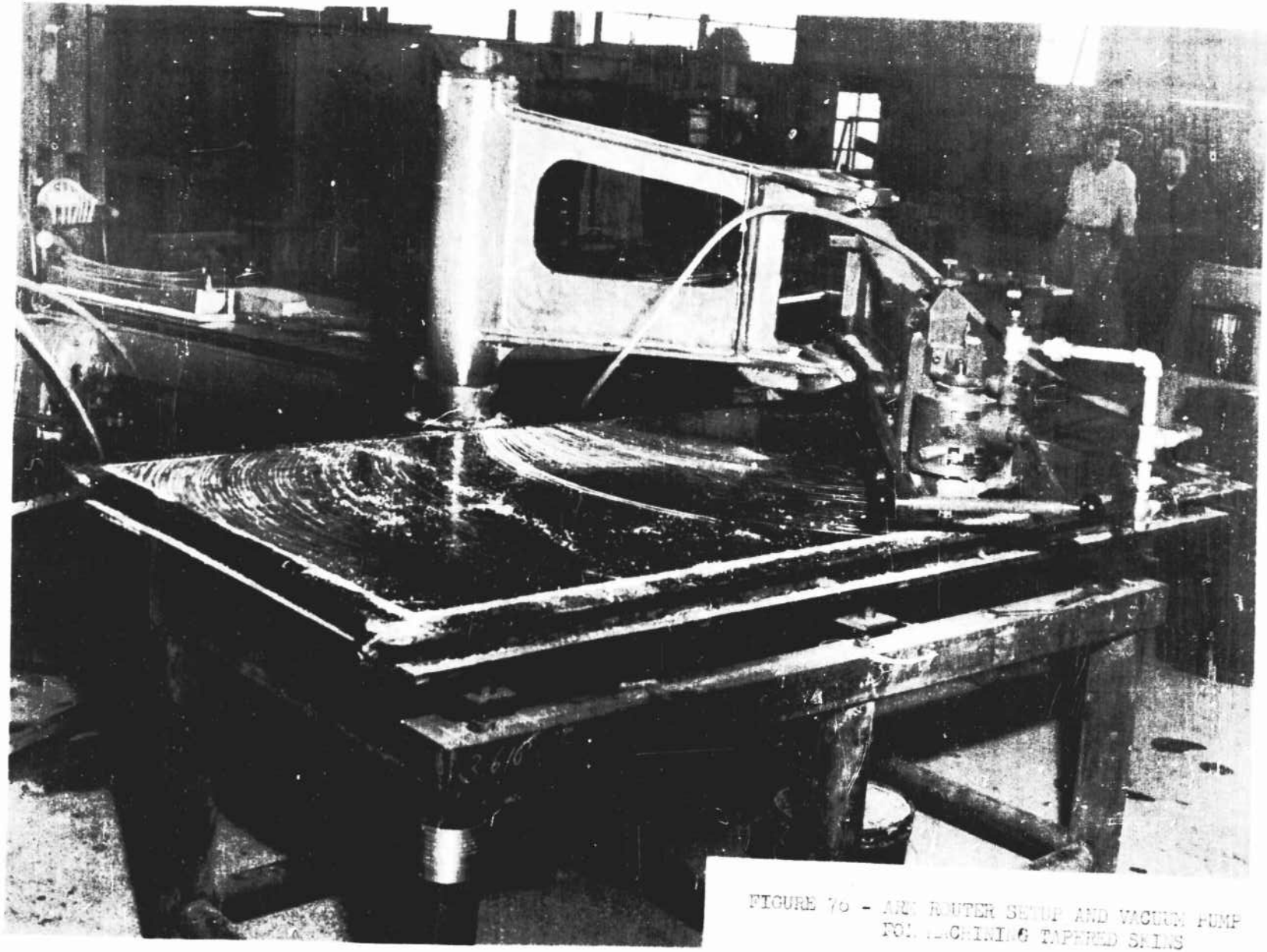

FIGURE 76 - ARC ROUTER SETUP AND VACUUM PUMP FOR MACHINING TAPERED SKINS

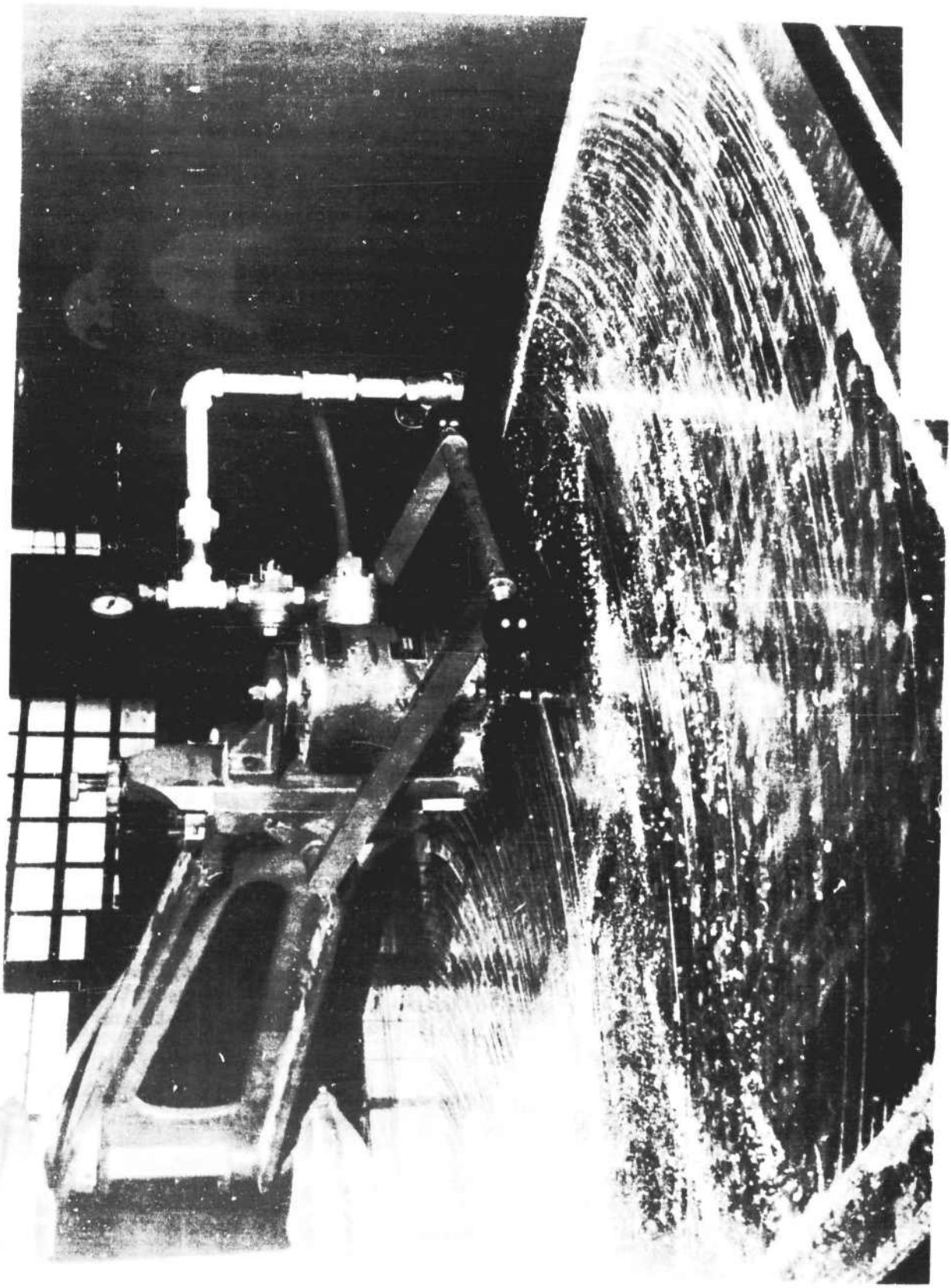

CASTING DESIGN

The design of magnesium alloy sand castings is essentially the same as for aluminum castings. It has been found that it is very important to provide generous filleting at intersections or at points where different thicknesses blend together. Adequate filleting will minimize stress concentrations and will improve metal flow during the casting process, thus avoiding shrinkage cracks and porosity.

Successful casting design depends upon the cooperation between the design engineer, foundryman, pattern maker, and the inspection department. It is advisable to let the casting manufacturer design the pattern and to consult him while the proposed casting design is still on the drawing board. For highly stressed castings, it is essential that the direction and magnitude of the principle stresses be indicated on the drawing. In such castings, design changes to improve soundness may prove necessary during the period of making the sample castings and developing the gating, chilling, and feeding technique.

The normal minimum section thickness of a magnesium sand casting is 5/32 inch; however, for large sand castings a 7/32 inch minimum section is recommended. For small castings, an 1/8 inch minimum is satisfactory providing gating conditions are favorable. The shrinkage allowance for magnesium alloy sand castings varies and depends on a number of factors similar to other alloys. For sand castings of large size or intricate design, the shrinkage allowance of each casting must be determined on the basis of the experience which the foundry has gained over a period of years in making similar castings.

In the following analysis, only the experiences gained in casting the large magnesium alloy sand castings for the structural bulkheads are discussed since the balance of the castings presented no problems.

The casting alloy concerned with in the following discussion is designated as H by the Dow Chemical Company, AM-265 by the American Magnesium Corporation, and QQ-M-56, Composition A alloy AZ63 by the Bureau of Federal Supply. This alloy is heat treatable and can be furnished in three conditions, as-cast (AC), solution heat-treated (HT), or solution heat-treated and aged (HTA). The as-cast (AC) condition is used for nonstructural parts requiring only moderate strength. For maximum ductility, elongation, and impact resistance the solution heat-treated condition is recommended. However, due to casting growth, the magnesium sand castings in this condition should not be specified if the castings are to be used at temperatures above 200 deg. F. The solution heat-treated and aged (HTA) condition should be used to minimize growth and to obtain maximum strength and hardness.

Reference to Table 4.111(b) of ANC-5 the design mechanical properties of magnesium alloy sand castings for AM-265 alloy are as follows:

	CONDITION		
	AC	HT	HTA
F_{tu} (psi)	24,000	34,000	34,000
F_{ty} (psi)	10,000	10,000	16,000
F_{cy} (psi)	10,000	10,000	16,000
F_{su} (psi)	16,000	17,000	19,000
F_{bru} (e/d = 1.5)	36,000	36,000	50,000
F_{bru} (e/d = 2.0)	50,000	50,000	65,000
F_{bry} (e/d = 1.5)	28,000	32,000	36,000
F_{bry} (e/d = 2.0)	30,000	36,000	45,000
e, Elongation %	4	7	3

In the design of the cast bulkhead patterns, the major problems encountered were shrinkage and warpage due to the semicircular shape of the bulkheads. At first an attempt was made to cast the bulkheads without providing secondary stiffeners to aid in maintaining the shape of the cast bulkhead. This did not prove successful since a great deal of warpage was encountered. The pattern was redesigned to provide secondary stiffeners similar to spokes of a wheel. These secondary stiffeners were square in cross-section and measured approximately 3/4 x 3/4 of an inch. Upon recasting the revised pattern, it was found that the stiffeners did not posses sufficient stiffness to prevent the casting from warping. This was apparent since all of the stiffeners or spokes deformed. It should be noted that the semicircular bulkhead ring did not warp as badly as the first attempt. Based upon these results, it was concluded that the secondary stiffeners should have a cross-section equal to that of the bulkhead. As a result, the square stiffeners were redesigned into the shape of an "I" beam. The final configuration is shown in Figure 78.

The above method of pattern design for the cast semicircular bulkheads did not eliminate all of the warpage but the degree of warpage was so small that it was found to be acceptable. The small degree of warpage was corrected prior to aging by cutting the stiffeners off and straightening the casting to the required shape.

Some typical magnesium sand castings are presented in Figures 79 to 82.

CORROSION PROTECTION

The protection of the magnesium alloy against corrosion was achieved by employing the following procedures. All of the magnesium parts used were dichromated per Specification MIL-M-3171 and then given two coats of zinc chromate primer per Specification MIL-P-6889 prior to installation. To guard against electrolytic corrosion, all rivet attachments were made by 56S aluminum alloy rivets. Rivet holes were primed with a wet coat of zinc chromate primer prior to insertion of the rivet.

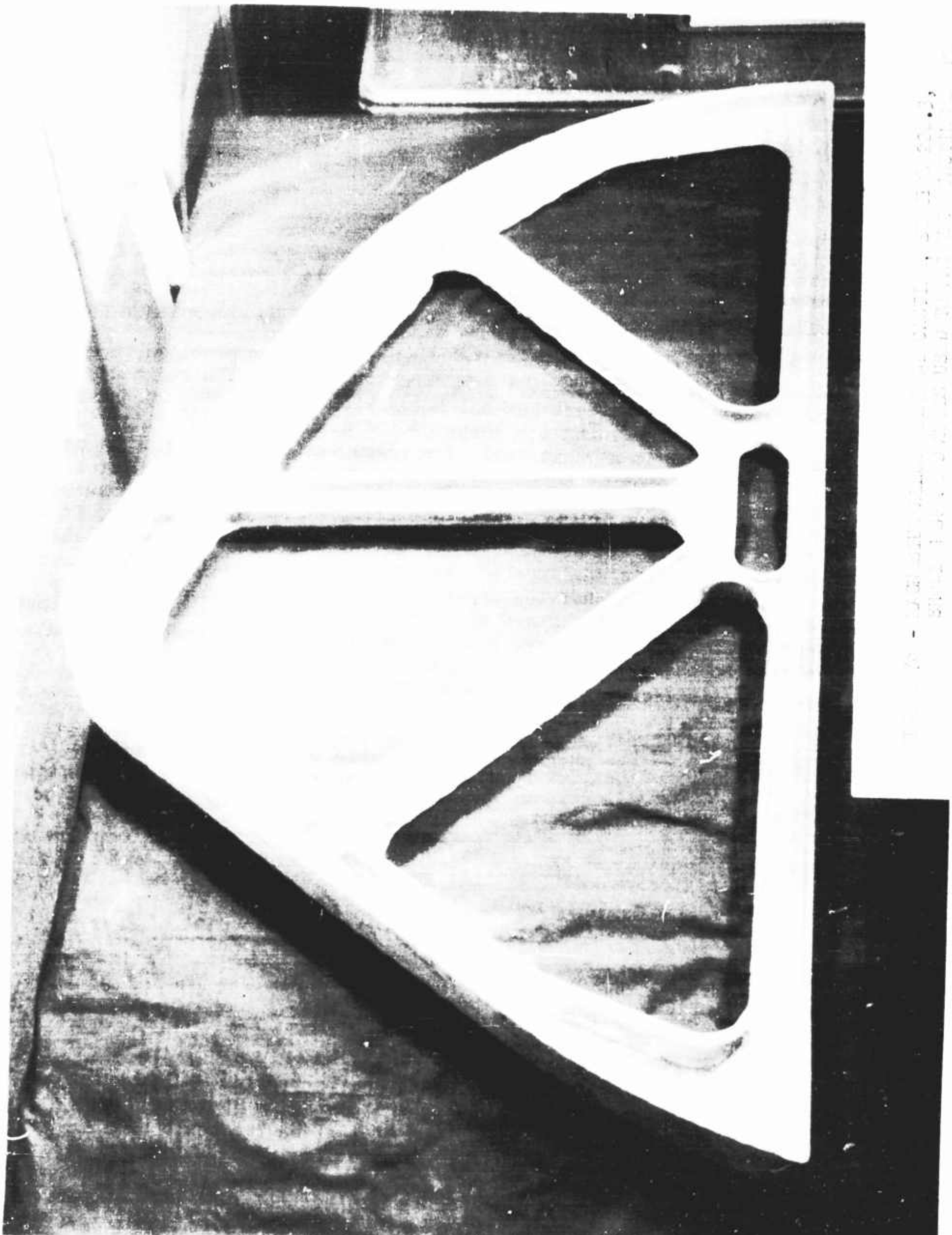

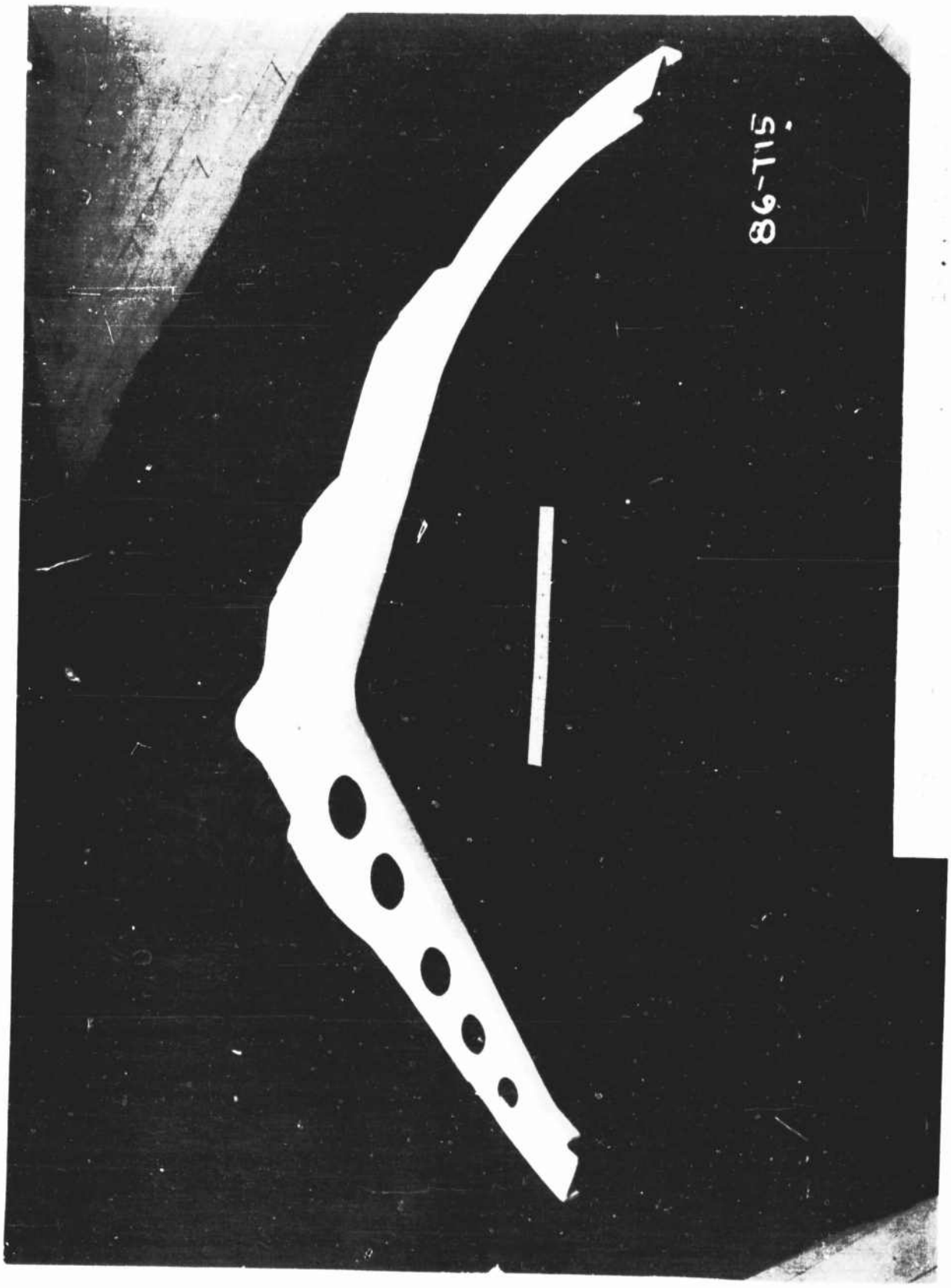
86-715

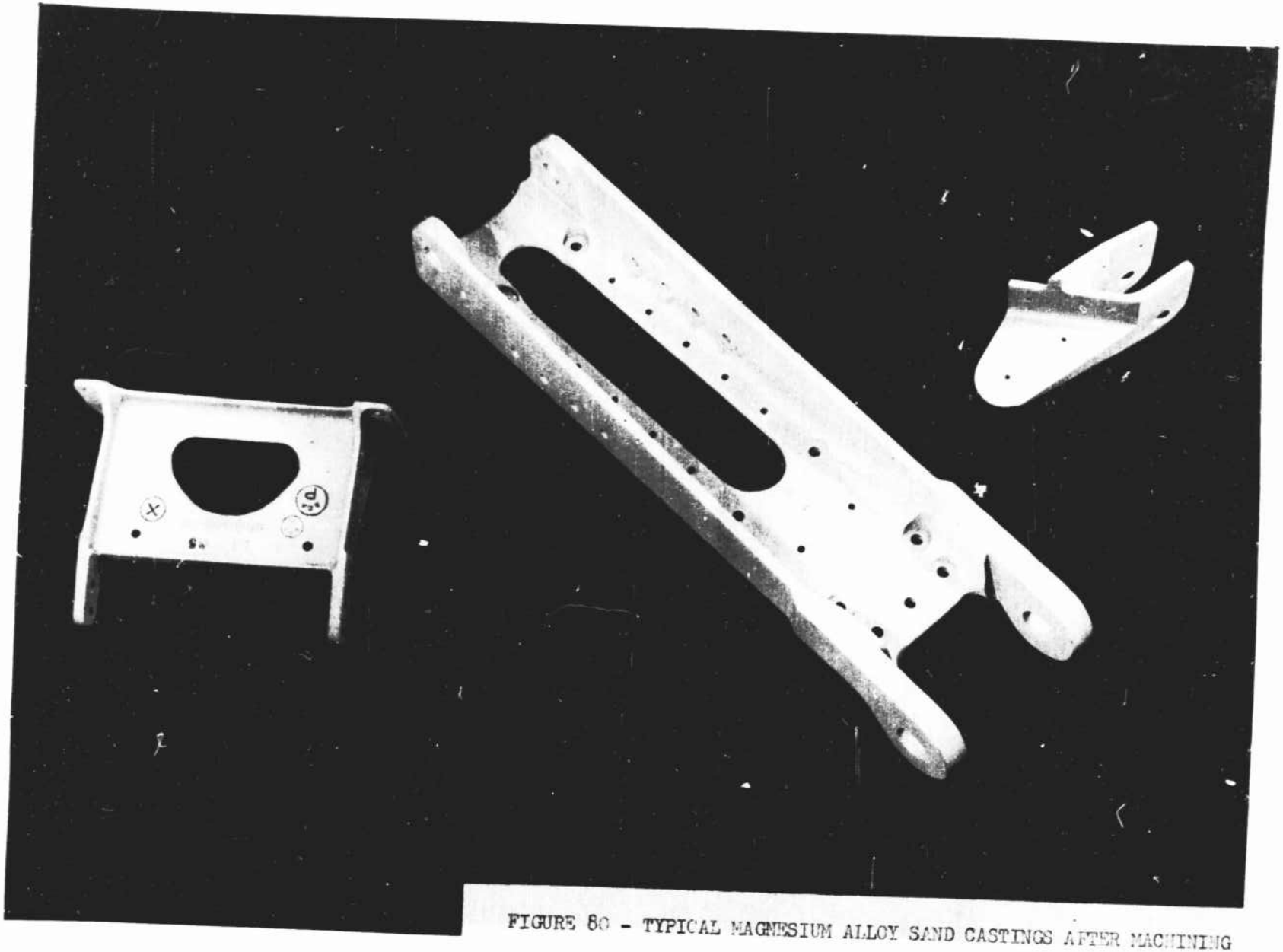

FIGURE 80 - TYPICAL MAGNESIUM ALLOY SAND CASTINGS AFTER MACHINING

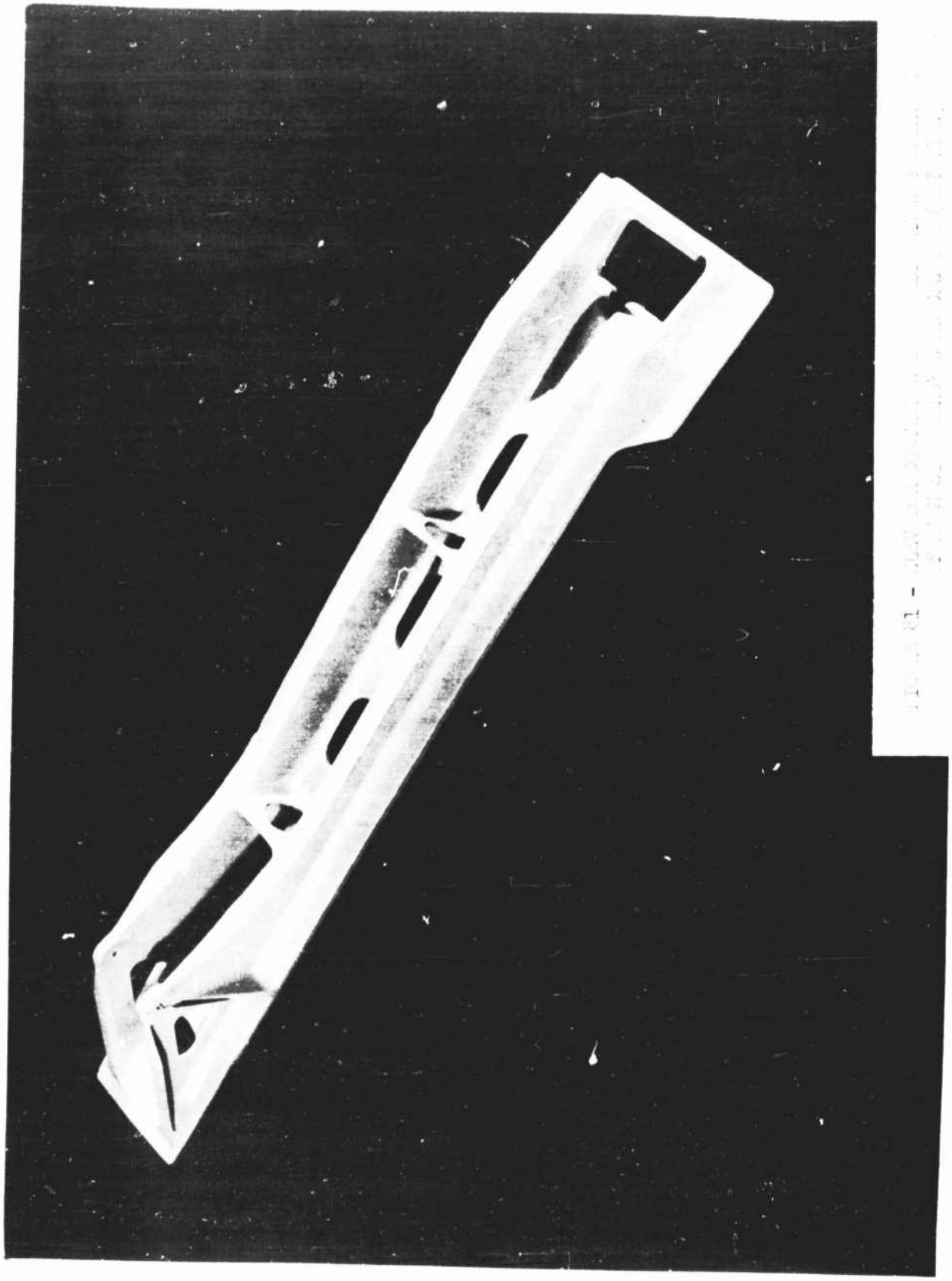

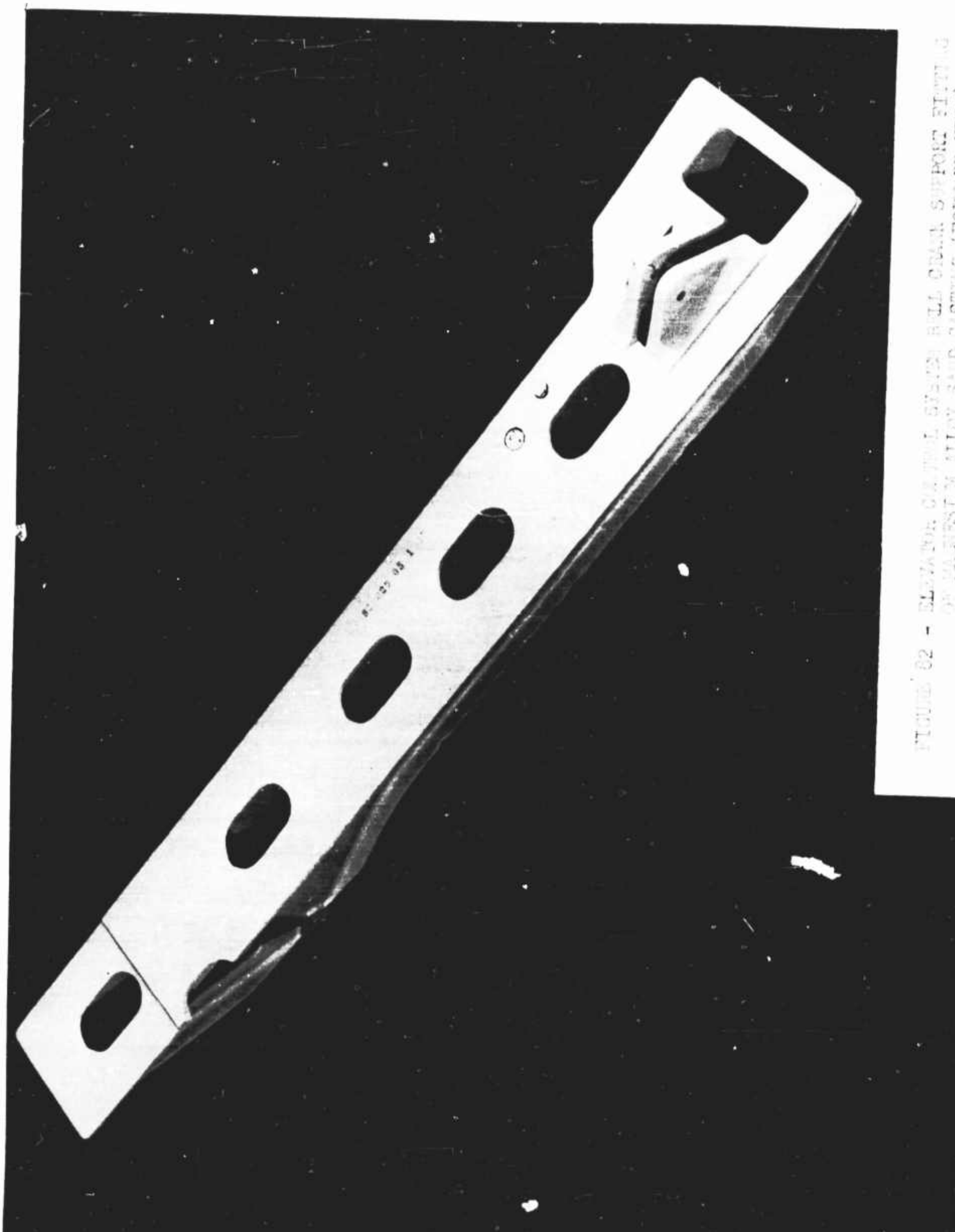

FIGURE 82 - ELEVATOR CONTROL SYSTEM BELL CRANK SUPPORT FITTING OF MAGNESIUM ALLOY SAND CASTING (FORWARD VIEW)

The problem of guarding against electrolytic corrosion when dissimilar metals were used was solved by employing an insulation of tape between the faying surfaces of dissimilar metals. This insulating tape extended at least one-eighth of an inch beyond the edge of the dissimilar metal. Fairprene tape was used as an insulator in all regions except in areas where relatively high temperatures were anticipated. In these areas, a .010 Silastic coated fiberglas tape, CHR #106, made by Triangle Pacific Co., Los Angeles, Calif. was used. In high stressed regions where the use of tape as an insulator was not practicable, the faying surfaces were coated with four coats of zinc chromate primer. When gang channels were used, a cellophane pressure sensitive tape was used as an insulator.

Prior to installation of the equipment, the interior and exterior surfaces of the basic structural airframe was coated with an additional coat of zinc chromate primer.

The exterior surface of the airplane was further protected by a finish coat of two coats of aluminized varnish; 16 ounches of aluminum powder or paste per Specification TT-A-468, Type II, Grade A to one gallon of varnish per Specification MIL-V-6893. The quantities for the mixture are based on a one gallon of packaged material before reduction.

WEIGHT ANALYSIS

The total weight of the contract structural items was 1685 pounds as compared with 1658 pounds for the aluminum prototype items. The magnesium structure was, therefore, 1.6% heavier than the aluminum prototype, which was well within the 3% tolerance permitted by the contract. A detailed weight comparison is given in the following table.

ITEM	ALUMINUM PROTOTYPE WEIGHT	MAGNESIUM STRUCTURE WEIGHT
Wing Group	(113.0)	(119.5)
Aileron	70.0	76.9
Flap	43.0	42.6
Tail Group	(241.0)	(263.7)
Stabilizer	105.0	128.8
Elevator	47.0	44.3
Fin	38.0	38.7
Rudder	27.0	27.4
Dorsal Fairing & Inst.	24.0	24.5
Body Group	(1304.0)	(1301.9)
Total Contract Structural Items	1658.0	1685.1

It should be noted that 6.3 pounds of the aileron weight increase was due to an increase in the static balance weights. This increase was necessary to offset a rearward shift of the C.G. of the magnesium structure.

REFERENCES

1. Forming Magnesium, Dow Chemical Company, Midland, Michigan, 1945.

2. East Coast Aeronautics, Inc., Report No. M-00-5, Effects of Heat Cycles on Physical Properties of Magnesium, October, 1949.

3. Designing with Magnesium, American Magnesium Corporation, 1947.

4. Metals Handbook, 1939 Edition, American Society for Metals, Cleveland, Ohio.

5. Machining Magnesium, Dow Chemical Company, Midland, Michigan, 1945.

6. ANC-5, Strength of Metal Aircraft Elements, Munitions Board Aircraft Committee, June, 1951.

7. Magnesium Alloys and Products, Dow Chemical Company, Midland, Michigan, 1950, page 24.

8. Dow Chemical Company, Effects of Forming Temperatures on Properties of Dowmetal FS1-H24 Sheet, Technical Memorandum No. 16, Midland, Michigan, 1950.

9. Dow Chemical Company, Bend Radii of Magnesium Alloy Sheet, Technical Memorandum No. 14, Midland, Michigan, January, 1949.

10. E. Sechler and L. Dunn, Airplane Structural Analysis and Design, John Wiley and Sons, Inc., 1942.

11. S. Timoshenko, Theory of Elastic Stability, McGraw-Hill Book Company, Inc., 1936.

12. E. Stowell, A Unified Theory of Plastic Buckling of Columns and Plates, NACA Tech. Note 1556.

13. S. Batdorf, M. Schildcrout, and M. Stein, Critical Combinations of Shear and Longitudinal Direct Stress for Long Plates with Transverse Curvature, NACA Tech. Note 1347.

14. S. Batdorf, M. Schildcrout, and M. Stein, Critical Shear Stress of Curved Rectangular Panels, NACA Tech. Note 1348.

15. S. Batdord, M. Schildcrout, and M. Stein, Critical Stress of Thin-Walled Cylinders, NACA Tech. Note 1343.

16. L. Levin, Ultimate Stresses Developed by 24S-T and Alclad 75S-T Aluminum Alloy Sheet in Incomplete Diagonal Tension, NACA Tech. Note 1756.

REFERENCES - CONT'D.

17. Lockheed Aircraft Company Report 4657, Basic Loads - Model P80A.

18. Lockheed Aircraft Company Report 4660, Control Surface Analysis.

APPENDIX A

STRESS ANALYSIS

HORIZONTAL STABILIZER

Discussion

The methods employed in calculating the stabilizer section properties, bending stresses, axial loads, and internal shear flows are illustrated in the following pages. The stabilizer is constructed completely of magnesium alloy and consists of three beams and tapered skins combined to produce a closed three-celled box structure. Since the relatively thick tapered skins are not expected to buckle until a point well above the limit load, the skins are assumed fully effective up to ultimate load.

The stabilizer is critical in bending and torsion for the dynamic loading conditions (forward and aft C.P. locations) set forth in Contract Change Notification No. 1 on subject contract: Exhibit "A", General and Detail Requirements.

The design ultimate shears, moments, and torques are summarized in Table 5 and were obtained by the following method.

1. The stabilizer deflection curve for dynamic loading was determined by assuming the total airload bending moments obtained from the aforementioned to act on the stabilizer alone. The elevator hinge reactions due to this deflection curve were then computed.

2. The elevator hinge reactions due to airloads on the elevator in the undeflected state were then determined for these conditions.

3. The design ultimate shears, moments, and torques were then determined by superposition of the hinge reactions obtained in steps 1 and 2 above and the data obtained from the Contract Change Notification No. 1 of the subject contract

The rolling pull-out condition is used solely to check the stabilizer center section and the stabilizer attachment fittings.

Section Properties

The stabilizer is designed symmetrically about the chord line. Therefore, spar cap and total skin areas are the same for corresponding upper and lower flange elements. The assumption of fully effective skins up to ultimate load permits the use of one set of section properties per station for either compression on the top or compression on the bottom surfaces. A further check of the stabilizer strength at ultimate load with buckled skins is also shown.

The section properties were computed at several stations along the stabilizer span. The thick skins were divided into elements of equal length and the area of each element was assumed acting at its centroid as illustrated in Figure 83.

A summary of the effective areas and ordinates of element centroids is shown in Table 6. The skins are assumed fully effective between front and rear spars at all stations. The nose skins are assumed 50% effective at stations 30, 45, and 60, and 0% effective at stations 0, 10, and 80. The three spars are assumed fully effective from root to tip.

Detailed calculations of the section properties at stations 30 and 45 placing either surface in compression are shown in Tables 7 and 8. A summary of the section properties at various stabilizer stations is presented in Table 9. In order to facilitate the shear flow calculations later in the report, the spar cap flange elements are assumed to act at the beam centerlines.

All section properties are computed using the section chord line and the rear beam mold line as the X and Z reference axes respectively. The rear beam mold line is located 3.075 inches forward of the elevator hinge ℄ which is at 75% of the section chord.

Bending Stresses and Axial Loads

In determining the bending stresses in the stabilizer, the following method was used. Since the stabilizer sections are symmetrical with respect to the chord line, the neutral axis corresponds to the chord line. The bending stress at an element dA located a distance "h" from the neutral axis is given by:

$$f_b = K_2 h \quad - \quad (1)$$

Where K_2 is a constant for each section determined by:

$$K_2 = \frac{M_x}{I_x} \quad - \quad (2)$$

The distance "h" corresponds to the Z ordinate of the element centroids so that:

$$f_b = K_2 Z \quad - \quad (3)$$

Values of Z are shown in Table 6. For convenience, values of K_2 are determined in Tables 7 and 8 and summarized in Table 9.

The detailed calculation of bending stresses in accordance with equation (3) for stations 30 and 45 is shown in Table 10 with a summary of the stresses at all stabilizer stations investigated given in Table 11.

TABLE 5 - FINAL STABILIZER SHEARS, MOMENTS, TORQUES - ULTIMATE DYNAMIC LOAD CONDITIONS

(1)	(2)	(3)	(4)	(5)	(6)	(7)	(8)	(9)	(10)	(11)	(12)	(13)	(14)	(15)	(16)	(17)	(18)	(19)	(20)
ITEM / STA.	CONDITIONS A & B		CONDITION A						CONDITION B						TORQUE ABOUT HINGE		S_e	TORQUE ABOUT REF. AXIS	
	PRELIM. NET SHEAR	PRELIM. NET MOMENT	AIRLOAD HINGE SHEAR	HINGE REACT. SHEAR	TOTAL SHEAR S	AIRLOAD HINGE MOMENT	HINGE REACT. MOMENT	TOTAL MOMENT	AIRLOAD HINGE SHEAR	HINGE REACT. SHEAR	TOTAL SHEAR S	AIRLOAD HINGE MOMENT	HINGE REACT. MOMENT	TOTAL MOMENT	COND. A T_{HL}	COND. B T_{HL}		COND. A $T_{ref.}$	COND. B $T_{ref.}$
Ref.	Note a		Note b	Note c	(2)+(4)+(5)	Note b	Note c	(3)+(7)+(8)	Note b	Note c	(2)+(10)+(11)	Note b	Note c	(3)+(13)+(14)	Note a		(6)x 3.075	(16) - (18)	(17) - (18)
91.7	0	0	0	0	0	0	0	0	0	0	0	0	0	0	0	0	0	0	0
80	784	4,390	0	0	784	0	0	4,390	0	0	784	0	0	4,390	7,320	3,650	2,410	4,910	1,240
-80	784	4,390	-50.2	3	737	0	-	-	-134.8	88	737	0	-	-	7,320	3,650	2,270	5,050	1,380
70	1,605	16,230	-50.2	3	1,558	-500	30	15,760	-134.8	88	1,558	-1,350	880	15,760	16,710	8,340	4,790	11,920	3,550
60	2,565	36,960	-50.2	3	2,518	-1,000	70	36,030	-134.8	88	2,518	-2,700	1,760	36,030	29,560	14,750	7,740	21,820	7,010
-60	2,565	36,960	-190.4	112	2,487	-1,000	-	-	-511.3	433	2,487	-2,700	-	-	29,560	14,750	7,650	21,910	7,100
50	3,665	68,000	-190.4	112	3,587	-2,910	1,180	66,270	-511.3	433	3,587	-7,810	6,080	66,270	46,420	23,200	11,030	35,390	12,170
40	4,905	110,730	-190.4	112	4,827	-4,810	2,300	108,220	-511.3	433	4,827	-12,920	10,410	108,220	67,810	33,840	14,840	52,970	19,000
30	6,282	166,540	-190.4	112	6,204	-6,720	3,420	163,240	-511.3	433	6,204	-18,040	14,740	163,240	94,280	47,050	19,080	75,200	27,970
-30	6,282	166,540	-435.7	546	6,392	-6,720	-	-	-1,170.2	1,280	6,392	-18,040	-	-	94,280	47,050	19,660	74,620	27,390
20	7,801	236,830	-435.7	546	7,911	-11,070	8,870	234,630	-1,170.2	1,280	7,911	-29,740	27,540	234,630	126,400	63,080	24,330	102,070	38,750
10	9,459	322,980	-435.7	546	9,569	-15,430	14,330	321,880	-1,170.2	1,280	9,569	-41,440	40,340	321,880	164,660	82,170	29,420	135,240	52,750
0	11,250	426,410	-471	471	11,250	-19,790	19,790	426,410	-1,265	1,265	11,250	-53,140	53,140	426,410	209,620	104,610	34,590	175,030	70,020

NOTES:

a. Preliminary net ultimate shears, moments, and torques are obtained from Contract Change Notification No. 1 on subject contract: Exhibit "A"

b. Airload hinge shears and moments are due to airloads on the elevator in the undeflected state.

c. The stabilizer deflection curve for dynamic loading was determined assuming the total airload bending moments obtained as noted in (a) to act on the stabilizer alone. The elevator hinge reactions due to this deflection were then computed.

d. Condition A represents 25% C.P. location.
Condition B represents 50% C.P. Location

e. Stabilizer torques about reference axis
- Reference axis located at ℄ rear spar
- Distance from reference axis to ℄ hinge = 3.075" = e

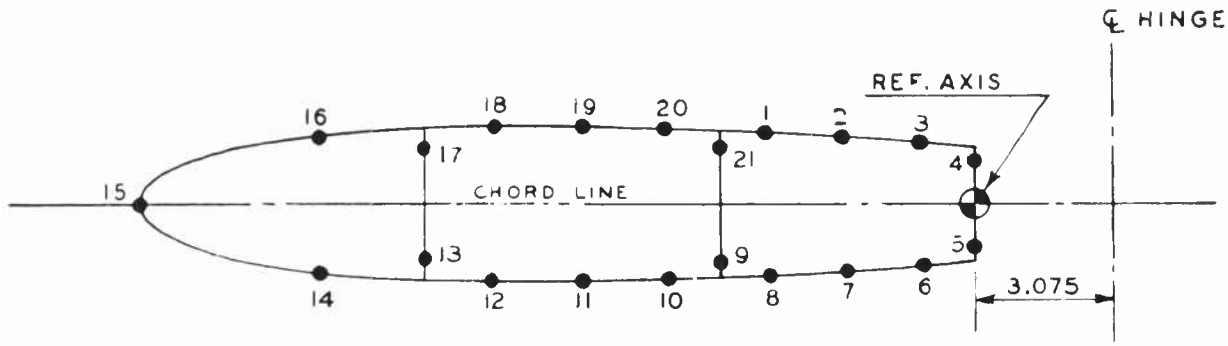

FIG. 83 FLANGE AND ELEMENT DESIGNATIONS

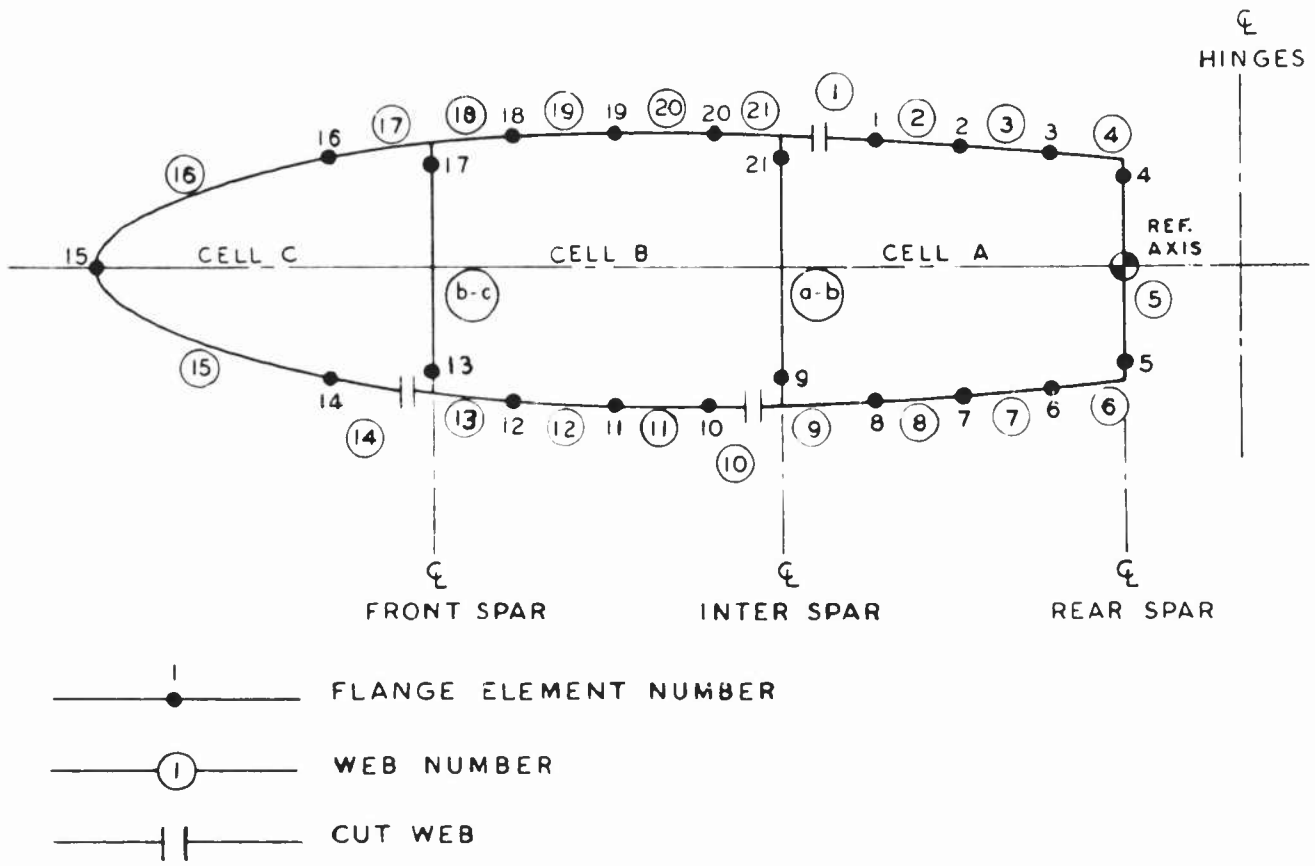

FIG. 84 FLANGE AND WEB DESIGNATIONS
SHEAR FLOW DETERMINATION
3-CELL BOX - STA. 10 TO 80.5

TABLE 6 - EFFECTIVE AREAS AND ORDINATES OF ELEMENT CENTROIDS

(1)	(2)	(3)	(4)	(5)	(6)	(7)	(8)	(9)	(10)	(11)	(12)	(13)	(14)	(15)	(16)	(17)	(18)	(19)
Flange or Element No.	STATION 0			STATION 10			STATION 30			STATION 45			STATION 60			STATION 80		
	Effect. Area Comp. In Either Surface	X	Z	Effect. Area Comp. In Either Surface	X	Z	Effect. Area Comp. In Either Surface	X	Z	Effect. Area Comp. In Either Surface	X	Z	Effect. Area Comp. In Either Surface	X	Z	Effect. Area Comp. In Either Surface	X	Z
1	.748	-10.88	2.45	.616	-9.87	2.27	.387	-7.86	1.91	.252	-6.36	1.64	.145	-4.86	1.37	.048	-2.85	1.01
2	.748	- 6.53	2.20	.616	-5.92	2.05	.387	-4.72	1.74	.252	-3.82	1.51	.145	-2.92	1.27	.048	-1.71	.97
3	.748	- 2.18	1.81	.616	-1.97	1.70	.387	-1.57	1.47	.252	-1.27	1.29	.145	- .97	1.11	.048	- .57	.89
4	.652	0	1.38	.502	0	1.29	.227	0	1.14	.222	0	1.02	.206	0	.91	.202	0	.72
5	.652	0	-1.38	.502	0	-1.29	.227	0	-1.14	.222	0	-1.02	.206	0	- .91	.202	0	- .72
6	.748	- 2.18	-1.81	.616	-1.97	-1.70	.387	-1.57	-1.47	.252	-1.27	-1.29	.145	- .97	-1.11	.048	- .57	- .89
7	.748	- 6.53	-2.20	.616	-5.92	-2.05	.387	-4.72	-1.74	.252	-3.82	-1.51	.145	-2.92	-1.27	.048	-1.71	- .97
8	.748	-10.88	-2.45	.616	-9.87	-2.27	.387	-7.86	-1.91	.252	-6.36	-1.64	.145	-4.86	-1.37	.048	-2.85	- .01
9	.355	-13.05	-2.29	.350	-11.84	-2.12	.340	-9.43	-1.77	.333	-7.63	-1.51	.194	-5.83	-1.21	.184	-3.42	- .86
10	.716	-15.13	-2.52	.601	-13.77	-2.34	.397	-11.04	-1.97	.274	-9.01	-1.68	.171	-6.98	-1.40	.070	-4.26	-1.03
11	.716	-19.29	-2.43	.601	-17.62	-2.25	.397	-14.27	-1.89	.274	-11.78	-1.62	.171	-9.28	-1.35	.070	-5.94	- .99
12	716	-23.45	-2.23	.601	-21.47	-2.07	.397	-17.50	-1.74	.274	-14.54	-1.49	.171	-11.57	-1.24	.070	-7.61	- .91
13	.675	-25.53	-1.80	.593	-23.39	-1.67	.432	-19.11	-1.40	.328	-15.92	-1.20	.238	-12.72	-1.00	.141	-8.45	- .73
14	-	-	-	-	-25.80	-1.69	.498	-21.13	-1.42	.344	-17.65	-1.22	.213	-14.16	-1.01	-	-9.50	- .73
15	-	-	-	-	-33.01	0	-	-27.18	0	-	-22.83	0	-	-18.46	0	-	-12.64	0
16	-	-	-	-	-25.80	1.69	.498	-21.13	1.42	.344	-17.65	1.22	.213	-14.16	1.01	-	-9.50	.73
17	.675	-25.53	1.80	.593	-23.39	1.67	.432	-19.11	1.40	.328	-15.92	1.20	.238	-12.72	1.00	.141	-8.45	..73
18	.716	-23.45	2.23	.601	-21.47	2.07	.397	-17.50	1.74	.274	-14.54	1.49	.171	-11.57	1.24	.070	-7.61	.91
19	.716	-19.29	2.43	.601	-17.62	2.25	.397	-14.27	1.89	.274	-11.78	1.62	.171	- 9.28	1.35	.070	-5.94	.99
20	.716	-15.13	2.52	.601	-13.77	2.34	.397	-11.04	1.97	.274	- 9.01	1.68	.171	- 6.98	1.40	.070	-4.26	1.03
21	.355	-13.05	2.29	.350	-11.84	2.12	.340	-9.43	1.77	.333	- 7.63	1.51	.194	- 5.83	1.21	.184	-3.42	.86

TABLE 7 - SECTION PROPERTIES AT STATION 30
COMPRESSION IN EITHER SURFACE

①	②	③	④	⑤	⑥	⑦	⑧	⑨
Elem. n	Area A	X	Z	AZ	AZ^2	Cross Products $X_n \cdot Z_{n-1}$	Cross Products $X_{n-1} \cdot Z_n$	C_n
Ref.	Tab. 6	Tab. 6	Tab. 6	② x ④	④ x ⑤	$③_n \times ④_{n-1}$	$③_{n-1} \times ④_n$	⑦ - ⑧
1	.387	-7.86	1.91	.739	1.41	-13.91	-18.01	4.10
2	.387	-4.72	1.74	.673	1.17	-9.01	-13.68	4.66
3	.387	-1.57	1.47	.569	.84	-2.73	-6.94	4.21
4	.227	0	1.14	.259	.30	0	-1.79	1.79
5	.227	0	-1.14	-.259	.30	0	0	0
6	.387	-1.57	-1.47	-.569	.84	-	-	1.79
7	.387	-4.72	-1.74	-.673	1.17	-	-	4.21
8	.387	-7.86	-1.91	-.739	1.41	-	-	4.66
9	.340	-9.43	-1.77	-.602	1.07	-	-	4.10
10	.397	-11.04	-1.97	-.782	1.54	19.54	18.58	.96
11	.397	-14.27	-1.89	-.750	1.42	28.11	20.87	7.24
12	.397	-17.50	-1.74	-.691	1.20	33.08	24.83	8.25
13	.432	-19.11	-1.40	-.605	.85	33.25	24.50	8.75
14	.498	-21.13	-1.42	-.707	1.00	29.58	27.14	2.44
15	-	-27.18	0	.000	0.00	38.60	0	40.24 *
16	.498	-21.13	1.42	.707	1.00	-	-	40.24 *
17	.432	-19.11	1.40	.605	.85	-	-	2.44
18	.397	-17.50	1.74	.691	1.20	-	-	8.75
19	.397	-14.27	1.89	.750	1.42	-	-	8.25
20	.397	-11.04	1.97	.782	1.54	-	-	7.24
21	.340	-9.43	1.77	.602	1.07	-	-	.96
						Web	a-b	33.38
						Web	b-c	53.51
Σ	7.698		0	0	21.60			

* Correction Factor Added.

2 x Area Cell A = 62.90
2 x Area Cell B = 70.53
2 x Area Cell C = 31.85

$$I_x = \Sigma ⑥ - \bar{z} \Sigma ⑤ = 21.60 \text{ in.}^4$$

M_x = 163,240"# (±) (Table 5)

$$K_2 = -\frac{163,240}{21.60} = -7557.4$$

TABLE 8 - SECTION PROPERTIES AT STATION 45
COMPRESSION IN EITHER SURFACE

①	②	③	④	⑤	⑥	⑦	⑧	⑨
Elem. n	Area A	X	Z	AZ	AZ^2	Cross Products		C_n
						$X_n \cdot Z_{n-1}$	$X_{n-1} \cdot Z_n$	
Ref.	Tab. 6	Tab. 6	Tab. 6	② x ④	④ x ⑤	$③_n \times ④_{n-1}$	$③_{n-1} \times ④_n$	⑦ - ⑧
1	.252	-6.36	1.64	.413	.677	-9.60	-12.51	2.91
2	.252	-3.82	1.51	.381	.575	-6.26	-9.60	3.34
3	.252	-1.27	1.29	.325	.419	-1.92	-4.93	3.01
4	.222	0	1.02	.226	.231	0	-1.30	1.30
5	.222	0	-1.02	-.226	.231	0	0	0
6	.252	-1.27	-1.29	-.325	.419	-	-	1.30
7	.252	-3.82	-1.51	-.381	.575	-	-	3.01
8	.252	-6.36	-1.64	-.413	.677	-	-	3.34
9	.333	-7.63	-1.51	-.503	.760	-	-	2.91
10	.274	-9.01	-1.68	-.460	.772	13.61	12.82	.79
11	.274	-11.78	-1.62	-.444	.719	19.79	14.60	5.19
12	.274	-14.54	-1.49	-.408	.608	23.55	17.55	6.00
13	.328	-15.92	-1.20	-.394	.473	23.72	17.45	6.27
14	.344	-17.65	-1.22	-.420	.512	21.18	19.42	1.76
15	-	-22.83	0	0	0	27.85	0	29.06 *
16	.344	-17.65	1.22	.420	.512	-	-	29.06
17	.328	-15.92	1.20	.394	.473	-	-	1.76
18	.274	-14.54	1.49	.408	.608	-	-	6.27
19	.274	-11.78	1.62	.444	.719	-	-	6.00
20	.274	-9.01	1.68	.460	.772	-	-	5.19
21	.333	-7.63	1.51	.503	.760	-	-	.79
						Web	a-b	23.04
						Web	b-c	38.21
Σ	5.610		0	0	11.492			

2 x Area Cell A = 44.16
2 x Area Cell B = 51.67
2 x Area Cell C = 23.43

$$I_x = \Sigma ⑥ - \bar{z} \Sigma ⑤ = 11.492 \text{ in.}^4$$

$M_x = 86{,}000$"# (+) (Table 5)

$$K_2 = -\frac{86{,}000}{11.492} = -7483.5$$

TABLE 9 - SUMMARY OF STABILIZER SECTION PROPERTIES AND BENDING CONSTANTS

STATION	0	10	30	45	60	80
$\bar{z}$	0	0	0	0	0	0
I_x	56.38	41.02	21.60	11.492	5.010	1.294
K_2	-6119.2	-7846.9	-7557.4	-7483.5	-7191.6	-3392.6

TABLE 10 - ULTIMATE BENDING STRESSES AND AXIAL LOADS
STATIONS 30 AND 45

①	②	③	④	⑤	⑥	⑦	⑧	⑨
Element	Station 30				Station 45			
	Z	A Comp. Either	F_b / K_2Z	P	Z	A Comp. Either	F_b / K_2 Z	P
Ref.	Tab. 6	Tab. 6	-7557.4 ②	③ x ④	Tab. 6	Tab. 6	-7483.5 ②	⑦ x ⑧
1	1.91	.387	-14,435	-5,586	1.64	.252	-12,273	-3.093
2	1.74	.387	-13,150	-5,089	1.51	.252	-11,300	-2,848
3	1.47	.387	-11,109	-4,299	1.29	.252	-9,654	-2,433
4	1.14	.227	-8,615	-1,956	1.02	.222	-7,633	-1,695
5	-1.14	.227	8,615	1,956	-1.02	.222	7,633	1,695
6	-1.47	.387	11,109	4,299	-1.29	.252	9,654	2,433
7	-1.74	.387	13,150	5,089	-1.51	.252	11,300	2,848
8	-1.91	.387	14,435	5,586	-1.64	.252	12,273	3,093
9	-1.77	.340	13,377	4,548	-1.51	.333	11,300	3,763
10	-1.97	.397	14,888	5,911	-1.68	.274	12,572	3,445
11	-1.89	.397	14,283	5,670	-1.62	.274	12,123	3,322
12	-1.74	.397	13,150	5,221	-1.49	.274	11,150	3,055
13	-1.40	.432	10,580	4,571	-1.20	.328	8,980	2,945
14	-1.42	.498	10,732	5,345	-1.22	.344	9,130	3,141
15	0	-	-	-	0	-	-	-
16	1.42	.498	-10,732	-5,345	1.22	.344	-9,130	-3,141
17	1.40	.432	-10,580	-4,571	1.20	.328	-8,980	-2,945
18	1.74	.397	-13,150	-5,221	1.49	.274	-11,150	-3,055
19	1.89	.397	-14,283	-5,670	1.62	.274	-12,123	-3,322
20	1.97	.397	-14,888	-5,911	1.68	.274	-12,572	-3,445
21	1.77	.340	-13,377	-4,548	1.51	.333	-11,300	-3,763

"K_2" values are from Tables 7 and 8.

TABLE 11 - SUMMARY - ULTIMATE BENDING STRESSES (NO BUCKLING)
- DYNAMIC LOADING CONDITIONS

Location	Sta. / Elem. No.	0	10	30	45	60	80
Aft Skin	1, 8	±14,990	±17,810	±14,440	±12,270	±9,850	±3,430
	2, 6	±13,460	±16,090	±13,150	±11,300	±9,130	±3,290
	3, 6	±11,080	±13,340	±11,110	± 9,650	±7,980	±3,020
Forward Skin	10, 20	±15,420	±18,360	±14,890	±12,570	±10,070	±3,490
	11, 19	±14,870	±17,660	±14,280	±12,120	±9,710	±3,360
	12, 18	±13,650	±16,240	±13,150	±11,150	±8,920	±3,090
Nose Skin	14, 16	-	-	±10,730	±9,130	±7,260	-
Front Spar	13, 17	±11,020	±13,100	±10,580	±8,980	±7,190	±2,480
Interm. Spar	9, 21	±14,010	±16,640	±13,380	±11,300	±8,700	±2,920
Rear Spar	4, 5	±8,440	±10,120	±8,620	±7,630	±6,540	±2,440

Shear Flow Determination

The method used in computing the internal shear flow in the stabilizer is described in this section. Since multi-cell structures are statically indeterminate, it is necessary to use deflection equations in addition to the equations of statics to obtain a solution for the distribution of shear flow within the structure. The shear flow in one web of each cell is taken as an initial unknown. The external torque on the section affords one relationship or equation which these unknowns must satisfy. It follows, therefore, that a structure with "n" cells is statically indeterminate to the (n-1)th degree.

The deflection equations used for multi-cell beams are derived from the angle of twist of the beam in the following manner. Since in this type of structure, the ribs prevent appreciable distortion of the cross section, the angle of twist per unit length, "θ", must be the same for every cell. This angle may be found for any cell in terms of the shear flow "Q" around the cell. If one cell of the beam is considered as shown in Figure 85(a), the angle of twist results from the shear distortion of each web due to the shear flow "Q" as shown in Figure 85(c). If a virtual torque, $Tv_o = 1.0$, is acting on the cell before the shear flows "Q" are applied, the virtual work of this torque, $Tv_o \times \theta = 1.0 \times \theta$ must be equal to the virtual internal work of the shear flows "Q_o", resulting from Tv_o. In this case $Q_o = Tv_o/2A_o = 1.0/2A_o$. These shear forces act through a displacement equal to Q/tG_e, as shown in Figure 85(c). Equating the work, we have:

$$1.0 \times \theta = \Sigma\, (1/2A_o)\, (\Delta s)\, (Q/tG_e)$$

or
$$\theta = (1/2A_o)\, \Sigma\, Q\, \Delta s/tG_e \quad - - - - - - - - - - - - \quad (4)$$

In Equation (4), A_o represents the area of the cell enclosed by the skin as shown in Figure 85(b), and G_e represents the effective modulus of rigidity, or the unit shear stress "Q/t" divided by the unit shear strain "γ". The thickness "t" is for the web of length "Δs". The summation of Equation (4) must extend all the way around the perimeter of the cell, in a clockwise direction. Thus, if any shear flows "Q" are in a counterclockwise direction, they must be considered as negative. Equation (4) applies to any number of cells, as long as the summation is performed in a closed path around the structure. If any interior vertical web in a multi-cell structure has a shear flow acting upward, it would be used in Equation (4) as positive when considering the cell to the right of the web and negative when considering the cell to the left of the web.

The effective modulus of rigidity "G_e" is a constant term which cancels out of all final equations if the webs are shear resistant. Since all webs are assumed shear resistant in this work, no correction is required in the value of "G", which is assumed constant.

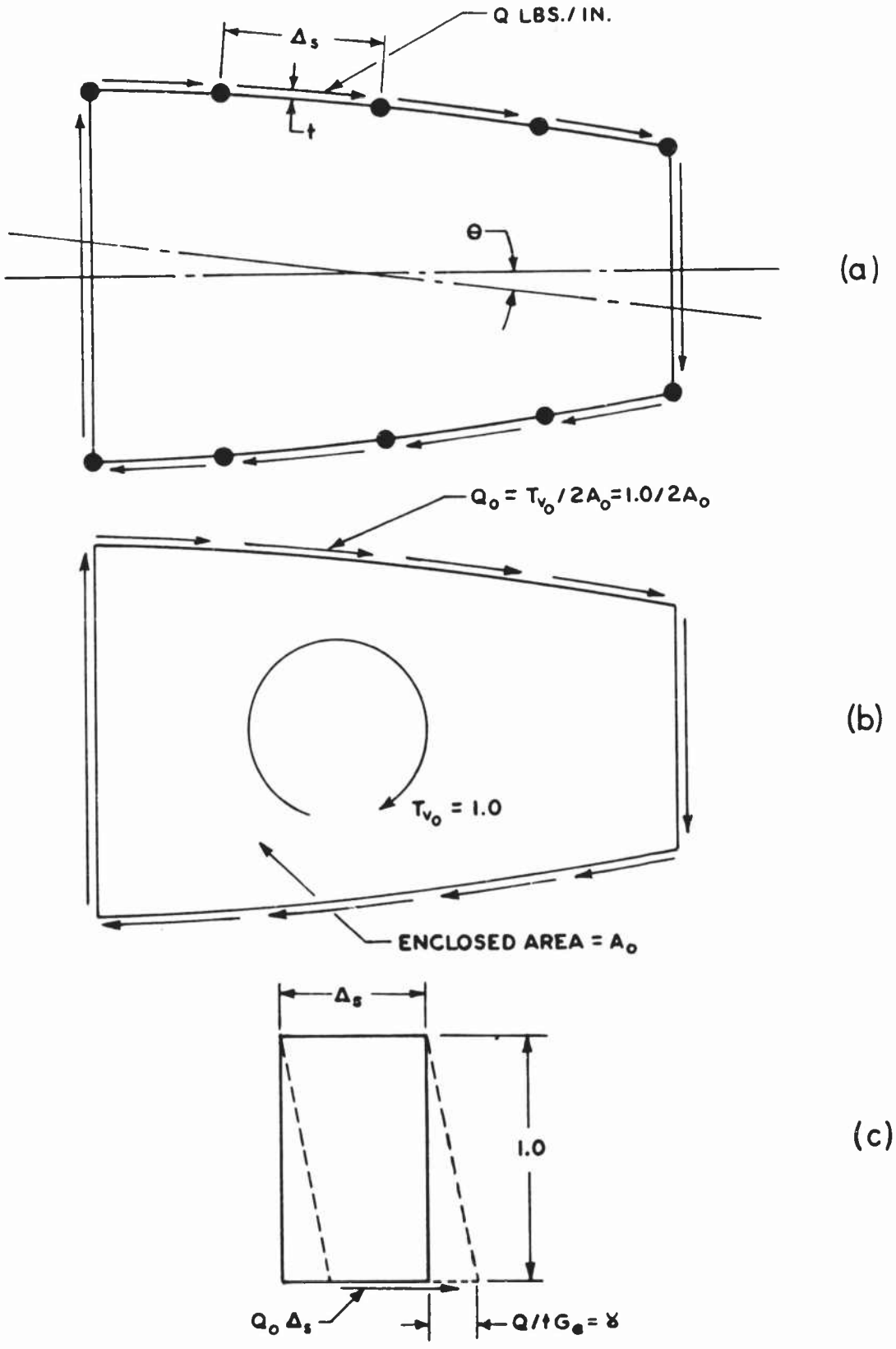

FIG. 85 NOTATION FOR DETERMINATION OF WORK DUE TO TWISTING OF A SINGLE CELL.

The general method of analysis of a multi-cell structure will be first to assume that the shear acts at the shear center with the angle of twist "θ" equal to zero. The external torque about the shear center is then computed and the shear flows from pure torque superimposed on the shear flows from transverse shear. In the tabular forms to be discussed presently, the torque about the shear center is computed without actually locating the shear center.

The determination of the shear flow in a three cell beam, such as illustrated in Figure 84, assuming the shear acting at the shear center, is described as follows. The shear in any external web of Cell A, Figure 84, may be expressed in terms of Q_1 as:

$$Q_n = Q_1 + \sum_{1}^{n-1} \Delta P/\Delta Y = Q_1 + Q^1_n \quad - - - - - - - - - - - - \quad (5)$$

Similarly the shear in any external web of Cells B and C can be expressed as:

$$\text{Cell B:} \quad Q_n = Q_{14} + \sum_{14}^{n-1} \Delta P/\Delta Y = Q_{14} + Q^1_n \quad - - - - - - - \quad (6)$$

$$\text{Cell C:} \quad Q_n = Q_{14} + \sum_{14}^{n-1} \Delta P/\Delta Y = Q_{14} + Q^1_n \quad - - - - - - - \quad (7)$$

The shear flows in the internal Webs a-b and b-c can be determined from consideration of the equilibrium conditions in the spanwise direction and may be expressed as follows; assuming positive shear flow to be upward:

$$Q_{a-b} = Q_1 + Q^1_{a-b} - Q_{10} \quad - - - - - - - - - - - - - - - \quad (8)$$

$$Q_{b-c} = Q_{10} + Q^1_{b-c} - Q_{14} \quad - - - - - - - - - - - - - - - \quad (9)$$

The shears Q^1_n are the shears in the beam of Figure 84 with the Webs 1, 10, and 14 assumed cut. The values of Q^1 for Cell A are obtained by a summation of the values of $\Delta P/\Delta Y$ between Web 1 and the section considered. This summation may be used to find Q^1 for the interior Web a-b. The values of Q^1 for Cell B are obtained by summation of the $\Delta P/\Delta Y$ values between Web 10 and the section considered. This summation starts from zero at Web 10 and includes the Q^1 for Web b-c. However, for the beam in Figure 84, Q^1 for Web 18 cannot be found until Q^1 for Web 17 is obtained. Therefore, the summation of $\Delta P/\Delta Y$ is interrupted at this point and the values of Q^1 around Cell C are determined. This summation starts from zero at Web 14 and proceeds in a clockwise direction around Cell C up to and including Q^1 for Web 17. Then the Q^1 for Web b-c is added to the value of Q^1 in Web 17 resulting in the required Q^1 for Web 18. It is then possible to complete the determination of Q^1 around Cell B in the usual manner.

As the shear had been assumed acting at the shear center, $\Theta = 0$ for each cell, therefore Equation (4) becomes

$$\Sigma q_{ns} \Delta s/t^1 = 0 \qquad - - - - - - - - - - - - - - - - - (10)$$

Around each cell, Equations (5), (8), and (10) give the following equation for Cell A.

$$\sum_A q_{ns} \Delta s/t^1 - q_{1S} \sum_A \Delta s/t^1 - q_{10S} (\Delta s/t^1)_{a-b} + \sum_A q^1{}_n \Delta s/t^1$$

$$= 0 \qquad - - - - - - - - (11)$$

The summation of Equation (11) must include all the webs around the circumference of Cell A. The notation $\sum_A$ will designate a summation for all webs of Cell A, with the shear considered as positive in a clockwise direction around the cell. The term $q_{10S} (\Delta s/t^1)$ for Web a-b in Equation (11) comes from Equation (8), which contains the additional terms q_{10S} not appearing in Equation (5). The evaluation of Equation (10) for Cell B using Equations (6), (8), (9), and (10) becomes:

$$\sum_B q_{ns} (\Delta s/t^1) = - q_{1S} (\Delta s/t^1)_{a-b} + q_{10S} \sum_B (\Delta s/t^1) - q_{14S} (\Delta s/t^1)_{b-c}$$

$$+ \sum_B q^1 (\Delta s/t^1) = 0 \qquad - - - - - - - - (12)$$

The evaluation of Equation (10) for Cell C using Equations (7), (9), and (10) becomes

$$\sum_C q_{ns} (\Delta s/t^1) = - q_{10S} (\Delta s/t^1)_{b-c} + q_{14S} \sum_C (\Delta s/t^1)$$

$$+ \sum_C q^1 (\Delta s/t^1) = 0 \qquad - - - - - - - - (13)$$

Abbreviating the coefficients of the "Q" terms in Equations (11), (12), and (13) we have

$$\Delta_{AA} q_{1S} - \Delta_{AB} q_{10S} + \Delta_{0A} = 0 \qquad - - - - - - - - - (14)$$

$$-\Delta_{AB} q_{1S} + \Delta_{BB} q_{10S} - \Delta_{BC} q_{14S} + \Delta_{0B} = 0 \qquad - - - - - - - - (15)$$

$$-\Delta_{BC} q_{10S} + \Delta_{CC} q_{14S} + \Delta_{0C} = 0 \qquad - - - - - - - - - - (16)$$

where $\Delta_{AA} = \sum_{A} (\Delta s/t^1)$ $\Delta_{BC} = (\Delta s/t^1)_{b-c}$

$\Delta_{BB} = \sum_{B} (\Delta s/t^1)$ $\Delta_{0A} = \sum_{A} q^1 (\Delta s/t^1)$

$\Delta_{CC} = \sum_{C} (\Delta s/t^1)$ $\Delta_{0B} = \sum_{B} q^1 (\Delta s/t^1)$

$\Delta_{AB} = (\Delta s/t^1)_{a-b}$ $\Delta_{0C} = \sum_{C} q^1 (\Delta s/t^1)$

- - - - - - - - - - - (17)

Equations (14), (15), and (16) can be solved for Q_{IS}, Q_{IOS}, and Q_{14S} after substitution of the numerical values for the Δ terms.

The torque about the shear center "T_{SC}" is determined as follows:

$$T_{SC} = T_O - \Sigma C_N \times Q_{ns} \quad - - - - - - - - - - - - - - - - (18)$$

where T_O is the external torque about the reference origin and the summation represents the moment of the shear flows, also about the reference origin. It is usually more convenient to use Equation (18) without actually finding the shear flow Q_{ns} for each web. From Equations (5), (6), (7), (8), (9), and (18)

$$T_{SC} = T_O - \Sigma C_N \times q^1_n - 2A_A \times Q_{IS} - 2A_B \times Q_{IOS} - 2A_C \times Q_{14} \quad - \quad (19)$$

since, for all the webs of any one cell, $\Sigma C_N = 2A$.

The shear flows resulting from the torque about the shear center must now be superimposed on those computed for zero torque. Since the pure torsion is assumed to produce no axial loads in the beam elements, the shear flows will have a constant value around each cell. (Q_{IT} for Cell A, Q_{IOT} for Cell B, etc.). The shear in the interior webs, assuming positive shear in external webs acts clockwise and positive shear in internal webs acts up, is expressed by -

$$Q_{a-b_T} = Q_{IT} - Q_{IOT} \quad - - - - - - - - - - - - - - - - - (20)$$

$$Q_{b-c_T} = Q_{IOT} - Q_{14T} \quad - - - - - - - - - - - - - - - - - (21)$$

From the condition that the angle of twist must be equal, Equation (4) yields -

$$(1/2A_A) \sum_A q_{nT} (\Delta s/t^1) = (1/2A_B) \sum_B q_{nT} (\Delta s/t^1)$$

$$= (1/2A_C) \sum_C q_{nT} (\Delta s/t^1) \quad - - - - \quad (22)$$

Substituting the subscript "T" for the "S" Equations (5), (6), (7), (8), and (9), and utilizing the abbreviation of Equations (17), Equation (22) becomes -

$$(1/2A_A)(\Delta_{AA} q_{IT} - \Delta_{AB} q_{1OT}) = (1/2A_B)(-\Delta_{AB} q_{IT} + \Delta_{BB} q_{1OT} - \Delta_{BC} q_{14T})$$

$$= (1/2A_C)(-\Delta_{BC} q_{IDT} + \Delta_{CC} q_{14T}) \quad - - - - \quad (23)$$

The condition that the torque of q_{IT}, q_{1OT}, and q_{14T} must equal the external torque T_{SC} about the shear center, yields the following equation.

$$T_{SC} = 2A_A \times q_{IT} + 2A_B \times q_{1OT} + 2A_C \times q_{14T} \quad - - - - - - - - - \quad (24)$$

Equations (23) and (24) can be solved for the values of q_{IT}, q_{1OT}, and q_{14T} after substitution of the numerical values of the Δ and A terms and T_{SC}.

The shear flows in the cut web of each cell may now be found by combining the results of the analysis for bending shears and for torsion, thus -

$$\left.\begin{aligned} q_1 &= q_{1S} + q_{1T} \\ q_{1O} &= q_{1OS} + q_{1OT} \\ q_{14} &= q_{14S} + q_{14T} \end{aligned}\right\} - - - - - - - - - - - - - - - \quad (25)$$

The final shear flows in the external webs of Cells A, B, and C are determined from the Equations (5), (6), and (7). The final shear flows for the internal webs a-b and b-c are obtained from Equations (8) and (9).

Detailed calculations were made for the determination of the shear flow between the various stabilizer stations for the dynamic loading conditions (A and B), which are the most critical. These shear flows represented average values in any given bay since the calculations were based upon averaged values of web moment coefficient "C_N" and the stiffness parameter " $\Delta s/t$ ". Since the stabilizer nose extends inboard only as far as Station 10, the stabilizer was analyzed as a three-cell structure outboard of Station 10. Inboard of Station 10, a "Center Section Analysis" was employed. Since the "Center Section Analysis" deals primarily with the attachment of the stabilizer to the fuselage and vertical fin, it is omitted from this report for reasons of brevity.

The following tables illustrate the application of the method of shear flow calculation as applied to the bay between Station 30 and 45.

Table 12 This table summarizes the average values of the stiffness parameter $\Delta s/t$ for each web in the various bays.

Table 13 This table summarizes the averages of the web moment coefficients C_N at the inboard and outboard ends of each bay.

Table 14 The values of Q^1 in the various webs are obtained in this table by the summation of $\Delta P/\Delta Y$ around each cell.

Table 15 The numerical values of the Δ coefficients used in Equations (14), (15), (16), (23), and (24) are computed in this table. This summation of $Q^1 C_N$ is also obtained in this table for subsequent use in evaluating the torque about the shear center.

Table 16 The solution of Equations (14), (15), and (16) for Q_{1S}, Q_{10S}, and Q_{14S} is performed in this table.

Table 17 The total unbalanced torque about the shear center, as expressed by Equation (19), is evaluated in this table.

Table 18 The coefficients of the three simultaneous equations developed from Equations (23) and (24) are determined in this table.

Table 19 This table shows the evaluation of Q_{1T}, Q_{10T}, and Q_{14T} such that Equations (23) and (24) are satisfied for a unit torque of 10^6 in.lbs.

Table 20 The final shear flows in the redundant webs are obtained in this table in accordance with Equations (25).

Table 21 The final ultimate shear flows in the various webs are calculated in this table in accordance with Equations (5) thru (9), inclusive.

The ultimate shear flows throughout the stabilizer for the dynamic loading conditions A and B are summarized in Table 22.

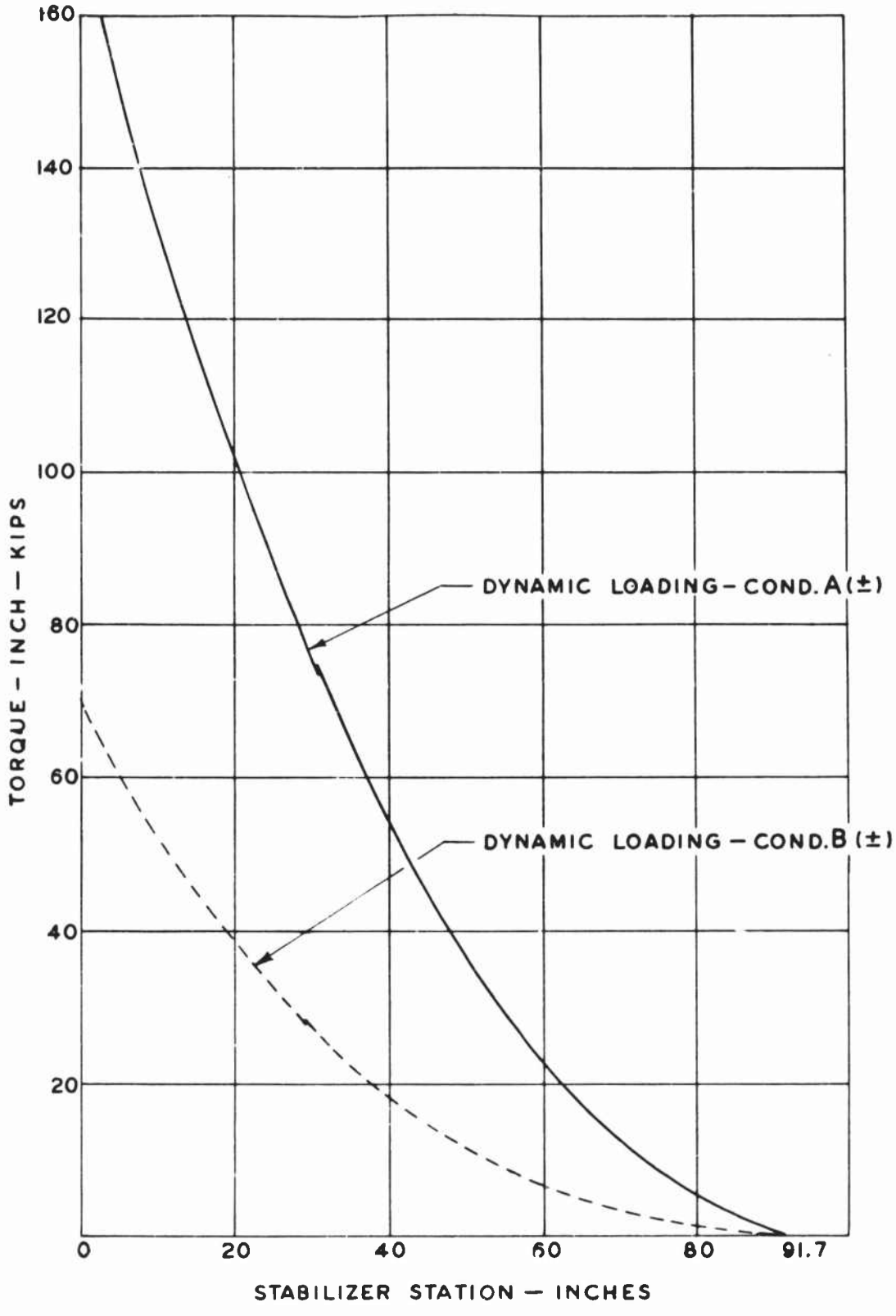

FIG. 86 NET STABILIZER TORQUES — ULTIMATE ABOUT REFERENCE AXIS (REF. TABLE 5)

TABLE 12 - SUMMARY OF AVERAGE VALUES OF $\Delta s/t$

Web \ Bay	10 to 30	30 to 45	45 to 60	60 to 80
1	12.64	12.79	12.87	13.28
2	25.36	25.59	25.75	26.55
3	25.36	25.68	25.86	26.55
4	12.64	12.79	12.87	13.28
5	12.79	16.67	14.85	27.17
6	12.64	12.79	12.87	13.28
7	25.36	25.68	25.86	26.55
8	25.36	25.59	25.75	26.55
9	12.64	12.79	12.87	13.28
10	12.43	13.51	14.60	17.24
11	25.29	27.03	29.08	34.31
12	25.29	27.03	29.08	34.14
13	12.43	13.51	14.60	17.24
14	15.86	16.94	18.16	21.55
15	49.79	53.33	57.24	67.07
16	49.79	53.33	57.24	67.07
17	15.86	16.94	18.16	21.55
18	12.43	13.51	14.60	17.24
19	25.29	27.03	29.08	34.14
20	25.29	27.03	29.08	34.31
21	12.43	13.51	14.60	17.24
a-b	48.63	41.00	34.00	25.88
b-c	18.06	18.84	19.91	22.18

TABLE 13 - SUMMARY OF AVERAGE WEB MOMENT COEFFICIENT ($C_{N_{AV}}$)

Web \ Bay	10 to 30	30 to 45	45 to 60	60 to 80
1	5.03	3.50	2.51	1.56
2	5.72	4.00	2.76	1.60
3	5.12	3.61	2.51	1.49
4	2.16	1.54	1.09	.64
5	0	0	0	0
6	2.16	1.54	1.09	.64
7	5.12	3.61	2.51	1.49
8	5.72	4.00	2.76	1.60
9	5.03	3.50	2.51	1.56
10	11.22	.88	.54	.22
11	8.74	6.22	4.38	2.74
12	10.04	7.12	5.06	3.12
13	10.66	7.51	5.24	3.16
14	3.00	2.10	1.54	1.04
15	49.18	34.65	24.26	14.54
16	49.18	34.65	24.26	14.54
17	3.00	2.10	1.54	1.04
18	10.66	7.51	5.24	3.16
19	10.04	7.12	5.06	3.12
20	8.74	6.22	4.38	2.74
21	1.22	.88	.54	.22
a-b	41.79	28.21	18.58	10.00
b-c	65.82	45.86	31.88	18.89

TABLE 14 - DETERMINATION OF Q^1
STATION 30 TO 45

DYNAMIC LOADING CONDITION (A & B)

①	②	③	④	⑤
Web	P Sta. 30	P Sta. 45	$\Delta P/\Delta Y$	Q'
Ref.	Table 10	Table 10	② - ③ /15	Σ④
1	-5586	-3093	-166.2	0
2	-5089	-2848	-149.4	-166.2
3	-4299	-2443	-124.4	-315.6
4	-1956	-1695	- 17.4	-440.0
5	1956	1695	17.4	-457.4
6	4299	2433	124.4	-440.0
7	5089	2848	149.4	-315.6
8	5586	3093	166.2	-166.2
9	4548	3763	52.3	0
a-b				52.3
10	5911	3445	164.4	0
11	5670	3322	156.5	164.4
12	5221	3055	144.4	320.9
13	4571	2945	108.4	465.3
b-c				573.7
14	5345	3141	146.9	0
15		-	-	146.9
16	-5345	-3141	-146.9	146.9
17	-4571	-2945	-108.4	0
b-c				573.7
18	-5221	-3055	-144.4	465.3
19	-5670	-3322	-156.5	320.9
20	-5911	-3445	-164.4	164.4
21	-4548	-3763	- 52.3	0
a-b				- 52.3

TABLE 15 - DETERMINATION OF SHEAR FLOW PARAMETERS
STATION 30 TO 45

①	②	③	④	⑤	⑥	⑦
Cell	Web	$\Delta s/t$	C_n	Dynamic Loading Cond. Q^1	$Q^1 \Delta s/t$	$Q^1 C_n$
Ref.	Fig. 6	Tab. 12	Tab. 13	Tab. 14	③ x ⑤	④ x ⑤
A	1	12.79	3.50	0	0	0
	2	25.59	4.00	-166.2	-4253	-665
	3	25.68	3.61	-315.6	-8105	-1139
	4	12.79	1.54	-440.0	-5628	-678
	5	16.67	0	-457.4	-7625	0
	6	12.79	1.54	-440.0	-5628	-678
	7	25.68	3.61	-315.6	-8105	-1139
	8	25.59	4.00	-166.2	-4253	-665
	9	12.79	3.50	0	0	0
	a-b	41.00	28.21	52.3	2144	1475
	Δ_{ab} = 41.00	Δ_{AA} = 211.37	$2A_A$ = 53.51		Δ_{oA} = 41453	
B	10	13.51	.88	0	0	0
	11	27.03	6.22	164.4	4444	1023
	12	27.03	7.12	320.9	8674	2285
	13	13.51	7.51	465.3	6286	3494
	b-c	18.84	45.86	573.7	10809	26310
	18	13.51	7.51	465.3	6286	3494
	19	27.03	7.12	320.9	8674	2285
	20	27.03	6.22	164.4	4444	1023
	21	13.51	.88	0	0	0
	a-b	41.00	-28.21	-52.3	-2144	-
	Δ_{bc} = 18.84	Δ_{BB} = 222.00	$2A_B$ = 61.11		Δ_{oB} = 47473	
C	14	16.94	2.10	0	0	0
	15	53.33	34.65	146.9	7834	5090
	16	53.33	34.65	146.9	7834	5090
	17	16.94	2.10	0	0	0
	b-c	18.84	-45.86	-573.7	-10809	-
		Δ_{CC} = 159.38	$2A_C$ = 27.64		Δ_{oC} = 4859	
Σ						46605

TABLE 16 - SOLUTION OF EQUATIONS FOR BALANCING
FLEXURAL SHEAR FLOW
STATION 30 TO 45

$$+ \Delta_{AA} q_{1S} - \Delta_{AB} q_{10S} + \Delta_{oA} = 0$$

$$- \Delta_{AB} q_{1S} + \Delta_{BB} q_{10S} - \Delta_{BC} q_{14S} + \Delta_{oB} = 0$$

$$\Delta_{BC} q_{10S} + \Delta_{CC} q_{14S} + \Delta_{oC} = 0$$

No.	Ref.	q_{1S}	q_{10S}	q_{14S}	Dynamic Loading Condition
(1)	Table 15	$+\Delta_{AA}$ = 211.37	$-\Delta_{AB}$ = -41.00	0	$-\Delta_{oA}$ = 41453
(2)	Table 15	$-\Delta_{AB}$ = -41.00	$+\Delta_{BB}$ = 222.00	$-\Delta_{BC}$ = -18.84	$-\Delta_{oB}$ = 47473
(3)	Table 15	0	$-\Delta_{BC}$ = -18.84	$+\Delta_{CC}$ = 159.38	$-\Delta_{oC}$ = -4859
(4)	(1)/Δ_{AA}	+1	K_1 = -.1940	0	K_2 = 196.12
(5)	(2)/Δ_{AB}	-1	5.4146	-.4595	-1157.0
(6)	(4) + (5)	0	K_3 = 5.2206	-.4595	-961.8
(7)	(6)/K_3		+1	K_4 = -.0880	K_5 = -184.23
(8)	(3)/Δ_{BC}		-1	8.4597	-257.91
(9)	(7) + (8)		0	K_6 = 8.3717	-442.14
(10)	(9)/K_6			+1	q_{14S} = -52.81
(11)	-(10) x K_4				-4.65
(12)	(11) + K_5				q_{10S} = -188.88
(13)	-(12) x K_1				-36.64
(14)	(13) + K_2				q_{1S} = 159.48

TABLE 17 - UNBALANCED TORSION ABOUT SHEAR CENTER
STATION 30 TO 45
DYNAMIC LOADING

No.	Item	Ref. \ Cond.	A	B
1	$2A_A$	Table 15	53.51	
2	$2A_B$		61.11	
3	$2A_C$		27.64	
4	Q_{1S}	Table 16	159.48	
5	Q_{10S}		-188.88	
6	Q_{14S}		-52.81	
7	T_o	Figure 86	57,500	21,200
8	$-\Sigma C_n Q^1$	Table 15	-46,605	
9	$-2A_A Q_{1S}$	-(1) x (4)	-8,534	
10	$-2A_B Q_{10S}$	-(2) x (5)	11,542	
11	$-2A_C Q_{14S}$	-(3) x (6)	1,460	
12	T_{SC}	Σ (7) to (11)	15,363	-20,937

TABLE 18 - CONSTANTS FOR SOLUTION OF TORSIONAL SHEAR FLOW EQUATIONS

No.	Item	Ref. \ Bay	30 to 45
(1)	Δ_{AA}	Table 15	211.37
(2)	Δ_{AB}		41.00
(3)	Δ_{BB}		222.00
(4)	Δ_{BC}		18.84
(5)	Δ_{CC}		159.38
(6)	$2A_A$		53.51
(7)	$2A_B$		61.11
(8)	$2A_C$		27.64
(9)	$\Delta_{AA}/2A_A$	(1)/(6)	3.9501
(10)	$\Delta_{BB}/2A_B$	(2)/(7)	.6709
(11)	$\Delta_{AB}/2A_A$	(2)/(6)	.7662
(12)	$\Delta_{BB}/2A_B$	(3)/(7)	3.6328
(13)	$\Delta_{BC}/2A_C$	(4)/(8)	.6816
(14)	$\Delta_{BC}/2A_B$	(4)/(7)	.3083
(15)	$\Delta_{CC}/2A_C$	(5)/(8)	5.7663
(16)	A_1	(9) + (10)	4.6210
(17)	A_2	(10)	.6709
(18)	B_1	(11) + (12)	4.3990
(19)	B_2	(12) + (13)	4.3144
(20)	C_1	(14)	.3083
(21)	C_2	(14) + (15)	6.0746

TABLE 19 - SOLUTION OF EQUATIONS FOR UNIT TORSIONAL SHEAR FLOW
STATION 30 TO 45

$$\left[1/2A_A\right]\left[\Delta_{AA}\, q_{1T} - \Delta_{AB}\, q_{10T}\right] - \left[1/2A_B\right]\left[-\Delta_{AB}\, q_{1T} + \Delta_{BB}\, q_{10T} - \Delta_{BC}\, q_{14T}\right] - \left[1/2A_C\right]\left[-\Delta_{BC}\, q_{10T} + \Delta_{CC}\, q_{14T}\right]$$

$$2A_A\, q_{1T} + 2A_B\, q_{10T} + 2A_C\, q_{14T} = T_{SC}$$

No.	Reference	q_{1T}	q_{10T}	q_{14T}	
1	Table 18	$+A_1$ = 4.6210	$-B_1$ = -4.3990	$+C_1$ = .3083	0
2		$-A_2$ = -.6709	$+B_2$ = 4.3114	$-C_2$ = -6.0746	0
3		$2A_A$ = 53.51	$2A_B$ = 61.11	$2A_C$ = 27.64	T_{SC} = +1,000,000
4	(1)/A_1	+1	K_1 = -.9520	K_2 = .06672	0
5	(2)/A_2	-1	6.4308	-9.0544	0
6	(4) + (5)	0	K_3 = 5.4788	-8.9877	0
7	(3)/$2A_A$	+1	1.1420	.5165	18,688
8	(4) - (7)	0	K_4 = -2.0940	-.4498	-18,688
9	-(8)/K_4		-1	K_5 = -.2148	K_6 = -8924.5
10	(6)/K_3		+1	-1.6405	0
11	(9) + (10)		0	K_7 = -1.8553	-8924.5
12	(11)/K_7			+1	q^1_{14T} = 4810.3
13	(12) x K_5				-1033.3
14	(13) - K_6				q^1_{10T} = 7891.2
15	-(14) x K_1				7512.4
16	-(12) x K_2				-320.9
17	(15) + (16)				q^1_{1T} = 7191.5

TABLE 20 - SHEAR FLOW IN REDUNDANT WEBS
STATION 30 TO 45
DYNAMIC LOADING

No.	Item	Cond. / Ref.	A	B
1	q^1_{1T}	Table 19	7191.5	
2	q^1_{10T}		7891.2	
3	q^1_{14T}		4810.3	
4	$T_{SO}/10^6$	Table 17	.015363	-.020937
5	Q_{1T}	(1) x (4)	110.5	-150.6
6	Q_{10T}	(2) x (4)	121.2	-165.2
7	Q_{14T}	(3) x (4)	73.9	-100.7
8	Q_{1S}	Table 16	159.5	
9	Q_{10S}		-188.9	
10	Q_{14S}		-52.8	
11	Q_1	(5) + (8)	270.0	8.9
12	Q_{10}	(6) + (9)	-67.7	-354.1
13	Q_{14}	(7) + (10)	21.1	-153.5

TABLE 21 - DETERMINATION OF RESULTANT SHEAR FLOW
STATION 30 TO 45

①	②	③	④	⑤	⑥	⑦	⑧
Web	Cell	Dynamic Load Cond. A			Dynamic Load Cond. B		
		Q'	Q_n	Q	Q'	Q_n	Q
Ref.	Fig. 84	Table 14	Table 20	③ + ④	Table 14	Table 20	⑥ + ⑦
1	A	0	270.0	270.0	0	8.9	8.9
2	↑	-166.2	↑	103.8	-166.2	↑	-157.3
3		-315.6		-45.6	-315.6		-306.7
4		-440.0		-170.0	-440.0		-431.1
5		-457.4		-187.4	-457.4		-448.5
6		-440.0		-170.0	-440.0		-431.1
7		-315.6		-45.6	-315.6		-306.7
8	↓	-166.2	↓	103.8	-166.2	↓	-157.3
9	A	0	270.0	270.0	0	8.9	8.9
10	B	0	-67.7	67.7	0	-354.1	-354.1
11	↑	164.4	↑	96.7	164.4	↑	-189.7
12	↓	320.9	↓	253.2	320.9	↓	-33.2
13	B	465.3	-67.7	397.6	465.3	-354.1	111.2
14	C	0	21.1	21.1	0	-153.5	-153.5
15	↑	146.9	↑	168.0	146.9	↑	-6.6
16	↓	146.9	↓	168.0	146.9	↓	-6.6
17	C	0	21.1	21.1	0	-153.5	-153.5
18	B	465.3	-67.7	397.6	465.3	-354.1	111.2
19	↑	320.9	↑	253.2	320.9	↑	-33.2
20	↓	164.4	↓	96.7	164.4	↓	-189.7
21	B	0	-67.7	-67.7	0	-354.1	-354.1
a-b	AB	52.3	337.7	390.0	52.3	363.0	415.3
b-c	BC	573.7	-88.8	484.9	573.7	-200.6	373.1

TABLE 22 - SUMMARY OF ULTIMATE SHEAR FLOWS

Web	Station 10 to 30		Station 30 to 45		Station 45 to 60		Station 60 to 80	
	Cond. A	Cond. B	Cond. A	Cond. B	Cond. A	Cond. B	Cond. A	Cond. B
1	456	133	270	9	194	-21	136	-5
2	186	-136	104	-157	83	-132	73	-68
3	-55	-377	-46	-307	-18	-233	14	-126
4	-251	-573	-170	-431	-103	-318	-36	-177
5	-407	-730	-187	-449	-126	-342	-79	-220
6	-251	-573	-170	-431	-103	-318	-36	-177
7	-55	-377	-46	-307	-18	-233	14	-126
8	-186	-136	104	-157	83	-132	73	-68
9	456	133	270	9	194	-21	136	-5
10	-19	-370	-68	-354	-28	-261	-34	-192
11	237	-114	97	-190	87	-146	40	-118
12	484	133	253	-33	198	-36	111	-46
13	711	360	398	111	300	67	177	19
14	398	184	21	-154	24	-117	8	-87
15	122	-92	168	-7	131	-11	86	-9
16	122	-92	168	-7	131	-11	86	-9
17	398	184	21	-154	24	117	8	-87
18	711	360	398	111	300	67	177	19
19	484	133	253	-33	198	-36	111	-46
20	237	-114	97	-190	87	-146	40	-118
21	-19	-370	-68	-354	-28	-261	-34	-192
a-b	539	567	390	415	361	379	227	244
b-c	473	336	485	373	358	266	237	174

Compression Surface Design

Panel Buckling

The buckling of curved plates under axial or edge compression is computed by Wenzek's method (Reference page 314 of "Airplane Structural Analysis and Design" by Sechler and Dunn), as follows:

$$\sigma_{cr_p} = \sigma_{cr_f} + \sigma_{cr_c} \qquad - - - - - - - - - - - - - - - (26)$$

where: σ_{cr_p} = allowable buckling stress for curved plate.

σ_{cr_f} = allowable buckling stress for flat plate with same t/b ratio as curved plate.

σ_{cr_c} = allowable buckling stress for cylinder with same R/t ratio as curved plate.

In the above equation, σ_{cr_f} and σ_{cr_c} are determined as follows:

$$\sigma_{cr_f} = K_f \left[\frac{2}{12\,(1-\mu^2)} \right] E \left(\frac{t}{b}\right)^2 \qquad - - - - - - - - - (27)$$

For $E = 6.5 \times 10^6$ and $\mu = .30$:

$$\sigma_{cr_f} = 5.88 \times 10^6\ (K_f)\ (t/b)^2 \qquad - - - - - - - - - - (27)$$

$$\sigma_{cr_c} = E \left[9(t/R)^{1.6} + .16(t/L)^{1.3} \right] \qquad - - - - - - - - - (28)$$

$$= E\,K_c \qquad - - - - - - - - - - - - - - - - - - - (28)$$

where: K_f = end fixity coefficient for flat plate.

K_c = allowable strain coefficient for cylinder.

t = plate thickness - inches.

b = width of plate - inches.

R = radius of cylinder - inches.

L = length of cylinder - inches.

TABLE 23 - CURVED PLATE - COMPRESSIVE BUCKLING ALLOWABLES

①	②	③	④	⑤	⑥	⑦	⑧	⑨	⑩	⑪	⑫	⑬	⑭	⑮
Sta.	Loc.	t	L	b	R	b/t	$(b/t)^2$	K_f	σ_{cr_f}	R/t	L/R	$K_c \times 10^6$	σ_{cr_c}	σ_{cr_p}
Ref.						⑤/③	$⑦^2$	See Note	Eq. (27)	⑥/③	④/⑥	Eq. (28)	6.5x⑬	⑩ + ⑭
0	Fwd	.172	10.0	10.60	124	61.63	3798	7.2 *	11147	721	.081	1054	6850	18000
	Aft	.172	10.0	11.52	124	66.98	4486	7.5 *	9831	721	.081			16680
10 in	Fwd	.156	10.0	9.99	114	64.04	4101	6.7 *	9606	731	.088	952	6190	15800
	Aft	.156	10.0	10.66	114	68.33	4669	7.3 *	9193	731	.088			15380
10_{out}	Fwd	.156	20.0	9.99	114	64.04	4101	8.2	11757	731	.175	527	3425	15180
	Aft	.156	20.0	10.66	114	68.33	4669	8.25	10390	731	.175			13810
20	Fwd	.140	20.0	9.16	104	65.43	4281	8.1	11125	743	.192	483	3140	14260
	Aft	.140	20.0	11.02	104	78.71	6195	8.3	7878	743	.192			11020
30 in	Fwd	.123	20.0	8.31	94	67.56	4564	7.8	10049	764	.213	433	2815	12860
	Aft	.123	20.0	9.81	94	79.76	6362	8.2	7579	764	.213			10390
30_{out}	Fwd	.123	30.0	8.31	94	67.56	4564	7.6	9791	764	.319	345	2240	12030
	Aft	.123	↑	9.81	94	79.76	6362	7.7	7117	764	.319			9360
40	Fwd	.107		7.49	84	70.00	4900	7.5	9000	785	.357	315	2050	11050
	Aft	.107		8.62	84	80.56	6490	7.7	6976	785	.357			9030
50	Fwd	.091		6.64	74	72.97	5325	7.5	8282	813	.405	284	1845	10130
	Aft	.091		7.43	74	81.65	6667	7.5	6615	813	.405			8460
60 in	Fwd	.0745	↓	5.66	64	75.97	5771	7.4	7540	859	.469	248	1610	9150
	Aft	.0745	30.0	6.23	64	83.62	6992	7.5	6307	859	.469			7920
60_{out}	Fwd	.0745	20.0	6.62	64	88.86	7896	7.7	5734	859	.313	294	1910	7640
	Aft	.0745	↑	6.23	64	83.62	6992	7.7	6475	859	.313			8380
70	Fwd	.058		5.81	54	100.17	10034	7.6	4454	931	.370	240	1560	6010
	Aft	.058		5.02	54	86.55	7491	7.5	5887	931	.370			7450
80	Fwd	.042	↓	5.01	44	119.29	14230	7.5	3099	1048	.455	185	1200	4300
	Aft	.042	20.0	3.82	44	90.95	8272	7.4	5260	1048	.455			6460

NOTE: - K_f based on Fig. 5.8, Page 168, "Airplane Structural Analysis and Design" by Sechler and Dunn.
- All panels outboard of Station 10 are assumed clamped along all four edges.
- *Panels inboard of Station 10 are assumed clamped at ribs and simply-supported at spars.

The percentage of limit load at which panel buckling may be expected is shown in Table 24. The values are based upon the curved plate buckling allowables in axial compression computed in Table 23 and neglect the effect of shear buckling, since the relatively thick skins employed result in very small shear stresses.

Ultimate Strength

The following analysis is presented to show the ultimate strength of the compression surface (skin and spar caps) after buckling of the skin panels has taken place.

The following method, (Reference page 318 of "Airplane Structural Analysis and Design" by Sechler and Dunn) is used to obtain ultimate strength checks of the various curved plates involved. The total compressive strength of a curved plate may be expressed as:

$$P_{total} = 2 W_e t \sigma_{YP} + (b-2W_e) t \sigma_{cr_c} \quad - - - - - - - (29)$$

where: P_{total} = allowable compressive load in plate-lbs.

W_e = effective width of plate at each edge-ins.

σ_{YP} = comp. yield strength of plate material-psi.

In Equation (29), effective widths (W_e) are conservatively obtained from the "Ultimate Curve" given in Figure 6.2, Page 205 of the above reference. To obtain W_e/b values from this curve, the stiffener edge stress, σ_{se}, is assumed as equal to σ_{YP} (= 24,000 psi for FS-1h sheet) and σ_{cr} is assumed equal to σ_{cr_f}.

In Table 25, the ultimate compressive surface load is derived from the basic section properties for fully effective skins and includes spar cap loads. This is compared, in Table 26, with P_{total} for the buckled skins as obtained from Equation (29), plus ΣP (allowable) for the spar caps. Allowable cap loads are based on a compressive yield stress of 27,000 psi for ZK-60 magnesium alloy extrusions.

TABLE 24 - PANEL BUCKLING - PERCENT LIMIT LOAD
DYNAMIC LOADING - CONDS. A AND B

①	②	③	④	⑤	⑥
Item / Panel *	Ultimate f_c (inbd)	Ultimate f_c (outbd)	Limit f_c (aver)	σ_{cr_p} (aver.)	% Limit Load -Buckling
Reference	Table 11	Table 11	$\frac{② + ③}{2 \times 1.5}$	Table 23	$\frac{⑤}{④} \times 100$
Sta. 0-10 (Fwd)	14,870	17,660	10,840	16,900	156%
Sta. 0-10 (Aft)	13,460	16,090	9,850	16,030	163
Sta. 10-30 (Fwd)	17,660	14,280	10,650	14,260	134
Sta. 10-30 (Aft)	16,090	13,150	9,750	11,020	113
Sta. 30-45 (Fwd)	14,280	12,120	8,800	11,300	128
Sta. 30-45 (Aft)	13,150	11,300	8,150	9,110	112
Sta. 45-60 (Fwd)	12,120	9,710	7,280	9,880	136
Sta. 45-60 (Aft)	11,300	9,130	6,810	8,320	122
Sta. 60-80 (Fwd)	9,710	3,360	4,360	6,010	138
Sta. 60-80 (Aft)	9,130	3,290	4,140	7,450	180

* Forward skin element is No. 19, Fig. 83

Aft skin element is No. 2, Fig. 83

TABLE 25 - ULTIMATE COMPRESSIVE LOAD IN UPPER SURFACE
DYNAMIC LOADING CONDITIONS

ΣP_{US} - ultimate compressive load in upper surface

$\Sigma P_{US} = \Sigma P$ (element Nos. 1, 2, 3, 4, 16, 17, 18, 19, 20, 21)

Reference Table 10 for axial loads.

Sta. / Elem. Load	0	10	30	45	60	80
P_1	-11214#	-10972#	-5586#	-3093#	-1429#	-165#
P_2	-10070	-9909	-5089	-2848	-1324	-158
P_3	-8285	-8217	-4299	-2433	-1158	-145
P_4	-5505	-5082	-1956	-1695	-1348	-493
P_{16}	0	0	-5345	-3141	-1547	0
P_{17}	-7435	-7771	-4571	-2945	-1712	-349
P_{18}	-9771	-9762	-5221	-3055	-1525	-216
P_{19}	-10647	-10611	-5670	-3322	-1660	-235
P_{20}	-11041	-11036	-5911	-3445	-1722	-245
P_{21}	-4975	-5822	-4548	-3763	-1688	-537
P_{US}	-78940	-79180	-48200	-29740	-15110	-2540

TABLE 26 - COMPARISON OF ULTIMATE COMPRESSIVE LOAD TO ALLOWABLE LOAD.

No.	Item	Ref.	Sta. 0	Sta. 10	Sta. 30	Sta. 45	Sta. 60	Sta. 80
(1)	$\sigma_{se} = \sigma_{yp}$ (Skin)	Pa. 153	24,000	24,000	24,000	24,000	24,000	24,000
(2)	σ_{yp} (Spar Caps)	Pa. 153	27,000	27,000	27,000	27,000	27,000	27,000
(3)	σ_{cr_c} psi	TAB. 23	6,850	3,425	2,240	1,950	1,910	1,200
(4)	t (Skin) ins.	TAB. 23	.172	.156	.123	.099	.0745	.042
	Forward Panel							
(5)	σ_{cr_f}	TAB. 23	11,150	11,760	9,790	8,640	5,730	3,100
(6)	$\sigma_{se}/\sigma_{cr_f}$	① / ⑤	2.15	2.04	2.45	2.78	4.19	7.74
(7)	We/b	Note a	.218	.220	.210	.200	.170	.130
(8)	b (℄ Spar to ℄ Spar)	TAB. 6	12.48	11.55	9.68	8.29	6.89	5.03
(9)	We	⑦ x ⑧	2.72	2.54	2.03	1.66	1.17	.654
(10)	b - 2We	⑧ -2 ⑨	7.04	6.47	5.62	4.97	4.55	3.72
(11)	$2(We)t\,\sigma_{yp}$	2 ⑨ × ④ ①	22,460	19,020	11,990	7,890	4,180	1,320
(12)	$(b - 2We)t\,\sigma_{cr_c}$	⑩ × ④ × ③	8,290	3,460	1,550	960	650	190
	Aft Panel							
(13)	σ_{cr_f}	TAB. 23	9,830	10,390	7,120	6,795	6,475	5,260
(14)	$\sigma_{se}/\sigma_{cr_f}$	① / ⑬	2.44	2.31	3.37	3.53	3.71	4.56
(15)	We/b	Note a	.210	.215	.185	.180	.175	.165
(16)	b (℄ Spar to ℄ Spar)	TAB. 2	13.05	11.84	9.43	7.63	5.83	3.42
(17)	We	⑮ x ⑯	2.74	2.55	1.74	1.37	1.02	.564
(18)	b - 2We	⑯ -2 ⑰	7.57	6.74	5.95	4.89	3.79	2.29
(19)	2 Wet σ_{yp}	2 ⑰ × ④ ①	22,620	19,090	10,270	6,510	3,650	1,140
(20)	$(b - 2We)t\,\sigma_{cr_c}$	⑱ × ④ × ③	8,920	3,600	1,640	940	540	120
(21)	Nose Skin: Area - Elem. "b"	TAB. 6	0	0	.498	.344	.213	0
(22)	P_{16} (Allow.) (b)	TAB. 6	0	0	5,980	4,130	2,560	0
(23)	ΣSpar Cap Areas (Up)	TAB. 6	1.682	1.445	.999	.883	.638	.527
(24)	ΣP_{caps} (Allowable)	27000 × ㉓	45,410	39,020	26,970	23,840	17,230	14,230
(25)	$\Sigma P_{U.S.}$ (Allowable	⑪ + ⑫ + ⑲ + ⑳ + ㉒ + ㉔	107,700	84,190	58,400	44,270	28,810	17,000
(26)	$\Sigma P_{U.S.}$ (Ultimate)	TAB. 25	78,940	79,180	48,200	29,740	15,110	2,450
(27)	M.S.	㉕ / ㉖ -1	+.36	+.06	+.21	+.49	+.91	Ample

Notes: (a) Reference Figure 6.2, Page 205, "Airplane Stress Analysis and Design" by Sechler and Dunn.

(b) Based on $We/b = .25$ for nose skin.

FUSELAGE

Introduction

The fuselage fabricated under Contract AF 33(038)-5121 is designed to be interchangeable with that of the Lockheed F-80C airplane. Consequently, it will carry the same equipment and useful load items for which the latter is designed and will house those items at the same locations as on the Lockheed F-80C.

The E.C.A. fuselage structure is of magnesium alloy material and semi-monocoque in construction. The external skin covering consists of FS-1h sheet varying in gage from .064 to .102. Bending moments are carried by three or four main longerons which are machined from ZK-60A extrusions or bar stock. Practically all the secondary stringers used in the Lockheed design have been eliminated in the E.C.A. article. Fuselage frames varying in spacing from 6" to 15" are placed at the same locations as on the Lockheed article so as to avoid internal interference with equipment items. In general, these frames are formed from FS-1h sheet. However, special highly loaded frames are made from AM 265-T6 (heat-treated and aged) magnesium alloy sand castings (Comp. A). In addition, several frames in the aft section are made from stainless steel because of high temperatures from the engine tail pipe. In general, most fittings are made from ZK-60 or ZK-60A bar stock; however, in some cases Lockheed type dural or steel fittings had to be employed due to space or interchangeability requirements.

The E.C.A. fuselage structural weight is designed to not exceed that of the Lockheed article by more than 3%. Since the equipment and useful load items are unchanged both in weight and location, the actual difference in total dead weight distribution will be less than 1% or negligible. Consequently, the E.C.A. fuselage is assumed to be subjected to the same loadings as the Lockheed article. Therefore, the fuselage loads and shears, moments, and torques used in this report are taken directly from Lockheed Report 4657, "Basic Loads, Model P-80A," except for the new "Rolling Pull-out" condition (unsymmetrical tail loading) which is explained in detail in this report.

The structure consists of three sections; nose, mid, and aft. The nose and mid-sections are attached by four tension fittings. The mid and aft sections are attached by three tension fittings which take axial loads and six pins which take shear loads. Both the fore and aft splices are designed to be interchangeable with those of the Lockheed F-80C.

Vertical loads at the wing-fuselage intersection are taken out by means of eight bolts on two bulkheads at the sides of the fuselage as was done on the Lockheed article. Similarly, fore and aft loads are transmitted through two serrated plates on the wing upper surface and two fuselage side skin panels. In addition, chord loads are transmitted through two tension fittings at the fuselage centerline, since the Station 0 wing rib lower cap affords continuity for the lower fuselage longeron.

The nose structure consists of two vertical beams formed by four ZK-60A extruded longerons and the .091 FS-1h skin between them. The guns are mounted on fittings which bolt to a stepped horizontal deck. The two armament hood doors are non-structural and the load carried by the upper hood door support is conservatively neglected.

In the mid-section, the four nose attaching longerons taper off and shed their loads to three main longerons which continue aft to the mid to aft section joint. Secondary longerons are also employed to carry axial and bending loads locally around cutouts. Most of the external skin covering in this section is .064 FS-1h sheet with slightly higher gages on the under side. As in the Lockheed design, the following areas are considered non-structural; cockpit opening, nose gear well, dive flap, upper engine access, and two lower engine access openings. The fuselage fuel tank cover and cockpit floor are considered as structural.

The aft section consists of the three main longerons from the mid-section and two secondary longerons which are used as longitudinal skin splice members in addition to carrying axial loads due to bending. The two upper main longerons and the two secondary or splice longerons run full length in the aft section whereas the lower main longeron stops at Station 352. No other longitudinal members are used to carry bending in this section. The skin covering in the aft section is all .064 FS-1h sheet forward of Station 400. Aft of this station .040 sheet (FS-1h) is employed.

In the following pages, sample calculations used in the analysis of the aft section are shown.

AFT SECTION STRUCTURE

Critical Conditions

The aft section structure is analyzed for the following critical conditions:

(a) Gust)
(b) Combined B)-- (Ref. LAC Report No. 4657, Pages 167 and 180)
(c) Rolling Pull-out (see below)

The aft section moments for the rolling pull-out condition are computed based on the following ultimate loads. (Reference Figure 87.)

Vertical Tail Load, P_V = 6,105 lbs.

Total Horizontal Tail Load, P_H = 5,600 lbs. (UP)

Load on Left Horizontal Tail, P_{H_L} = 3,500 lbs. (UP)

Load on Right Horizontal Tail, P_{HR} = 2,100 lbs. (UP)

Torque at ℄ Aircraft and W.L. 100, T_o = 354,000 in.-lbs.

In the calculation of the aft section moments the vertical tail C.P. location for rolling pull-out is assumed to be Station 388.55 and the horizontail tail C.P. is assumed to be Station 389.29. Since these locations are almost the same as the actual values used in the vertical and horizontal tail analyses, a change in calculations is not necessary.

The data shown above was obtained during a conference held with Wright Field personnel. It was this contractor's understanding that this requirement would be issued formally as a change in the subject contract, however, at the time this analysis was written, such change order had not been received. When the change order, Contract Change Notification No. 1 was received, it contained the following data for the rolling pull-out condition.

Vertical Tail Load, P_V = 6,410 lbs.

Total Horizontal Tail Load, P_H = 5,600 lbs.

Load on Left Horizontal Tail, P_{H_L} = 3,500 lbs.

Load on Right Horizontal Tail, P_{HR} = 2,100 lbs.

Torque at ℄ Aircraft and W.L. 100, T_o = 369,000 in.-lbs.

Since the increase between the assumed data and the Change Notification data was small, it was felt that the positive margins of safety indicated in the original analysis were adequate enough to justify leaving the original analysis unchanged. It should also be noted that during the static test program the structure was subjected to the higher loads.

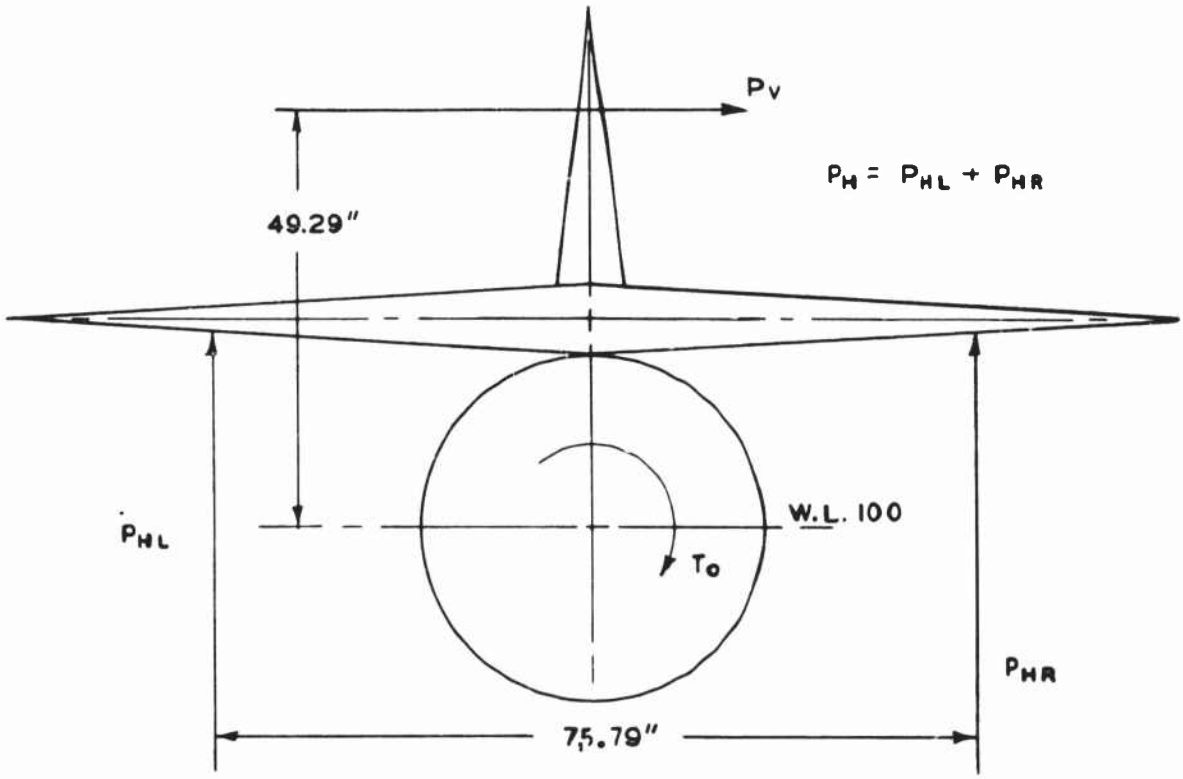

FIG. 87 TAIL LOADS

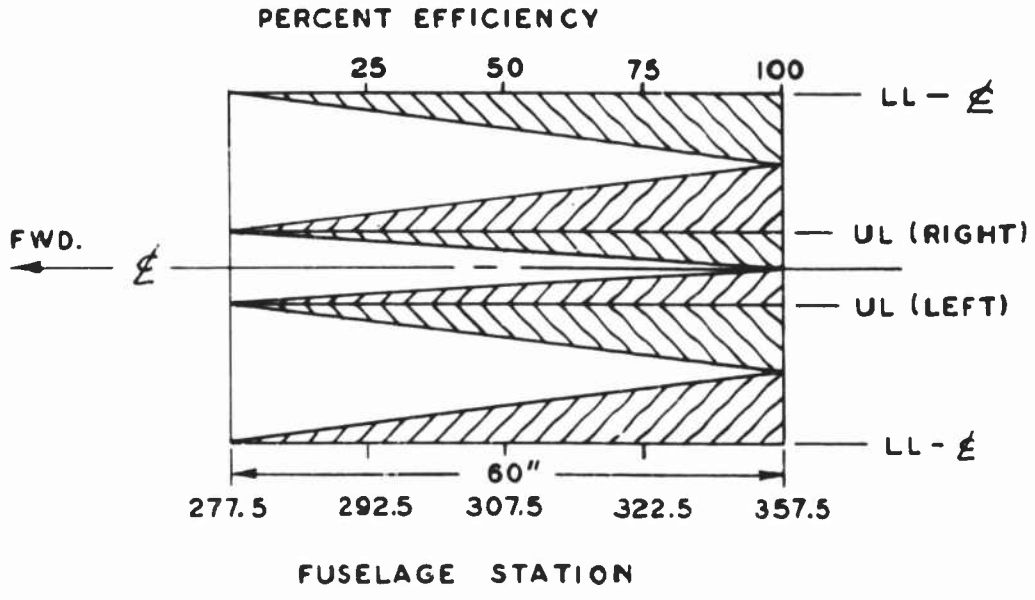

FIG. 88 SHELL SKIN EFFICIENCY

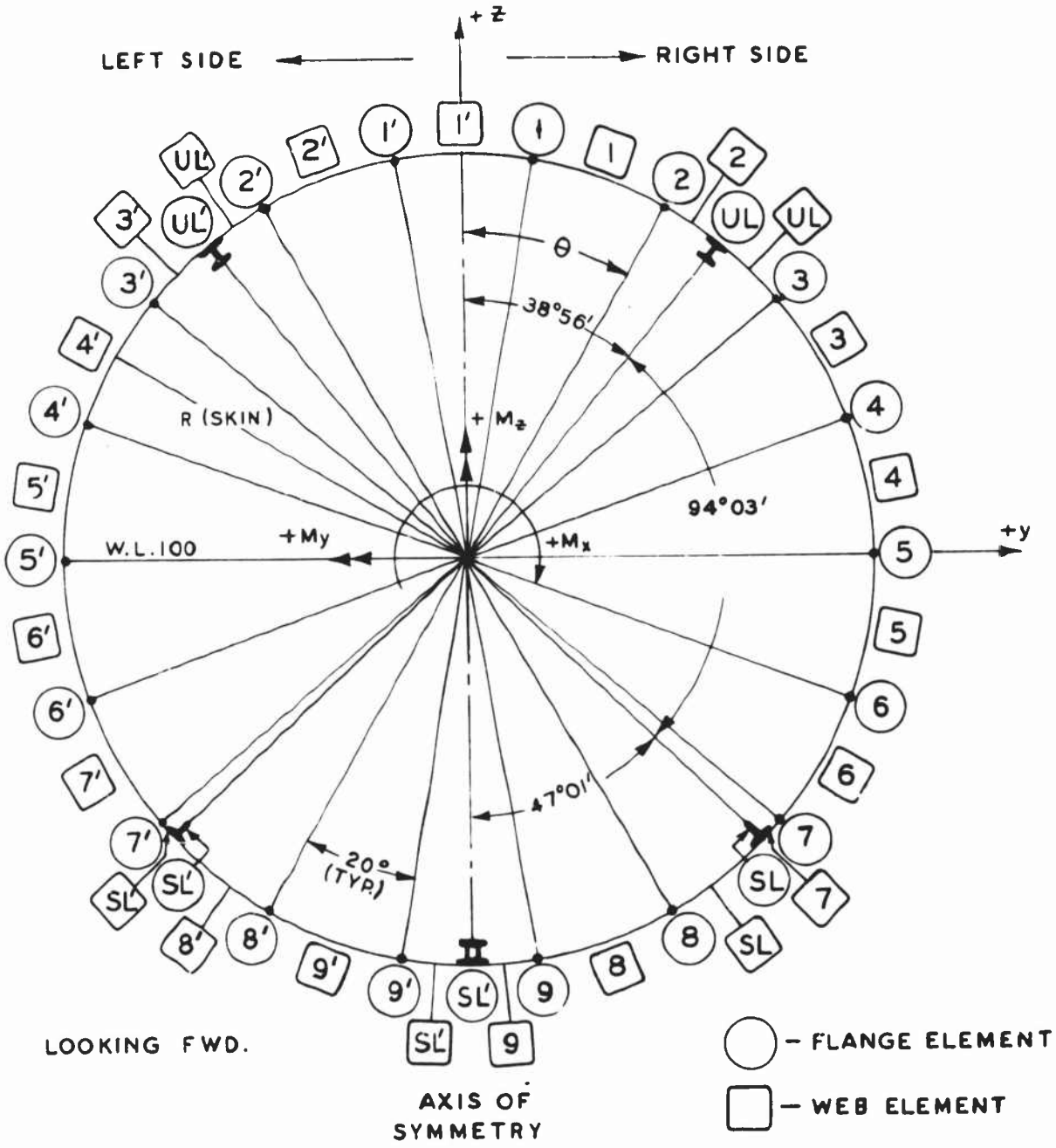

FIG. 89 AFT FUSELAGE STRUCTURE GEOMETRY
WEB AND FLANGE ELEMENTS

Therefore, referring to Figures 87 and 89, the bending moments due to the rolling pull-out condition may be expressed as follows:

$$M_X = T_o \quad - \quad (30)$$

$$M_Y = (5,600)\ (389.29 - F.S.) \quad - - - - - - - - - - - \quad (31)$$

$$M_Z = (6,105)\ (388.55 - F.S.) \quad - - - - - - - - - - - \quad (32)$$

Where F.S. is the fuselage station.

Table 27 summarizes the ultimate shears, moments, and torques used to analyse the aft section under the three most critical loading conditions.

Shear Lag Assumptions

The shell skin is assumed to vary in efficiency from zero at Station 277.5 to 100% at Station 337.5 as shown in Figure 88. The splice longerons (SL) are also assumed to vary in efficiency as the shell skin.

For the sake of simplicity the shell skin is assumed to act at a constant effectiveness due to shear lag around the entire periphery of the shell at any particular station. In other words it is assumed that any skin in compression will not buckle before ultimate load is reached and thus it behaves similar to the skin on the tension side as far as shear lag effects are concerned.

Section Properties

The shell skin is divided into 20° circular elements as shown in Figure 89. Since the fuselage section at any station is symmetrical about the Z axis and since all skin is assumed acting at the same efficiency, there is no rotation of the assumed axes. Therefore, only one set of section properties were calculated at any section. The final effective areas used in computing section properties, together with the ordinates of the element centers of gravity are given in Table 28. Table 29 shows the calculation of the C_n values. The effective skin element moments of intertia about the element centroids are summarized in Table 30.

Detailed calculations of the section properties for Stations 292.5 and 307.5 are shown in Tables 31 and 32. A summary of the section properties at various fuselage stations is shown in Table 33.

TABLE 27 - SUMMARY OF SHEARS, MOMENTS, AND TORSIONS

CONDITION		FUSELAGE STATION					
		277.5	292.5	307.5	322.5	337.5	352
Gust (1)	S_z	-12800	-12800	-12800	-12800	-12800	-12800
	M_y	-1,329,000	-1,138,000	-946,000	-753,000	-561,000	-376,000
Comb. B (2)	S_z	-11600	-11410	-11300	-11280	-11200	-11100
	S_y	-4520	-4520	-4520	-4520	-4520	-4520
	M_y	-1,178,600	-1,010,000	-840,000	-670,000	-498,000	-338,000
	M_z	-505,000	-437,000	-370,000	-302,000	-234,000	-168,000
	M_x	-278,000	-278,000	-278,000	-278,000	-278,000	-278,000
Rolling Pull-Out (3)	S_z	5600	5600	5600	5600	5600	5600
	S_y	6105	6105	6105	6105	6105	6105
	M_y	626,020	542,020	458,020	374,020	290,020	208,820
	M_z	677,960	586,390	494,810	403,240	311,660	223,140
	M_x	354,000	354,000	354,000	354,000	354,000	354,000

+ M_x - acts clockwise - looking forward.

+ M_y - compression on top fibres.

+ M_z - compression on right side.

+ S - acts up and to the right.

(1) Reference: LR 4657, page 167.
(2) Reference: LR 4657, page 180.
(3) Reference: Page 159

TABLE 28 - EFFECTIVE AREAS AND ORDINATES OF ELEMENT CENTROIDS

Elem. No.	FUSELAGE														
	292.5			307.5			322.5			337.5			352		
	Eff. Area	y	z	Eff. Area	y	z	Eff. Area	y	z	Eff. Area	y	z	Eff. Area	y	z
(1)(1')	.1495	±4.62	26.21	.2860	±4.42	25.08	.4060	±4.18	23.70	.5060	±3.91	22.19	.4690	±3.63	20.57
(2)(2')		±13.31	23.04		±12.74	22.06		±12.04	20.84		±11.27	19.51		±10.45	18.09
(3)(3')		±20.38	17.10		±19.51	16.37		±18.44	15.47		±17.26	14.48		±16.00	13.43
(4)(4')		±25.01	9.10		±23.93	8.71		±22.62	8.23		±21.17	7.71		±19.63	7.14
(5)(5')		±26.61	0		±25.47	0		±24.07	0		±22.53	0		±20.89	0
(6)(6')		±25.01	-9.10		±23.93	-8.71		±22.62	-8.23		±21.17	-7.71		±19.63	-7.14
(7)(7')		±20.38	-17.10		±19.51	-16.37		±18.44	-15.47		±17.26	-14.48		±16.00	-13.43
(8)(8')		±13.31	-23.04		±12.74	-22.06		±12.04	-20.84		±11.27	-19.51		±10.45	-18.09
(9)(9')	.1495	± 4.62	-26.21	.2860	±4.42	-25.08	.4060	±4.18	-23.70	.5060	±3.91	-22.19	.4690	±3.63	-20.57
(UL)(UL')	1.30	±16.00	19.88	.734	±15.52	19.21	.344	±15.02	18.59	.344	±14.04	17.39	.344	±13.01	16.10
(SL)(SL')	.086	±19.35	-18.03	.172	±18.51	-17.25	.258	±17.49	-16.30	.344	±16.35	-15.24	.344	±15.14	-14.11
(LL)	1.30	0	-25.56	.734	0	-24.70	.500	0	-23.58	.500	0	-22.03	.500	-	-

TABLE 29 - CALCULATION OF C_n VALUES

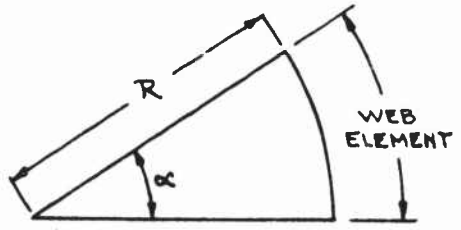

$C_n = 2A = R^2 \propto$

where

$\propto$ - Included angle in radians.

R - Radius to skin in inches.

Web El.	$\propto$°	$\propto$ Rad.	C_n VALUES					
			Sta. 277.5	Sta. 292.5	Sta. 307.5	Sta. 322.5	Sta. 337.5	Sta. 352
			R = 27.5	R = 26.75	R = 25.6	R = 24.2	R = 22.65	R = 21.0
1	20	.349	264.1	249.8	228.8	204.4	179.08	153.94
2	8.43	.156	118.0	111.6	102.2	91.4	79.98	68.75
UL	11.07	.193	146.1	138.2	126.6	113.0	99.10	85.19
3	20	.349	264.1	249.8	228.8	204.4	179.08	153.94
4	20	.349	264.1	249.8	228.8	204.4	179.08	153.94
5	20	.349	264.1	249.8	228.8	204.4	179.08	153.94
6	20	.349	264.1	249.8	228.8	204.4	179.08	153.94
7	2.98	.052	39.4	37.3	34.3	30.7	26.72	22.97
SL	17.02	.297	224.6	212.5	194.5	173.7	152.36	130.97
8	20	.349	264.1	249.8	228.8	204.4	179.08	153.94
9	10	.1745	132.0	124.9	114.4	102.2	89.54	76.97
LL	10	.1745	132.0	124.9	114.4	102.2	89.54	76.97
9'	20	.349	264.1	249.8	228.8	204.4	179.08	153.94
8'	17.02	.297	224.6	212.5	194.5	173.7	152.36	130.97
SL'	2.98	.052	39.4	37.3	34.3	30.7	26.72	22.97
7'	20	.349	264.1	249.8	228.8	204.4	179.08	153.94
6'	20	.349	264.1	249.8	228.8	204.4	179.08	153.94
5'	20	.349	264.1	249.8	228.8	204.4	179.08	153.94
4'	20	.349	264.1	249.8	228.8	204.4	179.08	153.94
3'	11.07	.193	146.1	138.2	126.6	113.0	99.10	85.19
UL'	8.93	.156	118.0	111.6	102.2	91.4	79.98	68.75
2'	20	.349	264.1	249.8	228.8	204.4	179.08	153.94
1'	20	.349	264.1	249.8	228.8	204.4	179.08	153.94

TABLE 30 - EFFECTIVE SKIN ELEMENT MOMENTS OF INERTIA ABOUT ELEMENT CENTROIDS

Fuselage Station	292.5	307.5	322.5	377.5	352
Eff. ΣI_{yo}; ΣI_{zo}	9.65	16.92	21.40	23.40	18.64

TABLE 31 - SECTION PROPERTIES AT STATION 292.5
COMPRESSION IN ANY SURFACE

(1)	(2)	(3)	(4)	(5)	(6)	(7)	(8)	(9)	(10)	(11)	(12)
Elem. n	Area A	y	Ay	Ay^2	z	Az	Az^2		CROSS PRODUCTS		C_n
Ref.	Tab.28	Tab. 28	(2) × (3)	(3) × (4)	Tab. 28	(2) × (6)	(6) × (7)	(4) × (6)	$(3)_n \times (6)_{n-1}$	$(3)_{n-1} \times (6)_n$	Tab. 29
1	.1495	4.62	0.691	3.2	26.21	3.918	513.8				249.8
2	.1495	13.31	1.990	26.5	23.04	3.444	79.3				111.6
UL	1.300	16.06	20.878	335.3	19.88	25.844	513.8				138.2
3	.1495	20.38	3.047	62.1	17.10	2.556	43.7				249.8
4	.1495	25.01	3.739	93.5	9.10	1.360	12.4				249.8
5	.1495	26.61	3.978	105.9	0	0	0				249.8
6	.1495	25.01	3.739	93.5	-9.10	-1.360	12.4				249.8
7	.1495	20.38	3.047	62.1	-17.10	-2.556	43.7				37.3
SL	.086	19.35	1.664	32.2	-18.03	-1.551	28.0				212.5
8	.1495	13.31	1.990	26.5	-23.04	-3.444	79.3				249.8
9	.1495	4.62	0.691	3.2	-26.21	-3.918	102.7				124.9
LL	1.300	0	0	0	-25.56	-33.228	849.3				124.9
9'	.1495	-4.62	-0.691	3.2	-26.21	-3.918	102.7				249.8
8'	.1495	-13.31	-1.990	26.5	-23.04	-3.444	79.3				212.5
SL'	.086	-19.35	-1.664	32.2	-18.03	-1.551	28.0				37.3
7'	.1495	-20.38	-3.047	62.1	-17.10	-2.556	43.7				249.8
6'	.1495	-25.01	-3.739	93.5	-9.10	-1.360	12.4				249.8
5'	.1495	-26.61	-3.978	105.9	0	0	0				249.8
4'	.1495	-25.01	-3.739	93.5	9.10	1.360	12.4				249.8
3'	.1495	-20.38	-3.047	62.1	17.10	2.556	43.7				138.2
UL'	1.300	-16.06	-20.878	335.3	19.88	25.844	513.8				111.6
2'	.1495	-13.31	-1.990	26.5	23.04	3.444	79.3				249.8
1'	.1495	-4.62	-0.691	3.2	26.21	3.918	102.7				249.8
Σ	6.763	0	0	1688.0	2.271	15.358	2885.3				4496.4

* Shell skin and aplice longeron efficiency = .25 (Reference Figure 88)

$\Sigma I_{y_o} = 9.65$ (Table 30)

$\Sigma I_{z_o} = 9.65$ (Table 30)

$I_y = \Sigma(8) - \bar{z}\,\Sigma(7) + \Sigma I_{y_o} = 2885.3 + 9.65 - 2.271(15,358) = 2860.1$

$I_z = \Sigma(5) - \bar{y}\,\Sigma(4) + \Sigma I_{z_o} = 1688.0 + 9.65 = 1697.7$

$I_{yz_z} = \Sigma(9) - \bar{y}\,\Sigma(7) = 0$

$I_y I_z - I_{yz}^2 = 4,855,600$

$C_o = 10^6/(I_y I_z - I_{yz}^2) = 0.20595$

$C_1 = I_y \times C_o = 589.04$

$C_2 = I_z \times C_o = 349.64$

$C_3 = I_{yz} \times C_o = 0$

NO	ITEM	REF \ COND	GUST	COMB B	ROLL. PULL.
(1)	$M_y/10^6$	Table 27	-1.138	-1.010	.5420
(2)	$M_z/10^6$	Table 27	0	-.437	.5864
(3)	$C_3 M_y$	0 x (1)	0	0	0
(4)	$-C_1 M_z$	-589.04 x (2)	0	257.41	-345.41
(5)	K_1	(3) + (4)	0	257.41	-345.41
(6)	$C_3 M_z$	0 x (2)	0	0	0
(7)	$-C_2 M_y$	-349.64 x (1)	397.14	353.14	-189.5
(8)	K_2	(6) + (7)	397.89	353.14	-189.5
(9)	$-K_1 \bar{y}$	-(5) x 0	0	0	0
(10)	$-K_2 \bar{z}$	-(8) x 2.271	-903.61	-801.98	430.35
(11)	K_3	(9) + (10)	-903.61	-801.98	430.35

TABLE 32 - SECTION PROPERTIES AT STATION 307.5
COMPRESSION IN ANY SURFACE

(1)	(2)	(3)	(4)	(5)	(6)	(7)	(8)	(9)	(10)	(11)	(12)
Elem. n	Area A *	y	A_y	A_y^2	z	A_z	A_z^2		CROSS PRODUCTS		C_n
Ref.	Tab.28	Tab. 28	(2)×(3)	(3)×(4)	Tab.28	(2)×(6)	(6)×(7)	(4)×(6)	$(3)_n \times (6)_{n-1}$	$(3)_{n-1} \times (6)_n$	Tab.29
1	.286	4.42	1.264	5.6	25.08	7.173	179.9				228.8
2	.286	12.74	3.644	46.4	22.06	6.309	139.2				102.2
UL	.734	15.52	11,392	176.8	19.21	14,100	270.9				126.6
3	.286	19.51	5.580	108.9	16.37	4.682	76.6				228.8
4	.286	23.93	6.844	163.8	8.71	2.491	21.7				228.8
5	.286	25.47	7.284	185.5	0	0	0				228.8
6	.286	23.93	6.844	163.8	-8.71	-2.491	21.7				228.8
7	.286	19.51	5.580	108.9	-16.37	-4.682	76.6				34.3
SL	.172	18.51	3.184	58.9	-17.25	-2.967	51.2				194.5
8	.286	12.74	3.644	46.4	-22.06	-6.309	139.2				228.8
9	.286	4.42	1.264	5.6	-25.08	-7.173	179.9				114.4
LL	.734	0	0	0	-24.70	-18.130	447.8				114.4
9'	.286	-4.42	-1.264	5.6	-25.08	-7.173	179.9				228.8
8'	.286	-12.74	-3.644	46.4	-22.06	-6.309	139.2				194.5
SL'	.172	-18.51	-3.184	58.9	-17.25	-2.967	51.2				34.3
7'	.286	-19.51	-5.580	108.9	-16.37	-4.682	76.6				228.8
6'	.286	-23.93	-6.844	163.8	-8.71	-2.491	21.7				228.8
5'	.286	-25.47	-7.284	185.5	0	0	0				228.8
4'	.286	-23.93	-6.844	163.8	8.71	2.491	21.7				228.8
3'	.286	-19.51	-5.580	108.9	16.37	4.682	76.6				126.6
UL'	.734	-15.52	-11.392	176.8	19.21	14.100	270.9				102.2
2'	.286	-12.74	-3.644	46.4	22.06	6.309	139.2				228.8
1'	.286	-4.42	-1.264	5.6	25.08	7.173	179.9				228.8
Σ	7.694	0	0	2141.2	.538	4.136	2761.6				4118.4

* Shell skin and splice longeron efficiency = .50 (Reference Figure 88)

$\Sigma I_{y_o} = 16.92$ (Table 30)

$\Sigma I_{z_o} = 16.92$ (Table 30)

$I_y = \Sigma(8) - \bar{z}\,\Sigma(7) + \Sigma I_{y_o} = 2761.6 + 16.92 - .538(4.136) = 2776.3$

$I_z = \Sigma(5) - \bar{y}\,\Sigma(4) + \Sigma I_{z_o} = 2141.2 + 16.92 = 2158.1$

$I_{yz_z} = \Sigma(9) - \bar{y}\,\Sigma(7) = 0$

$I_y I_z - I_{yz}^2 = 5{,}991{,}500$

$C_o = 10^6/(I_y I_z - I_{yz}^2) = 0.16690$

$C_1 = I_y \times C_o = 463.4$

$C_2 = I_z \times C_o = 360.2$

$C_3 = I_{yz} \times C_o = 0$

NO.	ITEM	REF \ COND.	GUST	COMB B	ROLL. PULL.
(1)	$M_y/10^6$	Table 27	-.946	-.840	.45802
(2)	$M_z/10^6$	Table 27	0	-.370	.49481
(3)	$C_3 M_y$	0 x (1)	0	0	0
(4)	$-C_1 M_z$	-463.4 x (2)	0	171.5	-229.3
(5)	K_1	(3) + (4)	0	171.5	-229.3
(6)	$C_3 M_z$	0 x (2)	0	0	0
(7)	$-C_2 M_y$	-360.2 x (1)	340.7	302.6	-165.0
(8)	K_2	(6) + (7)	340.7	302.6	-165.0
(9)	$-K_1 \bar{y}$	-(5) x 0	0	0	0
(10)	$-K_2 \bar{z}$	-(8) x .538	-183	-163	88.8
(11)	K_3	(9) + (10)	-183	-163	88.8

TABLE 33 - SUMMARY OF AFT FUSELAGE SECTION PROPERTIES
COMPRESSION IN ANY SURFACE

Station	$\bar{y}$	$\bar{z}$	I_y	I_z	I_{yz}	$C_1 \times 10^6$	$C_2 \times 10^6$	$C_3 \times 10^6$
292.5	0	2.271	2860.1	1697.7	0	589.04	349.64	0
307.5	0	.538	2776.3	2158.1	0	463.4	360.2	0
322.5	0	-.824	2784.1	2452.2	0	407.9	359.2	0
337.5	0	-.868	2937.4	2654.7	0	376.69	340.44	0
352.0	0	.139	2175.8	2134.8	0	468.43	459.60	0

TABLE 34 - SUMMARY OF BENDING CONSTANTS

Station	Gust Condition			Condition B			Rolling Pull Out		
	K_1	K_2	K_3	K_1	K_2	K_3	K_1	K_2	K_3
292.5	0	397.89	-903.61	257.41	353.14	-801.98	-345.41	-189.5	430.35
307.5	0	340.7	-183.0	171.5	302.6	-163.0	-229.3	-165.0	88.8
322.5	0	270.5	223.0	123.2	240.7	198.0	-164.6	-134.3	-110.7
337.5	0	190.99	165.78	88.15	169.54	147.16	-117.41	-98.73	-85.70
352.0	0	172.81	-24.02	78.70	155.34	-21.59	-104.51	-95.96	13.34

Bending Stresses and Axial Loads

The aft section shell is circular throughout. The method of analysis is as follows. The bending stresses are computed by means of the general formula:

$$f_b = \frac{M_y I_{y'z'} - M_z I_{y'}}{I_{y'} I_{z'} - I_{y'z'}^2} y' + \frac{M_z I_{y'z'} - M_y I_{z'}}{I_{y'} I_{z'} - I_{y'z'}^2} z' \quad - - - - - \quad (33)$$

letting

$$C_o = \frac{1}{I_{y'z'} - I_{y'z'}^2} \qquad C_3 = I_{y'z'} \times C_o$$

$$C_1 = I_{y'} \times C_o \qquad K_1 = C_3 M_y - C_1 M_z$$

$$C_2 = I_{z'} \times C_o \qquad K_2 = C_3 M_z - C_2 M_y \quad - - - \quad (34)$$

Utilizing the abbreviations of Equations (34), Equation (33) becomes:

$$f_b = K_1 y' + K_2 z' \quad - - - - - - - - - - - - - - - - \quad (35)$$

From Figure 90

$$y' = y - \bar{y} \quad \text{and} \quad z' = z - \bar{z} \quad - - - - - - - - - - - - \quad (36)$$

Therefore, the resulting expression for the bending stress is:

$$f_b = K_1 y + K_2 z + K_3 \quad - - - - - - - - - - - - - - - \quad (37)$$

where:

$$K_3 = -K_1 \bar{y} - K_2 \bar{z} \quad - - - - - - - - - - - - - - - \quad (38)$$

Detailed calculations of the bending stresses in accordance with Equation (37) for Stations 292.5 and 307.5, are shown in Tables 35 and 36 with a summary of the stresses at all aft fuselage stations investigated given in Table 37. For convenience of calculation, the constants, C_1, C_2, and C_3, shown in Equations (34), have been determined in Tables 31 and 32 for Stations 292.5 and 307.5 and summarized for all stations investigated in Table 33. The values of the bending constants K_1, K_2, and K_3, as defined by Equations (34), have also been calculated in Tables 31 and 32 and summarized for all stations in Table 34.

The axial load on each element is calculated in Tables 35 and 36 for Stations 292.5 and 307.5 by multiplying the ultimate bending stresses by the corresponding element effective area.

Since at the Station 277.5 splice, the bending moments are carried by tension-type fittings on the three main longerons, the longeron loads at Station 277.5 are determined as follows. Referring to Figure 92,

$$P_{UL'} \text{ (left)} = 1/2 \left(\frac{M_y}{46.693}\right) + \frac{M_z}{33.092} = -.010708\ M_y + .03022\ M_z \quad - - - - \quad (39)$$

$$P_{UL} \text{ (right)} = 1/2\left(\frac{M_y}{46.693}\right) - \frac{M_z}{33.092} = -.010708\ M_y - .03022\ M_z \quad - - - - \quad (40)$$

$$P_{LL} = \frac{M_y}{46.693} = .02142\ M_y \quad - - - - - - - - - - - - - \quad (41)$$

The calculation of the longeron loads in accordance with Equations (39), (40), and (41), for Station 277.5, is shown in Table 38.

The aft section longeron loads are summarized in the plot shown in Figure 93.

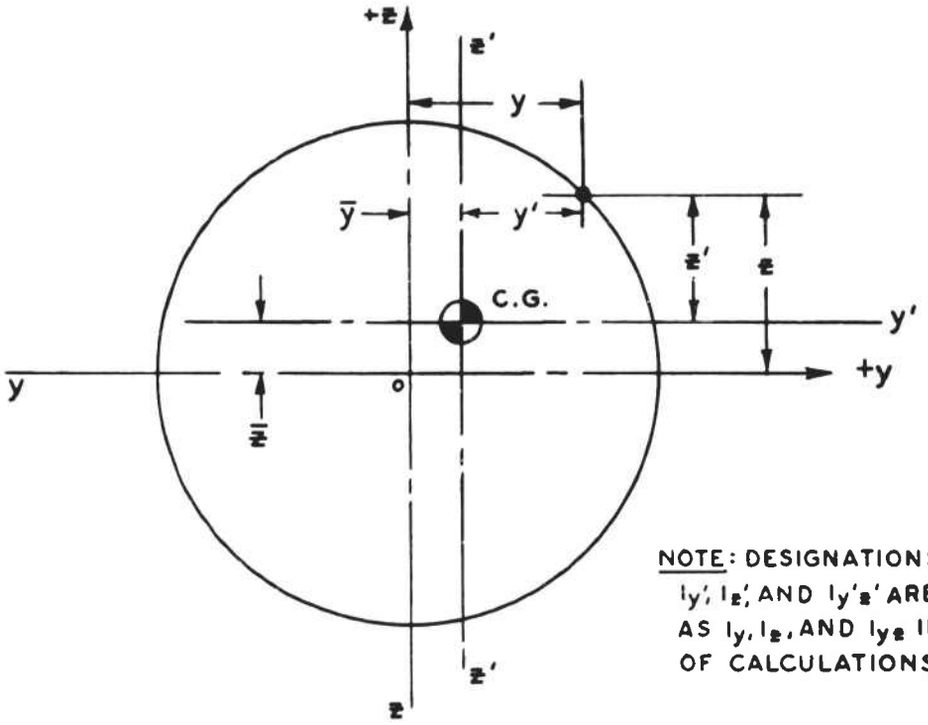

NOTE: DESIGNATIONS $I_{y'}$, $I_{z'}$, AND $I_{y'z'}$ ARE NOTED AS I_y, I_z, AND I_{yz} IN TABLES OF CALCULATIONS.

FIG. 90

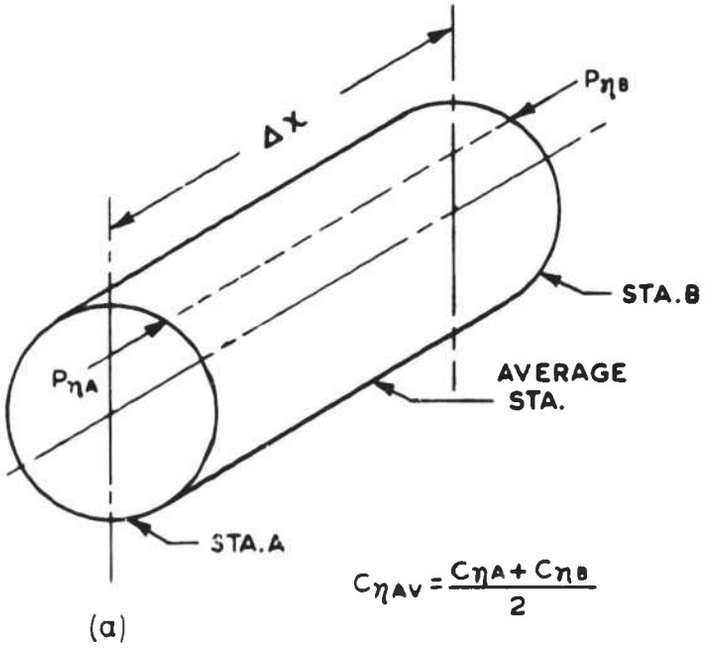

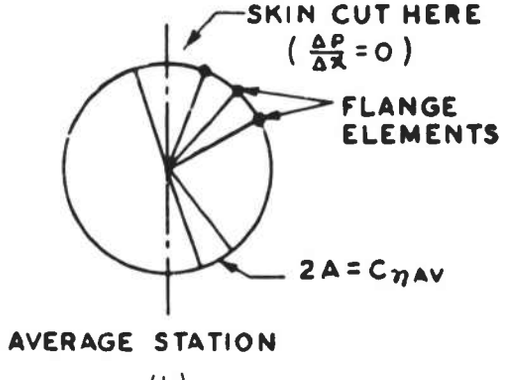

FIG. 91

TABLE 35 - ULTIMATE BENDING STRESSES AND AXIAL LOADS
STATION 292.5

(1)	(2)	(3)	(4)	(5)	(6)	(7)	(8)	(9)	(10)	(11)	(12)	(13)	(14)	(15)	(16)	(17)
ELEMENT	y	Z	A Comp. Upper or Lower	A Comp. Lower	CONDITION GUST				CONDITION COMB. B				CONDITION ROLLING PULL OUT			
					K_1y	K_2Z	F_b K_3=-903.61	P	K_1y	K_2Z	F_b K_3=-801.98	P	K_1y	K_2Z	F_b K_3=430.35	P
	Tab.28	Tab.28	Tab.28		0 x (2)	397.89 (3)	K_3+(6)+(7)	(4)x(8)	257.41 (2)	353.14 (3)	K_3(10)+(11)	(4) x (12)	-345.41 (2)	-189.5 (3)	K_3 (14)+(15)	(4)x(16)
1	4.62	26.21	.1495		0	10429	9525	1424	1189	9256	9643	1442	-1596	-4967	-6133	-917
2	13.31	23.04	.1495			9167	8263	1235	3426	8136	10760	1609	-4597	-4366	-8533	-1276
UL	16.06	19.88	1.300			7910	7006	9108	4134	7020	10352	13458	-5547	-3767	-8884	-11549
3	20.38	17.10	.1495			6804	5900	882	5246	6039	10483	1567	-7039	-3240	-9849	-1472
4	25.01	9.10	.1495			3621	2717	406	6438	3214	8850	1323	-8639	-1724	-9933	-1485
5	26.61	0	.1495			0	-904	-135	6850	0	6048	904	-9191	0	-8761	-1310
6	25.01	-9.10	.1495			-3621	-4525	-676	6438	-3214	2422	362	-8639	1724	-6485	-970
7	20.38	-17.10	.1495			-6804	-7708	-1152	5246	-6039	-1595	-238	-7039	3240	-3369	-504
SL	19.35	-18.03	.086			-7174	-8078	-695	4981	-6367	-2188	-188	-6684	3417	-2837	-244
8	13.31	-23.04	.1495			-9167	-10071	-1506	3426	-8136	-5512	-824	-4597	4366	199	30
9	4.62	-26.21	.1495			-10429	-11333	-1694	1189	-9256	-8869	-1326	-1596	4967	3801	568
LL	0	-25.56	1.300			-10170	-11074	-14400	0	-9026	-9828	-12776	0	4844	5274	6856
9'	-4.62	-26.21	.1495			-10429	-11333	-1694	-1189	-9256	-11247	-1681	1596	4967	6993	1045
8'	-13.31	-23.04	.1495			-9167	-10071	-1506	-3426	-8136	-12364	-1848	4597	4366	9393	1404
SL'	-19.35	-18.03	.086			-7174	-8078	-695	-4981	-6367	-12150	-1045	6684	3417	10531	906
7'	-20.38	-17.10	.1495			-6804	-7708	-1152	-5246	-6039	-12087	-1807	7039	3240	10709	1601
6'	-25.01	-9.10	.1495			-3621	-4525	-676	-6438	-3214	-10454	-1563	8639	1724	10793	1614
5'	-26.61	0	.1495			0	-904	-135	-6850	0	-7652	-1144	9191	0	9621	1438
4'	-25.01	9.10	.1495			3621	2717	406	-6438	3214	-4026	-602	8639	-1724	7345	1098
3'	-20.38	17.10	.1495			6804	5900	882	-5246	6039	-9	-1	7039	-3240	4229	632
UL'	-16.06	19.86	1.300			7910	7006	9108	-4134	7020	2084	2709	5547	-3767	2210	2873
2'	-13.31	23.04	.1495			9167	8263	1235	-3426	8136	3908	584	4597	-4366	661	99
1'	-4.62	26.21	.1495		0	10429	9525	1424	-1189	9256	7265	1086	1596	-4967	-2941	-440
								-6				+1				-3

"K" values are from Table 34.

TABLE 36 - ULTIMATE BENDING STRESSES AND AXIAL LOADS
STATION 307.5

(1)	(2)	(3)	(4)	(5)	(6)	(7)	(8)	(9)	(10)	(11)	(12)	(13)	(14)	(15)	(16)	(17)
ELEMENT	y	z	A COMP. UPPER OR LOWER	A COMP. LOWER	CONDITION GUST				CONDITION COMB.B				CONDITION ROLL. PULL OUT			
					$K_1 y$	$K_2 Z$	F_b / K_3=-183	P	$K_1 y$	$K_2 Z$	F_b / K_3=-163	P	$K_1 y$	$K_2 z$	F_b / K_3=89	P
	TABLE 28	TABLE 28	TABLE 28	PG	0 x (2)	340.7 x (3)	K_3+(6)+(7)	(4) x (8)	171.5 x (2)	302.6 x (3)	K_3+(10)+(11)	(4) x (12)	-229.3 (2)	-165 (3)	K_3+(14)+(15)	(4) x (16)
1	4.42	25.08	.286		0	8545	8362	2392	758	7589	8184	2341	-1014	-4138	-5063	-1448
2	12.74	22.06	.286			7516	7333	2097	2185	6675	8697	2487	-2921	-3640	-6472	-1851
UL	15.52	19.21	.734			6545	6362	4670	2662	5813	8312	6101	-3559	-3170	-6640	-4874
3	19.51	16.37	.286			5577	5394	1543	3346	4954	8137	2327	-4474	-2701	-7086	-2027
4	23.93	8.71	.286			2967	2784	796	4104	2636	6577	1881	-5487	-1437	-6835	-1955
5	25.47	0	.286			0	-183	-52	4368	0	4205	1203	-5840	0	-5751	-1645
6	23.93	-8.71	.286			-2967	-3150	-901	4104	-2636	1305	373	-5487	1437	-3961	-1133
7	19.51	-16.37	.286			-5577	-5760	-1647	3346	-4954	-1771	-507	-4474	2701	-1684	-482
SL	18.51	-17.25	.172			-5877	-6060	-1042	3174	-5220	-2209	-380	-4244	2846	-1309	-225
8	12.74	-22.06	.286			-7516	-7699	-2202	2185	-6675	-4653	-1331	-2921	3640	808	231
9	4.42	-25.08	.286			-8545	-8728	-2496	758	-7589	-6994	-2000	-1014	4138	3213	919
LL	0	-24.70	.734			-8415	-8598	-6311	0	-7474	-7637	-5606	0	4076	4165	3057
9'	-4.42	-25.08	.286			-8545	-8728	-2496	-758	-7589	-8510	-2434	1014	4138	5241	1499
8'	-12.74	-22.06	.286			-7516	-7699	-2202	-2185	-6675	-9023	-2581	2921	3640	6650	1902
SL'	-18.51	-17.25	.172			-5877	-6060	-1042	-3174	-5220	-8557	-1472	4244	2846	7179	1235
7'	-19.51	-16.37	.286			-5577	-5760	-1647	-3346	-4954	-8463	-2420	4474	2701	7264	2078
6'	-23.93	-8.71	.286			-2967	-3150	-901	-4104	-2636	-6903	-1974	5487	1437	7013	2006
5'	-25.47	0	.286			0	-183	-52	-4368	0	-4531	-1296	5840	0	5929	1696
4'	-23.93	8.71	.286			2967	2784	796	-4104	2636	-1631	-466	5487	-1437	4139	1184
3'	-19.51	16.37	.286			5577	5394	1543	-3346	4954	1445	413	4474	-2701	1862	533
UL'	-15.52	19.21	.734			6545	6362	4670	-2662	5813	2988	2193	3559	-3170	478	351
2'	-12.74	22.06	.286			7516	7333	2097	-2185	6675	4327	1238	2921	-3640	-630	-180
1'	-4.42	25.08	.286		0	84	8362	2392	-758	7589	6668	1907	1014	-4138	-3035	-686
Σ								+5				-3				-3

"K" values are from Table 34.

TABLE 37 - SUMMARY OF EFFECTIVE ULTIMATE BENDING STRESSES

(1)	(2)	(3)	(4)	(5)	(6)	(7)	(8)	(9)	(10)	(11)	(12)	(13)	(14)	(15)	(16)	(17)	(18)	(19)	(20)	(21)
EL. NO.	STATION 292.5				STATION 307.5				STATION 322.5				STATION 337.5				STATION 352			
	Eff. Factor	Gust	Comb.B	Rolling Pull Out	Eff. Factor	Gust	Comb. B	Rolling Pull Out	Eff. Factor	Gust	Comb.B	Rolling Pull Out	Eff. Factor	Gust	Comb.B	Rolling Pull Out	Eff. Factor	Gust	Comb.B	Rolling Pull Out
1	.25	2380	2410	-1533	.50	4181	4090	-2530	.75	4970	4810	-2990	1.00	4404	4253	-2736	1.00	3531	3459	-2340
2	.25	2070	2685	-2135	.50	3666	4340	-3235	.75	4400	5020	-3665		3892	4448	-3335		3102	3610	-2815
UL	1.00	7006	10352	-8884	1.00	6362	8312	-6640	1.00	5252	6523	-5080		3487	4333	-3465		2758	3503	-2892
3	.25	1476	2620	-2465	.50	2697	4070	-3540	.75	3310	4640	-3920		2932	4123	-3542		2297	3323	-2948
4		679	2210	-2485		1392	3285	-3415		1835	3720	-3700		1639	3320	-3333		1210	2632	-2724
5		-226	1513	-2193		-92	2103	-2875		167	2375	-3050		166	2133	-2731		-24	1622	-2170
6		-1133	606	-1620		-1575	653	-1980		-1502	754	-2045		-1307	706	-1811		-1258	414	-1354
7		-1930	-398	-842		-2880	-886	-842		-2975	-941	-802		-2600	-787	-682		-2345	-849	-370
SL		-2020	-547	-709		-3030	-1105	-655		-3140	-1177	-601		-2745	-996	-581		-2462	-1022	-215
8		-2520	-1380	50		-3850	-2327	404		-4060	-2500	530		-3560	-2168	517		-3150	-2010	657
9	.25	-2835	-2175	950	.50	-4364	-3497	1607	.75	-4640	-3740	1788		-4072	-3271	1646		-3579	-2931	1608
LL	1.00	-11074	-9828	5274	1.00	-8598	-7637	4165	1.00	-6155	-5478	3056		-4042	-3588	2089		-3653	-3284	2028
9'	.25	-2835	-2810	1750	.50	-4364	-4255	2651	.75	-4640	-4510	2820		-4072	-3959	2563		-3579	-3503	2366
8'		-2520	-3090	2350		-3850	-4512	3325		-4060	-4730	3500		-3560	-4154	3163		-3150	-3654	2850
SL'		-2020	-3035	2635		-3030	-4278	3590		-3140	-4410	3720		-2745	-3878	3339		-2462	-3406	2941
7'		-1930	-3020	2680		-2880	-4232	3632		-2975	-4350	3750		-2600	-3829	3370		-2345	-3367	2974
6'		-1133	-2610	2700		-1575	-3452	3507		-1502	-3430	3540		-1307	-3026	3160		-1258	-2676	2750
5'		-226	-1913	2407		-92	-2266	2965		167	-2075	2885		166	-1839	2559		-24	-1666	2196
4'		679	-1006	1837		1392	-816	2070		1835	-456	1880		1639	-412	1639		1210	-458	1380
3'	.25	1476	-2	1057	.50	2697	723	931	.75	3310	1237	635		2932	1081	510		2297	805	396
UL'	1.00	7006	2084	2210	1.00	6362	2988	478	1.00	5252	2823	-136		3487	1857	-155		2758	1455	-172
2'	.25	2070	977	1653	.50	3666	2164	-315	.75	4400	2800	-696		3892	2462	-689		3102	1966	-631
1'	.25	2380	1820	-736	.50	4181	3334	-1518	.75	4970	4035	-1955	1.00	4404	3565	-1818	1.00	3531	2887	-1582

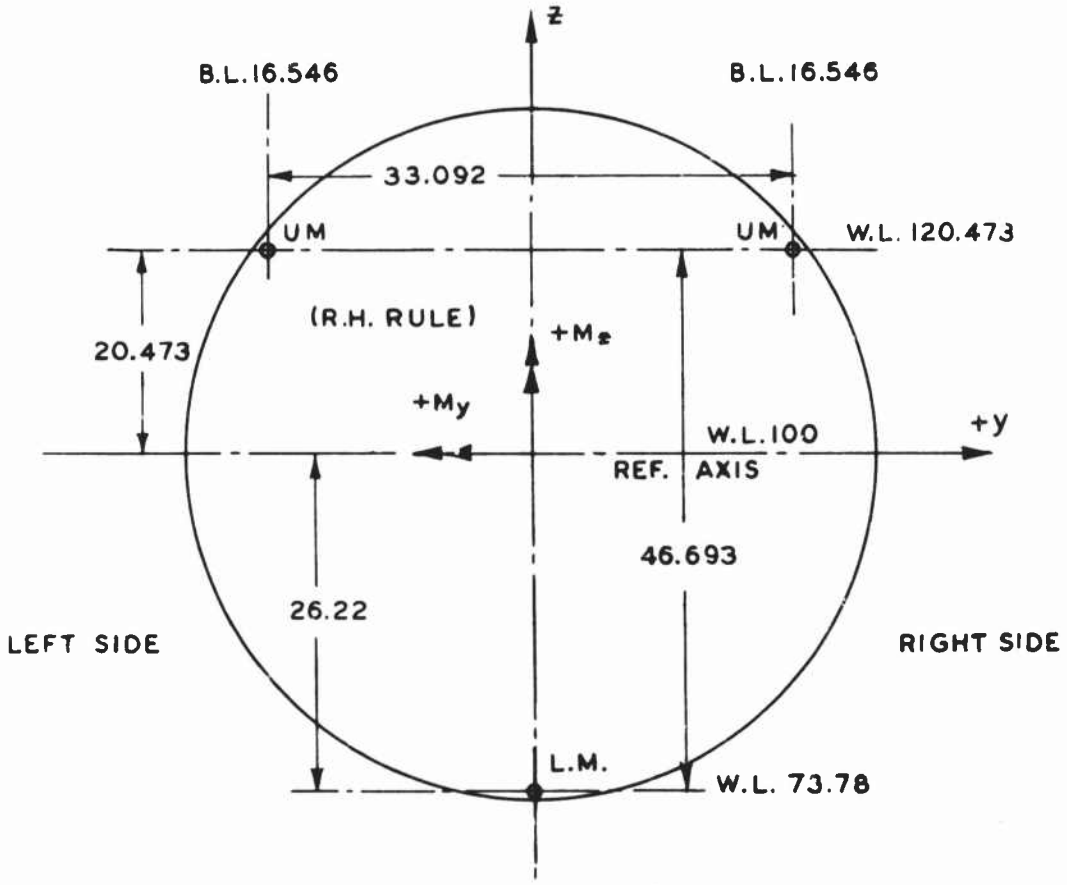

VIEW LOOKING FORWARD AT STA. 277.5

FIG. 92 LONGERON LOADS — STA. 277.5

TABLE 38 - LONGERON LOADS - STATION 277.5

①	②	③	④	⑤	⑥	⑦	⑧
Condition	M_y	M_z	.010708 M_y	.03022 M_z	P_{UL} (Left)	P_{UL} (Right)	P_{LL}
Ref.	Tab. 27	Tab. 27	.010708 ②	.03022 ③	⑤ - ④	- ④ - ⑤	.02142 ②
Gust	-1,329,000	0	-14,231	0	14,231	14,231	-28,462
Comb. B	-1,178,600	-505,000	-12,620	-15,261	-2,641	27,881	-25,240
Roll-Pull	626,020	677,960	6,703	20,488	13,785	-27,191	13,406

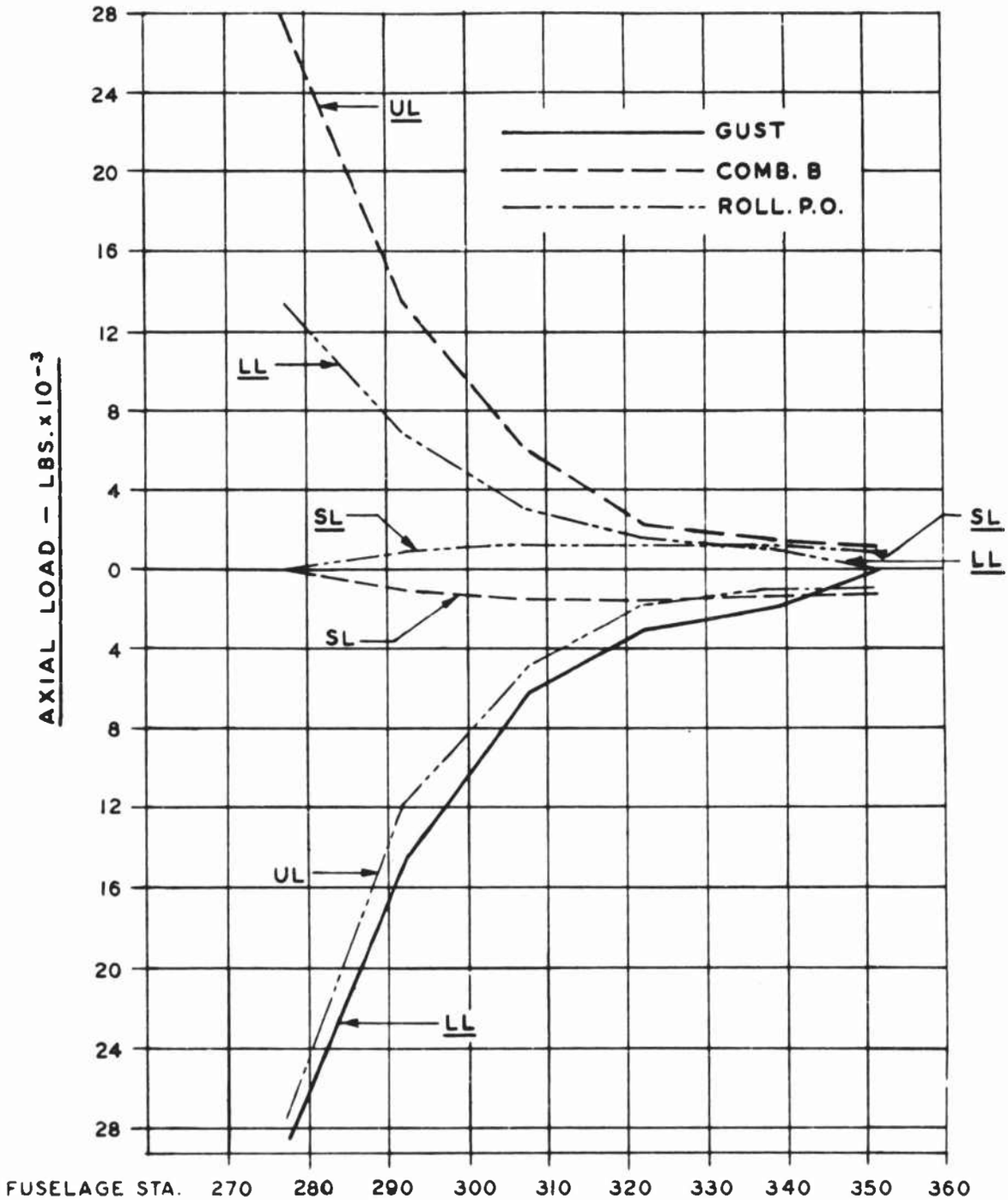

FIG. 93 AFT SECTION STRUCTURE — LONGERON LOADS

Shear Flow Calculations

The shear flow distribution is determined by the ΔP method for a single cell structure and follows the general method for a multi-cell structure outlined in the horizontal stabilizer analysis. After the flange loads are determined at the various sections, two adjacent stations are selected as shown in Figure 91(a). The skin is cut as shown in Figure 91(b). Where:

$$\frac{\Delta P}{\Delta X} = 0 \qquad - - - - - - - - - - - - - - - - - - \quad (42)$$

and the incremental shear flows are calculated by the expression

$$\frac{\Delta P}{\Delta X} = \frac{Pn_a - Pn_b}{\Delta X} \qquad - - - - - - - - - - - - - - - \quad (43)$$

then

$$q_n^1 = \sum_{n=1}^{n} \frac{\Delta P}{\Delta X} \qquad - - - - - - - - - - - - - - - \quad (44)$$

(q_n^1 = uncorrected shear flows in web, n)

Equation (44) yields uncorrected skin shear flows which must be corrected so that the summation of torque equals zero. Using Point O (see Figure 90) as a reference, the torque of the uncorrected shear flows about O is -

$$T = \Sigma q_n^1 \cdot C_{n_{AV}} \qquad - - - - - - - - - - - - - - - \quad (45)$$

Letting q_T be the correcting skin shear flow and to equal to the average applied torque between Station A and B we have:

$$q_T \cdot \Sigma C_{n_{AV}} + \Sigma q_n^1 \cdot C_{n_{AV}} = T_o \qquad - - - - - - - - - \quad (46)$$

therefore

$$q_T = (T_o - \Sigma q_n^1 \cdot C_{n_{AV}})/2A \qquad - - - - - - - - - - - - \quad (47)$$

where

$$\Sigma C_{n_{AV}} = 2A$$

The final shear flow is given by the expression -

$$q_n = q_T + q_n^1 \qquad - - - - - - - - - - - - - - - \quad (48)$$

Tables 39, 40, and 41 illustrate the application of the method of shear flow calculation as applied to the bay between Station 292.5 and 307.5. The ultimate shear flows throughout the fuselage aft section are summarized in Table 42.

TABLE 39 - CALCULATION OF RESULTANT SHEAR FLOWS
STATION 292.5 TO STATION 307.5

①	②	③	④	⑤	⑥	⑦	⑧
Web	P Fwd. Sta.	Aft Sta.	$\Delta P/\Delta x$	Q'	$C_{n_{AV}}$	Q' x $C_{n_{AV}}$	Q
Ref.	Tab. 35	Tab. 36	② - ③/15	Σ ④	*	⑤ x ⑥	Q_T + ⑤
1	1424	2392	-64.5	-64.5			-64.5
2	1235	2097	-57.5	-122.0			-122.0
UL	9108	4670	295.9	173.9			173.9
3	882	1543	-44.1	129.8			129.8
4	406	796	-26.0	103.8			103.8
5	-135	-52	-5.5	98.2			98.2
6	-676	-901	15.0	113.3			113.3
7	-1152	-1647	33.0	146.3			146.3
SL	-695	-1042	23.1	169.4			169.4
8	-1506	-2202	46.4	215.8			215.8
9	-1694	-2496	53.5	269.3			269.3
LL	-14400	-6311	-539.0	-269.3			-269.3
9'	-1694	-2496	53.5	-215.8			-215.8
8'	-1506	-2202	46.4	-169.4			-169.4
SL'	-695	-1042	23.1	-146.3			-146.3
7'	-1152	-1647	33.0	-113.3			-113.3
6'	-676	-901	15.0	-98.3			-98.3
5'	-135	-52	-5.5	-103.8			-103.8
4'	406	796	-26.0	-129.8			-129.8
3'	882	1543	-44.1	-173.9			-173.9
UL'	9108	4670	295.9	122.0			122.0
2'	1235	2097	-57.5	64.5			64.5
1'	1424	2392	-64.5	0			0

* $C_{n_{AV}} = (C_{n_{292.5}} + C_{n_{307.5}})/2$ (C_n values from Table 29)

$Q_T = (T_o - \Sigma Q' C_{n_{AV}})/2A = 0$

where $T_o = (T_{292.5} + T_{307.5})/2$ (Torsion values from Table 27)

TABLE 40 - CALCULATION OF RESULTANT SHEAR FLOWS
STATION 292.5 TO STATION 307.5

(1)	(2)	(3)	(4)	(5)	(6)	(7)	(8)
Web	P Fwd. Sta.	P Aft Sta.	$\Delta P/\Delta x$	Q'	$C_{n_{AV}}$	Q' · $C_{n_{AV}}$	Q
Ref.	Tab. 35	Tab. 36	(2) -(3)/15	Σ (4)	*	(5) x (6)	Q_T + (5)
1	1442	2341	-59.9	-59.9	239.3	-14334	-258.2
2	1609	2487	-58.5	-118.4	106.9	-12657	-316.7
UL	13458	6101	490.5	372.1	132.4	49266	173.8
3	1567	2327	-50.7	321.4	239.3	76911	123.1
4	1323	1881	-37.2	284.2	239.3	68009	85.9
5	904	1203	-19.9	264.3	239.3	63247	66.0
6	362	373	-.7	263.6	239.3	63079	65.3
7	-238	-507	17.9	281.5	35.8	10078	83.2
SL	-188	-380	12.8	294.3	203.5	59890	96.0
8	-824	-1331	33.8	328.1	239.3	78514	129.8
9	-1326	-2000	44.9	373.0	119.65	44629	174.7
LL	-12776	-5606	-478.0	-105.0	119.65	-12563	-303.3
9'	-1681	-2434	50.2	-54.8	239.3	-13114	-253.1
8'	-1848	-2581	48.9	-5.9	203.5	-1201	-204.2
SL'	-1045	-1472	28.5	22.6	35.8	809	-175.7
7'	-1807	-2420	40.9	63.5	239.3	15196	-134.8
6'	-1563	-1974	27.4	90.9	239.3	21752	-107.4
5'	-1144	-1296	10.1	101.0	239.3	24169	-97.3
4'	-602	-466	-9.1	91.9	239.3	21992	-106.4
3'	-1	413	-27.6	64.3	132.4	8513	-134.0
UL'	2709	2193	34.4	98.7	106.9	10551	-99.6
2'	584	1238	-43.6	55.0	239.3	13162	-143.3
1'	1086	1907	-54.7	0	239.3	0	-198.3
					4307.4	575898	

* $C_{n_{AV}} = (C_{n_{292.5}} + C_{n_{307.5}})/2$ (C_n values are from Table 29)

$Q_T = (T_o - \Sigma Q' C_{n_{AV}})/2A = (-278{,}000 - 575{,}898)/4307.4 = -198.3$

where $T_o = (T_{292.5} + T_{307.5})/2$ (Torsion values from Table 27)

TABLE 41 - CALCULATION OF RESULTANT SHEAR FLOWS
STATION 292.5 TO STATION 307.5

①	②	③	④	⑤	⑥	⑦	⑧
Web	P Fwd. Sta.	P Aft Sta.	$\Delta P/\Delta x$	Q'	$C_{n_{AV}}$	$Q' \cdot C_{n_{AV}}$	Q
Ref.	Tab. 35	Tab. 36	② - ③/15	Σ④	*	⑤ · ⑥	Q_T + ⑤
1	-917	-1448	35.4	35.4	239.3	8471	298.5
2	-1276	-1851	38.3	73.7	106.9	7879	336.8
UL	-11549	-4874	-445.0	-371.3	132.4	-49160	-108.2
3	-1472	-2027	37.0	-334.3	239.3	-79998	-71.2
4	-1485	-1955	31.3	-303.0	239.3	-72508	-39.9
5	-1310	-1645	22.3	-280.7	239.3	-67172	-17.6
6	-970	-1133	10.9	-269.8	239.3	-64563	-6.7
7	-504	-482	-1.5	-271.3	35.8	-9713	-8.2
SL	-244	-225	-1.3	-272.6	203.5	-55474	-9.5
8	30	231	-13.4	-286.0	239.3	-68440	-22.9
9	568	919	-23.4	-309.4	119.65	-37020	-46.3
LL	6856	3057	253.3	-56.1	119.65	-6712	207.0
9'	1045	1499	-30.3	-86.4	239.3	-20676	176.7
8'	1404	1902	-33.2	-119.6	203.5	-24339	143.5
SL'	906	1235	-21.9	-141.5	35.8	-5066	121.6
7'	1601	2078	-31.8	-173.3	239.3	-41471	89.8
6'	1614	2006	-26.1	-199.4	239.3	-47716	63.7
5'	1438	1696	-17.2	-216.6	239.3	-51832	46.5
4'	1098	1184	-5.7	-222.3	239.3	-53196	40.8
3'	632	533	6.6	-215.7	132.4	-28559	47.4
UL'	2873	351	168.1	-47.6	106.9	-5088	215.5
2'	99	-180	18.6	-28.5	239.3	-6820	234.6
1'	-440	-868	28.5	0	239.3	0	263.1
					4307.4	-779.173	

* $C_{n_{AV}} = (C_{n_{292.5}} + C_{n_{307.5}})/2$ (C_n values are from Table 29)

$Q_T = (T_o - \Sigma Q' C_{n_{AV}})/2A = (354{,}000 + 779{,}173)/4307.4 = 263.1$

where $T_o = (T_{292.5} + T_{307.5})/2$ (Torsion values from Table 27)

TABLE 42 - SUMMARY OF ULTIMATE SHEAR FLOWS

(1)	(2)	(3)	(4)	(5)	(6)	(7)	(8)	(9)	(10)	(11)	(12)	(13)	(14)	(15)	(16)	(17)	(18)	(19)	(20)	(21)
WEB	STATION 277.5 - 292.5				STATION 292.5 - 307.5				STATION 307.5 - 322.5				STATION 322.5 - 337.5				STATION 337.5 - 352			
	Gust	Comb.B	Rolling Pull Out		Gust	Comb.B	Rolling Pull Out		Gust	Comb.B	Rolling Pull Out		Gust	Comb.B	Rolling Pull Out		Gust	Comb.B	Rolling Pull Out	
1	-94.9	-468.7	557.5		-64.5	-258.2	298.5		-20.1	-166.2	205.5		31.0	-100.8	155.3		39.4	-108.3	170.0	
2	-177.2	-576.0	642.6		-122.0	-316.7	336.8		-38.9	-181.6	214.5		58.3	-69.6	135.4		74.8	-69.8	144.6	
UL	164.3	385.5	-400.2		173.9	173.8	-108.2		152.0	75.5	6.1		98.8	-19.4	98.3		92.1	-50.1	131.0	
3	105.5	281.0	-302.1		129.8	123.1	-71.2		135.5	63.0	12.4		119.2	9.2	76.4		120.2	-13.7	102.8	
4	78.4	192.8	-203.2		103.8	85.9	-39.9		122.3	54.0	15.7		130.2	31.6	55.1		138.3	17.1	74.5	
5	87.4	132.5	-115.9		98.3	66.0	-17.6		112.8	48.6	16.3		130.7	45.3	37.0		144.9	39.0	49.4	
6	132.5	108.4	-51.2		113.3	65.3	-6.7		106.9	46.3	14.6		120.6	48.7	24.2		140.0	50.2	30.0	
7	209.3	124.3	-17.6		146.3	83.2	-8.2		104.4	46.4	11.4		101.1	41.3	18.3		125.1	50.2	18.2	
SL	255.6	136.8	-1.3		169.4	96.0	-9.5		106.9	48.1	10.2		92.0	37.2	16.0		118.4	50.8	11.4	
8	356.0	191.7	-3.3		215.8	129.8	-22.9		106.6	49.6	6.5		65.5	20.1	17.7		96.1	40.2	8.2	
9	468.9	280.1	-41.2		269.3	174.7	-46.3		107.7	51.4	3.2		35.4	-4.7	26.7		69.8	20.9	13.6	
LL	-468.9	-550.8	395.5		-269.3	-303.3	207.0		-107.7	-139.7	105.1		-35.4	-67.7	58.9		-69.8	-102.8	85.7	
9'	-356.0	-438.7	325.8		-215.8	-253.1	176.7		-106.6	-139.0	103.2		-65.5	-97.2	74.2		-96.1	-127.6	98.6	
8'	-255.6	-315.5	232.2		-169.4	-204.2	143.5		-106.9	-140.5	103.6		-92.0	-127.6	93.9		-118.4	-154.4	116.7	
SL'	-209.3	-245.8	171.8		-146.3	-175.7	121.6		-104.4	-137.5	100.7		-101.1	-139.8	102.6		-125.1	-165.6	126.1	
7'	-132.5	-125.3	65.1		-113.3	-134.8	89.8		-106.9	-141.9	103.8		-120.6	-167.6	123.7		-140.0	-190.3	147.5	
6'	-87.4	-21.1	-42.5		-98.3	-107.4	63.7		-112.8	-149.8	109.9		-130.7	-189.2	144.8		-144.9	-209.3	167.8	
5'	-78.4	55.2	-138.4		-103.8	-97.3	46.5		-122.3	-161.3	118.7		-130.2	-201.3	162.7		-138.3	-219.6	187.1	
4'	-105.5	95.3	-211.6		-129.8	-106.4	40.8		-135.5	-175.9	129.8		-119.2	-204.5	175.3		-120.2	-219.6	202.4	
3'	-164.3	96.0	-253.7		-173.9	-134.0	47.4		-152.0	-193.3	142.5		-98.8	-196.3	181.0		-92.1	-207.4	204.7	
UL'	177.2	-260.7	473.8		122.0	-99.6	215.5		38.1	-111.8	169.0		-58.3	-174.3	181.4		-74.8	-187.9	190.2	
2'	94.9	-299.6	467.2		64.5	-143.3	234.6		20.1	-130.3	182.1		-31.0	-156.4	179.2		-39.4	-175.6	177.8	
1'	0	-372.6	496.4		0	-198.3	263.1		0	-148.5	194.2		0	-131.1	170.8		0	-144.9	189.8	

DESIGN OF MEMBERS

In this section the primary fuselage structure is designed to carry the axial loads and shear flows found in the preceding sections.

Longeron Design - Axial Loads

The aft section longerons carrying axial loads only are checked in Table 44. Since none of these longerons are critical in tension, only the check of those critical in compression are shown.

Detailed calculations of the section properties and allowable stresses are shown for the upper and lower longerons at Station 284 in Table 43. Referring to Figure 94 the allowable stresses of the longeron elements are determined as follows, based upon the crippling stress of flat elements under various conditions of edge support. Where (Ref. Timoshenko "Theory of Elastic Stability," Pg. 331)

$$F_{cr} = K\pi^2 E_R (t/b)^2/12(1-\mu^2) \quad - - - - - - - - - - - - \quad (49)$$

where K = coefficient dependent upon edge conditions of flange

E_R = effective modulus of elasticity

t = flange thickness

b = flange width

μ = Poisson's ratio, assumed equal to 0.3

Case I - Long Flange, One Unloaded Edge Simply Supported

(Reference Element (3))

K = .456 (Ref. Timoshenko, "Theory of Elastic Stability, Pg. 340)

E_R = Secant modulus of elasticity = E_S (Ref. Stowell, NACA TN 1556, P.4)

$$F_{CR} = .456\,\pi^2 E_S (t/b)^2/12(1-.3^2) = .4117\, E_S/(b/t)^2 \quad - - - \quad (50)$$

Case II - Long Plates, Both Unloaded Edges Simply Supported

(Reference Element (1), (2), and (5)

K = 4.0 (Ref. Timoshenko, Pg. 330)

$$E_R = E_S \left[.5 + .5(.25 + 75E_t/E_S)^{1/2} \right] \qquad \text{(Ref. Stowell, Pg. 4)}$$

$$F_{CR} = 4\pi^2 E_R (t/b)^2/12(1-.3^2) = 3.6116\, E_R/(b/t)^2 \quad - - - \quad (51)$$

Case III - Long Plate, Both Unloaded Edges Clamped

$K = 7.5$ (Ref. Sechler and Dunn, Pg. 168)

$E_R = E_S \left[.352 + .648(.25 + .75\ E_t/E_S)^{1/2} \right]$ (Ref. Stowell, Pg. 4)

$$F_{CR} = 7.5\pi^2\ E_R\ (t/b)^2/12(1 - .3^2) = 6.7717\ E_R/(b/t)^2 \quad - - - \quad (52)$$

Design of Shear Panels

The skin covering in the aft section is designed to carry axial loads as well as shear flows. Consequently, the skin panels in this region are analyzed to carry the combined shear and axial compression loads computed in the preceding section. In general, non-buckled skin panels up to limit load were desired. This was obtained in practically all cases as shown by the following. Note that the stress ratios were combined according to the formula,

$$R_b^2 + R_s^2 = 1.0 \quad - - - - - - - - - - - - - - - - - - \quad (53)$$

which holds for circular sections in bending and torsion as per ANC-5a, Page 28.

The allowable buckling shear stresses are computed in Table 45, in accordance with the formula,

$$F_{s_{cr}} = K_s\ \pi^2 E/12(1 - \mu^2)(b/t)^2 \quad - - - - - - - - - - \quad (54)$$

(Ref. NACA T.N. #1347)

where

K_s = shear stress coefficient

E = modulus of elasticity

μ = Poisson's ratio

b = width of plate (measured along the plate)

t = thickness of plate

R = radius of plate

The values of K_s were obtained from NACA T.N. #1348 where the variations of K_s with the curvature parameter Z for various ratios of panel width to length are plotted. The curvature parameter

$$Z = b^2(1 - \mu^2)^{1/2}/Rt \quad - - - - - - - - - - - - - - \quad (55)$$

The allowable buckling stresses due to edge compression are computed in Table 46. Since $R/t < 500$, the Kanemitsu and Nojima formula recommended in NACA T.N. #1343 is used as follows:

$$F_{c_{cr}} = E\left[.16(t/L)^{1.3} + 9(t/R)^{1.6}\right] \qquad - - - - - - - - (56)$$

The greatest shear flows occur in the region between Station 277.5 and 292.5 as shown in Table 42. The lowest value of $F_{s_{cr}}$ in this region is obtained in the panels between Stations 277.5 and 283.2 as shown in Table 45. Since the edge compression stresses in these skin panels are negligible, buckling of the panels is based on the shear flows only.

t_{skin} = .064 (FS-1h)

$q_{max.}$ = 643 lbs./in. (ultimate) (Roll. P.O.) Table 42

$$f_{s(max.)} = \frac{643}{.064} = 10{,}050 \text{ psi (ultimate)}$$

$$f_{s(max.)} = \frac{10{,}050}{1.50} = 6{,}700 \text{ psi (limit)}$$

$F_{s_{cr}}$ = 6,960 psi (Table 45)

Panel will buckle at $\frac{6{,}960}{6{,}700} \times 100 = 104\%$ of limit load.

Panel may be considered shear-resistant (K = 0)

Ultimate gross shear strength of skin

τ_s = 13,500 psi

$$\text{M.S. (Ultimate Shear)} = \frac{13{,}500}{10{,}500} - 1 = \underline{\underline{+.34}}$$

The above value for τ_s is based on the same value of τ_s/τ_{sh} obtained in Figure 4 of NACA T.N. #1756 for 24ST sheet.

The percent of limit load at which buckling will occur in various aft section skin panels is computed in Table 47.

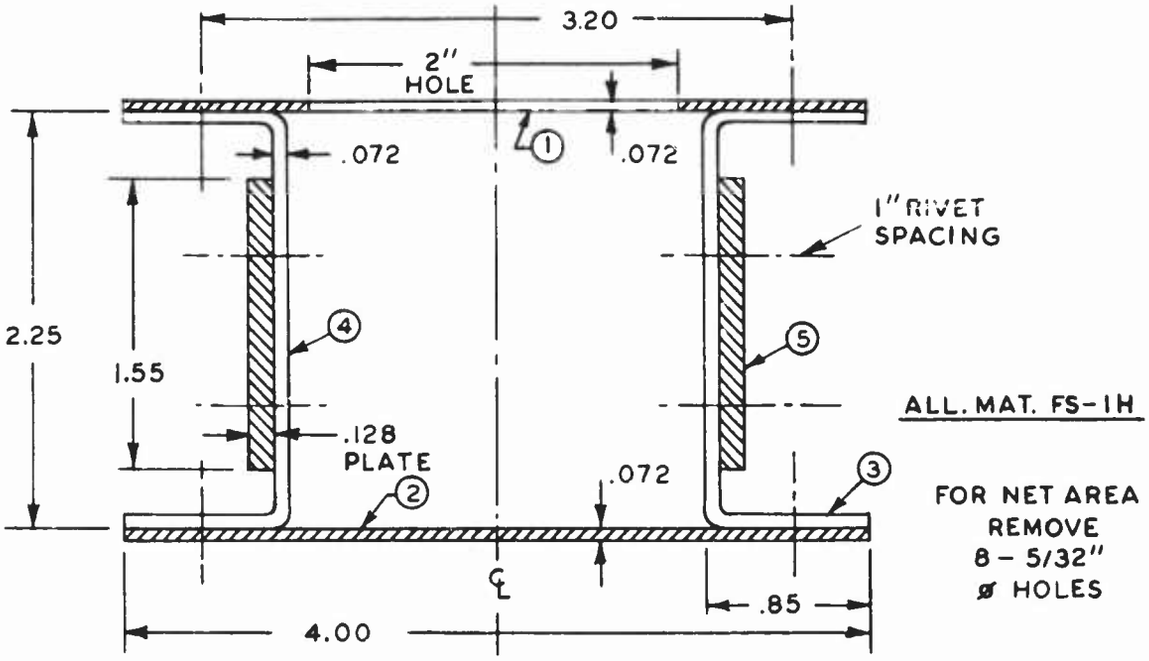

FIGURE 94 - UPPER AND LOWER LONGERON SECTION - STATION 284

TABLE 43 - SECTION PROPERTIES AND ALLOWABLE STRESSES
UPPER AND LOWER LONGERONS - STATION 284

ITEM	DIMENS.	NO PTS	b/t	Fcr	AREA	Pcr
REF	FIG. 94.				IN.^{2}	LBS.
1	2.0 x .072	1	44.5	11,700	.144	1685
2	4.0 x .072	1	44.5	11,700	.288	3370
3	.70 x .072	4	9.7	21,800	.202	4405
4	2.0 x .072	2	27.8	24,000	.288	6910
5	1.55 x .128	2	12.1	24,000	.397	9530
			F_{cr} (aver) = 19,640		1.319	25,900

NOTE: The above actual section differs slightly from the assumed section used to determine longeron loads (see Table 28). The difference is small enough to be considered negligible.

TABLE 44 - DESIGN OF MEMBERS - AFT SECTION LONGERONS CRITICAL IN COMPRESSION

(1)	(2)	(3)	(4)	(5)	(6)	(7)	(8)
Member	Fuselage Station	Gross Area	Comp. Load P	Condition	f_c	F_{cr}	M.S.
Ref.			Fig. (93)	Fig. (93)	(4) / (3)		(7)/(6) - 1
UL	284	1.319	20,400	Roll. P.O.	15,500	19,640	.27
UL	292.5	1.315	11,550	Roll. P.O.	8,800	21,700	1.47
UL	307.5	.727	4,870	Roll. P.O.	6,700	22,400	Ample
UL	322.5	.344	1,750	Roll. P.O.	5,100	21,800	Ample
LL	284	1.319	22,400	Gust	17,000	19,640	.16
LL	292.5	1.315	14,400	Gust	10,950	21,700	.98
LL	307.5	.727	6,310	Gust	8,700	22,400	1.58
LL	322.5	.507	3,080	Gust	6,100	25,600	Ample
SL	322.5	.344	1,520	Comb. B	4,400	21,800	Ample

TABLE 45 - ALLOWABLE BUCKLING SHEAR STRESSES

- All skin panels are FS-1h material

Skin Panels	t	b	a	R	Z	K_s	$F_{s_{cr}}$
Sta. 277.5 to 283.2	.064	5.7	45.0	27.4	17.7	9.40	6960
283.2 to 288.2	↕	5.0	44.6	27.2	13.7	8.40	8080
288.2 to 292.2	↕	4.3	44.1	26.9	10.2	7.50	9760
292.2 to 307.5	↕	15.0	43.0	26.2	128.0	32.8	3510
307.5 to 322.5	↕	15.0	40.8	24.9	134.7	34.0	3640
322.5 to 337.5	↕	15.0	38.4	23.4	143.2	35.5	3800
Sta. 337.5 to 352.0	.064	14.5	35.8	21.8	143.7	35.7	4080

$$F_{s_{cr}} = K_s \pi^2 E/12(1-\mu^2)(b/t)^2 \qquad E = 6.5 \times 10^6 \qquad \mu = .30$$

TABLE 46 - ALLOWABLE BUCKLING STRESSES - EDGE COMPRESSION

Skin Panels	t	L = b	R	$F_{c_{cr}}$
Sta. 277.5 to 283.2	.064	5.7	27.4	6650
283.2 to 288.2	↕	5.0	27.2	7250
288.2 to 292.5	↕	4.3	26.9	8090
292.5 to 307.5	↕	15.0	26.2	4750
307.5 to 322.5	↕	15.0	24.9	5060
322.5 to 337.5	↕	15.0	23.4	5510
Sta. 337.5 to 352	.064	14.5	21.8	6070

$$F_{c_{cr}} = E\left[.16(t/L)^{1.3} + 9\,(t/R)^{1.6}\right] \qquad E = 6.5 \times 10^6$$

TABLE 47 - LIMIT STRESSES AND BUCKLING RATIOS

LIMIT STRESSES							
(1)	(2)	(3)	(4)	(5)	(6)	(7)	(8)
Skin Panels	Web & Flange No.	Cond.	f_b (ult.) Fwd.	f_b (ult.) Aft	Average f_b(limit)	q (ult.)	f_s(limit)
Ref.	Fig.89		Table 37		$\frac{1}{1.5}\left[\frac{(4)+(5)}{2}\right]$	Tab.42	$\frac{(7)}{1.5(.064)}$
Sta. 292.5 to 307.5	2	Roll. P.O.	-2135	-3235	-1790	337	3510
307.5 to 322.5	2	Roll. P.O.	-3235	-3665	-2300	215	2240
322.5 to 337.5	7'	Comb. B	-4350	-3830	-2730	168	1750
Sta. 337.5 to 352.	7'	Comb. B	-3830	-3370	-2400	190	1980

BUCKLING RATIOS						
(1)	(9)	(10)	(11)	(12)	(13)	(14)
Skin Panels	$F_{C_{CR}}$	R_b	$F_{S_{CR}}$	R_S	$\sqrt{R_b^2 + R_s^2}$	Buckling @ % Limit
Ref.	Tab. 46	(6)/(9)	Tab. 45	(8)/(11)	$\sqrt{(10)^2+(12)^2}$	$\frac{1}{(13)} \times 100$
Sta. 292.5 to 307.5	4750	.377	3510	1.000	1.069	94%
307.5 to 322.5	5060	.455	3640	.616	.766	130
322.5 to 337.5	5510	.496	3800	.461	.677	148
Sta. 337.5 to 352.	6070	.396	4080	.486	.627	159

VERTICAL STABILIZER (FIN)

Introduction

The fin is of conventional design, with front and rear beams, and sheet metal skins combined to form a closed torque box.

All sheet metal conforms to Specification QQ-M-44, hard rolled magnesium alloy. Extrusions are fabricated from Dow Chemical Co. Spec. ZK-60, Certain of the hinge fittings are made from Spec. AN-M-36, Comp. A, heat-treated aged magnesium alloy castings. The main fin to stabilizer fittings are steel forgings, heat-treated to 150,000 psi tensile strength (minimum).

The method of analysis employed was identical with that shown in Lockheed Report #4660 and may be briefly described as follows:

(1) Preliminary shears, moments and torsions for the vertical tail surfaces based upon the net fin load and ignoring the rudder load were obtained directly from Lockheed Report #4660, pages 114 and 115, for the Balancing and Dynamic Conditions. The corresponding loads for the Rolling Pull-out Condition, a new contractual requirement, were obtained from the Balancing Condition by proportion.

(2) The fin deflection curve was calculated for the Balancing Condition and the rudder hinge reactions due to this deflection were then computed. The hinge reactions on the rudder due to fin deflection for the other flight conditions were then obtained by proportion.

(3) The rudder hinge reactions were then determined for the rudder air loads acting on the undeflected support system. These calculations were made in detail for the Balancing Condition and the hinge reactions for the other loading conditions obtained by proportion.

(4) The final rudder hinge reactions were obtained by adding the results of Steps 2 and 3.

(5) Using the results of Steps 1 and 4, the final fin and rudder shears, moments and torsions were calculated.

Loads on Vertical Tail Surfaces

Total Loads on Surfaces

(a) Balancing Condition

With reference to Lockheed Report #4660, page 111, the loads for this condition are as follows:

Load on fin = 5900 lbs.
Load on rudder = 975 lbs. acting opposite to the air load on the fin.
Net tail load = 5900 - 975 = 4925 lbs.

The chordwise distribution of the air load is as shown in Figure 95. The preliminary shears, bending moment and torsion about the hinge line are obtained from Lockheed Report #4660, page 114, and are tabulated in Table 48.

(b) Dynamic Condition

With reference to Lockheed Report #4660, page 112, the loads for this condition are as follows:

Load on fin = 3880 lbs.
Load on rudder = 640 lbs.
Total tail load = 3880 + 640 = 4520 lbs.

The chordwise distribution of air load on the vertical tail for this condition is shown in Figure 95. The shears and bending moments are obtained from Lockheed Report #4660, page 115, and are tabulated in Table 48. The values of torsion about the hinge line shown in Figure 95 are obtained by multiplying the torsion from the Balancing Condition by the following factor.

$$(3880/5900)(.538/.605) = .585$$

The above factor is made necessary by the difference in chordwise center of pressure (see Figure 95).

(c) Rolling Pull-out Condition

The loads on the vertical tail for this condition are as follows: (Ref. p. 159)

Load on fin = 6105 lbs.
Load on rudder = 0

The chordwise distribution of air load on the vertical tail for this condition is as shown in Figure 95. The shears and bending moments are obtained by multiplying the values from the Balancing Condition by the ratio (6105/5900) = 1.035. The torsion about the hinge line is obtained by multiplying the torsion from the Balancing Condition by the ratio (6105/5900)(.640/.605) = 1.095. The resultant shear, bending moment and torsion about the hinge line are tabulated in Table 48.

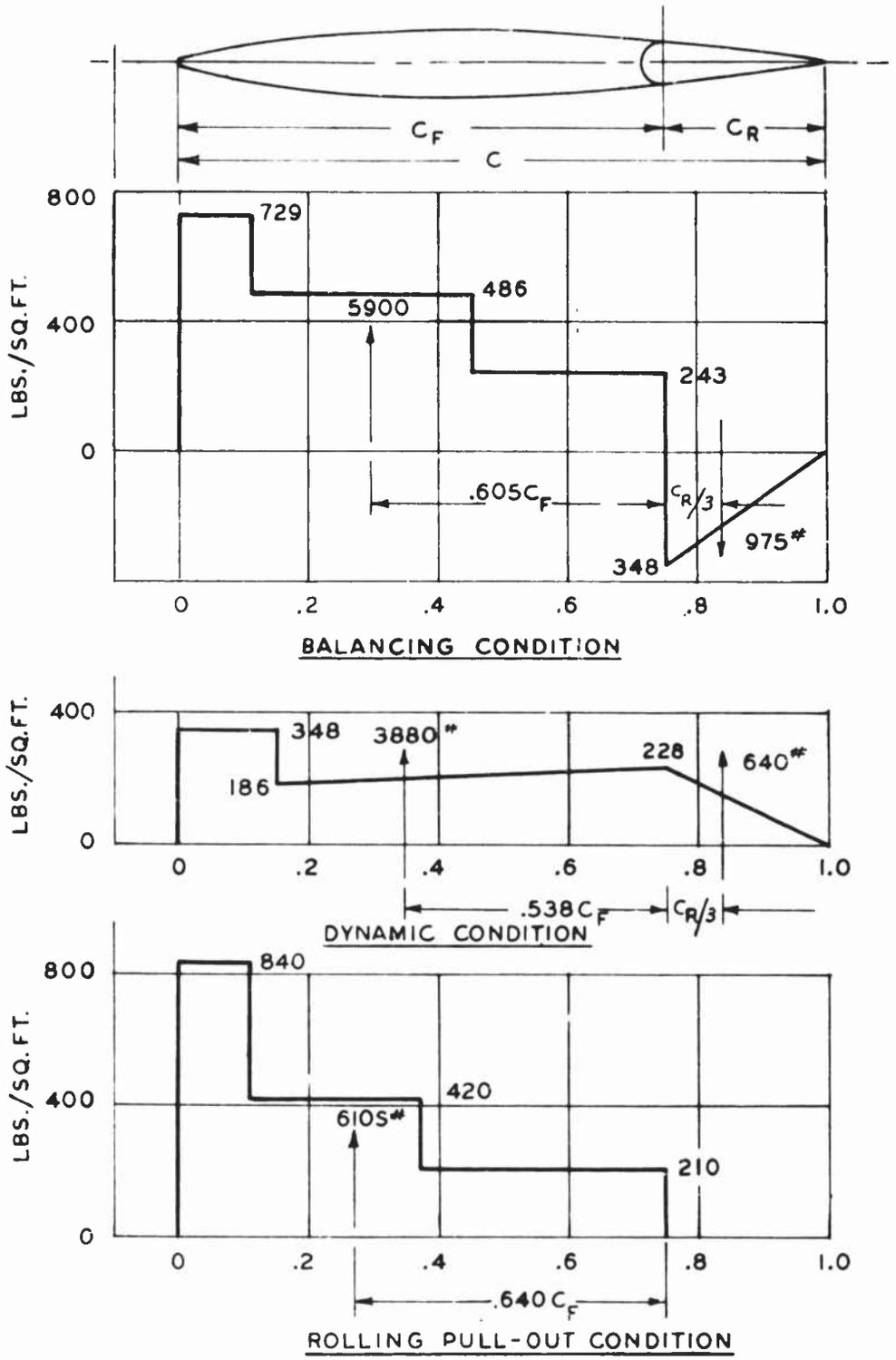

FIG. 95 CHORDWISE LOAD DISTRIBUTIONS

TABLE 48 - PRELIMINARY SHEARS, BENDING MOMENTS AND TORSION ABOUT HINGE LINE

(Reference Figure 95)

(1)	(2)	(3)	(4)	(5)	(6)	(7)	(8)	(9)	(10)
Fin Station	Balancing Condition			Dynamic Condition			Rolling Pull-Out Condition		
	Shear S_{AL}	Bending Moment BM_{AL}	Torsion about Hinge T_{AL}	Shear S_{AL}	Bending Moment BM_{AL}	Torsion about Hinge T_{AL}	Shear S_{AL}	Bending Moment BM_{AL}	Torsion about Hinge T_{AL}
Ref.	Note 1	Note 1	Note 1	Note 2	Note 2	Note 3	1.035 (2)	1.035 (3)	1.095 (4)
192.79	0	0	0	0	0	0	0	0	0
180	614	3720	7020	404	2450	4110	636	3850	7680
170	1210	12740	15420	794	8380	9020	1250	13190	16880
160	1920	28290	27670	1270	18620	16200	1990	29300	30300
151	2660	48860	42170	1750	32150	24700	2750	50600	46200
143	3400	73040	58190	2240	48060	34100	3520	75700	63700
135	4200	103400	77510	2760	68010	45300	4350	107200	84800
128	4960	135400	97280	3270	89090	56900	5130	140200	106500
120	5900	178800	123500	3880	117600	72300	6110	185000	135200

Notes: (1) These values are from Lockheed Report #4660, pg. 114.
(2) These values are from Lockheed Report #4660, pg. 115.
(3) Torque about hinge line = .585 (4) (Ref. page 191)

Fin Section Properties

The section properties of the fin are computed on the basis of the following assumptions:

1. The crippling stress of the beam in compression is assumed the limiting value for the section.

2. The effective width of skin acting at the rivet line attaching skin to beam is based upon the following equation, obtained from page 206 of Sechler and Dunn.

$$W_E/_b = 0.25(1 + F_{CR}/F_C)\ (F_{CR}/F_C)^n \quad - - - - - - - - - - (57)$$

where $$n = 0.37\ F_C/F_{CY} \quad - - - - - - - - - - - - - - - - - - (58)$$

W_E = effective width of sheet acting on one side of rivet line attaching sheet to stiffener.

F_{CR} = critical buckling stress of panel (simply-supported edges).

F_C = compression stress in stiffener.

F_{CY} = compression yield stress of sheet material.

b = panel width

t = sheet thickness

The critical buckling stress (F_{CR}) of a flat panel with all edges simply supported and with a length to width ratio greater than 1.0 is given by Equation (51), where

$$F_{CR} = 3.6116\ E_R/(b/t)^2 \quad - - - - - - - - - - - - (51)$$

The compression stress of a stiffener is calculated using Equation (50), where

$$F_C = .4117\ E_S/(b/t)^2 \quad - - - - - - - - - - - - - - - (50)$$

3. The effective section is assumed symetrical.

Sample calculations of the fin section properties are shown for Fin Station 121 in Figure 96. A summary of the fin section properties for all the sections investigated is shown in Table 49.

FIGURE 96 - FIN SECTION PROPERTIES - STATION 121

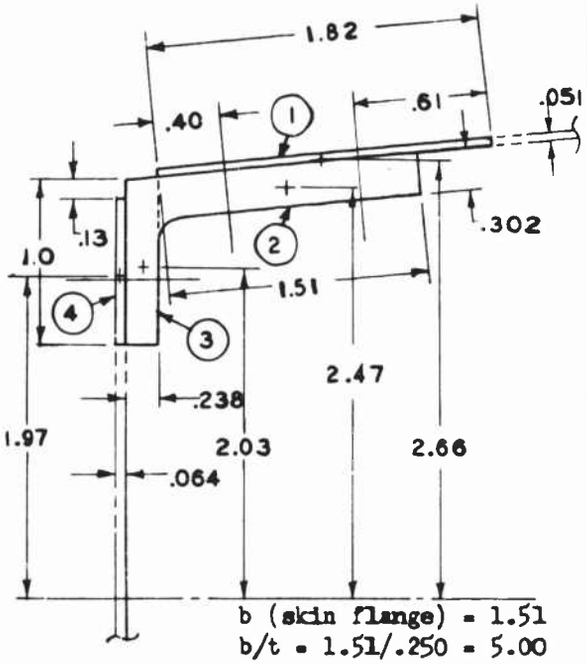

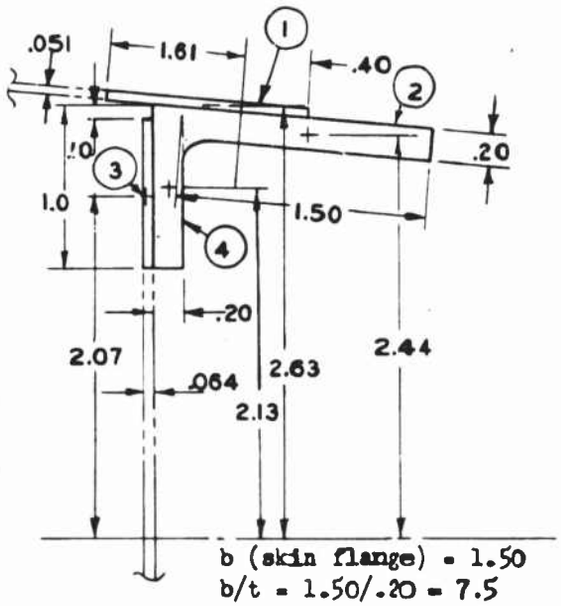

F_c = 27000 lbs/sq.in. (Ref. Equation 50)

b_s = 24.75 ins. b/t = 24.75/.051 = 485

$F_{CR} = 3.612 \times 6.50 \times 10^6/485^2 = 100$ lbs/sq.in.

$n = .37 \times 27000/24000 = .416$

$w_e/b_s = .25(1 + 100/27000)(100/27000)^{.416} = .0245$

$w_e = .0245 \times 24.75 = .61$ ins.

Item	Dimension	A	y	Ay^2
(1)	1.82 x .051	.0928	2.66	.657
(2)	1.51 x .302	.456	2.47	2.780
(3)	1.0 x .238	.238	2.03	.980
(4)	.87 x .064	.0557	1.97	.216
Σ				4.633

$I_{FB} = 2 \times 4.633 = 9.266$ ins.^{4}

$(I_F/y)_{FB} = (9.266 + 6.590)/2.66 = 5.96$ ins.^{3}

F_c = 27000 lbs/sq.in. (Ref. Equation 50)

w_e = .61 in. (same as for front beam)

Item	Dimension	A	y	Ay^2
(1)	1.01 x .051	.0515	2.63	.356
(2)	1.50 x .20	.300	2.44	1.785
(3)	1.0 x .20	.200	2.13	.907
(4)	.90 x .064	.0576	2.07	.247
Σ				3.295

$I_{RB} = 2 \times 3.295 = 6.590$ ins.^{4}

$(I_F/y)_{RB} = 15.86/2.63 = 6.03$ ins.^{3}

TABLE 49 - SUMMARY OF FIN SECTION PROPERTIES

(1)	(2)	(3)	(4)	(5)	(6)	(7)	(8)
Fin Section	Front Beam		Rear Beam		Total		
	I_{FB}	$(I_F/y)_{FB}$	I_{RB}	$(I_F/y)_{RB}$	I_F	I_{FB}/I_F	I_{FB}/I_F
Ref.					(2) + (4)	(2) / (6)	(4) / (6)
121	9.266	5.96	6.590	6.03	15.86	.584	.416
128	7.430	5.36	5.790	5.36	13.22	.562	.438
135	6.170	4.85	5.078	4.99	11.25	.548	.452
143	4.620	3.94	3.676	4.03	8.30	.557	.443
151	3.604	3.17	2.594	3.32	6.20	.582	.418
160	2.500	2.42	1.690	2.56	4.19	.597	.403
170	1.866	1.93	.978	2.03	2.84	.655	.345
180.4	1.402	1,57	.576	1.68	1.98	.709	.291

Determination of Fin Shears, Moments and Torques

Distribution of Final Fin Shear Along Hinge Line

The loading on the fin due to its own air load and the hinge loads from the rudder are as indicated in Figure 97.

The shear at any station "n" is given by the following expression.

$$S_n = - S_{AL} - S_H \qquad (59)$$

where S_{AL} = summation of shear due to air load from Station 192.79 to Station "n".

S_H = summation of hinge loads acting between Station "n" and tip of fin.

The values of S_H are determined as follows:

From Sta. 180.0 to 170.5	$S_H = R_{180}$
From Sta. 170.5 to 135.5	$S_H = R_{180} + R_{170.5}$
From Sta. 135.5 to 120.0	$S_H = R_{180} + R_{170.5} + R_{135.5}$

where R is the hinge reaction determined by the method outlined on Page 190 These hinge reactions are summarized and the resultant fin shear determined in Table 50 for the various loading conditions.

The final fin shear distribution is determined, using Equation (59) in Table 51, and plotted in Figure 98.

FIGURE 97 - FIN LOADING

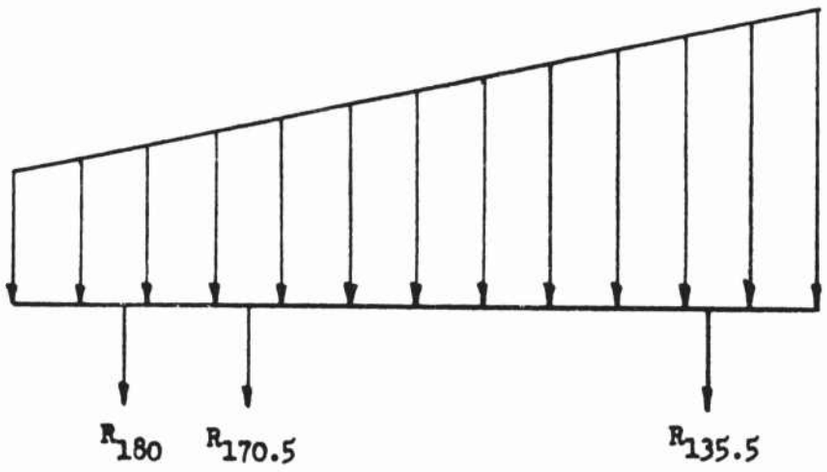

TABLE 50 - SUMMARY OF HINGE REACTIONS AND RESULTANT FIN SHEAR

(1)	(2)	(3)	(4)	(5)	(6)	(7)
Fin Station	Balancing Cond.		Dynamic Cond.		Roll. Pull-Out Cond.	
	R	S_H	R	S_H	R	S_H
Ref.		Σ (2)		Σ (4)		Σ (6)
192.79	-	0	-	0	-	0
-180.0	-	0	-	0	-	0
+180.0	-224	-224	+10	+10	-108	-108
-170.5	-	-224	-	+10	-	-108
+170.5	-290	-514	+108	+118	-65	-173
-135.5	-	-514	-	+118	-	-173
+135.5	-153	-667	+719	+837	+486	+313
120.0	-	-667	-	+837	-	+313

TABLE 51 - FINAL FIN SHEAR ALONG HINGE LINE

(1)	(2)	(3)	(4)	(5)	(6)	(7)	(8)	(9)	(10)
Fin Station	Balancing Condition			Dynamic Condition			Roll. Pull-Out Cond.		
	$-S_{AL}$	$-S_H$	S	$-S_{AL}$	$-S_H$	S	$-S_{AL}$	$-S_H$	S
Ref.	Tab.50	Tab.50	(2) + (3)	Tab. 48	Tab.50	(5) + (6)	Tab.48	Tab.50	(8) + (9)
192.79	0	0	0	0	0	0	0	0	0
-180	-614	0	-614	-404	0	-404	-636	0	-636
+180	-614	+220	-394	-404	-10	-414	-636	+110	-526
-170	-1210	+220	-990	-794	-10	-804	-1250	+110	-1140
+170	-1210	+510	-700	-794	-120	-914	-1250	+178	-1080
160	-1920	↑	-1410	-1270	↑	-1390	-1990	↑	-1820
151	-2660	|	-2150	-1750	|	-1870	-2750	|	-2580
143	-3400	↓	-2890	-2240	↓	-2360	-3520	↓	-3350
-135	-4200	+510	-3690	-2760	-120	-2880	-4350	+178	-4180
+135	-4200	+670	-3530	-2760	-840	-3600	-4350	-310	-4660
128	-4960	↕	-4290	-3270	↕	-4110	-5130	↕	-5440
120	-5900	+670	-5230*	-3880	-840	-4720*	-6110	-310	-6420*

* Net fin shear does not equal net tail load since lower rudder hinge is attached directly to fuselage.

(REF. TABLE 51)

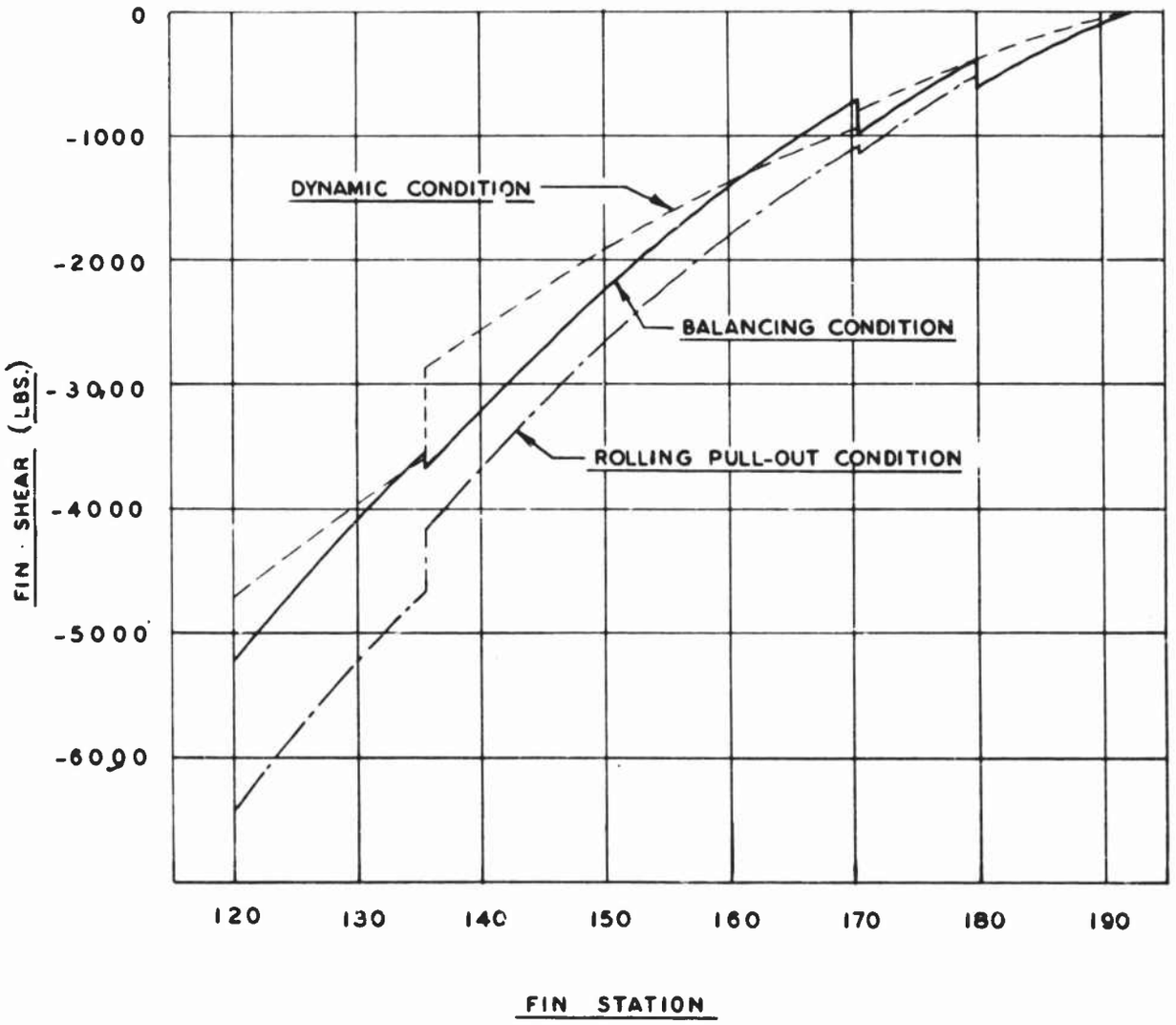

FIG. 98 DISTRIBUTION OF FINAL FIN SHEAR ALONG HINGE LINE

Distribution of Final Fin Bending Moment

With reference to Figure 97, the bending moment at any fin station "n" is given by the expression

$$M = M_{AL} - M_H = - M_{AL} - \sum_{n}^{192.79} (S_H)_{n-1} \Delta X \quad - - - - - - - - \quad (60)$$

where M_{AL} = bending moment due to air load only.

$(S_H)_{n-1}$ = shear due to hinge loads at previous station.

ΔX = distance to previous station.

The bending moment distributions for the various loading conditions are calculated in Table 52 and plotted in Figure 99.

Distribution of Final Fin Torsion About Hinge Line

Since the rudder hinge loads are applied to the fin at the hinge line, they do not affect the torsion in the fin. Therefore, the torsion values calculated in Table 48 are final ultimate values, and are plotted in Figure 100.

TABLE 52 - DISTRIBUTION OF FINAL FIN BENDING MOMENT

①	②	③	④	⑤	⑥	⑦	⑧	⑨	⑩	⑪	⑫	⑬	⑭	⑮	⑯	⑰
FIN STATION	ΔX	BALANCING CONDITION					DYNAMIC CONDITION					ROLLING PULL OUT CONDITION				
		$-(S_H)_{n-1}$	$-(S_H)_{n-1}\cdot\Delta X$	M_H	$-M_{AL}$	M	$-(S_H)_{n-1}$	$-(S_H)_{n-1}\cdot\Delta X$	M_H	$-M_{AL}$	M	$-(S_H)_{n-1}$	$-(S_H)_{n-1}\cdot\Delta X$	M_H	$-M_{AL}$	M
Ref.	$①_n - ①_{n-1}$	Tab.51	②×③	Σ④	Tab.48	⑤+⑥	Tab.51	②×⑧	Σ⑨	Tab.48	⑩+⑪	Tab.51	②×⑬	Σ⑭	Tab.48	⑮+⑯
192.79	0	0	0	0	0	0	0	0	0	0	0	0	0	0	0	0
180.0	12.79	0	0	0	-3720	-3720	0	0	0	-2450	-2450	0	0	0	-3850	-3850
170.0	10.00	220	+2200	2200	-12740	-10540	-10	-100	-100	-8380	-8480	+110	+1100	+1100	-13190	-12090
160.0	10.00	510	5100	7300	-28290	-20990	-120	-1200	-1300	-18620	-19920	+170	+1700	+2800	-29300	-26500
151.0	9.00	↕	4590	11890	-48860	-36970	↕	-1080	-2380	-32150	-34530	↕	+1530	+4330	-50600	-46270
143.0	8.00	↕	4080	15970	-73040	-57070	↕	-960	-3340	-48060	-51400	↕	+1360	+5690	-75700	-70010
135.0	8.00	510	4080	20050	-103400	-83350	-120	-960	-4300	-68010	-72310	+170	+1360	+7050	-107200	-100200
128.0	7.0	670	4690	24740	-135400	-110660	-840	-5880	-10180	-89090	-99270	-310	-2170	+4880	-140200	-135300
120.0	8.0	670	5360	30100	-178800	-148700	-840	-6720	-16900	-117600	-134500	-310	-2480	+2440	-185000	-182600

(REF. TABLE 52)

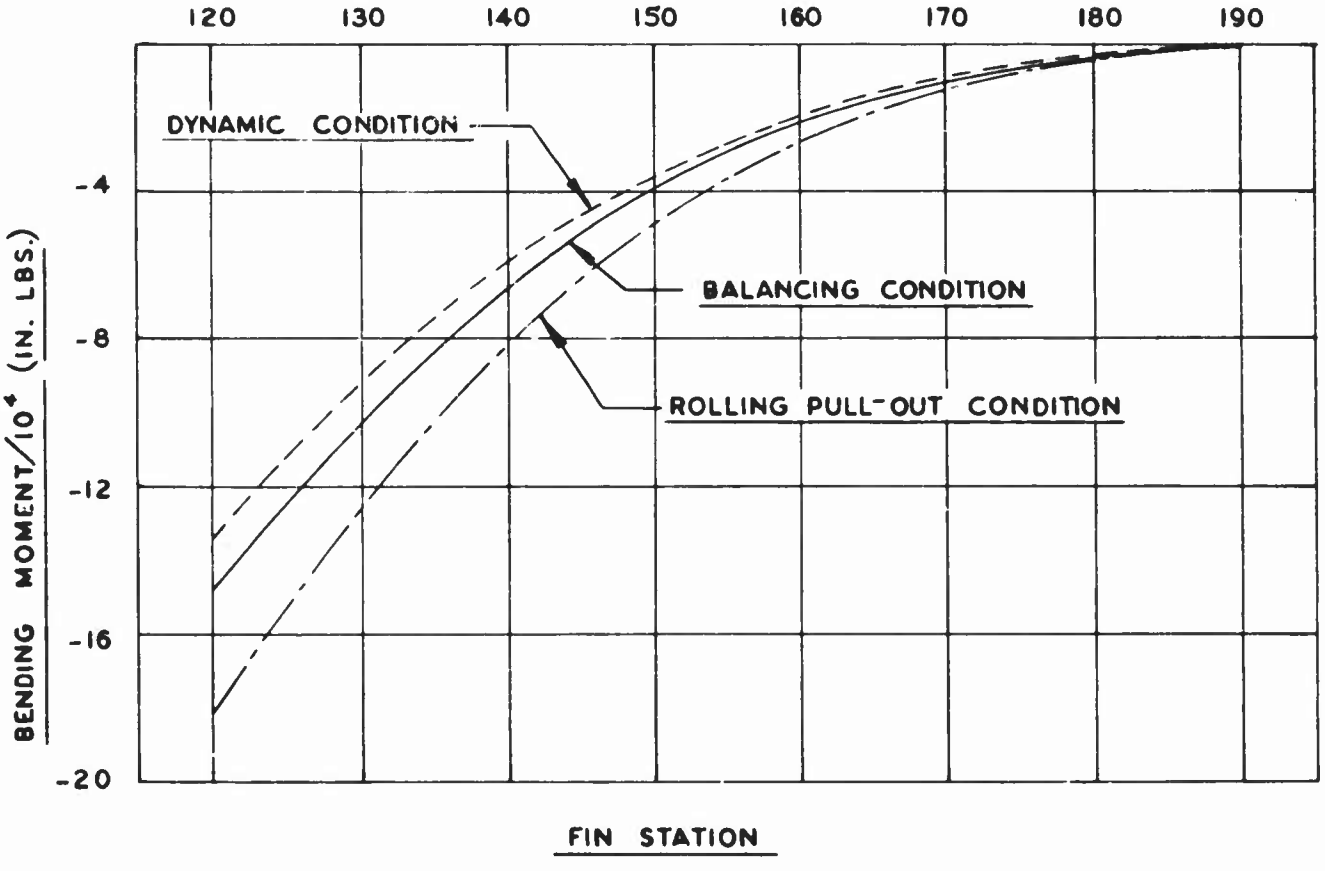

FIG. 99 FINAL FIN BENDING MOMENT DISTRIBUTION

(REF. TABLE 48)

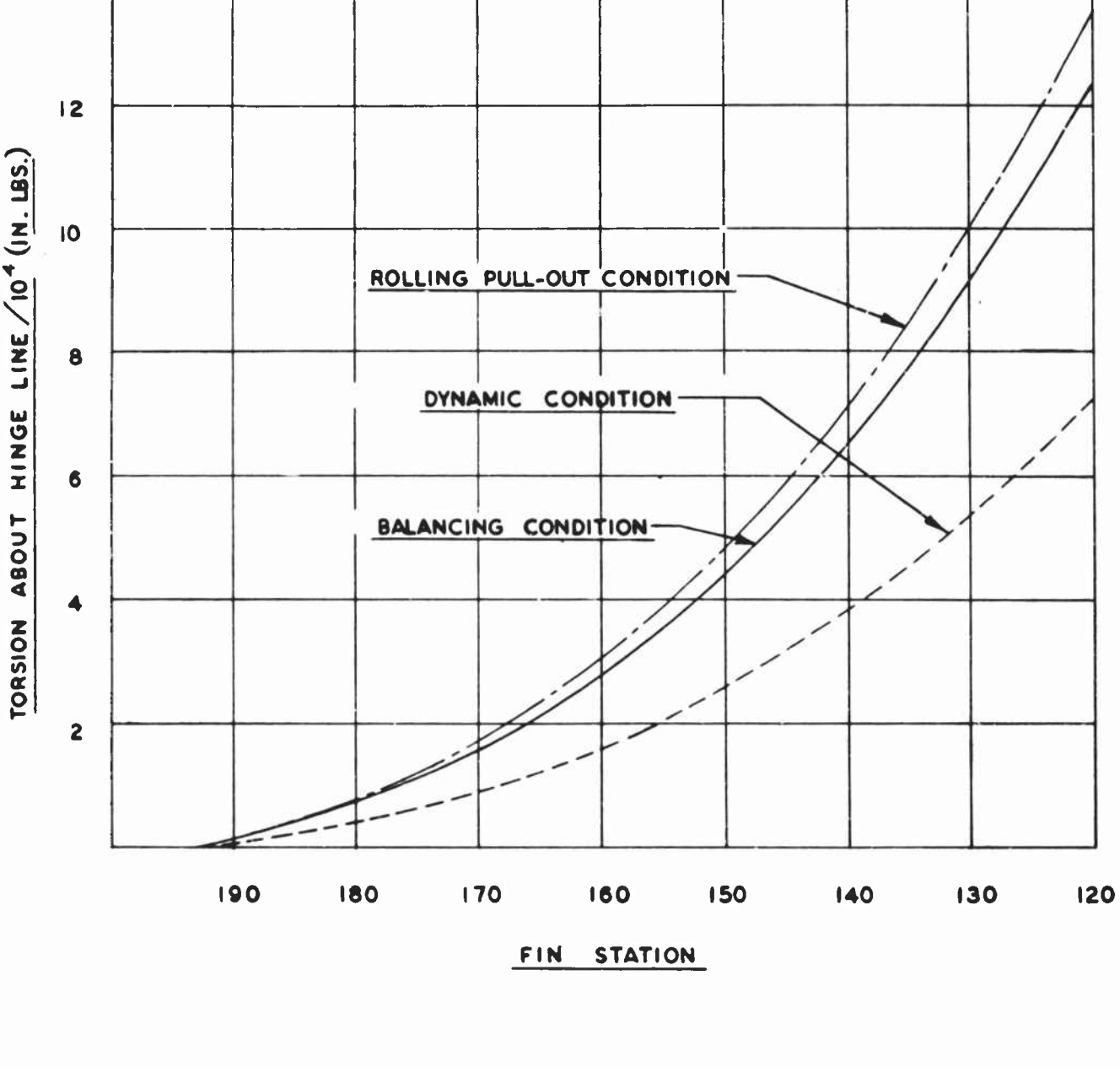

FIG. 100 DISTRIBUTION OF FIN TORSION ABOUT HINGE LINE

Design of Fin

Bending Strength of Fin Beams

Front Beam

The front beam makes an angle of approximately 18 deg. with the vertical. (Ref. LAC Report #4660, page 141.) For conservative design the stresses due to bending are increased by dividing by the cosine of this angle. The bending stresses and margins of safety at several stations are determined in Table 53.

Rear Beam

The bending stresses in the rear beam and the margins of safety at several stations are determined in Table 54.

Shear Flow in Fin Due to Torsion

The shear flow due to torsion is calculated by the same methods utilized in the Lockheed Report #4660, page 142. The shear center of the box beam at any station is assumed to lie at the center of gravity of the fin beam moments of inertia. Torsion about the shear center consists of two parts. One part is due to external loads and is obtained by transferring the external loads to the shear center. The other part is that torsion induced in the fin skin by bending of the inclined front and rear beams.

The distance from the shear center to the hinge line at any fin station "n" is obtained as follows:

$$X_{CG} = (I_{FB}/I_F)\, X_{FB} + (I_{RB}/I_F)\, X_{RB} \qquad - - - - - - - - - (61)$$

where I_{FB} = moment of inertia of front beam

I_{RB} = moment of inertia of rear beam

I_F = total moment of inertia = $I_{FB} + I_{RB}$

X_{FB} = distance from hinge line to front beam

X_{RB} = distance from hinge line to rear beam

The front beam is located at 18.85% chord, the rear beam at 58.2% chord and the hinge line at 75% chord. The chord at any station "n" is also given as 65.00 - .5821 (n-118). Therefore -

$$X_{FB} = (.75 - .1885)\left[\, 65.00 - .5821\,(n-118)\,\right] = 36.50 - .3268(n-118)$$

$$- - - - - - - - - (62)$$

$$X_{RB} = (.75 - .582)\left[\, 650 - .5821(n-118)\,\right] = 10.92 - .0978(n-118)$$

$$- - - - - - - - - (63)$$

TABLE 53 - BENDING STRESSES AND MARGINS OF SAFETY - FRONT BEAM

①	②	③	④	⑤	⑥	⑦	⑧
Fin Station	M	Critical Condition	$(I_F/y)_{FB}$	$(I_F/y)_{FB}$ x cos.18°	f_b	F_c	Margin of Safety
Ref.	Tab. 52	Fig. 99	Tab.49	.951 ④	② / ⑤	Pg.183	⑦/⑥ -1.0
128	135300	R. Pull-out	5.36	5.10	26500	27000	+.02
135	100000	"	4.85	4.61	20600	27000	+.31
143	700000	"	3.94	3.75	18670	27000	+.44
151	46300	"	3.17	3.01	15400	26700	+.73
160	26500	"	2.42	2.30	11530	22750	+.97
170	12090	"	1.93	1.83	6270	13900	+1.22
180	3850	"	1.57	1.49	2690	6250	+1.32

TABLE 54 - BENDING STRESSES AND MARGINS OF SAFETY - REAR BEAM

①	②	③	④	⑤	⑥	⑦
Fin Station	M	Critical Condition	$(I_F/y)_{RB}$	f_c	F_c	Margin of Safety
Ref.	Tab. 52	Tab. 99	Tab. 49	② / ④	Pg.183	⑥/⑤ -1.0
128	135300	R. Pull-out	5.36	25200	27000	+.07
135	100000	"	4.99	20000	27000	+.35
143	70000	"	4.03	17350	26500	+.52
151	46300	"	3.32	13950	25750	+.84
160	26500	"	2.56	10350	24500	+1.37
170	12090	"	2.03	5960	21250	High
180	3850	"	1.68	2290	18300	High

The locations of the shear center at various fin stations are determined in Table 55, using Equations (61), (62), and (63).

The external loads are assumed acting on the fin as shown in Figure 101.

The torque about the shear center due to the external loads acting on the fin is given by

$$T_{SC_{AL}} = T_{HL} - SX_{CG} \qquad - - - - - - - - - - - - - - - - (64)$$

The values of $T_{SC_{AL}}$ at the various fin stations for the three loadings are determined as follows. (Ref. Lockheed Report #4660, page 142)

$$(T_{SC})_{BM} = - BM \left[(I_{FB}/I_F) \text{ TAN } 18^\circ\ 06' + (I_{RB}/I_F) \text{ TAN } 5^\circ\ 35' \right]$$

$$= - BM \left[(.327)(I_{FB}/I_F) + (.0978)(I_{RS}/I_F) \right] - - - - - - (65)$$

The values of $(T_{SC})_{BM}$ at various fin stations "n" for the three loading conditions are determined in Table 57. The sign of the bending moment is taken such that a positive moment induces negative torsion in section (see Fig. 101).

The final torque distribution about the shear center of the fin,

$$T_{SC} = (T_{SC})_{AL} + (T_{SC})_{BB} \qquad - - - - - - - - - - - - - - - - (66)$$

and the resulting shear flows,

$$q_T = T_{SC}/2A \qquad - - - - - - - - - - - - - - - - - (67)$$

where

A = area of section

are determined in Table 58. The shear flows are summarized in Figure 102.

TABLE 55 - SHEAR CENTER LOCATION

①	②	③	④	⑤	⑥	⑦	⑧
Fin Station n	I_{FB}	I_{HB}	(I_{FB}/I_F)	(I_{RB}/I_F)			X_{CG}
Ref.	Eq. 62	Eq. 63	Tab. 49	Tab. 49	② x ④	③ x ⑤	⑥ + ⑦
120	35.85	10.72	.584	.416	20.90	4.46	25.36
128	33.23	9.94	.562	.438	18.69	4.35	23.04
135	30.94	9.26	.548	.452	16.95	4.18	21.13
143	28.33	8.48	.557	.443	15.79	3.76	19.55
151	25.72	7.69	.582	.418	14.95	3.22	18.17
160	22.77	6.81	.597	.403	13.60	2.75	16.35
170	19.50	5.83	.655	.345	12.78	2.01	14.79
180	16.24	4.86	.709	.291	11.52	1.41	12.93

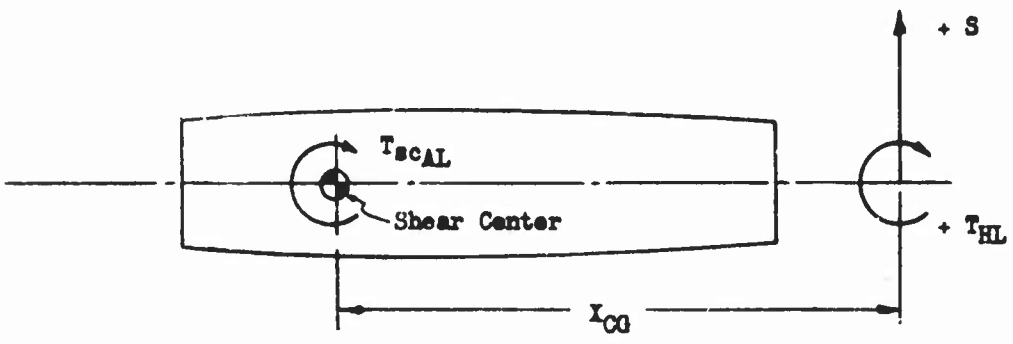

TABLE 56 - TORQUE ABOUT SHEAR CENTER DUE TO EXTERNAL LOADS

①	②	③	④	⑤	⑥	⑦	⑧	⑨	⑩	⑪	⑫	⑬	⑭
Fin Station	S_{CG}	Balancing Condition				Dynamic Condition				Roll. Pull-Out Cond.			
		S	$X_{CG} \cdot S$	T_{HL}	$(T_{SC})_{AL}$	S	$X_{CG} \cdot S$	$X_{CG} \cdot S$	$(T_{SC})_{AL}$	S	$X_{CG} \cdot S$	T_{HL}	$(T_{SC})_{AL}$
Ref.	Tab. 55	Tab. 51	② x ③	Tab.48	⑤ - ④	Tab.51	② x ⑦	Tab. 48	⑨ - ⑧	Tab.51	② x ⑪	Tab.48	⑬ - ⑫
192.79	-	0	0	0	0	0	0	0	0	0	0	0	0
-180.0	12.93	-614	-7940	-7020	+920	-404	-5220	-4110	+1110	-636	-8230	-7680	+550
+180.0	12.93	-394	-5090	-7020	-1930	-414	-5350	-4110	+1240	-526	-6810	-7680	-870
-170.0	14.79	-990	-14640	-15420	-780	-804	-11890	-9020	+2870	-1140	-16870	-16860	-10
+170.0	14.79	-700	-10350	-15420	-5070	-914	-13520	-9020	+4500	-1080	-15980	-16880	-900
160	16.35	-1410	-23050	-27670	-4620	-1390	-22730	-16200	+6530	-1820	-29750	-30300	-550
151	18.17	-2150	-39070	-42170	-3100	-1870	-33980	-24700	+9280	-2580	-46800	-46200	+600
143	19.55	-2890	-56500	-58190	-1690	-2360	-46140	-34100	+12040	-3350	-65500	-63700	+1800
-135	21.13	-3690	-77970	-77510	+460	-2880	-60850	-45300	+15500	-4180	-88300	-84800	+3500
+135	21.13	-3530	-74590	-77510	-2920	-3600	-76070	-45300	+30700	-4660	-98500	-84800	+13700
128	23.04	-4290	-98840	-97280	+1560	-4110	-94690	-56900	+37790	-5440	-125300	-106500	+18800
120	25.36	-5230	-132630	-123500	+9130	-4720	-119700	-72300	+47400	-6420	-162800	-135200	+27600

TABLE 57 - TORQUE ABOUT SHEAR CENTER DUE TO BENDING

①	②	③	④	⑤	⑥	⑦	⑧	⑨	⑩	⑪	⑫
Fin Station	(I_{FB}/I_F)	I_{RB}/I_F				Balancing - BM	Balancing - $(T_{SC})_{BM}$	Dynamic BM	Dynamic $(T_{SC})_{BM}$	Roll. Pull-Out BM	Roll. Pull-Out $(T_{SC})_{BM}$
Ref.	Tab.49	Tab.49	.327 ②	.0978 ③	④ + ⑤	Tab.52	- ⑥ × ⑦	Tab.52	- ⑥ - ⑨	Tab. 52	- ⑥ - ⑪
192.79	-	-									
180	.709	.291	.232	.0293	.261	-3720	+970	-2450	+640	-3850	+1005
170	.655	.345	.214	.0337	.248	-10540	+2620	-8480	+2100	-12090	+2990
160	.597	.403	.195	.0395	.235	-20990	+4930	-19920	+4680	-26500	+6220
151	.582	.418	.190	.0409	.231	-36970	+8540	-34530	+7970	-46270	+10700
143	.557	.443	.182	.0433	.225	-57070	+12800	-51400	+11560	-70010	+15750
135	.548	.452	.179	.0442	.2233	-83350	+18600	-72310	+16170	-100200	+22300
128	.562	.438	.183	.0428	.226	-110660	+24900	-99270	+22400	-135300	+30550
120	.584	.416	.191	.0407	.232	-148700	+34400	-134500	+31200	-182600	+42300

TABLE 58 - FINAL TORQUE DISTRIBUTION AND SHEAR FLOWS

①	②	③	④	⑤	⑥	⑦	⑧	⑨	⑩	⑪	⑫	⑬	⑭
Fin Station	2A	Balancing Cond.				Dynamic Cond.				Rolling Pull-Out Cond.			
		$(T_{SC})_{AL}$	$(T_{SC})_{BM}$	T_{SC}	q_T	$(T_{SC})_{AL}$	$(T_{SC})_{BM}$	T_{SC}	q_T	$(T_{SC})_{AL}$	$(T_{SC})_{BM}$	T_{SC}	q_T
Ref.		Tab.56	Tab.57	③ + ④	⑤ / ②	Tab.56	Tab.57	⑦ + ⑧	⑨ / ②	Tab.56	Tab.57	⑪ + ⑫	⑬ / ②
-180	58.2	+920	+970	+1890	+32	+1110	+640	+1750	+30	+550	+1005	+1560	+27
+180	58.2	-1930	+970	-960	-17	+1240	+640	+1880	+32	-870	+1005	+125	+2
-170	84.4	-780	+2620	+1840	+22	+2870	+2100	+4970	+59	-10	+2990	+2980	+35
+170	84.4	-5070	+2620	-2450	-29	+4500	+2100	+6600	+78	-900	+2990	+2090	+25
160	115.6	-4620	+4930	+310	+3	+6530	+4680	+11210	+97	-550	+6220	+5670	+49
151	150.6	-3100	+8540	+5440	+36	+9280	+7970	+17250	+115	+600	+10700	+11300	+75
143	182.6	-1690	+12800	+11110	+61	+12040	+11560	+23600	+129	+1800	+15750	+17550	+96
-135	218.6	+460	+18600	+19060	+87	+15500	+16170	+31670	+145	+3500	+22300	+25800	+118
+135	218.6	-2920	+18600	+15680	+72	+30700	+16170	+46870	+214	+13700	+22300	+36000	+165
128	252.4	+1560	+24900	+26460	+105	+37790	+22400	+60190	+238	+18800	+30550	+49350	+196
120	289.8	+9130	+34400	+43530	+150	+47400	+31200	+78600	+272	+27600	+42300	+69900	+241

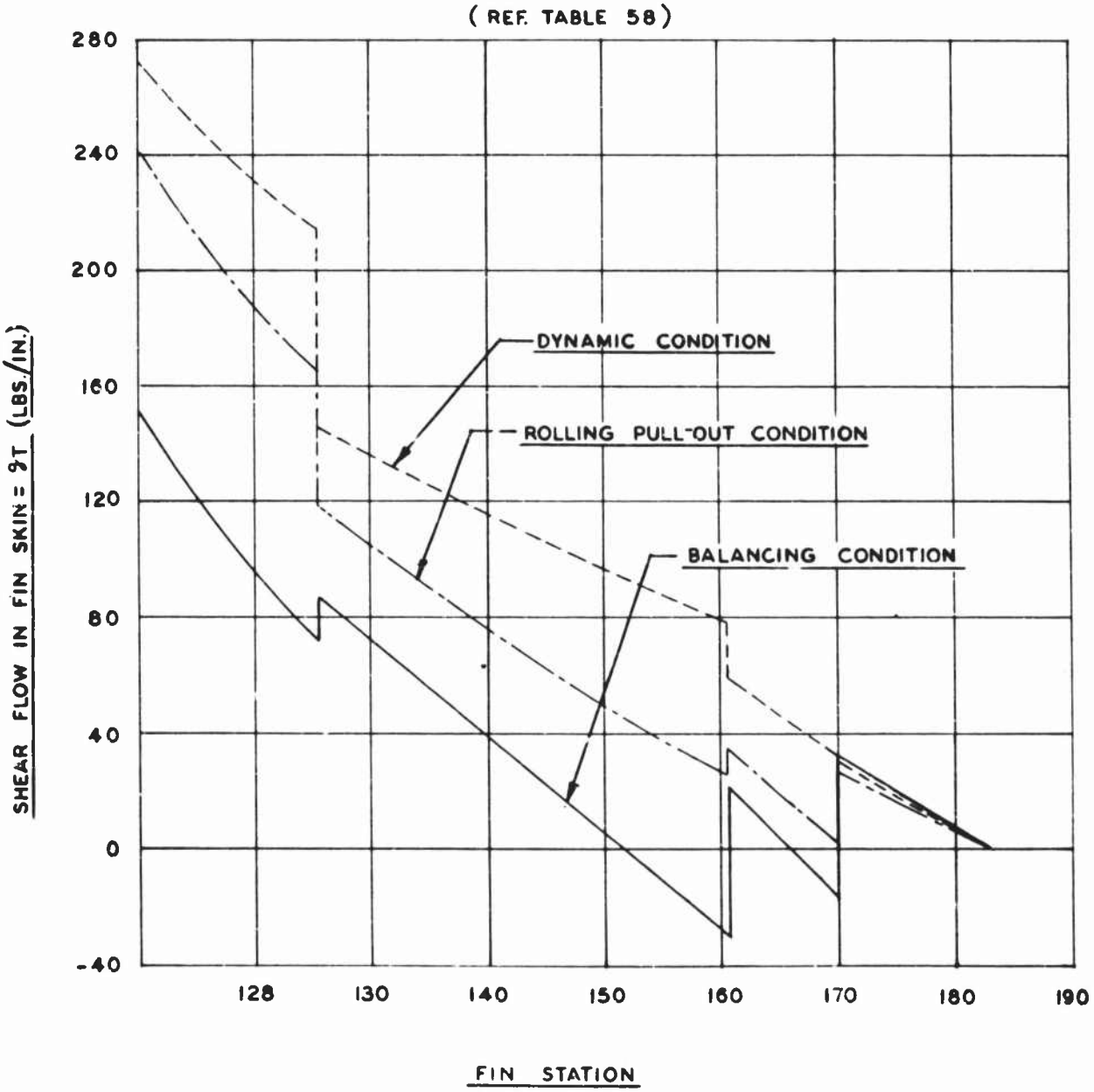

FIG. 102 SHEAR FLOW IN FIN SKIN DUE TO TORSION

Shear Flow in Fin Beam Webs

The shear in the fin beam webs is composed of two parts, that due to bending and that due to torsion. Distributing the total fin shear to the front and rear beams in proportion to their moments of inertia, the total shear flow in each beam is given by -

$$q_{FB} = q_{B_F} + q_T = S(I_{FB}/I_F)/h_{FB} + q_T \quad - - - - - - - - - - \quad (68)$$

$$q_{RB} = q_{B_R} - q_T = S(I_{RB}/I_F)/h_{RB} - q_T \quad - - - - - - - - - - \quad (69)$$

where S = total shear in fin at station

(I_{FB}/I_F) and (I_{RB}/I_F) = ration of front and rear beam moments of inertia to total fin moment of inertia.

h_{FB} and h_{RB} = distance between cap rivet lines at front and rear beams.

The resultant shear flows in the web of the front and rear beams are determined in Tables 59, 60, and 61 and summarized in Figure 103.

TABLE 59 - SHEAR FLOWS FRONT AND REAR BEAM WEBS - BALANCING CONDITION

①	②	③	④	⑤	⑥	⑦	⑧	⑨	⑩	⑪
Fin Station	(I_{FB}/I_F)	(I_{RB}/I_F)	h_{FB}	h_{RB}	q_T	S	q^B_F	q^B_R	q_{FB}	q_{RB}
Ref.	Tab.49	Tab.49			Tab.58	Tab.51	②⑦/④	③⑦/⑤	⑥ + ⑧	- ⑥ + ⑨
-180	.709	.291	1.16	1.30	+32	-614	-376	-137	-344	-169
+180	.709	.291	1.16	1.30	-17	-394	-241	-88	-258	-71
-170	.655	.345	1.58	1.74	+22	-990	-411	-196	-389	-218
+170	.655	.345	1.58	1.74	-29	-700	-291	-139	-320	-110
160	.597	.403	2.14	2.26	+3	-1410	-394	-251	-391	-254
151	.582	.418	2.60	2.70	+36	-2150	-481	-333	-445	-369
143	.557	.443	2.84	3.12	+61	-2890	-567	-410	-506	-471
-135	.548	.452	3.26	3.50	+87	-3690	-620	-477	-533	-564
+135	.548	.452	3.26	3.50	+72	-3530	-594	-456	-522	-528
128	.562	.438	3.64	3.84	+105	-4290	-663	-490	-558	-595
120	.584	.416	3.94	4.14	+150	-5230	-775	-526	-625	-676

TABLE 60 - SHEAR FLOWS FRONT AND REAR BEAM WEBS - DYNAMIC CONDITION

①	②	③	④	⑤	⑥	⑦	⑧	⑨	⑩	⑪
Fin Station	(I_{FB}/I_F)	(I_{RB}/I_F)	h_{FB}	h_{RB}	q_T	S	q_{BF}	q_{BR}	q_{FB}	q_{RB}
Ref.	Tab.49	Tab.49			Tab.58	Tab.51	②⑦/④	③⑦/⑤	⑥ + ⑧	- ⑥ + ⑨
-180	.709	.291	1.16	1.30	+30	-404	-247	-91	-217	-121
+180	.709	.291	1.16	1.30	+32	-414	-253	-93	-221	-125
-170	.655	.345	1.58	1.74	+59	-804	-333	-159	-274	-218
+170	.655	.345	1.58	1.74	+78	-914	-379	-181	-301	-259
160	.597	.403	2.14	2.26	+97	-1390	-388	-248	-291	-345
151	.582	.418	2.60	2.70	+115	-1870	-418	-290	-303	-405
143	.557	.443	2.84	3.12	+129	-2360	-462	-336	-333	-465
-135	.548	.452	3.26	3.50	+145	-2880	-484	-372	-339	-517
+135	.548	.452	3.26	3.50	+214	-3600	-605	-465	-391	-679
128	.562	.438	3.64	3.84	+238	-4110	-635	-469	-397	-707
120	.584	.416	3.94	4.14	+272	-4720	-700	-475	-428	-747

TABLE 61 - SHEAR FLOWS FRONT AND REAR BEAMS WEBS - ROLL. PULL-OUT CONDITION

①	②	③	④	⑤	⑥	⑦	⑧	⑨	⑩	⑪
Fin Station	(I_{FB}/I_F)	(I_{RB}/I_F)	h_{FB}	h_{RB}	q_T	S	q_{B_F}	q_{B_R}	q_{FB}	q_{RB}
Ref.	Tab.49	Tab.49			Tab.58	Tab.51	②⑦/④	③⑦/⑤	⑥+⑧	-⑥+⑨
-180	.709	.291	1.16	1.30	+27	-636	-389	-143	-362	-170
+180	.709	.291	1.16	1.30	+2	-526	-322	-118	-320	-120
-170	.655	.345	1.58	1.74	+35	-1140	-472	-226	-437	-261
+170	.655	.345	1.58	1.74	+25	-1080	-448	-214	-423	-239
160	.597	.403	2.14	2.26	+49	-1820	-508	-325	-459	-374
151	.582	.418	2.60	2.70	+75	-2580	-578	-399	-503	-474
143	.557	.443	2.84	3.12	+96	-3350	-658	-476	-562	-572
-135	.548	.452	3.26	3.50	+118	-4180	-704	-540	-686	-658
+135	.548	.452	3.26	3.50	+165	-4660	-785	-589	-620	-754
128	.548	.452	3.26	3.50	+165	-4660	-785	-589	-620	-754
120	.584	.416	3.94	4.14	+241	-6420	-951	-464	-710	-887

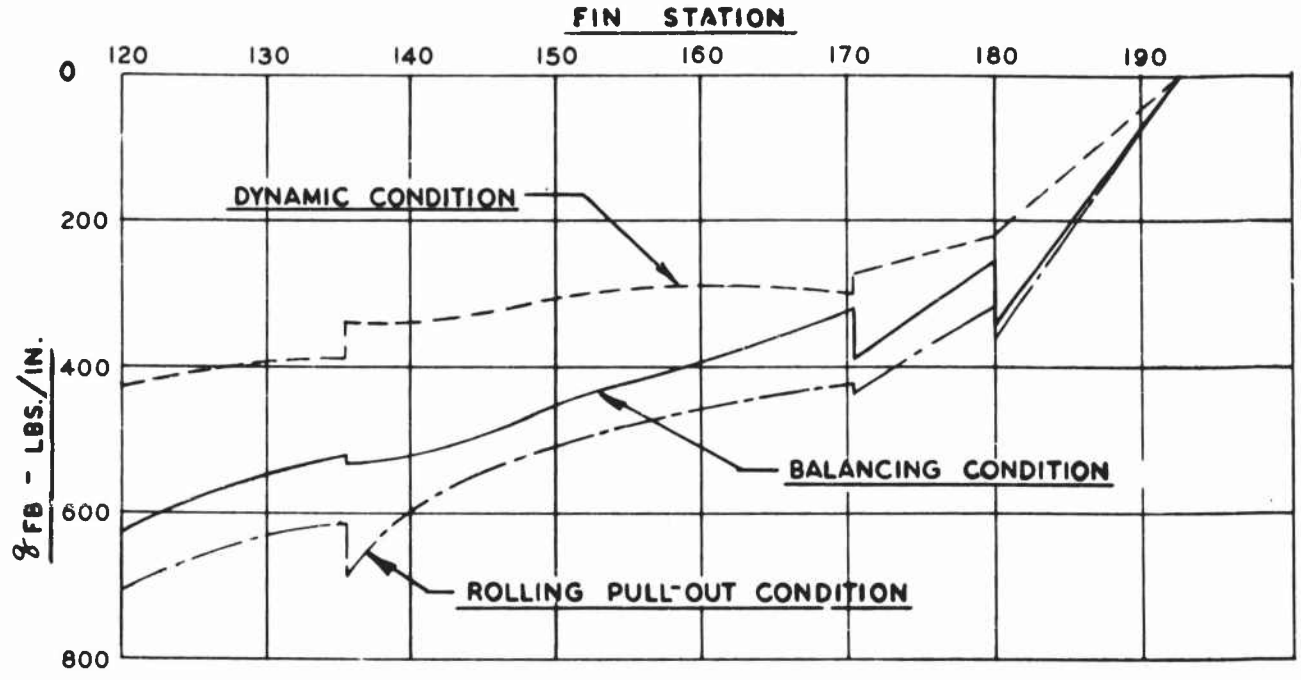

(REF. TABLES 59, 60, & 61)

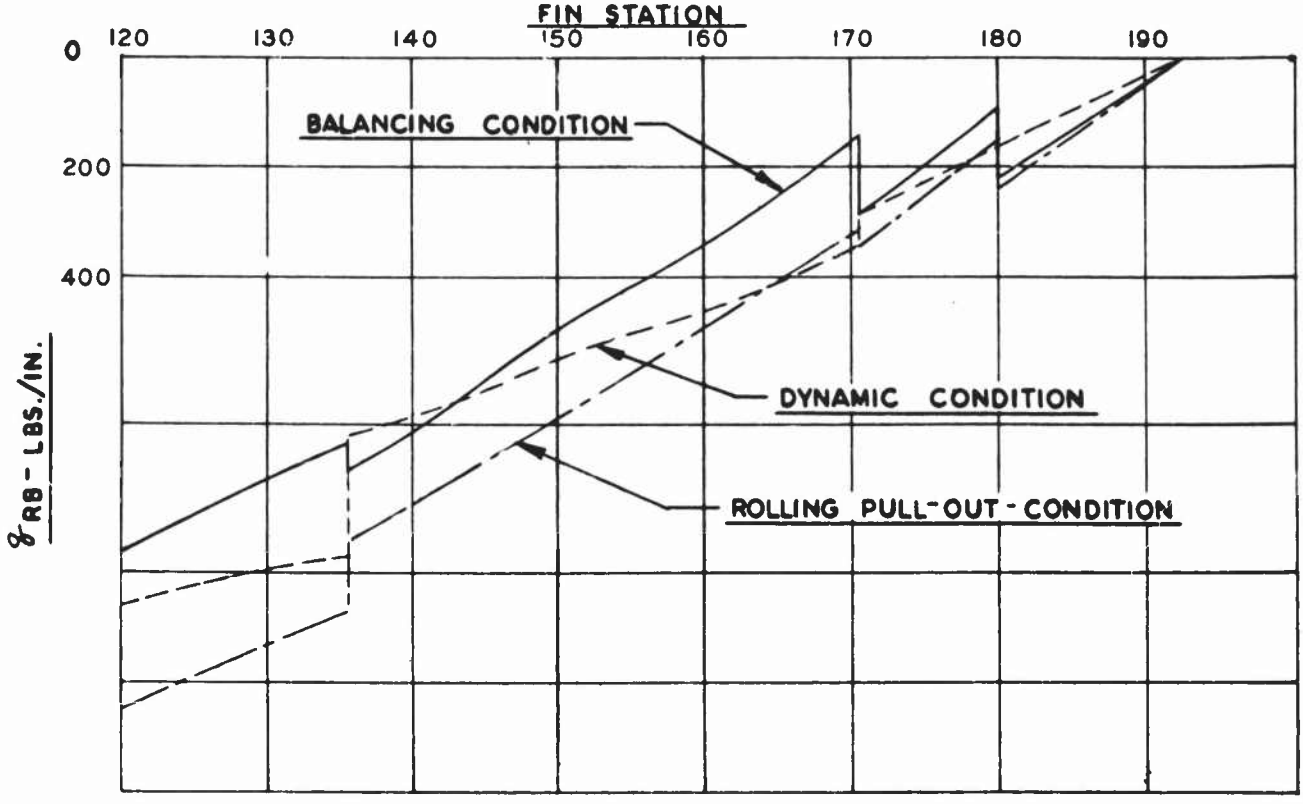

(REF. TABLES 59, 60 & 61)

FIG. 103 SHEAR FLOWS FRONT AND REAR BEAM WEB